

AD-A192 821

FRACTURE PHYSICS OF DELAMINATION OF COMPOSITE MATERIALS

1/3

(U) TEXAS A AND M UNIV COLLEGE STATION MECHANICS AND

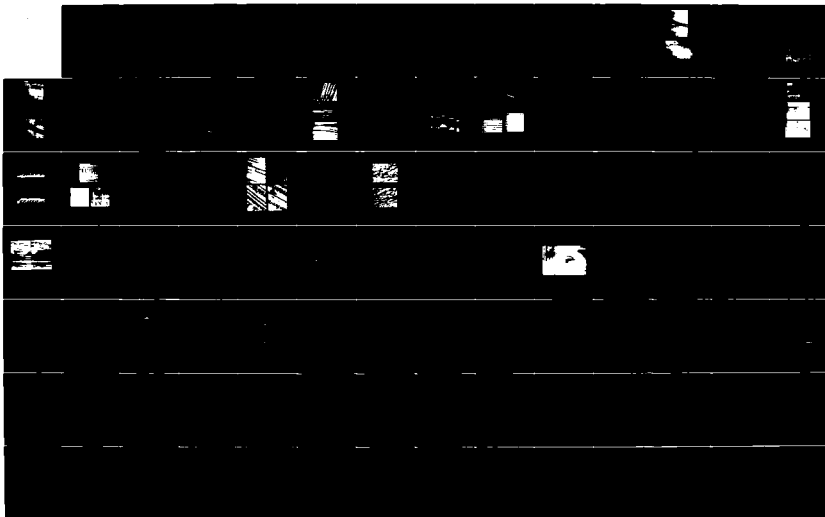
MATERIALS CE. H. P. STANLEY ET AL. OCT 87 NP-8821-87-12

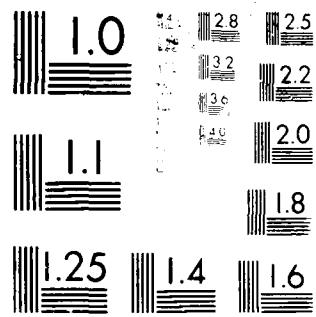
UNCLASSIFIED


AFOSR-1A-88-0020 AFOSR-84-0064

F/C 11/4

NE







AFOSR-TR- 88-0020

AD-A192 021

FRACTURE PHYSICS OF DELAMINATION OF COMPOSITE MATERIALS

~~FINAL~~ TECHNICAL REPORT

W.L. BRADLEY

C.R. CORLETO

D.P. GOETZ

DTIC
ELECTE
FEB 25 1988

DIRECTOR, FBI (100-441100)
 FROM: SAC, NEW YORK (100-100000)
 SUBJECT: MURDER OF MARTIN LUTHER KING, JR.
 RE: NEW YORK TELETYPE TO BUREAU, APRIL 19, 1968.
 NEW YORK OFFICE IS CURRENTLY REVIEWING ALL INFORMATION
 RECEIVED FROM SOURCE IN CONNECTION WITH THIS CASE.
 NEW YORK OFFICE WILL ADVISE BUREAU OF ANY DEVELOPMENTS.
 WJH:KMP
 ENCL. 1
 INFORMATION DIVISION

AIR FORCE OFFICE OF SCIENTIFIC RESEARCH
OFFICE OF AEROSPACE RESEARCH
UNITED STATES AIR FORCE
GRANT No. AFOSR-84-0064

MM 5021-87-12

OCTOBER 1987

88 2 24 1 50

ADA192021

REPORT DOCUMENTATION PAGE

1a. REPORT SECURITY CLASSIFICATION Unclassified			1b. RESTRICTIVE MARKINGS		
2a. SECURITY CLASSIFICATION AUTHORITY			3. DISTRIBUTION / AVAILABILITY OF REPORT Approved for public release; distribution is unlimited.		
2b. DECLASSIFICATION / DOWNGRADING SCHEDULE			5. MONITORING ORGANIZATION REPORT NUMBER(S) AFOSR-TR- 88 - 0020		
4. PERFORMING ORGANIZATION REPORT NUMBER(S)					
6a. NAME OF PERFORMING ORGANIZATION Texas A&M University		6b. OFFICE SYMBOL (If applicable)		7a. NAME OF MONITORING ORGANIZATION AFOSR	
6c. ADDRESS (City, State, and ZIP Code) Box 3578 College Station		7b. ADDRESS (City, State, and ZIP Code) Bldg 410 Bolling AFB, DC 20332-6448			
8a. NAME OF FUNDING / SPONSORING ORGANIZATION AFOSR		8b. OFFICE SYMBOL (If applicable) NA		9. PROCUREMENT INSTRUMENT IDENTIFICATION NUMBER AFOSR-84-0064	
8c. ADDRESS (City, State, and ZIP Code) same as 7b.		10. SOURCE OF FUNDING NUMBERS			
		PROGRAM ELEMENT NO. 61102F		PROJECT NO. 2301	
				TASK NO. B2	
				WORK UNIT ACCESSION NO.	
11. TITLE (Include Security Classification) "FRACTURE PHYSICS OF DELAMINATION OF COMPOSITE MATERIALS (U)					
12. PERSONAL AUTHOR(S) Drs. W L. Bradely, C. Corleto, D. Goetz					
13a. TYPE OF REPORT ANNUAL		13b. TIME COVERED FROM 84/2/01 to 87/6/31		14. DATE OF REPORT (Year, Month, Day) October 1987	
15. PAGE COUNT 263					
16. SUPPLEMENTARY NOTATION					
17. COSATI CODES			18. SUBJECT TERMS (Continue on reverse if necessary and identify by block number)		
FIELD	GROUP	SUB-GROUP			
			Microstructure Observations, Delamination of Composites		
19. ABSTRACT (Continue on reverse if necessary and identify by block number) Real time observations in the scanning electron microscope have delineated the detail of the fracture processes that result in mode I and mode II delamination of composite materials. These observations give clear explanation of why GII/GIC ratio for brittle materials is three times that for ductile materials. These in-situ observations of fracture also indicate that distinctively different damage zone develops ahead of growing cracks for mode I and mode II delamination. Two techniques have been developed to measure the strain field around a crack tip. Stereo-imaging and direct measurement of distortion of a fine array of dots placed on the surface. Both are effective in measuring the strain field around a crack tip. A surprising result which emerged from these measurements is that the local strain to failure at the crack tip is much greater than the elongation measured in a tensile test (up to six times as high). A linear, orthotropic finite element code has been used to calculate the stress fields around the crack tip for					
20. DISTRIBUTION / AVAILABILITY OF ABSTRACT <input type="checkbox"/> UNCLASSIFIED/UNLIMITED <input checked="" type="checkbox"/> SAME AS RPT <input checked="" type="checkbox"/> DTIC USERS			21. ABSTRACT SECURITY CLASSIFICATION UNCLASSIFIED		
22a. NAME OF RESPONSIBLE INDIVIDUAL GEORGE K. HARITOS, Lt Colonel, USAF			22b. TELEPHONE (Include Area Code) (202) 767-0463		22c. OFFICE SYMBOL NA

UNCLASSIFIED

(Block No. 19) Continued

mode I and mode II loading. A J-integral approach for mode I has been used to investigate the delamination of multi-directional composites. Initial results using this approach look very promising for characterizing systems which can not be characterized with conventional analysis.

TABLE OF CONTENTS

	page
1.0 SUMMARY OF SIGNIFICANT ACCOMPLISHMENTS	1
2.0 OBJECTIVES	2
3.0 SUMMARY WORK STATEMENT	3
4.0 SUMMARY OF ACCOMPLISHMENTS BY AREAS STATED IN WORK STATEMENT	4
4.1 IN-SITU FRACTURE OBSERVATIONS	4
4.1.1 IN-SITU OBSERVATIONS IN SEM OF FRACTURE OF NEAT RESINS	4
4.1.2 IN-SITU OBSERVATIONS IN SEM OF DELAMINATION FRACTURE OF COMPOSITE MATERIALS	13
4.2 STRAIN FIELD MAPPING	26
4.2.1 STRAIN FIELD MAPPING BY STEREO-IMAGING	26
4.2.2 STEREO-IMAGING	30
4.3 ANALYSIS AND MODELING	51
4.3.1 LINEAR, ORTHOTROPIC FINITE ELEMENT ANALYSIS OF MODE I AND MODE II DELAMINATION	52
4.3.2 MODELING THE EFFECT OF FIBERS ON MODE I DELAMINATION TOUGHNESS	60
4.4 FRACTURE MECHANICS CHARACTERIZATION OF MATERIALS	67
4.4.1 MODE I DELAMINATION	68
4.4.2 MIXED MODE AND MODE II DELAMINATION OF COMPOSITE	107
4.4.2.1 COMPARISON OF THE END NOTCH FLEXURE TEST AND THE END-LOADED SPLIT LAMINATE TEST FOR DELAMINATION OF COMPOSITE MATERIALS	107
4.4.2.2 J-INTEGRAL APPROACH FOR MODE II DELAMINATION FRACTURE TOUGHNESS EVALUATION	126
4.5 FRACTOGRAPHY AND FAILURE ANALYSIS	
5.0 PUBLICATION RESULTING IN WHOLE OR IN PART FROM WORK SUPPORTED BY AFOSR	155
6.0 PRESENTATIONS MADE THAT WERE BASED ON WHOLE OR IN PART ON WORK PERFORMED UNDER SPONSORSHIP OF THIS AFOSR GRANT	158
7.0 PROFESSIONAL PERSONNEL ASSOCIATED WITH RESEARCH EFFORT	161
Appendix I	163
Appendix II	167



Availability For	
1.0	✓
2.0	
3.0	
4.0	
Distribution/	
Availability Codes	
Avail and/or	Spec'd
1.0	
2.0	
3.0	
4.0	
5.0	
6.0	
7.0	
Appendix I	
Appendix II	

1.0 SUMMARY OF SIGNIFICANT ACCOMPLISHMENTS

The significant accomplishments from this research project fall into five areas.

1.1 Real time observations in the scanning electron microscope have delineated the details of the fracture processes that result in mode I and mode II delamination of composite materials. These observations give clear explanation of why G_{IIC}/G_{IC} ratio for brittle materials is 3.0 or larger while for ductile materials it is closer to 1.1. These in-situ observations of fracture also indicate that distinctively different damage zones develop ahead of growing cracks for mode I and mode II delamination.

1.2 Two techniques have been developed to measure the strain field around a crack tip. Stereo-imaging and direct measurement of distortion of a fine array of dots placed on the surface have both been found to be effective in measuring the strain field around a crack tip. One of the surprising results from these measurements is that the local strain to failure at the crack tip is much greater than the elongation measured in a tensile test (48% versus 8% for Hexcel F185).

1.3 A linear, orthotropic finite element code has been used to calculate the stress fields around the crack tip for mode I and mode II loading. The relative size and shape of the stress fields for these two different loading conditions explains the different sizes and shapes of the damage/deformation zones seen in-situ (as noted in 1.1). A phenomenological model has been developed to try to explain

why G_{IC} and G_{IIC} for delamination of a composite material made from a tough resin are so much lower than the neat resin G_{IC} .

1.4 A J-integral approach for mode I has been used to investigate the delamination of multi-directional composites. A comparison of the end notch flexure test and the loaded flexure test for measuring G_{IIC} has found that they give consistent results. A J-integral approach for the measurement of J_{IIC} for composites made from more ductile resin has been developed. Initial results using this approach look very promising for characterizing systems which previously could not be characterized with conventional analyses.

1.5 A combination of in-situ fracture observations with postmortem fractography has clarified some long standing questions with regard to fractographic interpretation in failure analysis.

2.0 OBJECTIVES

The objectives of the research program whose results are summarized in this report have been:

2.1 to better define the deformation and fracture physics of delamination fracture in graphite/epoxy composite materials so that realistic micromechanics models of matrix dominated fracture can be developed; and

2.2 to develop reliable experimental and analytical techniques to measure mode I, mode II, and mixed mode

delamination fracture toughness of both unidirectional and multidirectional composite laminates to provide meaningful design parameters and benchmarks against which predictions of the various micromechanics models may be tested.

3.0 SUMMARY WORK STATEMENT

The following areas of work have been performed to achieve the stated objectives.

3.1 In-situ fracture studies in a scanning electron microscope (SEM) have been undertaken to better define the deformation and fracture processes which accompany mode I and mode II delamination fracture.

3.2 Two techniques to measure the displacement fields around crack tips in neat resins and composites from direct observations made in the scanning electron microscope have been developed and utilized.

3.3 A simple phenomenological model consistent with observations made in 3.1 and 3.2 which is capable of predicting the results obtained in 3.4 is being developed.

3.4 Testing and analytical techniques have been developed for characterizing mode I, mode II, and mixed mode delamination of split laminates which give very nonlinear load-displacement curves; e.g. ones made from more ductile resins and/or split laminates with multi-directional layups.

3.5 The results from the in-situ observations of fracture in the SEM have been utilized in conjunction with post-mortem fractography to develop a failure analysis methodology.

4.0 SUMMARY OF ACCOMPLISHMENTS BY AREAS STATED IN WORK STATEMENT

4.1 In-Situ Fracture Observations

A summary of significant results will be given in this section with more complete results and discussion available in the twelve papers that have been published based on this work. These papers are listed in section 5.0 with copies of each in Appendix II.

In this research program, in-situ fracture observations have been made for both neat resin loaded in mode I and graphite/epoxy composite materials loaded to give mode I and mode II delamination. The primary objective of these observations have been to determine the crack tip processes that lead to fracture and to relate the size and shape of the damage zone observed around the tip of a growing crack to the macroscopically measured fracture toughness.

4.1.1 In-Situ Observations in SEM of Fracture of Neat Resins

In-situ observations of neat resin fracture have been made on standard 0.5T compact tension specimens (see ASTM-E399¹), except that the thicknesses were typically about 3-4 mm rather than the specified 12.5 mm.

Typical in-situ fracture observations are presented in Fig. 1 for the relatively brittle resin Hercules 3502 (highly crosslinked epoxy) and for the much more ductile Hexcel F185 (moderately crosslinked epoxy with 14% rubber added to

enhance toughness). The very fine microcracking observed in these figures is due either to deformation and fracture of the 150A thick gold/palladium film that is sputter coated onto the polished surface of the neat resin compact tension specimens to avoid charging or real microcracking in the specimen. It has been determined that the film microcracking begins at about 3-5% tensile strain. (This was done by coating a rubber band and stretching it in the SEM.) Thus, the microcracked zone gives some indication of the volume of material surrounding the crack tip which experiences either significant deformation (at least 3%) or real resin microcracking.

F185 Resin--The "butterfly wings" pattern of the microcrack distribution as well as the very fine scale of cracking in the in-situ observations of fracture of F185 neat resin (Fig. 1) indicate this to be only film cracking resulting from the considerable plastic deformation occurring in this very ductile resin prior to crack advance. A comparison of the fracture surface of the F185 observed post mortem to the fracture surface of the 3502 which fails brittlely clearly indicates that the F185 experiences a ductile fracture (see Fig. 2). This further substantiates our contention that the microcracking observed in-situ in the F185 is coating microcracking due to resin deformation.

The viscoelastic nature of the Hexcel 185 resin gives a very discontinuous crack growth behavior, as seen in Fig.3. The initial loading is occurring under displacement control

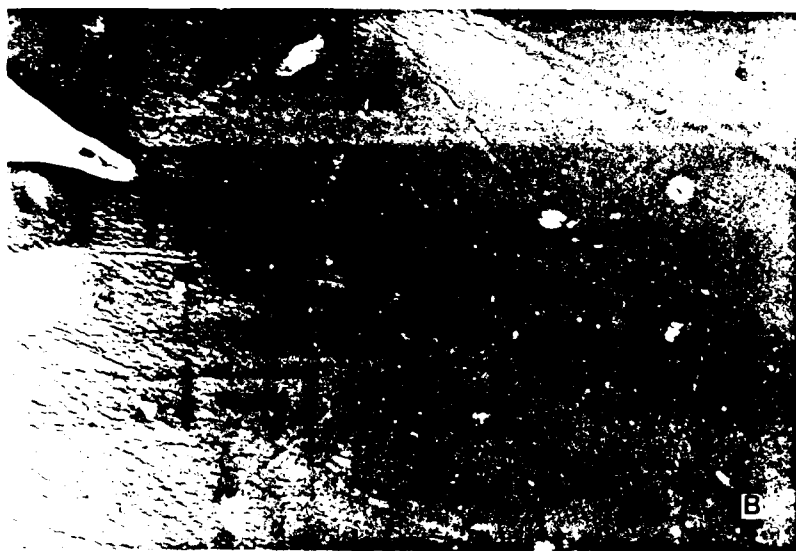


Figure 1. In-situ fracture of (a) 3502 (4300X) and (b) F185(1000X). The white region along the crack is due to charging of uncoated resin, exposed by the fracture process. The point lines especially evident in the 3502 arc polishing scratches introduced during specimen preparation.

at a very slow rate. Crack tip deformation and blunting are noted, with the deformation zone indicated by the microcracking of the 100A thick gold/palladium film. Once the strain in the crack tip reaches a critical value, a sharp crack emerges from the blunted notch. The material is unable to support this slightly longer and much sharper crack at its current load level. Furthermore, the blunting process previously observed requires some time to be realized, time which was formerly provided by the slow, monotonic loadup. With the specimen now already at full load, the crack will tend to propagate unstably and quickly with much less deformation until the specimen unloads sufficiently to give crack arrest. For slow monotonic loading in displacement control, this process of crack tip blunting, rapid advance, and arrest will be repeated many times.

Post-mortem fractography of the F185 specimens indicates a considerable difference in the amount of deformation that occurs during unstable crack propagation as compared to reinitiation of crack growth during monotonic loading (in displacement control). The individual "platelets" seen in Fig. 2 represent unstable advance of the crack tip. (Compare the length of unstable crack advance in Fig. 3 to platelet size in Fig. 2.) The steps between "platelets" are the result of the crack tip blunting that occurs during reloading to give further crack advance. Ductile fracture is indicated for both, but the amount of deformation is much less during rapid crack advance. The

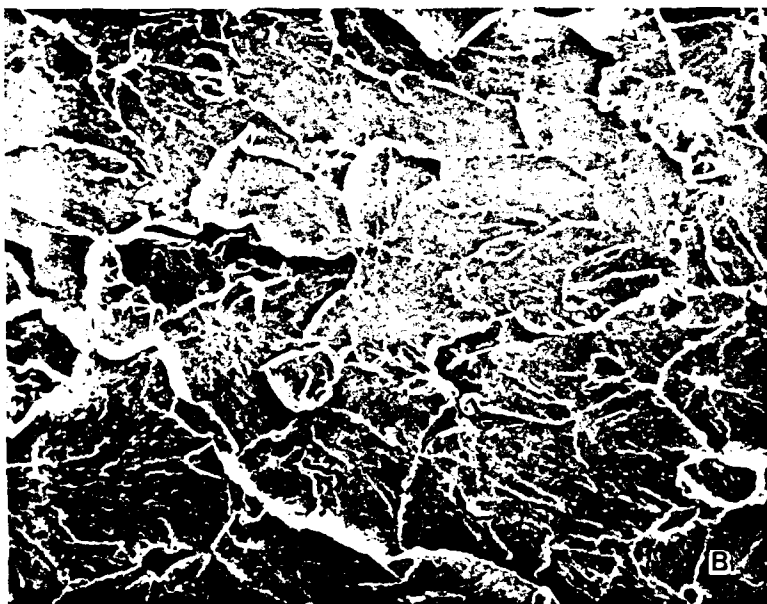
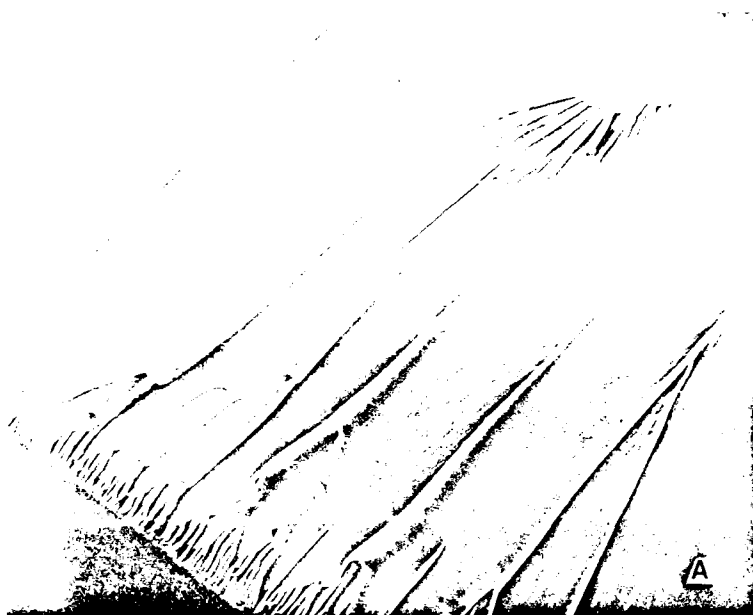


Figure 2. Post-mortem fractography of (a) 2000x, 3502 epoxy resin, and (b) 1000x, F185 epoxy resin.



Figure 3. Microcracking ahead of crack tip of F185 resin showing crack growth sequence under constant applied displacement. (a) 3000x. Detail of crack tip, blunt crack. (b) 9000x. Crack propagation through microcrack coalescence to form a very sharp narrow crack. (c) 5000x. Crack extension occurred. New crack tip is very sharp.

fine holes are due to cavitation of the rubber particles added to the F185 resin to enhance toughness.

3502 Resin--The microcracking in the brittle 3502 is much more localized around the crack tip, and the observation of these microcracks in real time indicates that they coalesce to give macrocrack advance, as seen in Fig. 2. With a monotonic increase in mouth opening displacement, microcracking around the crack tip develops which partially shields the crack tip, reducing locally the crack tip stresses. However, once these microcracks coalesce giving local crack tip advance, unstable crack growth follows due to the presence of the new sharp crack tip without the benefit of microcrack shielding. Advance proceeds under displacement control until sufficient unloading occurs that the running crack arrests. Subsequent quasi-static, monotonic increase in the mouth opening displacement again causes the formation of new microcracks surrounding the crack tip, with the density increasing with mouth opening displacement until coalescence occurs, again giving additional, unstable crack extension.

The river pattern seen in Fig. 2 is due to coalescence with growth of the many microcracks that develop in the vicinity of the crack tip during quasi-static, monotonic loading. Once coalescence has occurred, the crack advances rapidly to the new arrest location, with little opportunity for new microcrack formation. The river patterns that form at the arrest lines as well as the almost smooth fracture

surface in between arrest lines strongly supports the scenario just presented for crack growth in brittle resin systems.

Comparison of 3502 and F185 Resins--The relative deformation/damage zone sizes seen in Fig. 1 for F185 and 3502 resins may be better understood by comparing the constitutive behavior of the two materials as determined in tensile tests, the results of which are presented in Fig. 4. It is clear that the lower yield strength of the F185 as well as the much more nonlinear constitutive behavior combine to give a much larger deformation zone and much greater load redistribution away from the crack tip, postponing the fracture event. The result is a much greater resistance to crack propagation, and thus, a much greater macroscopically measured fracture toughness.

It should be emphasized that the strain to failure measured in tensile tests greatly underestimates the local strain to failure in the crack tip region. For example, the F185 resin gave 8-9% elongation in a 2.5 cm gage length. By contrast, the local strain to failure as measured in a 10 micron gage length at the tip of the crack indicated 48% strain (as will be explained in more detail in section 4.2 of this report). In similar fashion the tensile elongation in a 2.5 cm gage length of 3502 resin was only 1.5% whereas the elongation measured in a 10 micron gage length at the tip of a mode I delamination crack was 15%. However, to the degree that crack tip strain to failure is some constant times the

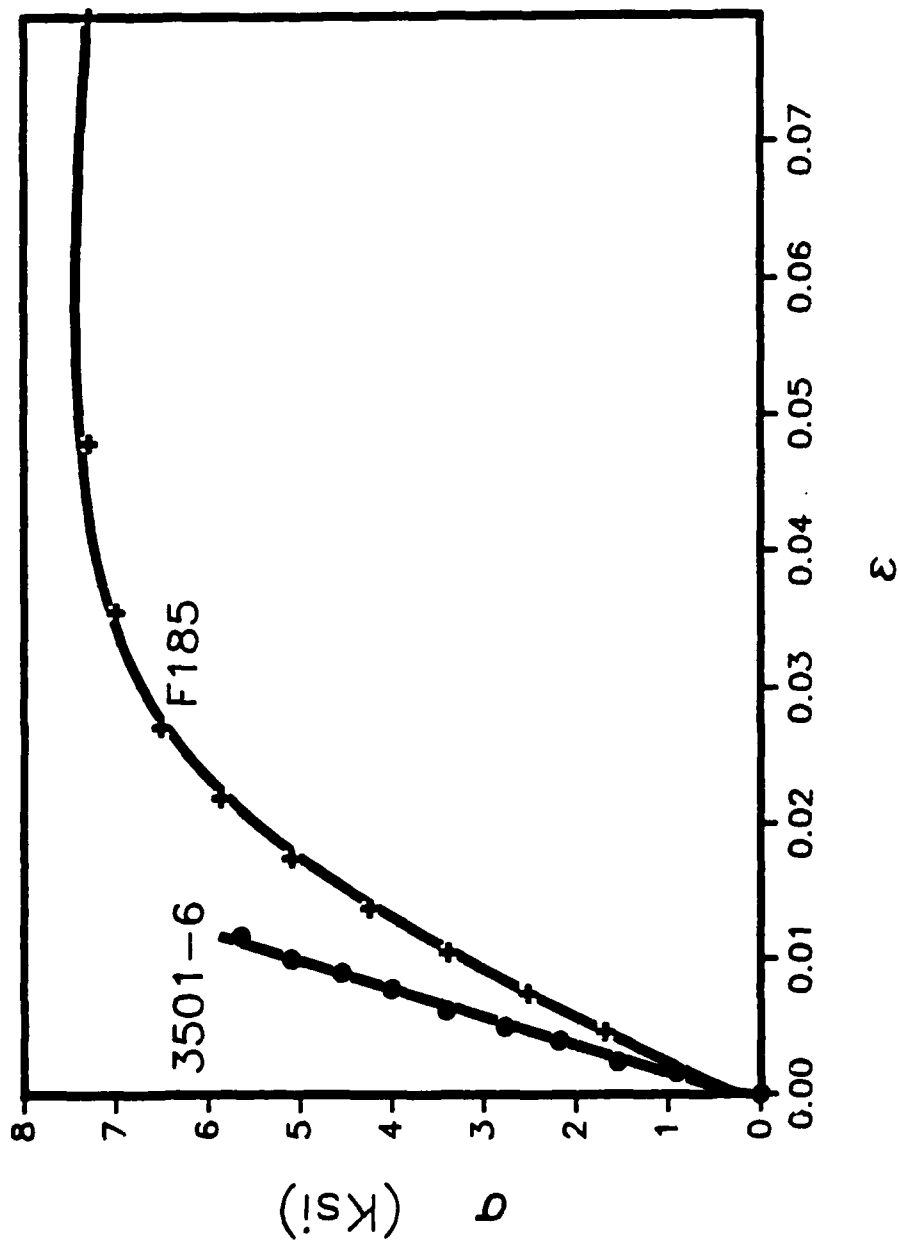


Figure 4. Longitudinal Stress-strain curve of F185 and 3501-6 epoxy resins.

tensile elongation, or more likely times the nonlinear component of the tensile elongation, tensile data may still be useful to rank resins, though the tensile elongation would obviously not be a useful fracture parameter in a micromechanics model.

4.1.2 IN-SITU OBSERVATIONS IN SEM OF DELAMINATION FRACTURE OF COMPOSITE MATERIALS

Direct observation of the delamination fracture process in composite materials allows one to determine the micromechanical processes responsible. For example, delamination crack growth may occur by interfacial debonding or by resin cracking, as seen in Fig. 5. Furthermore, the size and shape of the deformation/damage zone is seen to be quite variable, depending on both the resin toughness and the state of stress (i.e., mode I, mode II, or mixed mode).

Figure 6 presents in-situ fracture observations of the deformation/damage zone sizes for mode I and mode II delamination fracture of brittle AS4/3501-6. The extent of the damage zone ahead of the crack tip is much greater for the mode II loading than for the mode I loading. A much slower decay in the stress field ahead of the crack tip (to be reported in section 4.3 of this document) for mode II loading than for mode I loading is responsible for the difference in the respective damage zone sizes.

The deformation/damage zone for mode I and mode II delamination fracture of the much more ductile T6T145/F185 is



Figure 5

Crack extension by resin fracture and interfacial debond are seen in three composites made with ductile resins. (a) AS41Q6, Dow Chemical (1100X)1; (b) T6T145/F185, Hexcel (1000X), and (c) T6145/F155, Hexcel (1200X).

seen in Fig. 7. It is obvious that the deformation/damage zone for both mode I and mode II delamination of the T6T145/F185 is much greater than that observed in the more brittle AS4/3501-6. A schematic representation of the relative damage zone sizes for these two composite systems, loaded in mode I and mode II, is seen in Fig. 8.

The deformation/damage zone size has been measured for several systems and an effort has been made to see how the size of the deformation/damage zone correlates with the delamination fracture toughness. The results are presented in Table 1. In general, larger deformation/damage zone sizes correlate with higher delamination fracture toughness; however, the correlation is not monotonic.

Micromechanisms of Mode I Delamination--The details of the fracture process have also been noted during in-situ observations of fracture. In most systems studied, mode I crack advance occurs after the development of a deformation/damage zone ahead of the crack tip. In brittle systems, this zone consists of microcracks which coalesce with each other and the macrocrack to give crack advance. Sometimes, crack advance occurs by debonding before microcrack coalescence occurs. When this takes place, fiber bridging and fiber breakage will be observed. In ductile systems, local deformation around the crack tip precedes crack advance, but with no true specimen microcracking, only the superficial coating cracks which are indicative of large deformation. Crack advance generally occurs by ductile

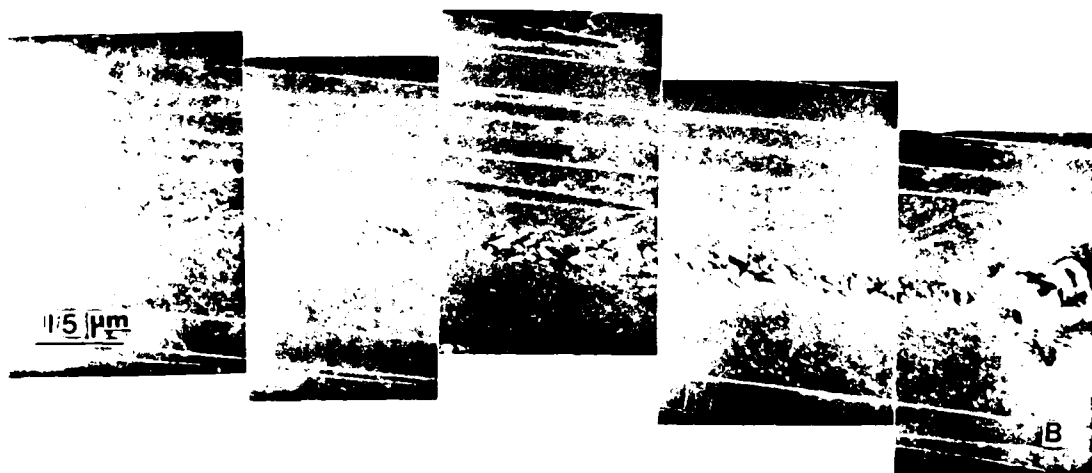
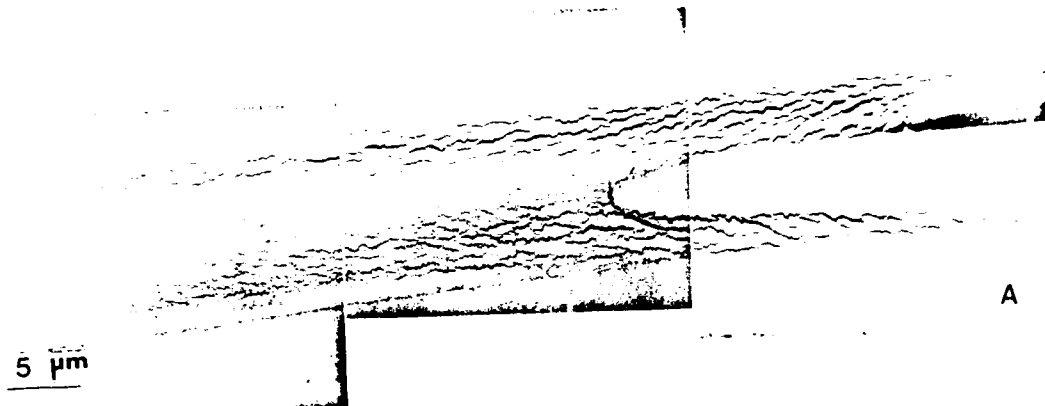


Figure 6. Damage zones ahead of the crack tip of AS4/3501-6 under (a) mode I loading, and (b) mode II loading.

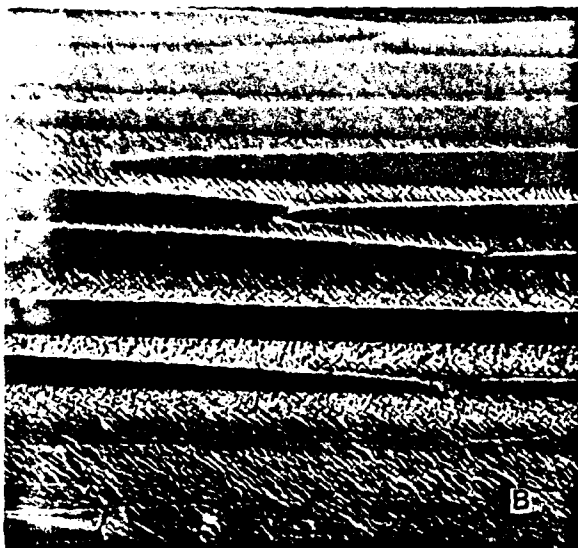


Figure 7. Damage zone ahead of crack tip of T6T145/F185 under (a) 750x, mode I loading. (b) 1000x, mode II loading. (c) 1000x, mode II loading.

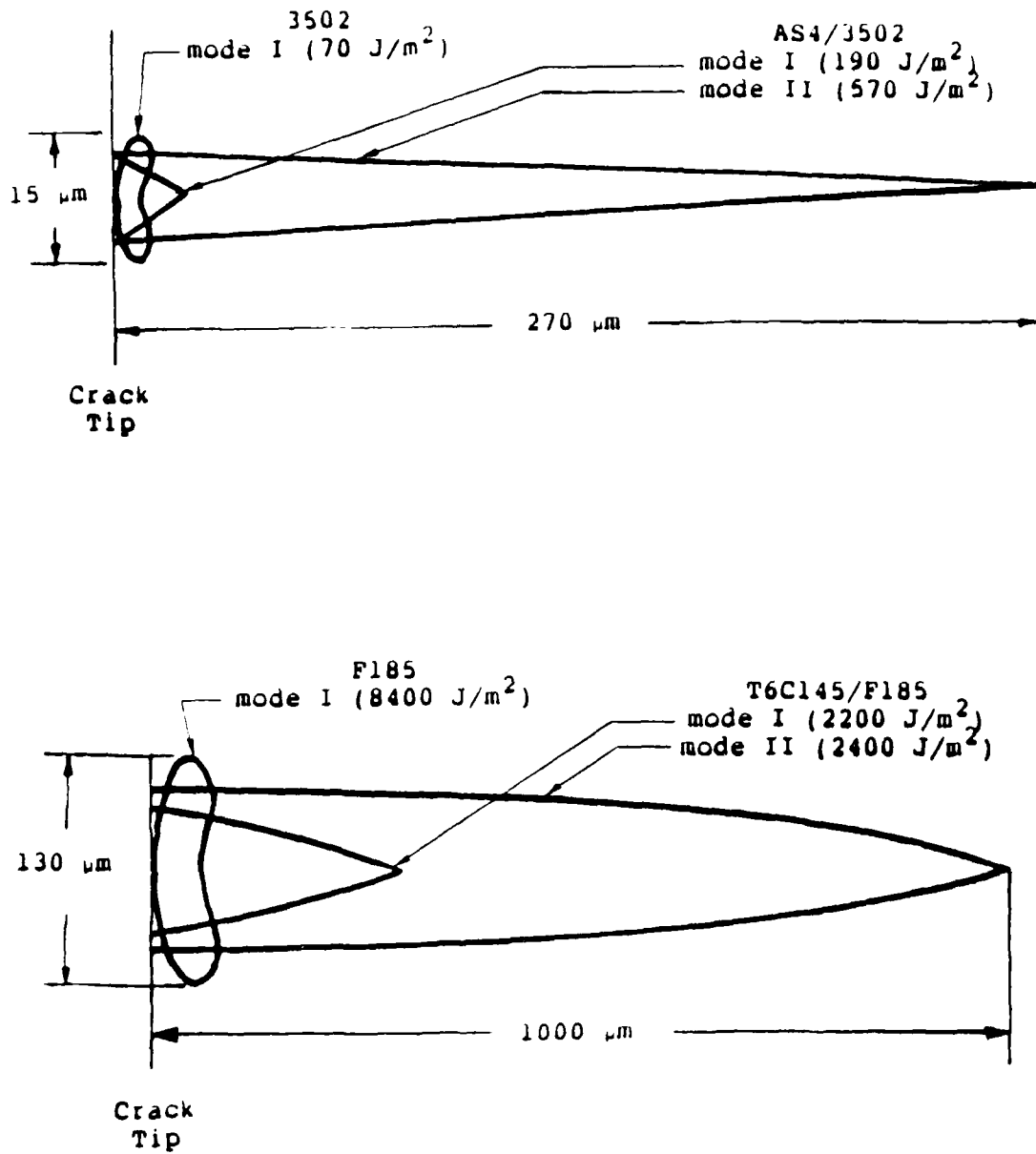


Figure 8. Schematic of relative damage zone sizes for mode I and mode II. (a) 3502 neat resin and AS4/3502 composite. (b) F185 neat resin and T6C145/F185 composite.

Composite System	Fiber Density (vol.%)	Size of Damage Zone ahead of crack (μm)	Size of Damage Zone above/below crack (μm)	G_{Ic} (J/m^2)
AS4/3502	76.4	20	5	190
F155 NR		20	7	135
T6T145/F155	59.6	30	20	1015
T6T145/F155	70.5	20	10	615
T6T145/F155	68.8	20	10	520
F185 NR		75	35	455
F185		200	50	2205

Table I. Deformation/Damage zone sizes for composites; determined from in-situ fracture observations for mode I delamination fracture.

tearing, but crack advance by interfacial debonding was also commonly observed in composites made with more ductile resins.

Micromechanisms of Mode II Delamination--Mode II delamination of brittle systems occurs in a very distinctive way. Microcracks form for a considerable distance ahead of the crack tip at a 45° angle to the plane of the ply, which is the plane perpendicular to the principal normal stress. These cracks grow until they reach the fibers which bound the resin rich region between plies. It sometimes appears that they stop in the resin short of the nearest visible fiber (see Fig. 6, for example). However, there are certainly fibers just beneath the surface which are responsible for arresting these growing microcracks. Coalescence of these microcracks is required for macrocrack advance. This coalescence generally occurs at the fiber/matrix interface, giving a corrugated roof appearance along with the formation of "hackles" in the resin between fibers, as seen in Fig. 9. It is apparent that the final orientation of the microcracks and the resulting hackles is greater than 45° . This is a result of the fact that hackles are often rotated into a more nearly upright position by the mode II loading prior to final microcrack coalescence, as shown schematically in Fig. 10. It has been noted by several investigators (e.g., Bradley and Cohen²) that the G_{IIC}/G_{IC} ratio for delamination of composites made with brittle resins is typically 3 or greater. This is understandable when one considers the

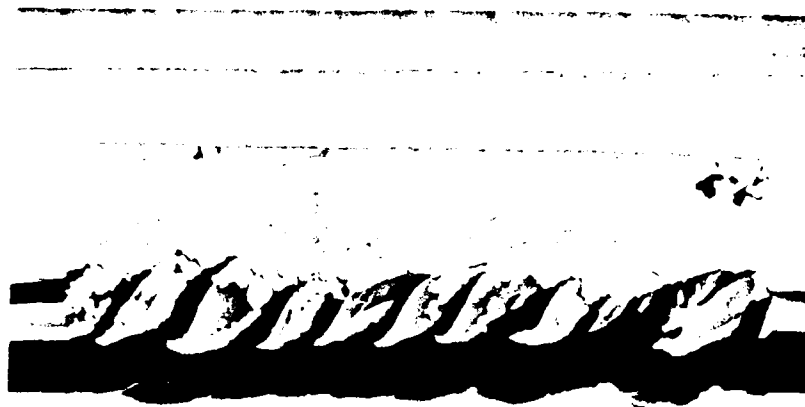
following factors: (1) a much more extensive damage zone ahead of the crack tip; (2) the greater difficulty in getting microcrack coalescence; (3) the more torturous path taken by the crack; and (4) the much greater evidence of crack interaction with the fibers via the microcracks which form and arrest temporarily at the fibers.

Mode II delamination of the more ductile T6T145/F185 gave no evidence of resin microcracking. Rather, only a very fine coating cracking was noted (see Fig. 7), indicating resin deformation. Thus, the fracture process for mode II delamination (like that for mode I delamination) appears to be ductile rupture, with occasional fiber debonding. Thus, it is not surprising that the G_{IIC}/G_{IC} ratio for delamination of composites made with ductile resins is approximately 1.

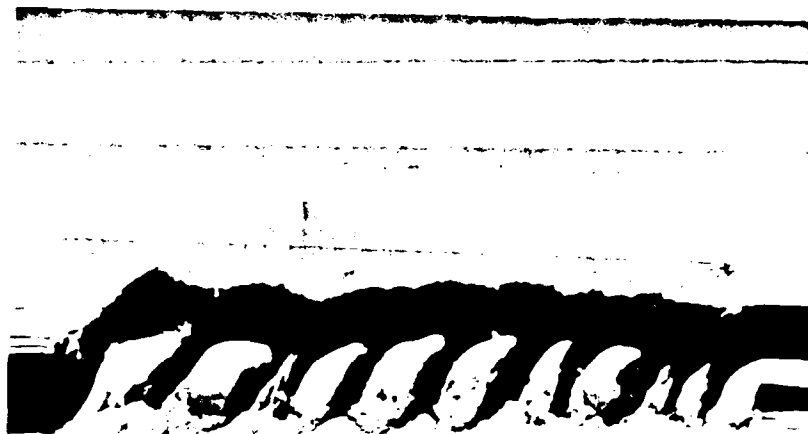
Mixed-Mode Delamination--A series of mixed mode delamination experiments were run in which the percentage of mode II energy release rate, G_{IIC} , was systematically varied from 0% to 100%. These tests were performed on several resin systems. Where the brittle AS4/3502 was used, the density of the hackles as well as their orientation relative to the delamination planes were found to increase with increasing percentage of mode II loading, as seen in Fig. 11. The total critical energy release rate was also found to monotonically increase with increasing percentage of mode II energy release rate, as seen in Fig. 12 for composites made with brittle resins. No such systematic variation in either fracture surface appearance or critical energy release rate was noted



Figure 9. In situ and post mortem fractography of AS4/3502 under mode II delamination. (a) 3000x. Microcrack formation at 45 degrees followed by opening of microcracks. (b) 3000x. Microcrack coalescence. (c) 3000x. Microcrack coalescence with rotation at root of hackles.



A



B

Figure 9. (Continued) (d) 2000x. (e) 2000x. Final coalescence of microcracks results in macroscopic crack formation showing the typical hackles characteristic of mode II delamination of brittle composites.

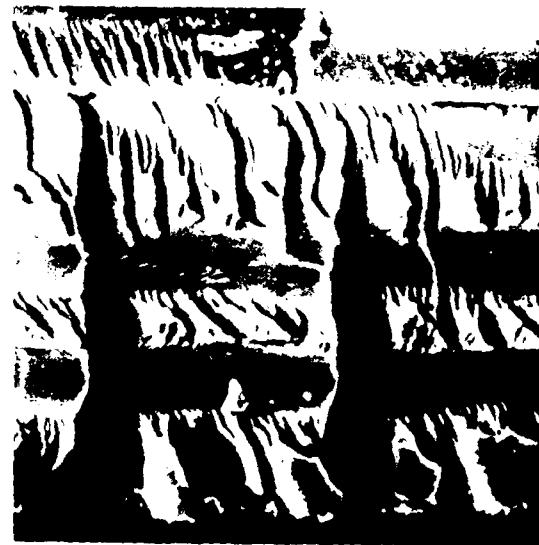
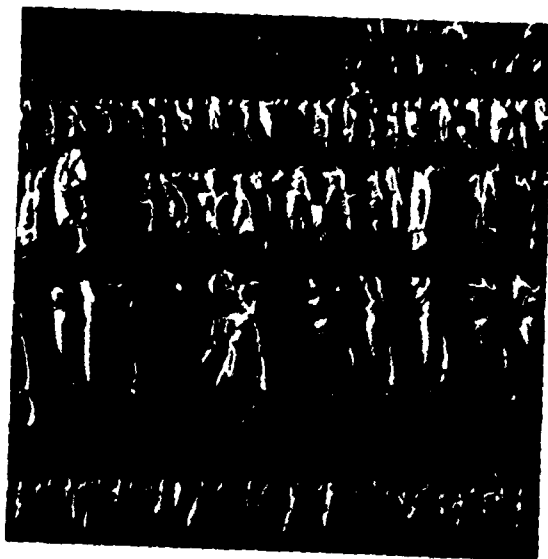


Figure 9. (Continued). Post-mortem fractography showing the highly hackled fracture surface. (f) 1000x. (g) 1000x. (h) 2000x.

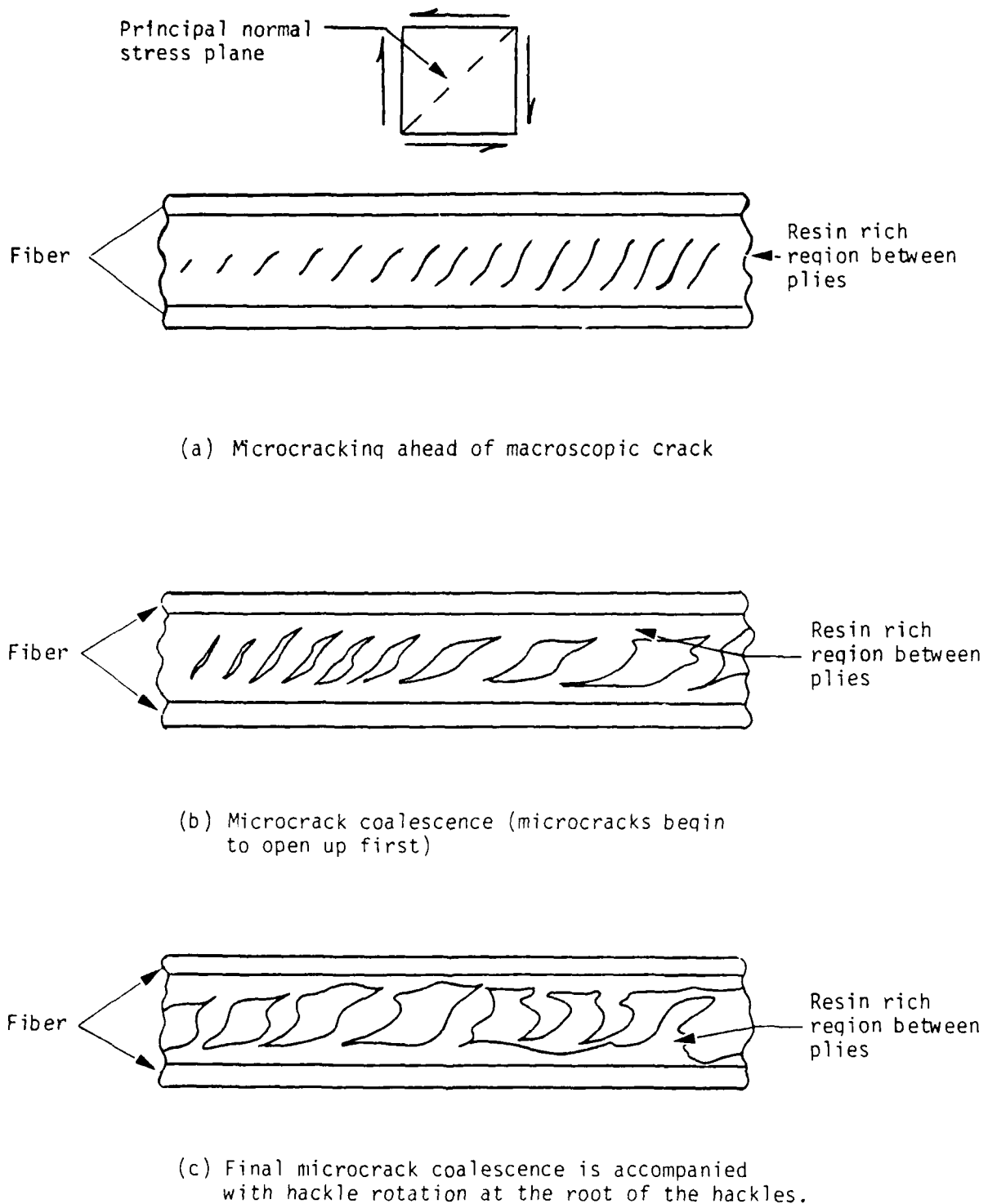


Figure 10. Schematic of mode II delamination crack formation (hackle formation process).

for the ductile T6T145/F185 as the percentage of mode II loading was increased.

While most of the laminates studied in this work were unidirectional layups, a few multi-directional layups were also investigated. Typical results for mode I delamination of a specimen containing $\pm 45^\circ$ plies across the delamination plane are seen in Fig. 13.

4.2 Strain Field Mapping

In the previous section, the physical details of the mode I and mode II delamination fracture process as determined by direct, real-time observations in the SEM were summarized. It was decided early in this program that quantifying the strain field around the crack tip would be essential to assist in the development and verification of micromechanics models. Two different approaches were taken to try to achieve this objective: (1) the stereo-imaging approach developed for metals by Davidson and Lankford at Southwest Research Institute and (2) the direct measurement of the distortion of a dot pattern placed on the surface with the electron beam of the SEM. These two approaches will be explained and results from each presented next.

4.2.1 Strain Field Mapping by Stereo-Imaging

Recent works by Davidson and Lankford³⁻⁵ have described a method of accurately determining the in-plane displacements and strain fields developed during the



Figure 11. Hackles increasing in orientation with increasing mode II loading of AS4/3501-6. (a) 1500x. 0% mode II (mode I). (b) 10000x. 20% mode II. (c) 2000x. 43% mode II. (d) 3000x. 100% mode II.

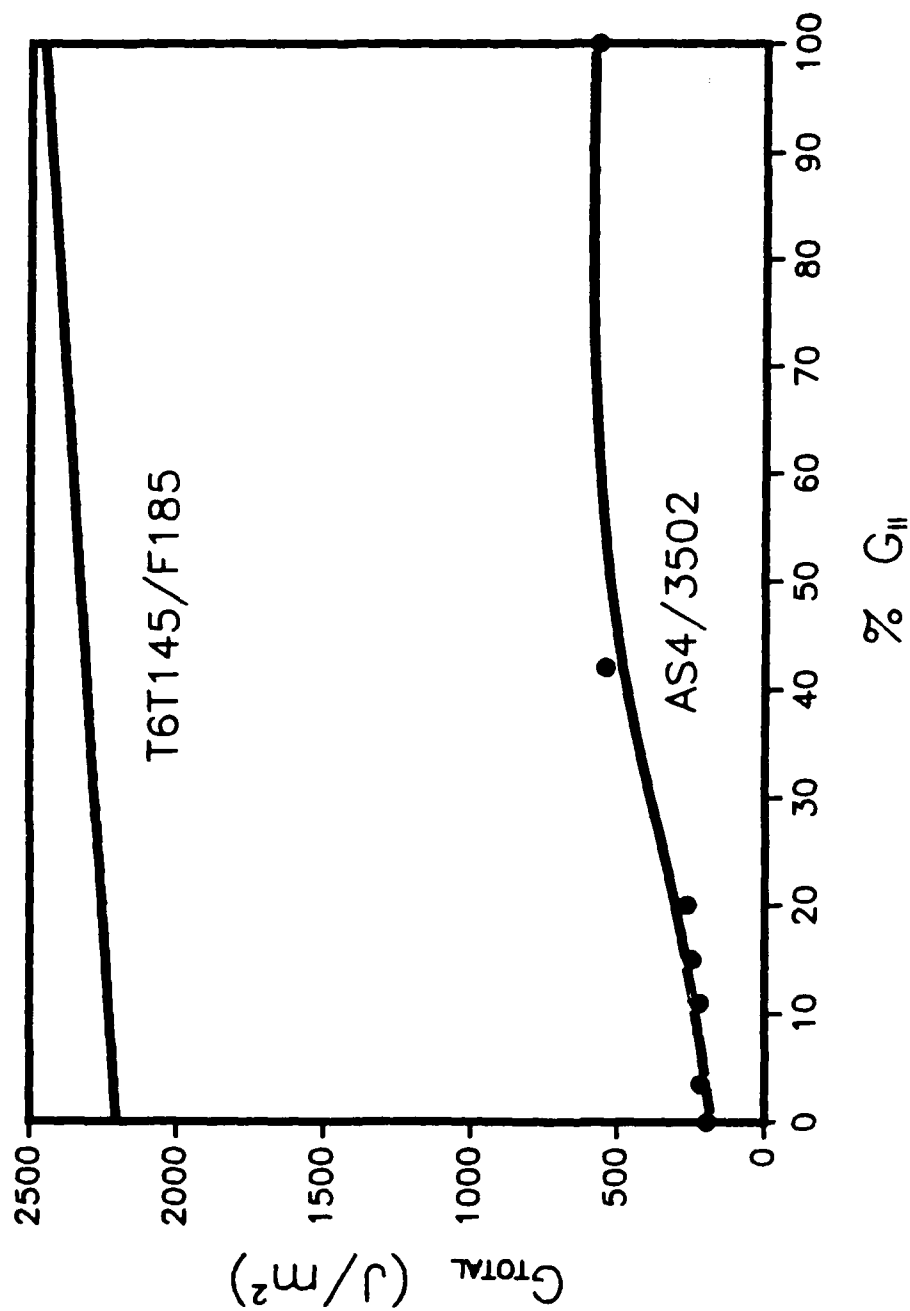


Figure 12. Total G vs. % mode II showing increase in brittle systems (AS4/3501-6) and little change in ductile systems (T6T145/F185).

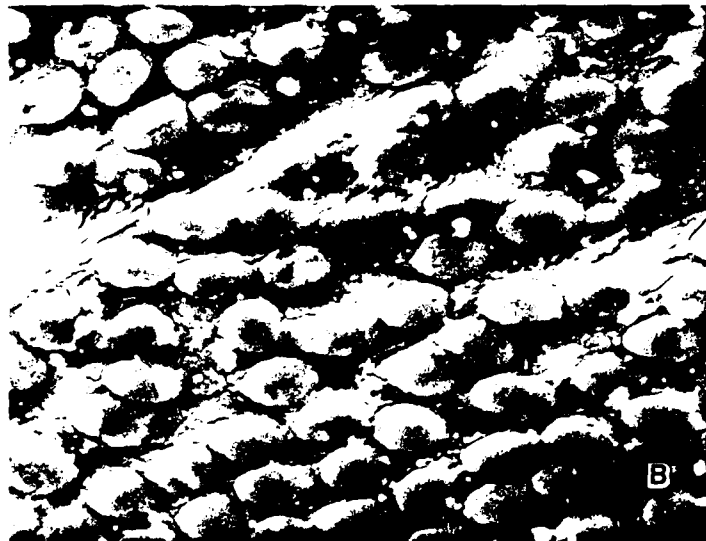
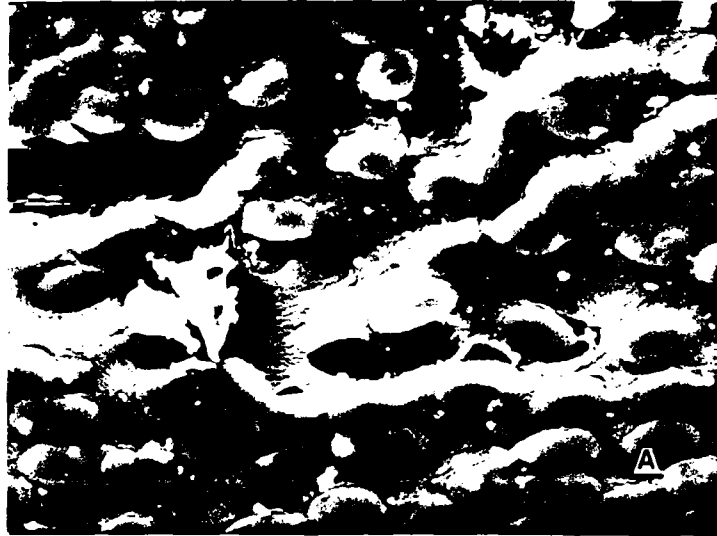


Figure 13. Multi-axial layup delamination of F155 composite system. (a) 1000x.
(b) 1000x.

deformation of a specimen. The technique involves photographing the crack tip region of the specimen both before loading and while loaded, and then using stereo-imaging to determine the displacement field. The in-plane strains are then calculated by differentiating this displacement field. The advantage of this technique is that high-resolution strain field maps can be obtained for any level of loading, including loading that produces nonlinear deformation around the crack tip.

Previously this experimental approach has only been utilized to determine the strain field around the crack tip of metals subjected to fatigue stressing³⁻⁵. In this study, similar stereo-imaging techniques have been developed to examine the strain fields associated with delamination in graphite/epoxy composites. Stereo-photograph pairs (one of the loaded specimen, a second of the unloaded specimen) of a delamination crack tip for both mode I and mode II loading conditions are made in a scanning electron microscope (SEM). From the displacement and strain field maps generated, the effects of macroscopic loading as well as the role of fiber constraint on the deformation and resin yielding in the region of the crack tip were examined. All data reduction routines used in the strain field analysis were performed on an Apple Computer.

4.2.1.1 Stereo-Imaging

We perceive three dimensions, or depth of field,

because our eyes view our surroundings from slightly different angles. The apparent position of foreground objectives relative to the distant background seen from one eye is slightly displaced from that seen through the other eye. As the brain melds these two images into one, it takes note of the relative displacements of the foreground objects and interprets it as depth.

In determining the in-plane delamination displacements, an area well ahead of the crack tip in an unloaded specimen is photographed, ensuring an unloaded reference condition. The specimen is then loaded and the crack allowed to grow into the field of view, which is subsequently rephotographed. In the second case, due to the loading, localized deformation in the crack tip region will appear as displacements relative to the surrounding unstrained regions, as captured in the photograph of the specimen prior to loading. When the two photographs are observed in a stereoscope, these relative surface displacements are perceived as relief in the out of plane or Z-direction. It is noted that a state of triaxial displacement may exist at the loaded crack tip, but only the in-plane displacement can be observed using this technique.

4.2.1.2 Experimental and Analytical Procedures

The graphite-epoxy systems examined in this study were Hercules AS4/3501-6 and AS4/DOW P-7. These resin systems were selected because of their differences in ductility and

interfacial adhesion strengths. The Hercules AS4/3501-6 system consisted of a brittle resin ($G_{IC} = 70 \text{ J/m}^2$) along with unsized fibers, resulting in a composite delamination toughness of $G_{IC} = 140 \text{ J/m}^2$ and $G_{IIC} = 634 \text{ J/m}^2$. The AS4/Dow P7 system used sized fibers with a tougher Novolac resin, modified to increase both toughness and resin/fiber adhesion, resulting in a composite delamination toughnesses of $G_{IC} = 340 \text{ J/m}^2$ and $G_{IIC} = 862 \text{ J/m}^2$.

Small (25 mm x 11 cm), unidirectional double cantilever beam specimens, 14 plies in thickness, were cut from cured laminate panels of the two systems. A thin 0.03 mm teflon sheet inserted at one edge during the layup of the laminate panels before curing provided a starter crack between the mid-plyes. Delamination loading of the specimens within the SEM was accomplished by using a tensile stage. Mode I loading was achieved by driving the precracked portion of the specimen onto a fixed wedge (see Fig. 14). The wedge was sufficiently blunt to ensure that it remained well behind the crack tip. A three point bend fixture was used to provide pure shear or mode II loading at the crack tip (see Fig. 14).

For neat resin testing, compact tension specimens of size 1T were used as per ASTM E399¹, except that the thickness was 3-4 mm instead of the 12.5 mm prescribed by the standard. The same loading fixtures were originally used for the in-situ fracture observations reported in section 4.1 of this report.

As described before, an area well ahead of the crack

tip was photographed, and then rephotographed after the crack was allowed to grow into the field of view, representing the unloaded and loaded conditions respectively. These photographs were then viewed with a TOPCON stereoscope. A 1/4-inch reference grid is marked on one photograph to enable the location on the specimen to be identified. A parallax bar is then used to measure the apparent height (Z_x) of the surface at each of the points of the reference grid. A reference point far ahead of the crack tip outside of the deformation zone is selected to provide a reference point (RP) of zero displacement (see Fig. 2). Displacement (D_x) is calculated at each point on the reference grid using a standard stereo imaging analysis by the following relationship⁵:

$$D_x = (1/M) (dP)/(P+dP) \quad (1)$$

where M is the photographic magnification, dP is the difference in the parallax bar measurement at a given point on the reference grid minus the parallax bar measurement at the reference point (Z_x -RP), and P is the average separation between the conjugate center and conjugate principal points for the two pictures used in the stereo pair. A more complete discussion by Avery⁶ of this technique is available.

Since only displacements along the eye axis can be observed in the stereoscope, the photographs must be rotated 90 degrees and the procedure repeated to obtain the Y-direction displacements (D_y). Additional details may be found in a soon to be published dissertation by Hibbs.

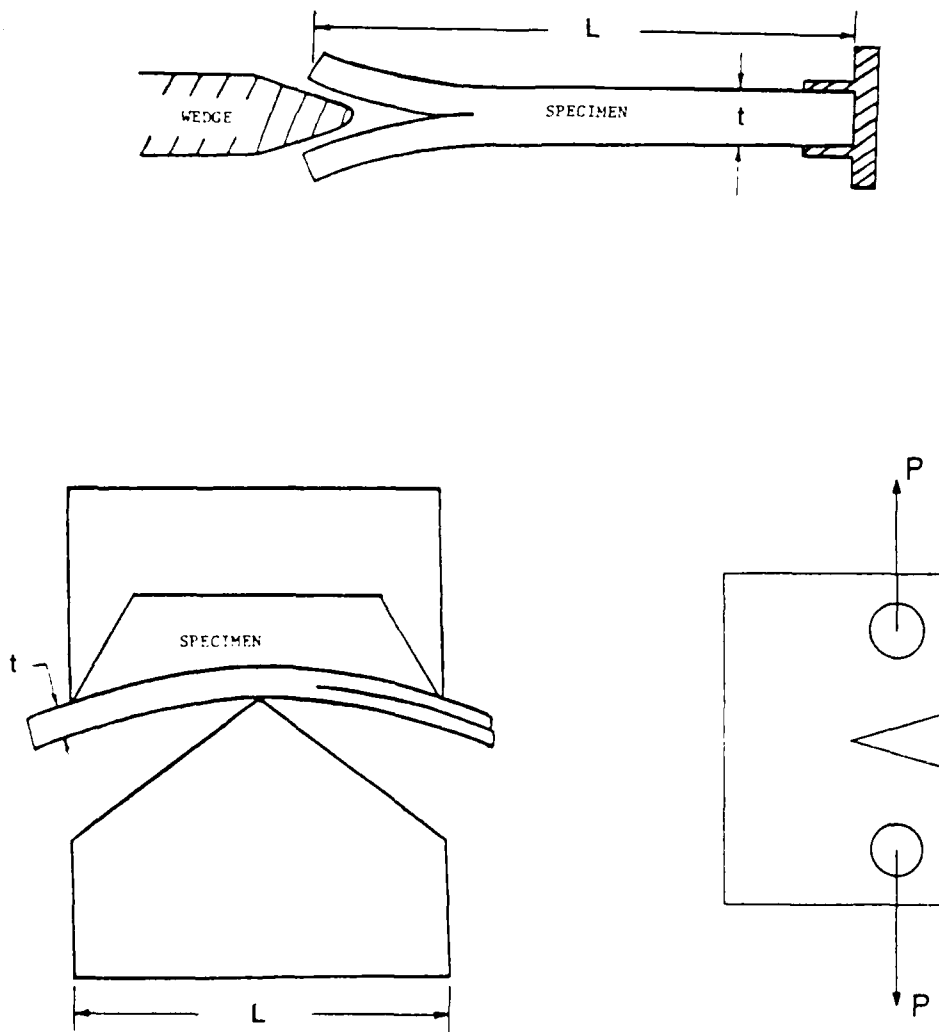


Figure 14 (a) Schematic of mode I delamination of scanning electron of microscopy specimens. (b) Schematic of mode II delamination of scanning electron microscopy specimens. (c) Schematic of mode I fracture of scanning electron microscopy CT specimens.

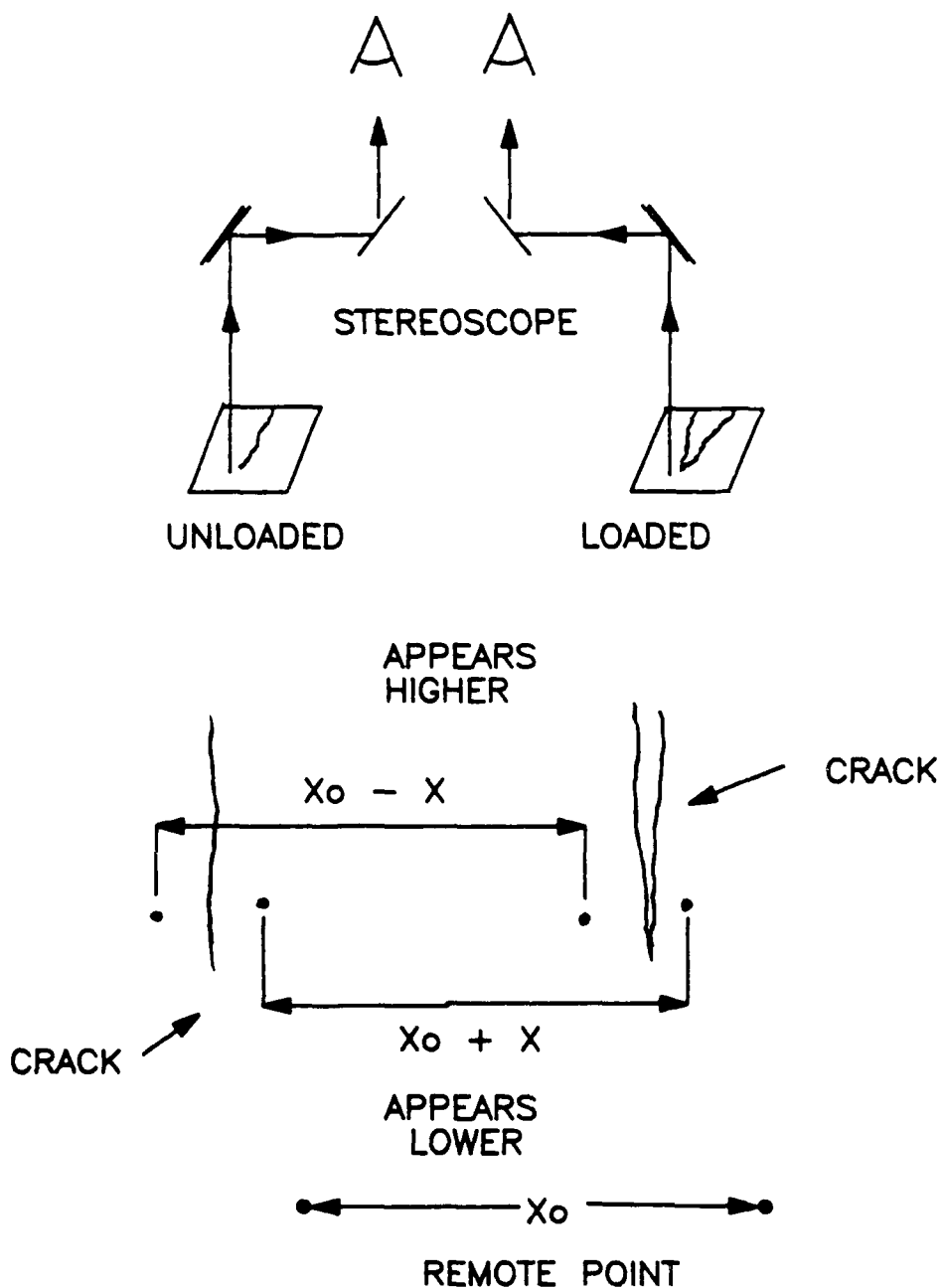


Figure 14d. Relative displacement of points near the crack tip resulting from the loading of the specimen. When view with a stereoscope these relative displacements are seen as vertical relief. The point x_0 is selected far ahead of the deformation zone and is used as a reference point of zero displacement.

4.2.1.3 Experimental Results

Results for mode I loading of the AS4/Dow P7 system and mode II loading of the AS4/3501-6 system will be presented in this report with more extensive results to be presented in Michael Hibbs' dissertation.

Mode I Displacement and Strain Fields--The unloaded/loaded stereo pair for the AS4/Dow P7 composite system loaded in mode I conditions is given in Fig. 15. To show the displacement field more clearly, the displacement vectors as determined from the photographs in Fig. 15 using the TOPCON stereoscope are represented graphically in Fig. 16. The displacement field is not symmetric about the crack tip. This probably results from asymmetric constraints due to the asymmetric distribution of fibers on either side of the plane of the crack. The maximum displacements are seen to be approximately 0.25 microns. At the crack tip the loading is shown to be essentially pure mode I.

The resulting strain field seen in Fig. 17 shows that the maximum shear strain is for the most part confined to the resin rich area between the fibers, with a maximum of about 20% strain at the crack tip. A more ductile resin would be expected to have deformation outside the resin rich region between plies. With increasing distance ahead of the crack tip, the magnitude of the strain decreases, reaching a value of 7% strain at a distance of 33 microns. It is interesting to note that the tensile elongation measured for this

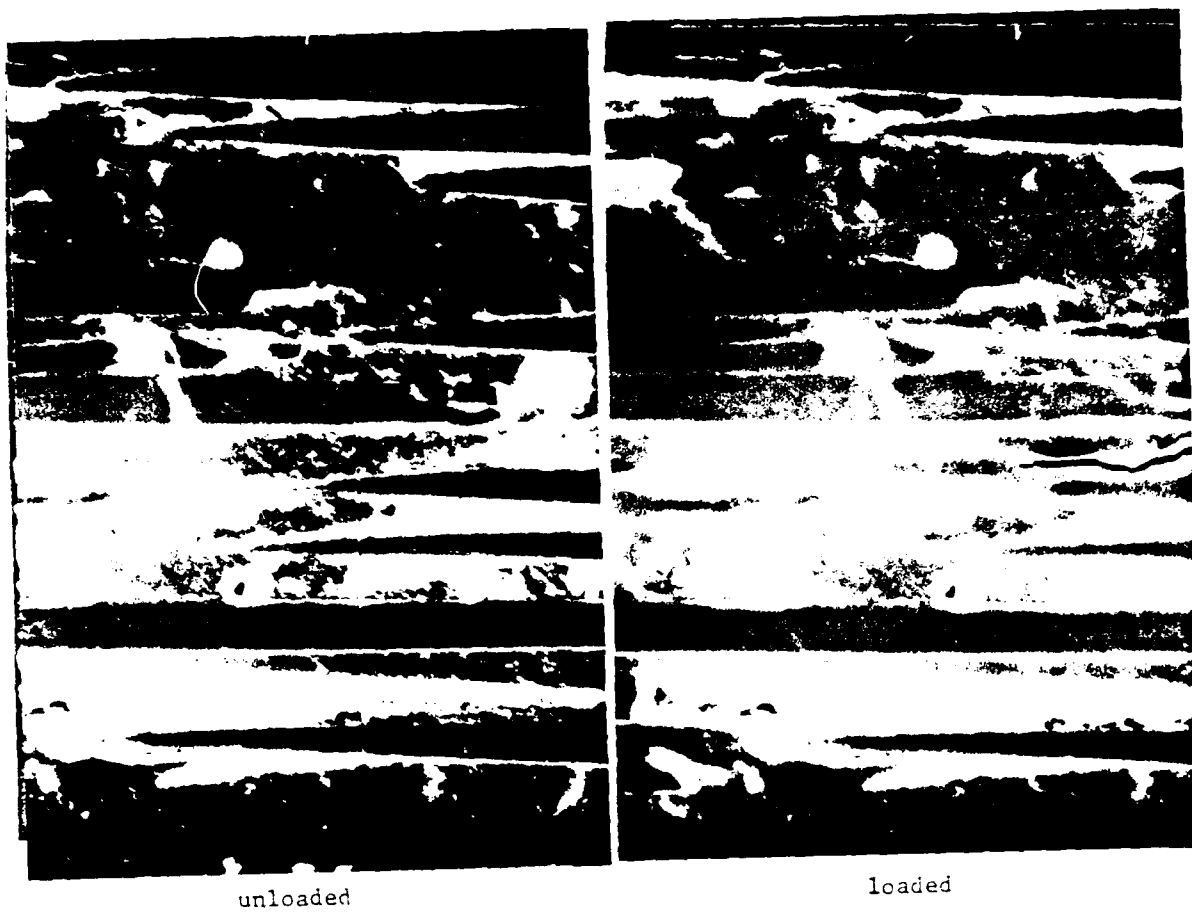


Figure 15. The unloaded/loaded stereo photographs of the composite AS4/Dow P7 loaded in mode I conditions. (1000X)

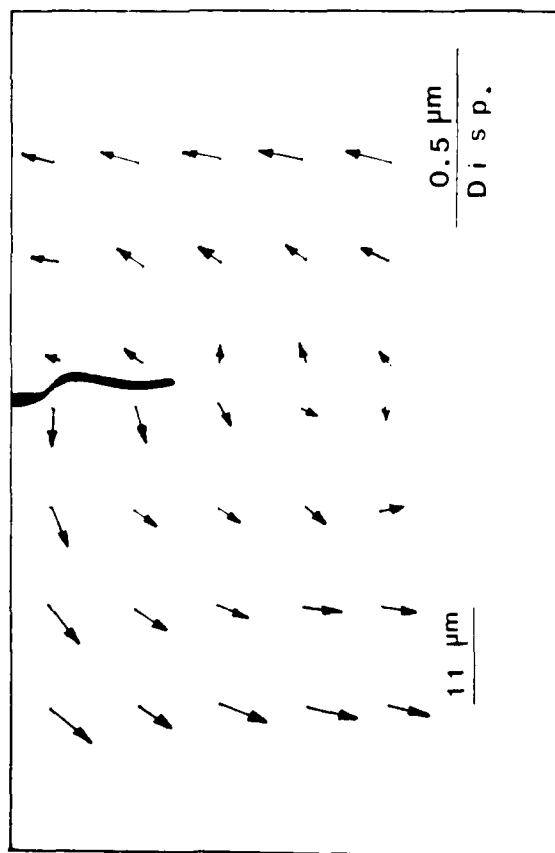


Figure 16. An expanded view of the mode I loading displacement field of AS4/Dow P7. The displacements are not symmetric in the region of the crack, but at the crack tip mode I loading is seen to exist.

relatively brittle resin is less than 2%. We should hasten to add that the indicated crack tip shear strain of 20% is not true resin strain because of the fine microcracking that develops in the crack tip region. The true resin strain would be less. Nevertheless, displacements due to resin deformation and microcracking combine to give deformation shear equivalent to 20% strain.

The displacement field that results for mode II loading of AS4/3501-6 is given in Fig. 18, where a symmetric displacement field with essentially pure mode II loading at the crack tip is seen. In this field, the magnitude of the displacements are on the order of 0.75 microns.

The resulting strain field (Fig. 19), as in the case for the mode I loading of the Dow P7 system, is seen to be confined in the resin rich region between the fibers, again a result that would not be true for a composite made with a more ductile resin. A maximum shear strain of approximately 100% occurs at the crack tip, with a very slow reduction in magnitude with increasing distance ahead of the crack tip. At the edge of the observed field, 33.0 microns ahead of the crack tip, the magnitude of the shear strain was still 85%.

It is difficult to see how a composite with such a brittle resin as the AS4/3501-6 could have such a large local strain to failure until one recognizes that most of the measured displacements are (as was the case for mode I) due to extensive microcracking, hackle formation, and hackle rotation. These can be seen in Figs. 6, 9 and 10 in section

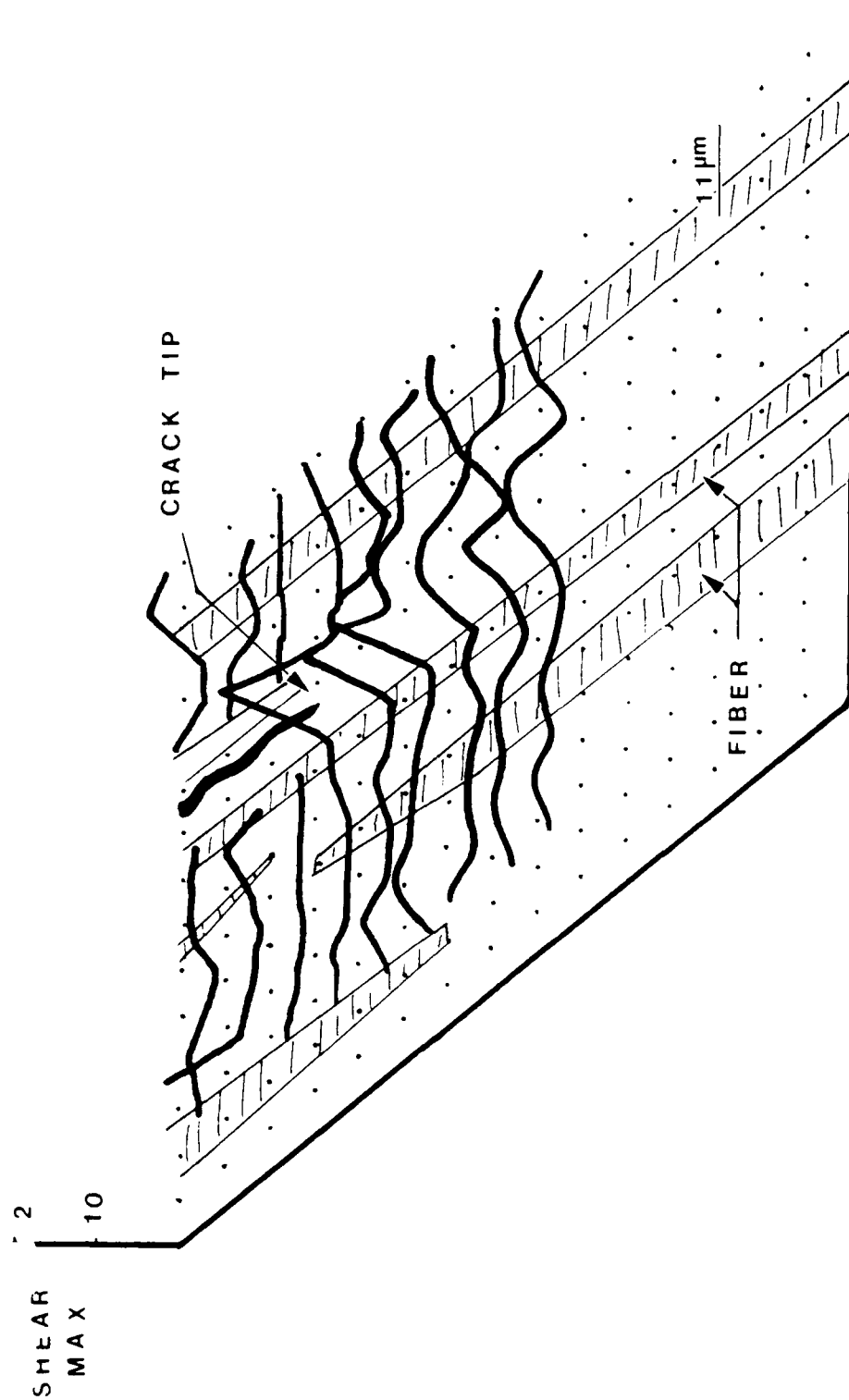


Figure 17. The three dimensional strain field map in the region of the mode I delamination crack tip for AS4/Dow P7. The strain is seen to be confined in the resin region between the fibers (shaded areas). The maximum strain occurs at the crack tip and decreases rapidly ahead of the crack tip.

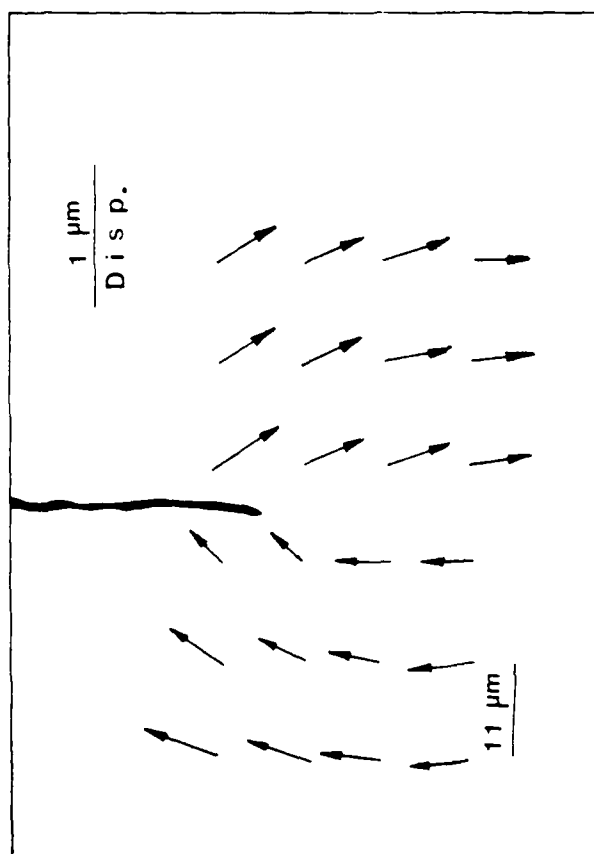


Figure 18. An expanded view of the mode II loading displacement field of AS₄/3501-6. The displacements in the region of the crack tip are seen to be nearly pure mode II shear.

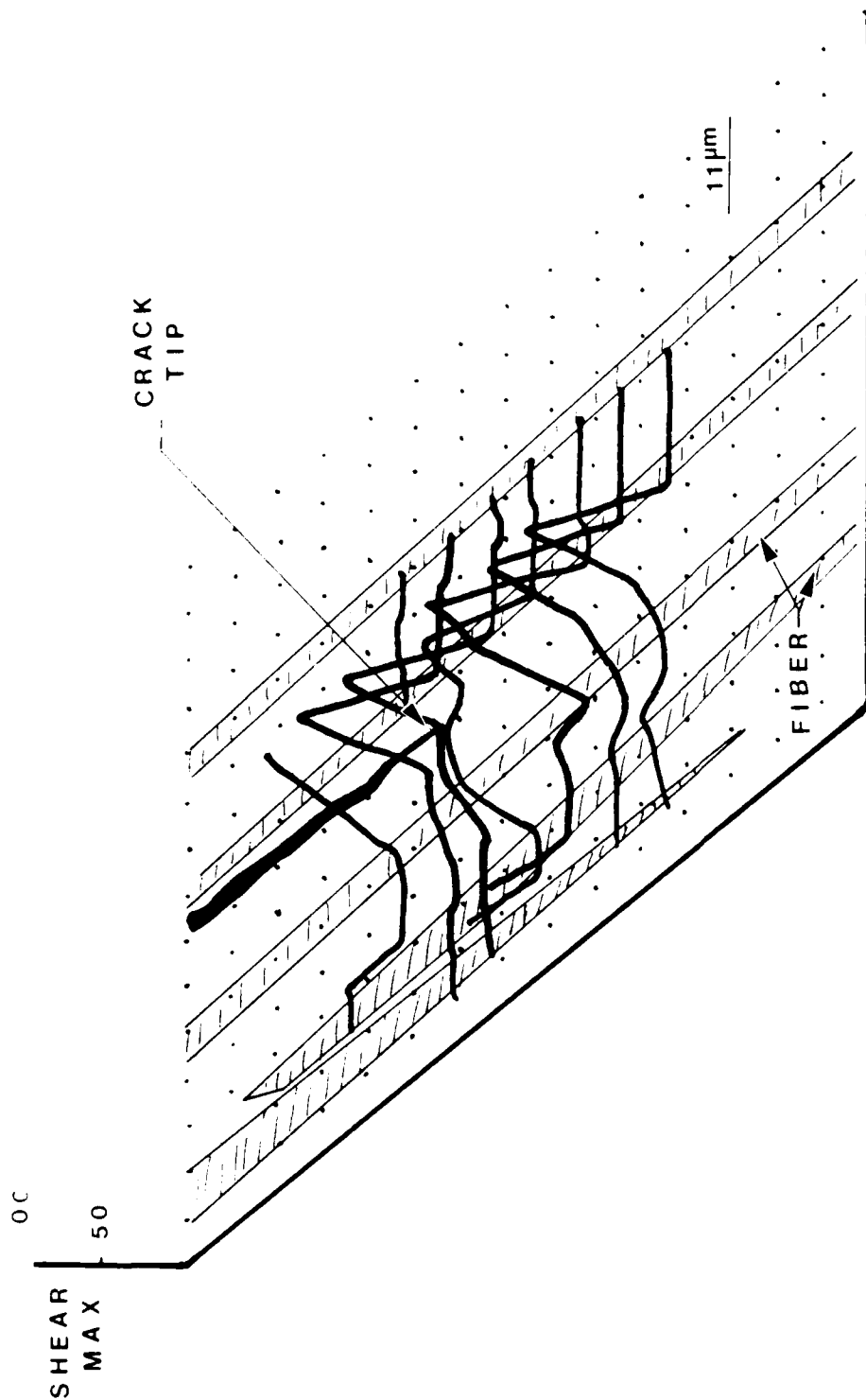


Figure 19. The three dimensional strain field map in the region of the mode II delamination crack tip for AS4/3501-6. The strain is seen to be confined in the resin region between the fibers (shaded areas). The maximum strain occurs at the crack tip and remains fairly constant in the remaining field of view ahead of the crack tip.

4.1.

These results for the strain field for mode I and mode II delamination are consistent with the observations of deformation/damage zone size previously reported in 4.1 and will be seen later in this report (section 4.3) to be qualitatively consistent with finite element calculations of the strain field decay ahead of a crack for these two loading conditions.

4.2.2 Direct Measurement of Strain Field Using a Dot Pattern

The purpose of this study has been to develop a technique which would permit the direct measurement of the strain field around a crack tip with sufficient resolution to make a comparison of the fields for cracks in neat resin versus delamination cracks in composites made from the same resin. The approach used has been to burn a very fine array of dots onto the polished surface (perpendicular to the plane of the crack) of a specimen using the electron beam in a scanning electron microscope. The exact coordinates for each of these points are determined before and after loading the specimen, allowing the determination of the displacement of each point. This displacement field may then be differentiated to give the strain field around the crack tip.

4.2.2.1 Experimental Procedure

With considerable trial and error, a technique has been developed to burn a very systematic dot pattern onto the

polished surface of the specimens. The beam of the electron microscope was adjusted to give dots that were sufficiently large to remain easily recognizable after considerable deformation but small enough to give adequate resolution and minimal damage to the specimen. The very regular dot pattern seen in Fig. 20 was burned onto the surface using a JEOL-35 scanning electron microscope with the assistance of an image processing system manufactured by Kontron. The dot spacing seen in Fig. 20 is approximately 10 microns. A finer dot spacing is possible, but not very useful unless the size of the dots can also be reduced, while retaining their visibility after large deformation.

The resin system selected for use in this study was Hexcel F185. This resin was selected because it is known to be relatively ductile (8% elongation in a tensile test), and therefore would be expected to give significant strain in the vicinity of the crack tip prior to failure.

Hexcel F185 resin was cast into rectangular plates. Compact tension specimens were machined from these plates and subsequently fatigue precracked. Then the CT specimens were polished on a microprocessor-controlled automatic polisher to a 0.03 micron finish. Finally, a dot pattern was burned on the surface using the electron beam in the SEM, as shown in Fig. 20. The crack tip is seen at the bottom of Fig. 20, just below the dot pattern. After loading to grow the crack a small amount into the dot array, the deformation field was determined using the distortion of the dot pattern. The

displacement field and the associated strain field were determined using the image processing system in conjunction with a computer program written to numerically differentiate the displacement field data.

4.2.2.2 Results and Discussion

The results are presented in Figs. 21-23. The normal strains as well as the principal shear strain are seen as a function of x-y coordinates. The crack tip has coordinates of $y=57.48$, $x=59.14$. The compact tension specimen was loaded in the x-direction with crack growth in the x-direction.

It should be emphasized that the three dimensional plotting routine used to present the results graphically does local smoothing prior to plotting. The polynomial curve fit for the smoothing operation interpolates as well, giving a much finer grid in the graphical results than was actually used on the specimen surface. (Contrast actual grid size, Fig. 20, to grid size seen in the three dimensional plots, Figs. 21-23.)

The strain at yielding in F185 as measured in a tensile test is about 1.2%. Thus, the region of nonlinear deformation around the crack tip is seen to be quite extensive. If it is remembered that carbon fibers typically have diameters of about 7 microns, then the nonlinear deformation zone would extend to at least five fiber diameters above and below the plane of delamination if the composite has a similar strain field around the tip of a

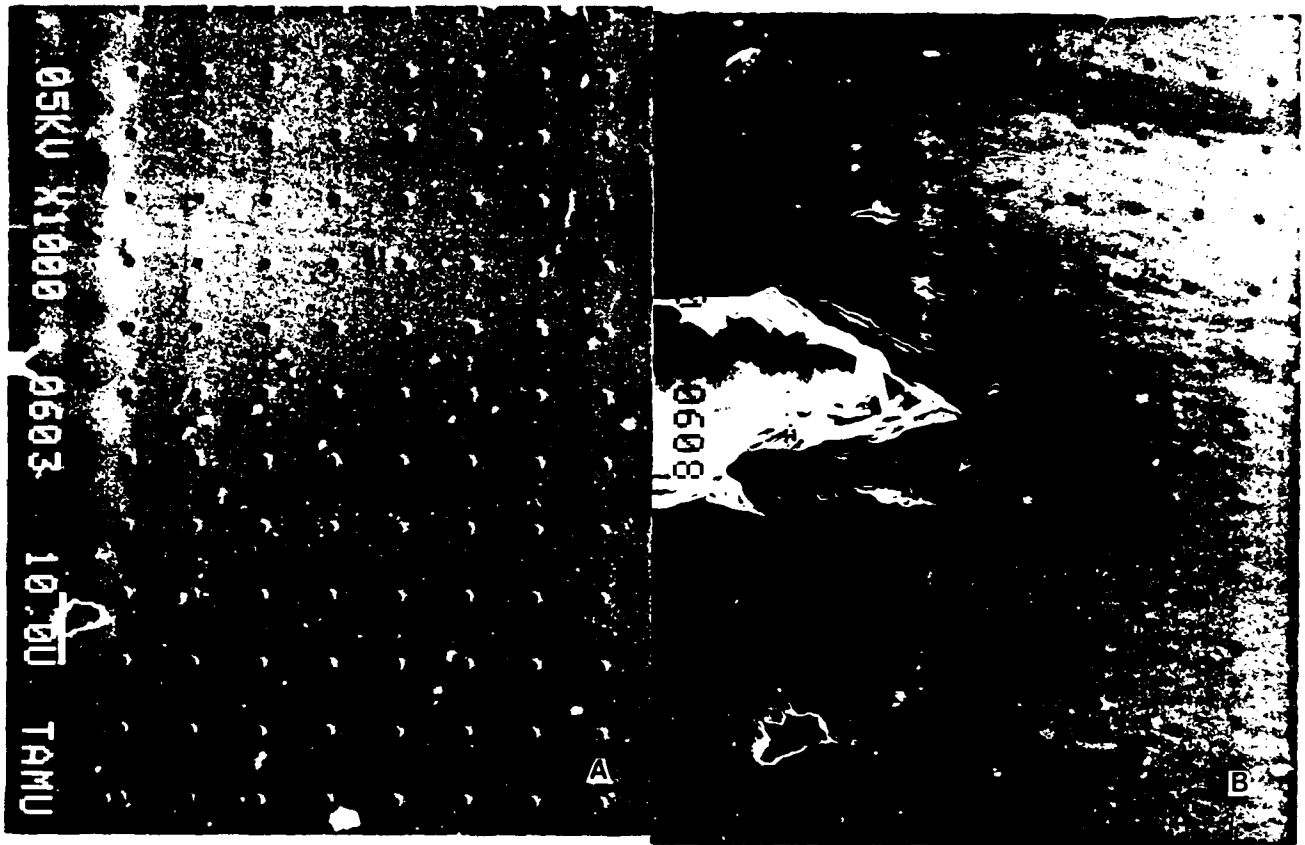


Figure 20. Dot spacing (a) before and (b) after loading (mode I loading) of F185 epoxy resin.

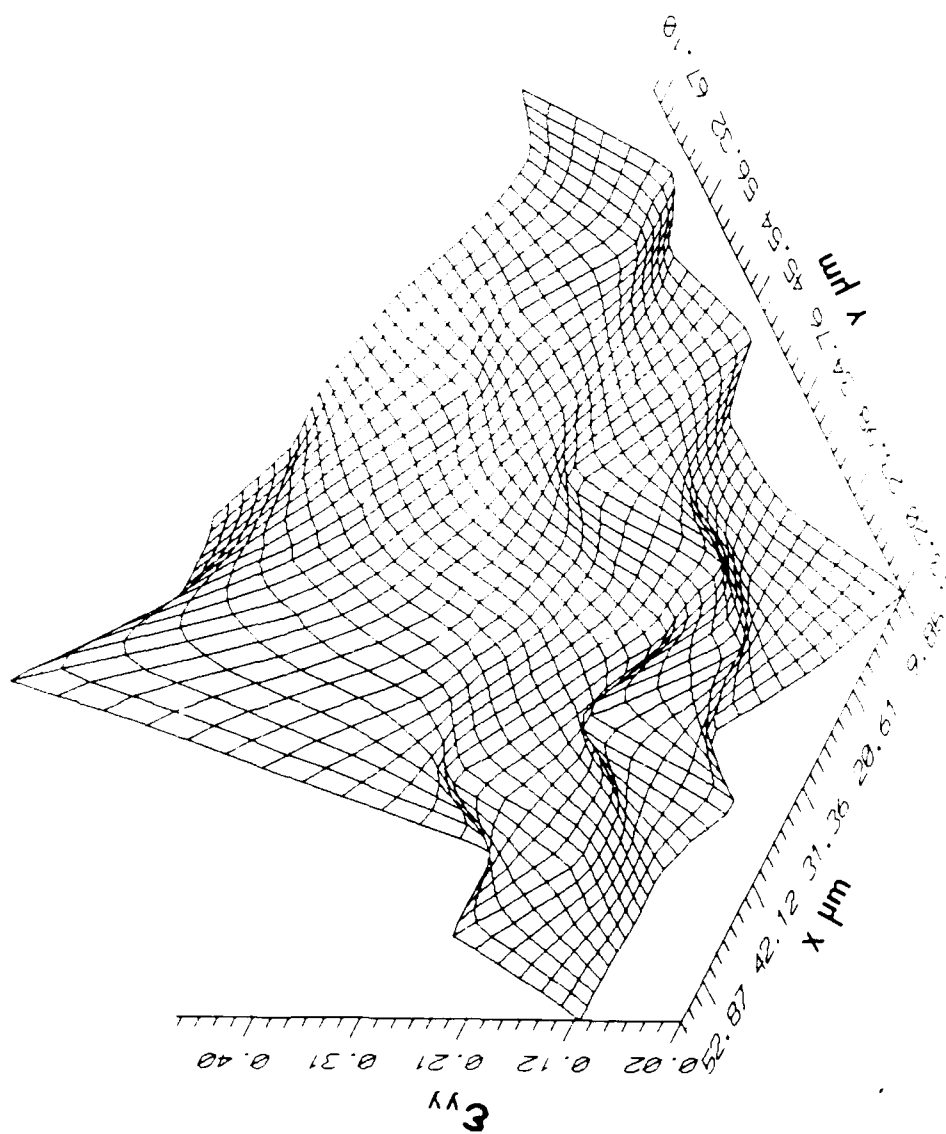


Figure 21. Mode I strain ϵ_{yy} ahead of crack tip of F185 epoxy resin.

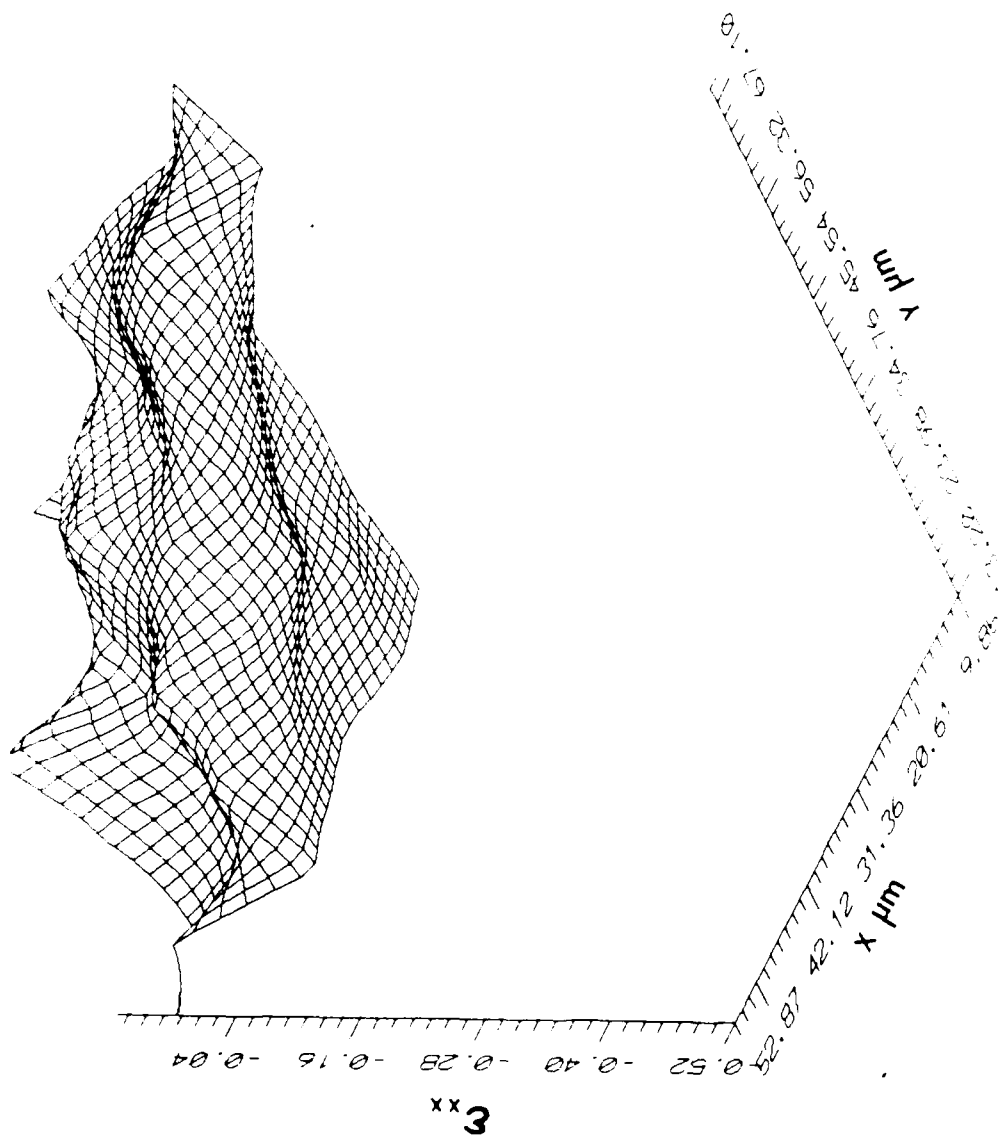


Figure 22. Mode I strain ϵ_{xx} ahead of crack tip of F185 epoxy resin.

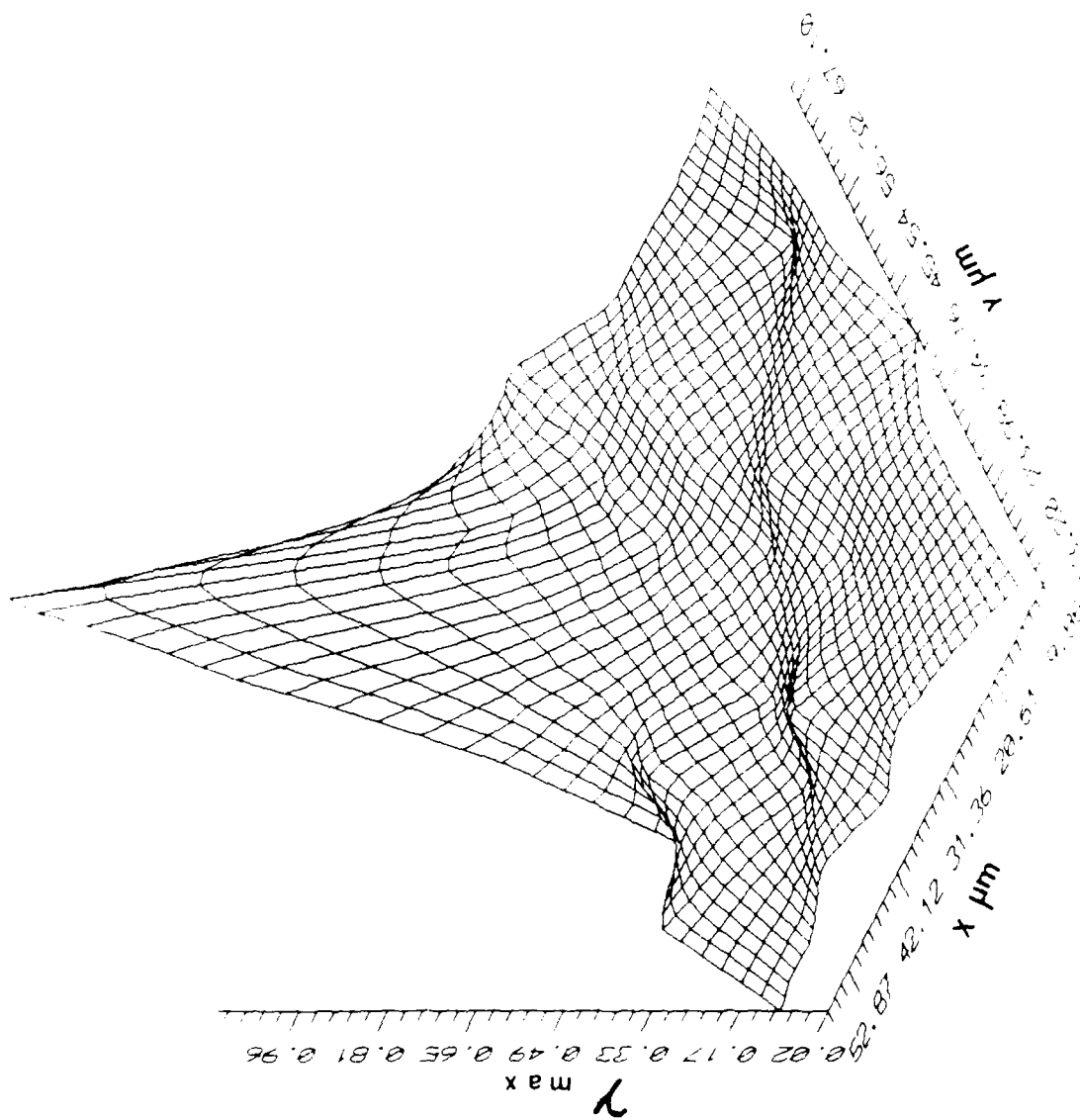


Figure 23. Mode I strain γ_{\max} ahead of crack tip of F185 epoxy resin.

growing delamination crack to that observed in Figs. 21-23 for the F185 neat resin. A qualitative indication of a deformation zone of this size in a delaminating T6T145/F185 composite, is seen in Fig. 7 (section 4.1) and has previously been noted by Bradley and Cohen².

A second important observation concerns the magnitude of the local strain at the crack tip. The elongation measured in a tensile test of F185 is 8%, with no apparent necking. Thus, one might have assumed for micromechanics modelling that the local strain to failure would be 8%, or possibly less due to the effects of constraint. However, it is clear that the tensile elongation greatly underestimates the true local strain to failure at the tip of a growing crack in F185. The measured value of 48% should be considered a lower bound since it is measured over a 10 micron gage length at the crack tip in a very steep strain gradient and would increase to an even higher value as crack advance caused ductile fracture. The critical value for local strain to failure for delamination crack growth is probably somewhat lower than the value for crack growth in the neat resin measured here due to debonding and constraint produced by the fibers. Comparable results for crack growth in a delaminating T6145/F185 composite were not available at the time of the preparation of this report but should be available soon in the new grant period.

One concern that should be mentioned is the question of whether the surface strain measurements are in any way

representative of the bulk strain distribution. In materials where cavitation or microcracking does not occur, one would expect a significant difference between the strain distribution for the plane-stress state of stress that exists at the surface and the strain distribution that would exist for the more nearly plane-strain state of stress in the bulk. However, F185 with rubber particle toughening does cavitate, relaxing the through-thickness stress. Thus, for this system we believe the surface strain distribution is representative of the bulk strain distribution.

Direct comparison of results from stereo-imaging with results based on dot pattern distortion will also be available soon under the new contract.

4.3 Analysis and Modeling

Analysis and modeling have been used in two ways to better understand the experimental results of sections 4.1, 4.2, and 4.4. First, the very different size and shape of the damage zone for mode I loading compared to mode II loading has been studied using a finite element analysis in which the constitutive relationship for a linear, orthotropic continuum is assumed. While ignoring the details that would be treated explicitly in a micromechanics model, this approach has been quite successful in accounting for the major distinctives between mode I and mode II delamination. Second, a simple model has been proposed to account for the observed differences in neat resin toughness compared to mode

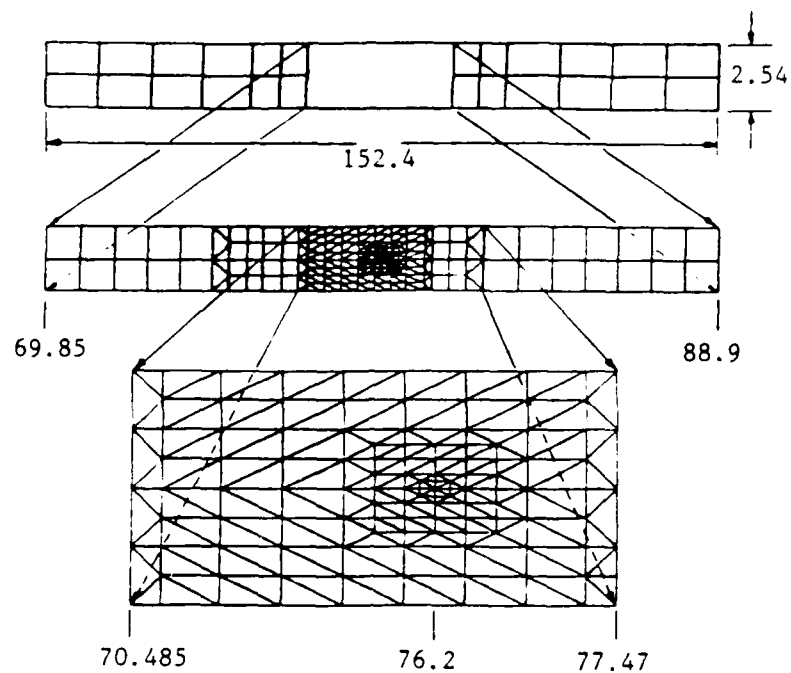
I delamination toughness for composites made with ductile resins. The results of these two areas of investigation will be presented in this section.

4.3.1 Linear, Orthotropic Finite Element Analysis of Mode I and Mode II Delamination

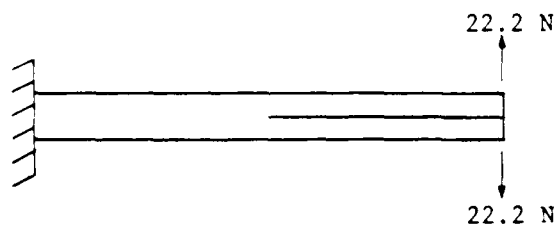
In this investigation, the stress fields ahead of the crack tip of a split laminate specimen loaded to give mode I delamination and mode II delamination have been determined by means of a finite element analysis. The results are compared to the observed damage zones developed ahead of the crack tip for the same loading conditions, as reported in section 4.1. A comparison with the direct strain field measurements of section 4.2 is made.

4.3.1.1 Materials and Methods

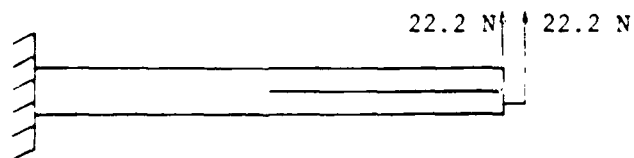
The determination of the stress field ahead of the crack tip of the split laminate specimen loaded under mode I and mode II was accomplished by first generating a two dimensional mesh 152.4 mm long by 2.54 mm thick consisting of 791 nodes and 294 elements as shown in Fig. 24a. Triangular six-noded elements were used around the crack tip with mid-side nodes displaced to the quarter point⁷, and a substantial refinement of the mesh around the crack tip was made to overcome the difficulty imposed by the stress singularity present at the crack tip. This linear orthotropic analysis has been made with a finite element



(a) Finite element mesh consisting of 791 nodes and 264 elements.
(Dimensions in millimeters)



(b) Mode I boundary conditions.



(c) Mode II boundary conditions.

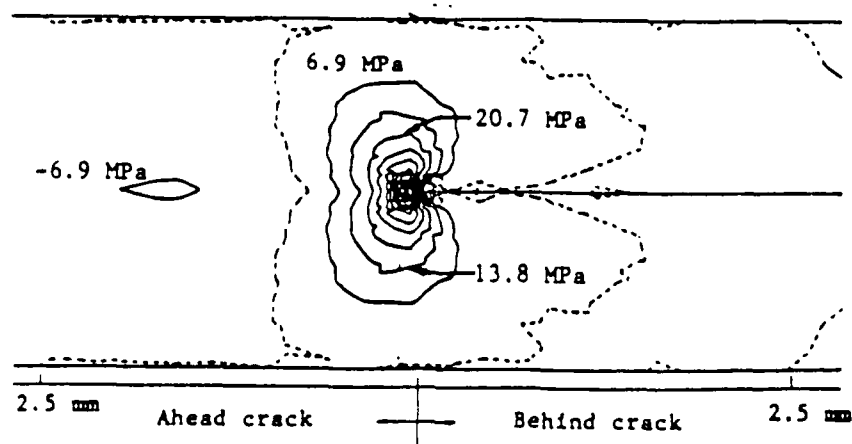
Figure 24. Finite element mesh and boundary conditions.

algorithm developed by Henriksen⁸. The algorithm is based on a nonlinear code updated with Lagrangian formulation using six and/or eight noded isoparametric elements with two degrees of freedom per node. Elastic constants for a unidirectional laminate of AS4/3502 graphite/epoxy composite to be used in the analysis were obtained from Hercules⁹.

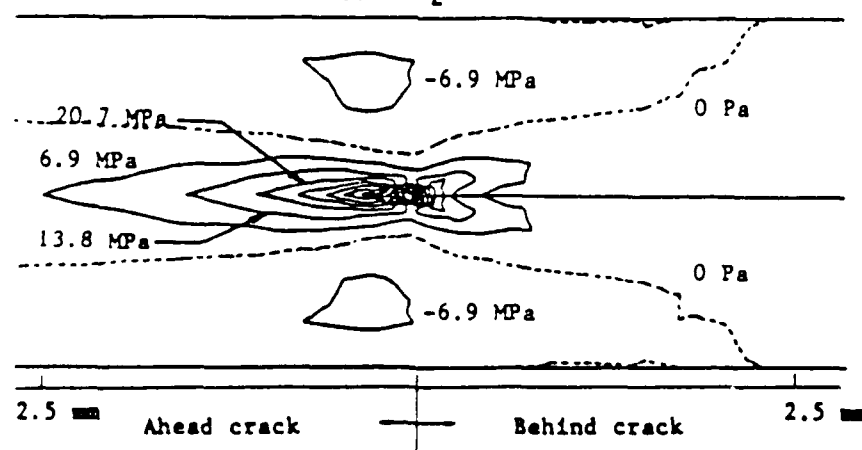
Mode I loading was simulated by applying a symmetric load at the cracked end of the mesh as shown in Fig. 24b. Mode II loading was introduced by asymmetrically loading the cracked end (see Fig. 24c). The load level applied corresponds to approximately the load at onset of crack growth for these two modes of failure, as determined from experimental measurements in combination with beam linear beam theory.¹⁰ Stresses were obtained and were plotted as a function of distance ahead of the crack tip.

4.3.1.2 Results and Discussion

Figures 25 and 26 show the finite element results for both mode I and mode II loading. Figure 25a is a S_{yy} (normal) stress contour plot from the vicinity of the crack tip for mode I loading. The normal stress S_{yy} which for this loading and geometry is the principal normal stress S_2 , rapidly decreases ahead of the crack tip. Figure 25b corresponds to the S_{xy} (shear) stress contour plot for a mode II condition. Note how the shear stress drops off much more slowly with distance ahead of the crack tip than does the normal stress for mode I loading (Fig. 25a). Furthermore,



(a) $S_{yy} = S_2$, mode I.



(b) $S_{xy} = S_1$, mode II.

Figure 25. Stress contour plots for mode I and mode II loading

the shape of the stress field is more narrow and elongated. For this loading condition, S_{xy} = maximum shear stress = S_1 . Figure 26 shows the stress distribution as a function of distance ahead of the crack tip for mode I and mode II. In the case of the normal stress for mode I, the stress drops off rapidly until it is compressive at a distance of 0.76 mm ahead of the crack tip. Finally, it gradually approaches a zero stress level at approximately 8 mm from the crack tip which is maintained all the way to the end of the beam. It should be noted that the compressive stresses observed for mode I loading are not expected to significantly influence the fracture mode at the crack tip because they occur far enough away from the crack tip. The mode I damage zones sizes presented in section 4.1 (see Table 1) were between .020 mm and .200 mm, well below the .76 mm indicated in the analysis as the distance ahead of the crack beyond which the stresses are compressive.

In the case of the shear stress distribution ahead of the crack tip for mode II, it monotonically decreases to a constant value. As can be seen, the shear stress ahead of the crack tip for mode II loading decays much more slowly than the normal stress for mode I loading. These results indicate that the stress concentration at the crack tip is distributed over a larger distance for mode II loading than for mode I loading. For mode II, the extent of the stress field above and below the center plane is much smaller than for mode I, as seen in the stress contour plots in Fig. 25.

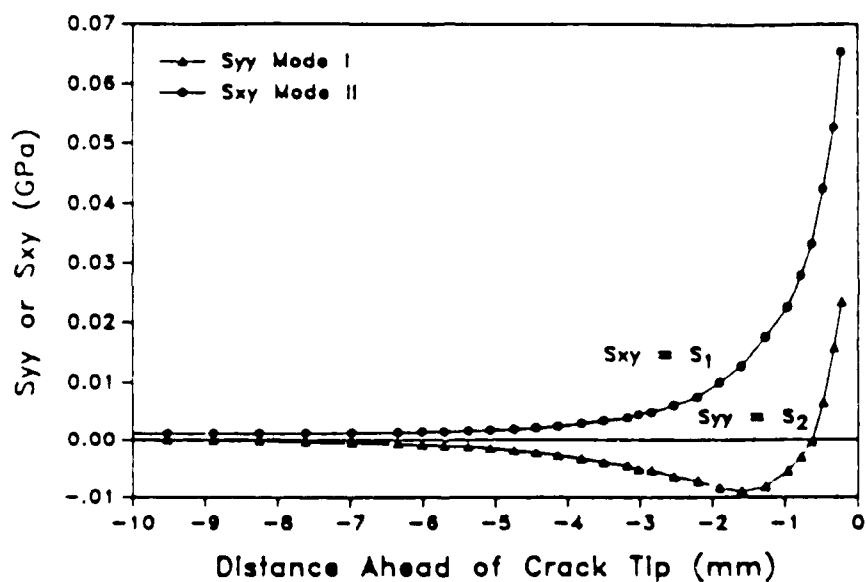
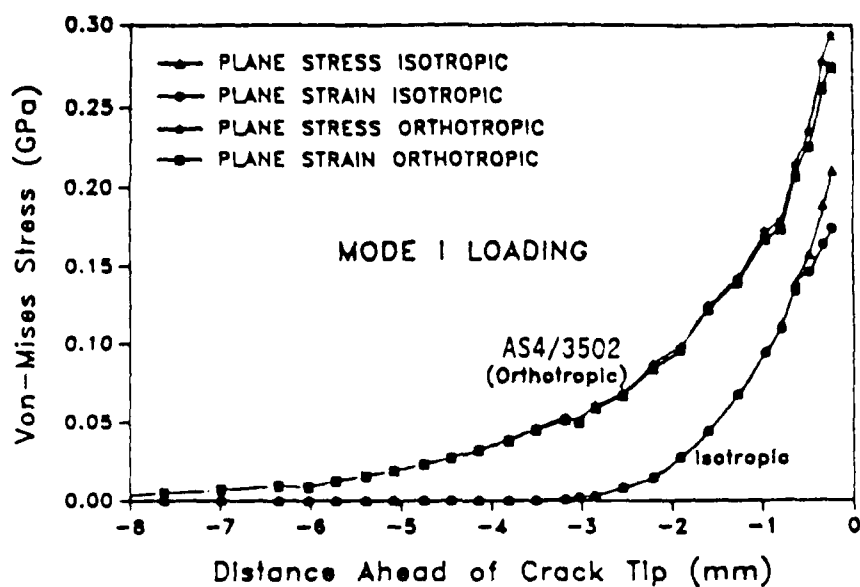
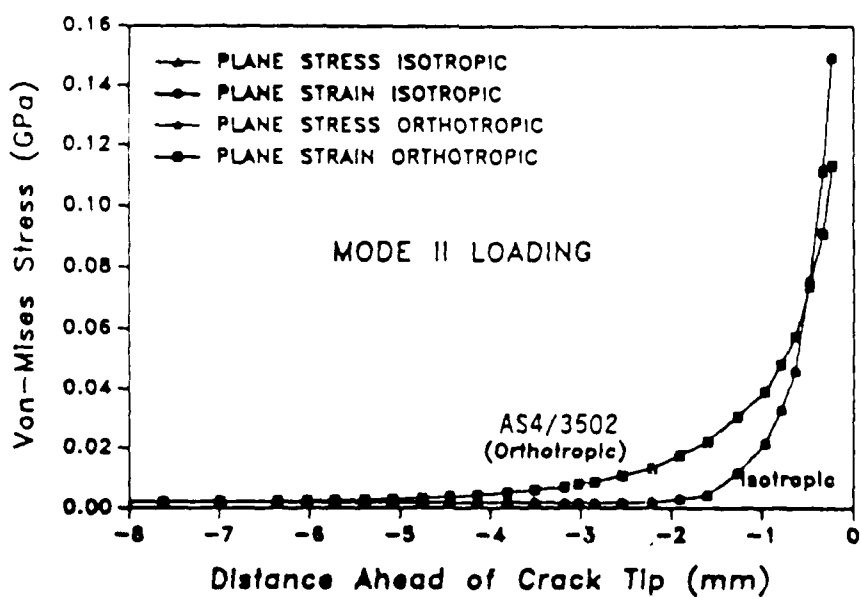


Figure 26

Stress distributions ahead of the crack tip for mode I and mode II loading. Note for mode I, the first principal normal stress, S_1 , is parallel to the fibers. However, S_2 ($=S_{yy}$) is the stress responsible for delamination crack growth, and thus, the one of primary interest. For mode II loading, the maximum shear stress is equal to S_1 .



(a)



(b)

Figure 27. Von-Mises stress distribution ahead of the crack tip for mode I and mode II loading.

A careful comparison of the stress fields of Figs. 25 and 26 with the damage zone shown in Figs. 6-8 for mode I and mode II delamination reveals a direct correspondence between them. The much longer and more narrow stress field predicted by the linear, orthotropic analysis is clearly reflected in the observed damage zones for mode I and mode II delamination. There is also quantitative agreement with measured strain fields, which also indicate a much more gradual decay of the strain field ahead of the crack tip for mode II loading than for mode I. It should be emphasized that quantitative agreement between the directly measured strain field and the calculated stress field would not be expected. The stress field calculations ignored both nonlinear behavior and microstructural details (fibers and resin) since they assumed linear, orthotropic behavior. Furthermore, there is no easy way to get from the measured strain to the associated stress, since the nonlinear constitutive relationship is unknown.

When dealing with damage zone development, the effect of the state of stress, namely plane stress versus plane strain, may be important. This is particularly true where the principle shear stress plays a role in the deformation of fracture process. The damage zones shown in Figs. 6 and 7 were obviously made at the edge of the specimen where a plane stress condition occurs. Therefore, in order to have a first order approximation as to the effect the difference in the state of stress at the surface of the specimen where our

direct observations are made, and at the center where plane strain conditions prevail, the Von-Mises stress for mode I and mode II were plotted as functions of distance ahead of the crack tip. The results in Fig. 27a indicate that for mode I, the difference in the Von-Mises stress (or root mean square shear stress) in plane stress versus plane strain is approximately 10%. In the case of mode II, the difference is negligible, as is evident in Fig. 27b. Therefore, it appears that for these orthotropic materials, the difference between plane stress and plane strain is not too significant and our surface observations of damage zone size and detail should not be very different than subsurface behavior. Previous studies in which the postmortem appearance of the fracture surface near a free edge to that at the center of a specimen are consistent with this interpretation¹¹. A final observation from Fig. 27 is that the stress field ahead of a crack tip decays much more slowly for an orthotropic material with the crack parallel to the fibers than for an isotropic material.

4.3.2 Modeling the Effect of Fibers on Mode I Delamination Toughness

A first order estimate of the delamination fracture toughness may be obtained by assuming that the delamination fracture process is essentially the same as the fracture process in the neat resin, except that the fibers act as a rigid filler, reducing the volume of resin available to

$$G_{lc} = \int_0^{\epsilon_{ij}^0} \int_{-h}^h \sigma_{ij} dy d\epsilon_{ij}$$

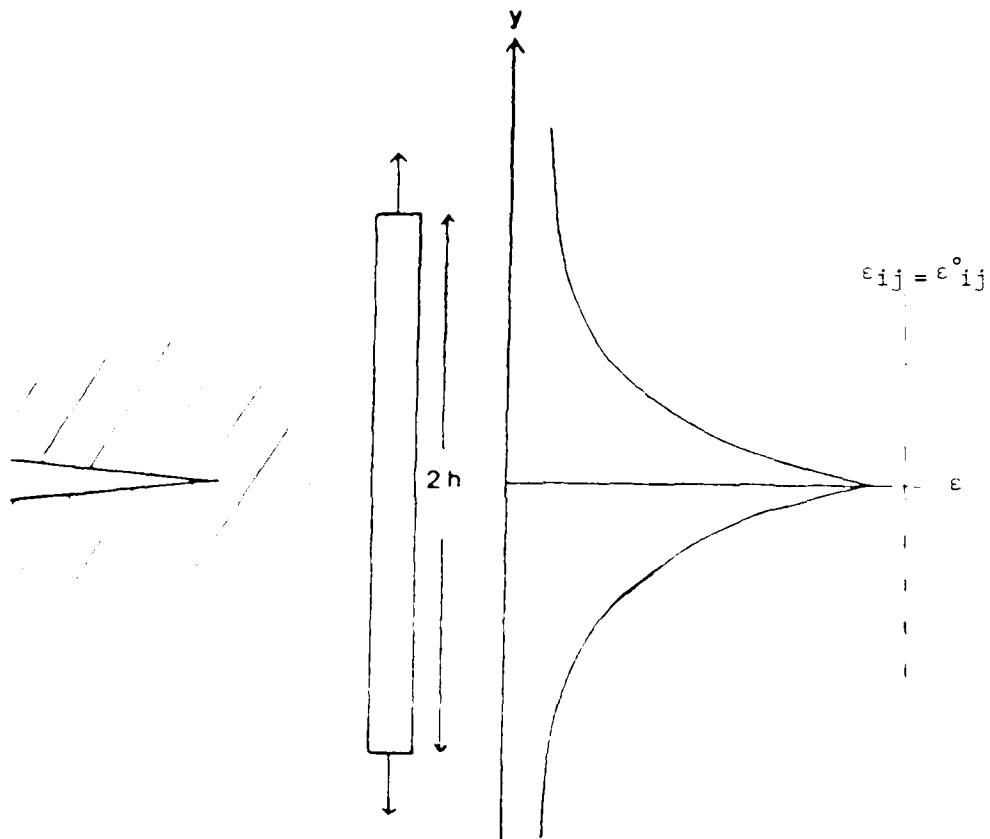


Figure 28. Schematic of hypothetical tensile bar ahead of the crack tip with the strain distribution across it.

deform in the crack tip region. It has previously been suggested by Bradley and Cohen² that the energy dissipation per unit area of crack extension may be calculated by picturing a small tensile specimen ahead of the crack tip, which is slowly stretched as the crack tip approaches and finally breaks as the crack tip passes (Fig. 28). The energy absorbed per unit area of crack extension would be calculated for such a model by summing the energy absorbed per unit volume of material over the volume of the hypothetical tensile specimen. Such a summation may be written mathematically as follows:

$$G_{IC} = \int \sigma_{11} d\epsilon_{11} dy \quad (1)$$

where G_{IC} is the fracture toughness of the material, $2h$ is the height of the hypothetical tensile bar, and σ_{11} is the component of the stress tensor normal to the plane of the crack. Until recently, neither the strain field nor the constitutive relationship required to calculate stress from strain was known. Thus, a direct evaluation of Eq. 1 was not possible. A phenomenological approach has been taken to try to evaluate this energy release rate for delamination.

The addition of fibers to the neat resin can perturb the energy calculation in Eq. 1 in several ways. First, the extent of the deformation zone might be changed due to the additional constraint imposed by the fibers, changing the value of h (i.e., the height of our hypothetical tensile

specimen) in Eq. 1. Second, rigid filler would further reduce the effective gage length of material capable of deforming in our hypothetical tensile specimen. Third, fiber debonding and/or constraint could change the local strain to fracture. These three factors could potentially account for the observed decrease in fracture toughness from 8100 J/m^2 in the F185 resin to 1900 J/m^2 in the composite delamination fracture toughness. The first two of these three factors can be quantified based on actual observations. If one assumes that coating microcracking begins for strains above the threshold strain; (say 3%), then the extent of the microcracked zone can be used to approximately quantify the magnitude of the h in Eq. 2.

A cross-section of the composite prepared metallographically to reveal the microstructure (Fig. 29) may be used to determine the volume fraction of fibers in the hypothetical tensile specimen ahead of the crack tip. Since the volume fraction is quite nonuniform, the microstructure can be divided into three regions: the resin rich region between plies with a fiber volume fraction of 19%; the ply region with a volume fraction of fibers of 76%, and a transition zone with a volume fraction of approximately 33%. The relative heights of these three regions are shown in the schematic in Fig. 30 along with the height of the microcracked zone in the F185 resin. Using a simple rule of mixtures approach, and taking account of the smaller microcracked (and deformed) zone, $2h$, one may estimate the

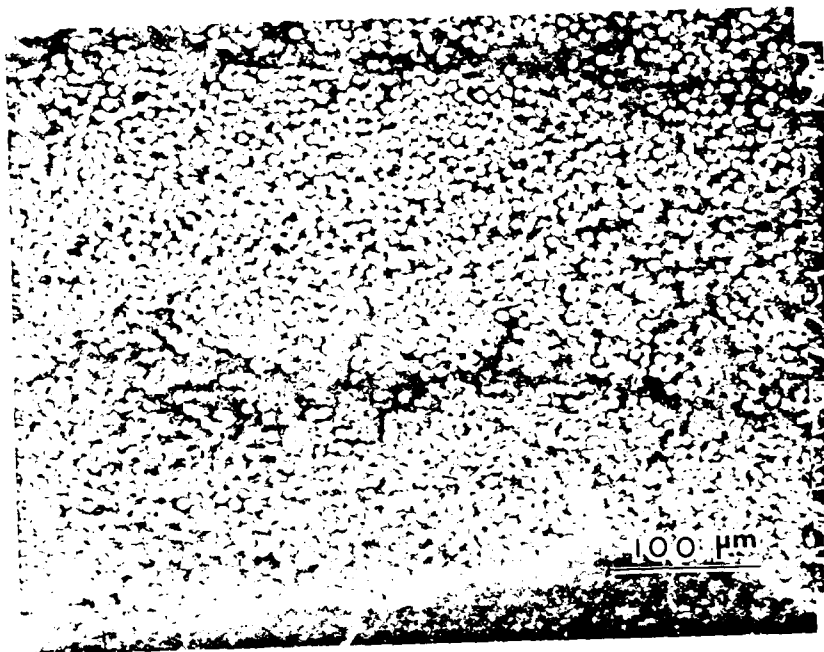


Figure 29. Cross section of T6T145-F185 showing interlaminar resin-rich regions.

delamination fracture toughness to be 4000 J/m^2 as shown below:

$$\begin{matrix} G_{IC} \\ \text{(composite} \\ \text{delamination)} \end{matrix} = \frac{G_{IC}}{h_o} [h_a(1-v_f^A) + h_b(1-v_f^B) + h_c(1-v_f^C)] \quad (2)$$

where G_{IC} refers to composite delamination and G_{IC} refers to the neat resin. This calculation implicitly assumes that the local strain to fracture in the F185 resin and the composite are the same and that the stress distribution is also similar, at least on average. It is recognized that these are crude assumptions at best.

The calculated value of Mode I delamination fracture toughness of 4000 J/m^2 is clearly much larger than the observed value of 1900 J/m^2 . This discrepancy is due to the assumptions in the calculation that the strain field distribution as well as the local strain to failure are similar. In reality, fracture at the fiber/resin and/or constraint due to the presence of the fibers should cause the strain to failure in the composite to be somewhat less than that in the neat resin. Furthermore, the decay of the strain field ahead of the crack tip is different for an orthotropic material than for an isotropic one (See Fig. 27).

Thus, the incorporation of the recent measurements of the strain field described in section 4.2 into this model should bring the predictions more in line with the observed delamination toughness. This is currently being done under

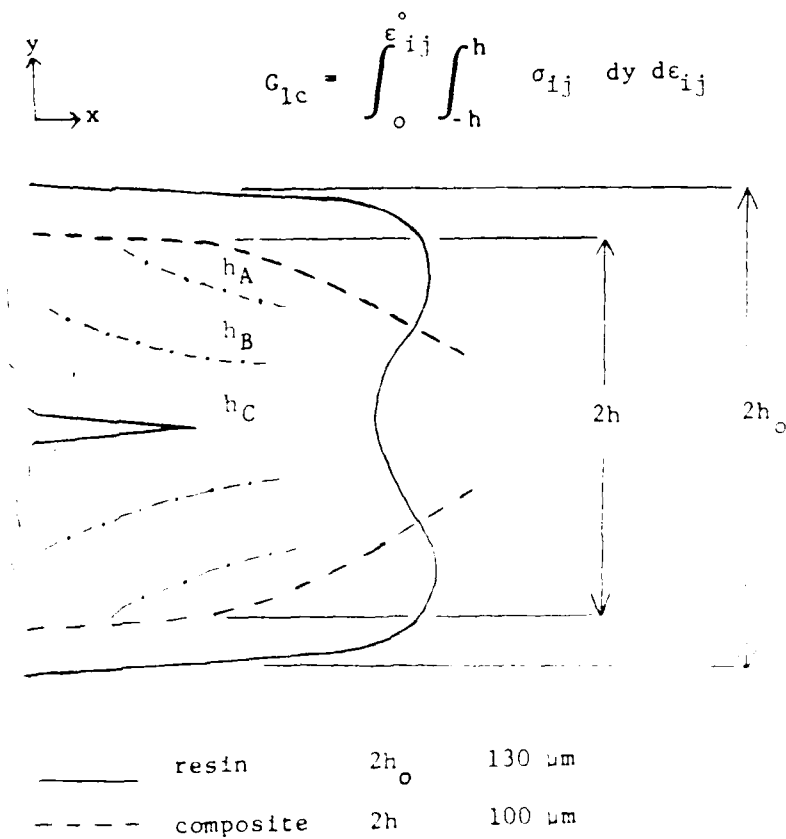


Figure 30. Schematic showing relative height of damage zone in F185 resin and T6T145/F185 composite.

the new contract. A constitutive relationship will have to be either determined or assumed before this approach can be fully implemented. With a constitutive relationship and the measured strain fields, it would be possible to evaluate directly Eq. 1 rather than using the more indirect, phenomenological approach expressed in Eq. 2.

4.4 FRACTURE MECHANICS CHARACTERIZATION OF MATERIALS

In this section our work to develop better test methods and analysis to determine the mode I and mode II delamination fracture toughness of composite materials will be described. The newer resin systems are significantly tougher than the first generation resins for which the current test methodology was developed. For these early systems which were quite brittle, linear load-displacement curves for split laminate testing is the norm and linear elastic analysis is adequate to extract meaningful fracture toughness parameters from the experimental data. As it has become necessary to characterize some of the newer, tough resins such as PEEK, both nonlinear and inelastic behavior are frequently observed in the load-displacement records, and thus, the usual linear beam theory is not adequate to obtain meaningful fracture mechanics parameters from these test results.

It has also been found that mode II testing with the generally much higher critical energy release rates observed for this mode of fracture is also much more likely than mode

I testing to exhibit nonlinear behavior. The delamination fracture toughness characterization of multi-axial laminates with the associated reduction in stiffness along the axis of the split laminate being tested has also been found to often give nonlinear behavior unless very thick specimens are utilized.

Our efforts in response to these challenges have been to develop a J-integral approach to delamination fracture characterization for both mode I and mode II loading. These two efforts will be described in the two subsections that follow. The presentation in these subsections will be somewhat more detailed than those in 4.1, 4.2 and 4.3 as most of the results have not yet been published.

4.4.1 Mode I Delamination

The subject of the work reported in this section is the means of determining the mode I delamination fracture toughness of multidirectional composites. Material characterization is a prerequisite for systematic design and analysis of composite structures. The intent is to develop and verify a theoretically-based method for characterizing delamination fracture despite the complicating factors which will be discussed.

4.4.1.1 Current Status of the Problem

Delamination of Unidirectional Composites--The delamination of unidirectional composites, though not

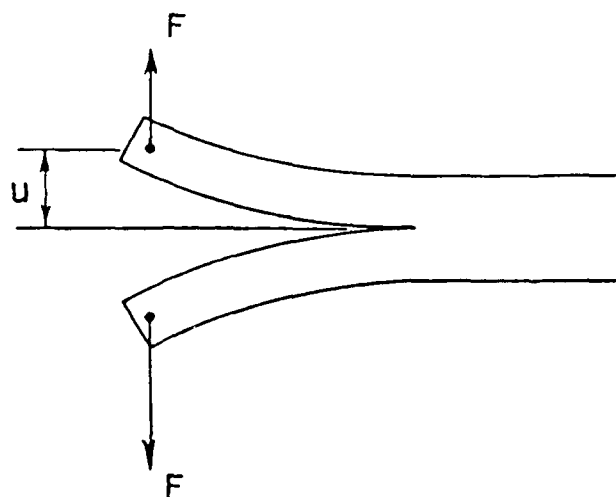


Figure 31 . Schematic of the double cantilevered beam (DCB) specimen for delamination studies

directly the subject of the present study, nevertheless forms the background for it. Therefore, this discussion of the current status of the problem begins with its review.

The great majority of studies of delamination toughness have involved unidirectional composites. A major motivation for this activity has been to understand the relationship between neat resin fracture toughness and composite interlaminar toughness¹². Several different specimen designs have been used by various investigators¹³⁻¹⁶. Of special interest because of its wide use and apparent utility is the double cantilevered beam (DCB) specimen, as shown in Fig. 31. Numerous investigators have studied it as applied to unidirectional composites¹⁶⁻¹⁸. The DCB specimen has also been applied to a planar isotropic short-fiber reinforced composite¹⁹. In these studies the necessary analyses have been developed and the procedure's viability has been demonstrated by experiment.

Several different ways of analyzing DCB data have been proposed. Various assumptions about material and specimen behavior are made in each method. Analyses based on linear beam theory, large displacement theory, empirical compliance calibration, the area under the load-displacement curve, and an energy rate interpretation of the J integral have been used^{16,17,20}. The effectiveness of a particular method depends on the situation at hand. For the case where there is permanent deformation due to material damage, Keary et al.²⁰ determined that the J integral is superior to

approaches based on linear beam theory and empirical compliance calibration. This observation is salient to this study since such damage has been observed in multidirectional composites.

A similar conclusion can be drawn from Fig. 32 which shows data generated in this program using DCB specimens. The delamination fracture toughness determined using the area method (G) and using a damage-dependent J integral (J) are plotted versus crack length. One G and one J curve were determined from each of three specimens. Not only does J appear to give results which are more consistent over the range of crack lengths, but it gives lower toughness values. The overestimation of fracture energy using the area method reflects that methods' unsuitability when damage is present away from the crack tip. The stacking sequence used results in damage in the legs of the specimens; the material was Hexcel's T2C145/F155 in a 24-ply plate with the stacking sequence $[-+45/(+45)_2/(-+45)_2/(+45)_2/(-+45)_2/+45]$.

4.4.1.2 Delamination of Multidirectional Composites

In actual structures, laminate layups are not generally unidirectional. Therefore data from unidirectional tests can only be used directly in structural design and analysis if it can be shown that the unidirectional data reflects the response of the more complex material. Recent studies show that this is not always the case. For example, Nicholls and Gallagher²¹ have observed in their DCB tests

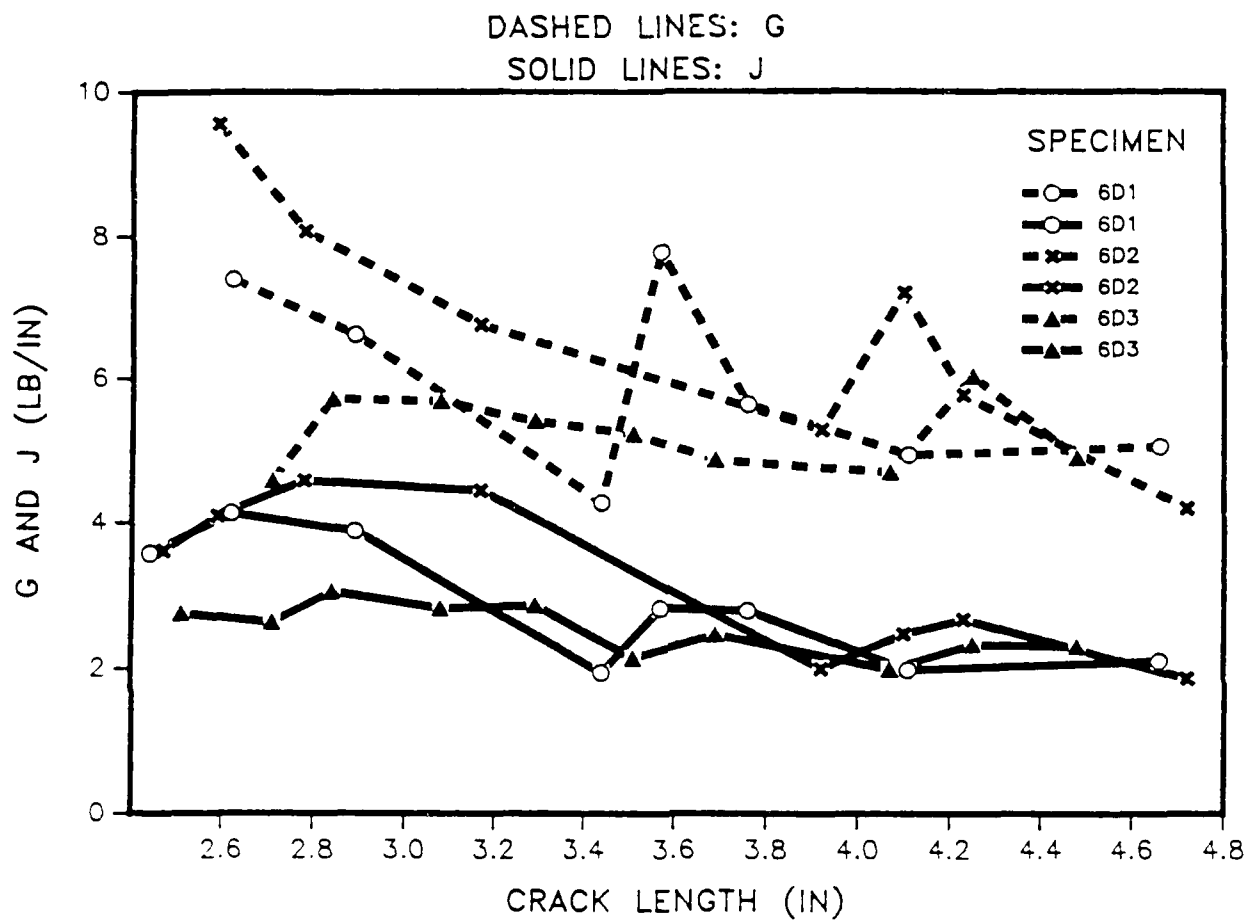


Figure 32. Fracture energy versus crack length using the area method (G) and a damage-dependent J integral (J) to analyze DCB data. The material is T2C145/F155 with a lay-up of $[\pm 45/(\mp 45)_2/(\pm 45)_2/(\mp 45)_2/(\pm 45)_2/(\mp 45)_2/\pm 45]$.

almost a twofold increase in fracture energy over the unidirectional value when a crack travels at a $\pm 30^\circ$ or $\pm 45^\circ$ interface in AS1/3502 graphite/epoxy. The fracture surfaces evidenced a change in mechanism which was responsible for the greater toughness.

In this study just mentioned, several notable results were obtained which were reflected in the recommendations for further work. First, it was observed that when the crack was propagating at the interface of two plies, neither of which was parallel to the propagation direction, the crack tended to jump between plies by forming another crack parallel to the original crack, but on a different plane. They suggested that a more detailed knowledge of the crack front shape in this region would be helpful in understanding this phenomenon. A second subject for additional work was the transition between a region where the crack broke through a ply and a region where growth occurred between two plies, one of which had fiber parallel to the propagation direction. As shown in Fig. 33, the transition zone was V-shaped, with the first region tapering off into the second. This shape suggests an edge effect, and thus a width effect. Knowledge of the stress state across the width of the specimen would be needed to explain this behavior. Thirdly, a wide range of fracture toughness values was observed. There is therefore reason to consider how to interpret the results in a way that is relevant to analysis of crack growth in structures.

Given the complex delamination behavior of

multidirectional composites, how can one compare the results from the delamination testing between various layups? Also, how do the toughness measurements correlate with the values for the neat resin? By understanding the relationship between the behavior of various layups, one hopes to be able to predict the delamination performance of a proposed layup based on the results of a few baseline tests, rather than needing to make and test each potential layup. Also, understanding the critical parameters which determine toughness would lead to guidelines for the choice and development of materials.

Chai²² also used the DCB geometry to study delamination at various interfaces in multidirectional layups. Like Nicholls and Gallagher, he found that delamination energy correlated strongly with fracture morphology. He observed that various mechanisms operated during the course of a single test, and that transitions between fracture mechanisms occurred unpredictably. In general, the crack did not continue to grow in its plane, but shifted interfaces as it propagated. Large differences in the angles of the plies at the crack plane were noted to encourage ply jumping. Recent tests by Goetz have demonstrated that in the absence of 0° fibers to contain the crack, it can leave the midplane and jump from ply to ply until finally reaching the surface; during the process the specimen behavior is radically altered. Such behavior is not seen in the testing of unidirectional composites.

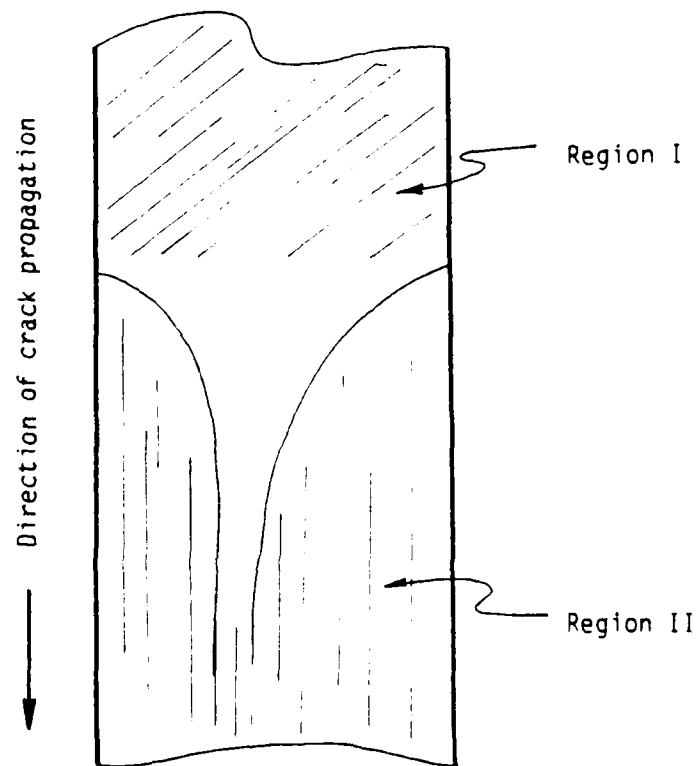


Figure 33. Schematic of transition between two regions on a fracture surface. Region I corresponds to the crack front breaking through a ply. Region II appears as the crack propagates between two dissimilarly oriented plies one of which is oriented parallel to the direction of crack propagation. (After [12].)

Chai observed local toughness changes on the order of 100% due to transitions in fracture mechanism. High fracture energies were not necessarily due to fiber breakage; for example, even when the crack traveled between two 0° plies, the multiplanar character of the fracture lead to variations in roughness prompting his statement that, "The range in fracture energies found in the region of the 0₂ plies as opposed to a single value may be cause for concern in the fracture testing of unidirectional laminates."

A major conclusion in Chai's paper was that the mode I interlaminar fracture energy was independent of test specimen geometry (crack length and width), independent of ply orientations at the delamination surface, and dependent only on the matrix constituent. It should be noted, however, that in order to make this statement Chai had to exclude from consideration all regions of the fracture surface where fiber breakage, pull-out, and ply-jumping were observed. Essentially, by excluding fracture processes where the fibers made a difference (on the basis of fracture surface morphology), Chai insured that the matrix consistence was determinative in the toughnesses measured. Indeed, in the absence of such a screening of data on the basis of surface morphology, a constant value of delamination toughness is not obtained. When he compared the results of other investigators with the hypothesis, it was largely unsupported. In general, fracture energy appears to be dependent on interface angle and potentially on fiber

properties as well.

The evidence he presents suggests that a less strong, more precise conclusion is that minimum toughness is obtained for matrix-dominated mechanisms, and that similar toughness is sometimes obtained despite varying fracture morphology details. Because a lower bound gives the most conservative result in analysis, this is very significant. However, identifying a constant lower bound does not fully explain the data. Understanding the higher energy processes which lead to higher delamination resistance is still necessary.

Another aspect of the paper's conclusion bears scrutiny. The delamination toughness is stated to be independent of DCB width. The results for specimens with a range of widths agreed. For one material, the width was varied from 4.2 to 8 mm and for another from 7.2 to 10.4 mm. However, the thickness of the 48 ply layups were 6.1 and 6.7 mm, respectively. Since edge effects would be expected to be seen over a distance on the order of the thickness²³, these specimens were not nearly wide enough to produce a change in behavior, even if such a transition does occur in wider specimens. Furthermore, evidence of edge effects is seen in some of the fracture morphologies shown in the paper. Aside from the effect of width, Chai cites the effect of specimen geometry on the crack tip damage zone as a complicating factor making interpretation of the toughness he reported more difficult.

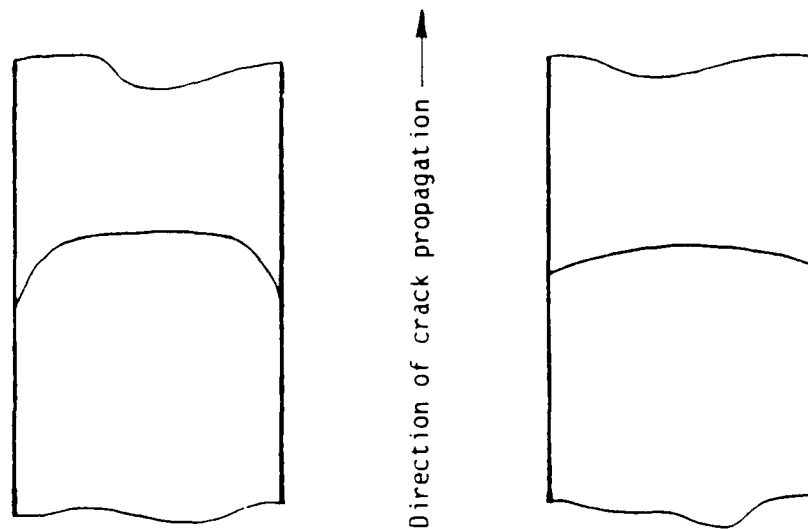
Jordan²⁴ conducted delamination tests on

multidirectional laminates. Tests were performed using layups with 0° fibers except at the fracture plane, at which there was a ± 10 or ± 45 degree interface. For these cases, the stiffnesses of the laminates were similar to that of the unidirectional layup, and the toughness values were also similar. However, he noted that as the percentage of off-axis plies was increased and the axial modulus decreased, the size of the zone of microcracking at the crack tip increased, as did the amount of damage in the specimen away from the crack tip. Analytical methods which did not account for the effect of the far field damage gave results showing a large increase in apparent fracture toughness. However, when data reduction was performed using a damage-dependent J integral, the intrinsic fracture energy was found to be comparable to that for the unidirectional composite in three of the four systems studied. This suggests, in accord with Chai's conclusions, that there is an intrinsic fracture energy which is independent of interface angle. In another recent study²⁵, a similar result was found by applying the J integral to delamination. Such layup insensitivity of toughness suggests that the local normal interface stress, rather than local layup-induced shear stress, is the primary factor in delamination²⁴. It should be noted that this conclusion is based on limited data. Whether local shear stress was insignificant or whether any amount of local shear stress would be unimportant is not clear. Jordan's results from mixed-mode tests on one composite suggest that when

externally-produced G_{II} is over about 40% of the total energy release rate ($G_T = G_I + G_{II}$), G_T will become sensitive to the percentage of G_{II} and will increase. Thus, if the results from load-induced mixed-mode tests are relevant to the analysis of delamination based on the local stress state, one would expect local mode II conditions to be evidenced by an increase in toughness.

The determination of mode I delamination fracture toughness of multidirectional composites poses numerous questions--many of which do not exist for unidirectional composites. When performing delamination tests, one is seeking a geometry-independent material parameter. The question of geometry dependence has not been adequately addressed for multidirectional DCB specimens. The crack front often takes the shape seen in Fig. 34a. The change in curvature near the edge seems to be an edge effect. The difference in crack length at the edge and the center is typically .15 to .2 inches for a one inch wide specimen. Compare this to the relatively mild curvature seen for a unidirectional specimen (Fig. 34b). The difference in curvature implies that the crack tip stress field is significantly different for the two cases. To my knowledge, the causes and significance of this have not been addressed in the open literature. However, related work is currently being done at Texas A&M University.

Figure 35 shows a record of the load versus applied displacement curve for a typical DCB test. The smooth curve



a) Multidirectional Laminate

b) Unidirectional Laminate

Figure 34. Schematic of crack front curvature in DCB specimens

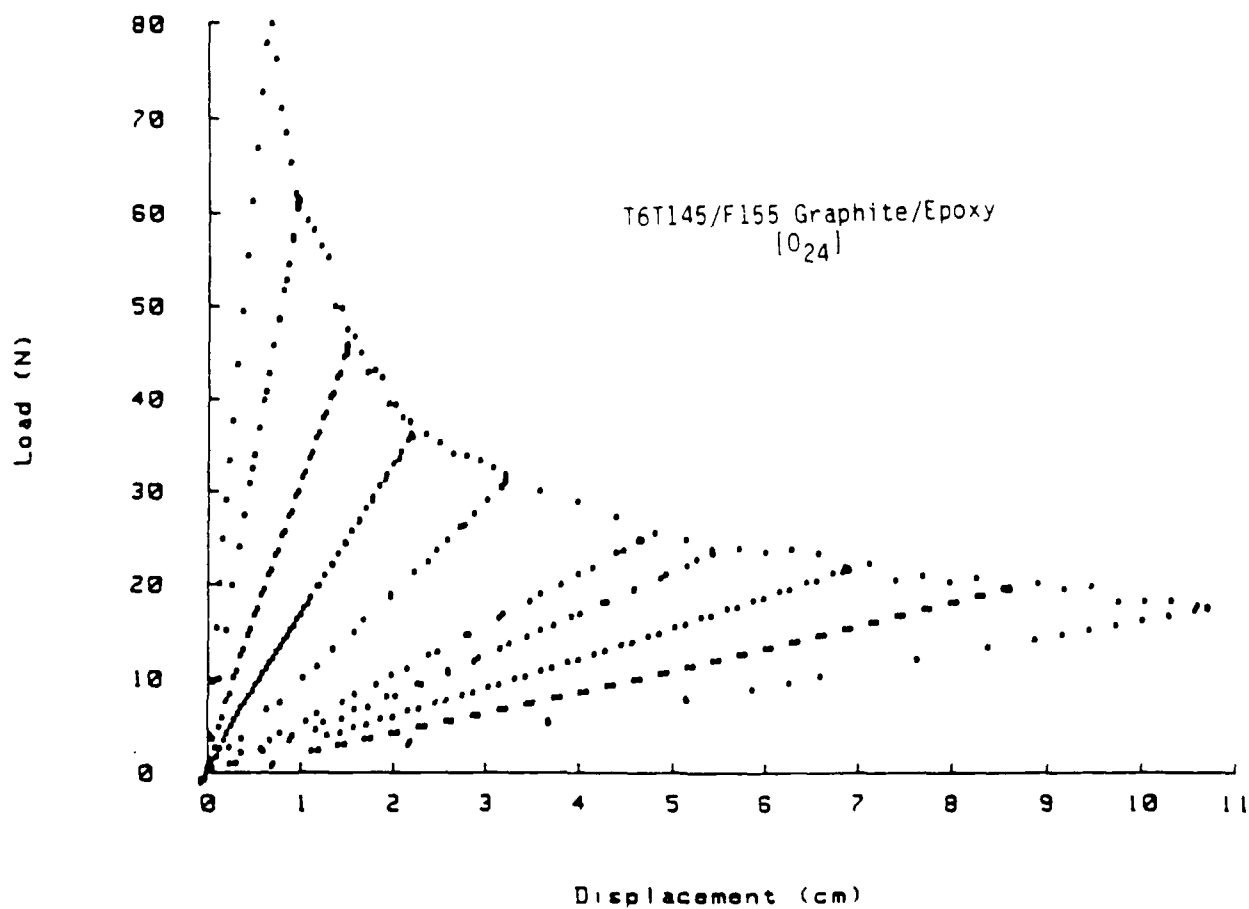


Figure 35. Load vs. applied displacement record for a typical DCB test illustrating stable crack growth

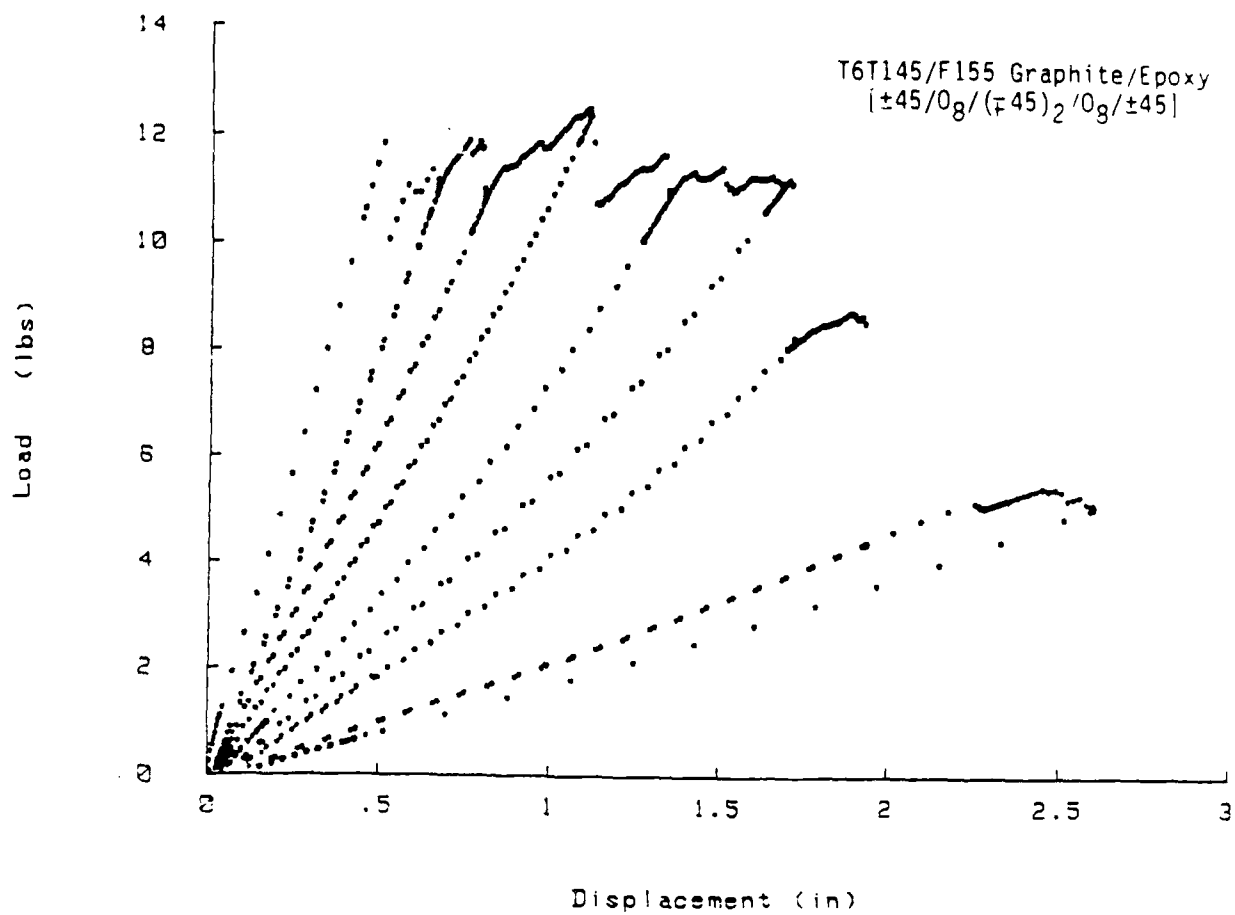


Figure 36 . Load vs. applied displacement for a DCB test illustrating unstable crack growth

is the result of stable crack growth. In contrast, the curve in Fig. 36 shows evidence of intermittent unstable growth during the displacement-controlled test. Such data are more difficult to interpret than those in Fig. 35. Tests conducted on the current grant have shown that regions of fast crack growth are generally regions of lower fracture toughness. What is the significance of the arrest energy? What is its geometry dependence? A second question is raised by the parts of the curve which show increasing load with increasing displacement coming from what is evidently damage zone growth or stable crack growth. Is there some significance of this behavior analogous to that seen in the resistance curves commonly determined for metals? Such questions have yet to be answered.

As mentioned previously, studies have shown that the fracture energy of a specimen can vary widely with crack length if fracture mode transitions (e.g., ply jumping) take place. This creates a problem in data interpretation and reporting. Chai addressed this by screening his results to isolate the lowest energy mechanisms, and then reporting the lowest value as the interlaminar fracture toughness. Often data reduction techniques are used which smooth out the data, such as the area method²⁵. There is a need for data analysis which is able to capture the details of the various fracture processes.

It has been reported that in some instances multidirectional fracture toughness is similar to the

unidirectional value and in some it is not. The limits of the generality of the former statement have yet to be explored. The potential significance of such a correlation is very great, since it would allow one to perform a simple test to obtain information for many complex layups.

Previously, the generation of far-field damage (damage away from the crack tip, e.g., in the legs of a DCB specimen) was cited as a complicating factor in delamination testing. Care must be taken to differentiate between energy going into the fracture process and energy going into generation of the far-field damage. Only a handful of investigators have attempted to develop analyses and tests which compensate for it ^{20,25}. The degree of far-field damage is known to be dependent on stacking sequence. More matrix-dominated layups and layups with large differences in interface angles generate more damage. In a DCB specimen, damage can be due not only to bending stresses, but also to tensile stresses in the legs near the loading points when the angle of rotation of the legs is large.

Besides affecting the introduction of far-field damage, the stacking sequence can potentially affect the delamination process by producing local shear and twisting at the crack tip, which may lead to partial crack closure or cause local mode II or mode loading²⁶.

4.4.1.3 Objectives of Current Study

The primary objective of the present study has been to

develop a theoretically-based procedure for determining the mode I delamination fracture toughness of multidirectional composite materials.

The nature of the questions to be answered was expressed in the previous section. Here are some of the fundamental questions underlying the objective of the proposed research:

- o Under what conditions can a geometry-independent measure of fracture energy be obtained?
- o What is the cause and significance of crack front curvature?
- o What data analysis is necessary to capture the details of the delamination process?
- o What is the significance and geometry dependence of the intermittent growth reflected in data such as seen Fig. 34? What is the significance of the increasing crack growth resistance?
- o Under what conditions do various fracture morphologies occur?
- o How do observed toughness values relate to the corresponding fracture morphologies?
- o For a given crack tip damage state (constant intrinsic fracture energy), what is the effect of varying stacking sequence, i.e., changing the amount of far-field damage?
- o What is the effect of changing the crack tip stress state through altering the stacking sequence?

- o How does damage due to tensile stress (as opposed to bending stress) impact the apparent toughness?
- o How does the fracture energy depend on crack speed?

4.4.1.4 Experimental Investigation

To date, the focus of the work has been on application of the J integral to double cantilever beam (DCB) tests in order to investigate the importance of geometry, layup, rate effects, and fracture morphology. The goal is to synthesize principles which can guide the prediction of delamination performance using limited material data. The following discussion highlights the method used and results obtained to date.

4.4.1.4.1 Materials and Layups--The material used in this study is T2C145/F155, manufactured by Hexcel. It uses a rubber-toughened epoxy matrix with about 6% rubber by weight. The nominal fiber volume fraction for all the material tested was 57%. This material system was chosen in order to accentuate possible non-linear and viscoelastic responses for a commercially available, toughened composite. It is also currently being used for other work on this contract and other contracts at Texas A&M, allowing sharing of material data. Three layups were used. Hereafter, they will be referred to using the following designations:

<u>Designation</u>	<u>Layup</u>	<u>No. Plies</u>
unidirectional	[0 ₂₄]	24

fiber-dominated $[+45/0_8/-+45]_{\text{antisym}}$ 24

angle-ply $[+45/(-+45)_2/(-+45)_2/-+45]_{\text{antisym}}$. 24

The unidirectional layup is the one which has been most commonly used in the literature to characterize delamination. In this study it was used not only to examine delamination between zero degree plies where ply interpenetration could occur, but to give a baseline for evaluating data for multidirectional layups. The fiber-dominated layup was used to study delamination at a ± 45 degree interface. Each leg of the DCB specimen was made balanced and symmetric in order to eliminate stretching-shearing and stretching-bending coupling. Antisymmetry about the midplane of the laminate was designated in order to put the delamination plane at a ± 45 degree interface. The stacking sequence for the angle-ply layup was chosen to minimize bending-twisting coupling as well.

4.4.1.4.2 Experimental Results--All data shown in the following figures were generated using DCB specimens. The fracture toughness was calculated using the J integral method of Schapery²⁷. In this formulation J is calculated using the moment at the crack tip during crack extension and the moment-curvature relationship for one leg of the specimen. The J integral is twice the area to the left of the moment-curvature curve, as shown in Fig. 37. In the following discussion, J will correspond to this path integral definition. The energy release rate was also calculated for

comparison. The symbol G will signify the energy release rate calculated by the area method¹⁶. The area method derives from the derivative definition of energy release rate, and provides an average value for an increment of crack growth. The symbol G_1 will refer to the energy release rate calculated using the equation

$$G_1 = \frac{3P_c \delta_c}{2ba} \quad (3)$$

where P_c is the load at crack extension, δ_c is the load line displacement at crack extension, b is the specimen width, and a is the crack length. This equation is based on the assumptions of linear beam theory and material linearity.

Comparison of J_c and G_c for Delamination of Angle Ply Composites--Motivation for using a J integral comes from the need for an analysis which would account for continuum damage such as might be generated throughout the legs of a DCB specimen during testing. The area method of calculating the energy release rate allows for geometric and material nonlinearity, as does J , but does not differentiate between energy which goes into driving the delamination and that which causes general damage away from the crack tip, leading to an overestimation of the delamination fracture toughness. The difference is illustrated in Fig. 32, where G and J are plotted versus crack length for three angle-ply DCB specimens. Note that for each specimen, G is significantly higher than J . The presence of damage is illustrated by the

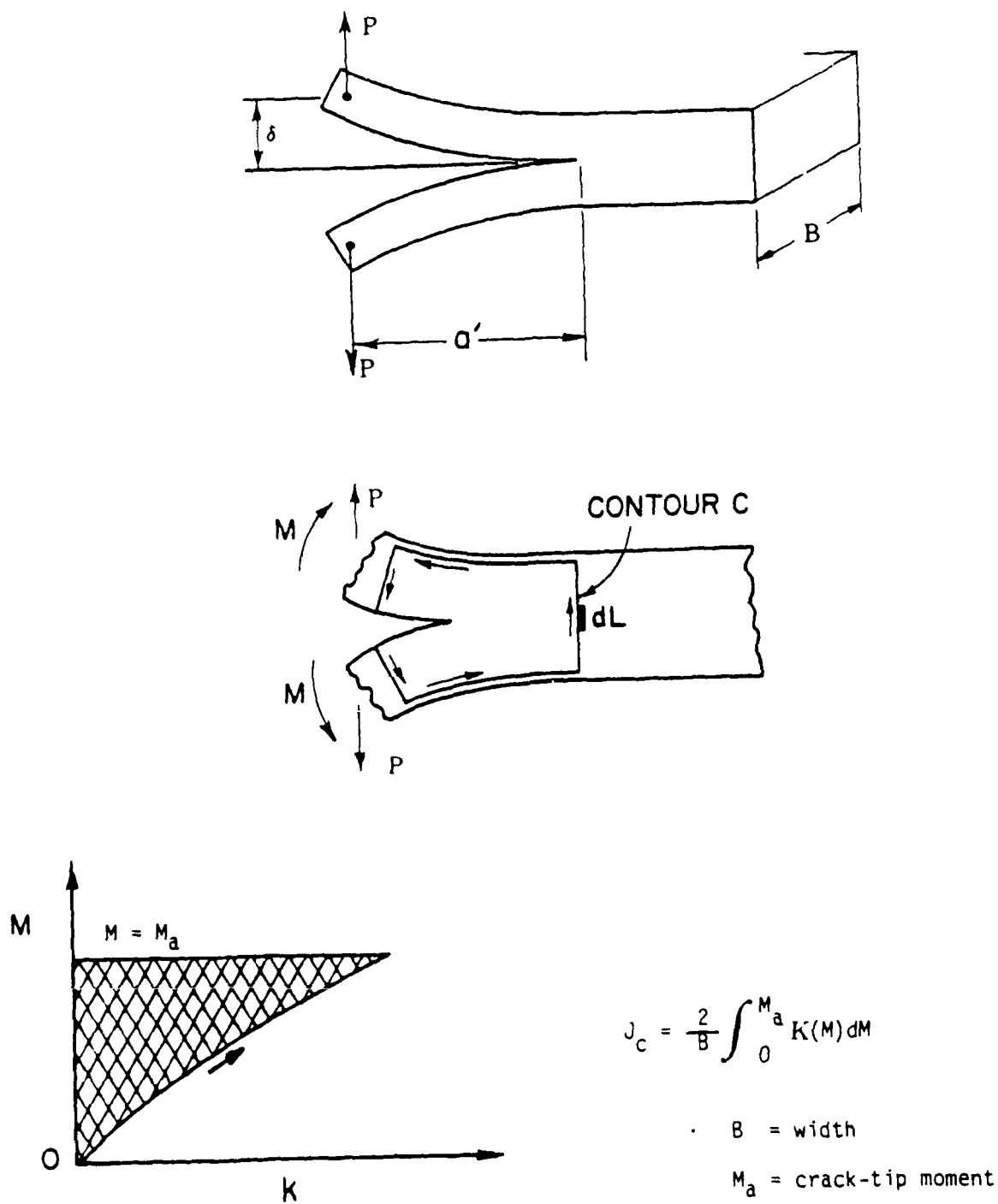


Figure 37. Double cantilever beam specimen, integration path, and moment-curvature diagram for calculation of J [after 1]

moment-curvature relationship for the angle-ply layup, as shown in Fig. 38. Note that the unloading portion of the moment-curvature plot does not retrace the loading portion.

For layups containing a high percentage of 0 degree fibers, one would expect that G and J would give better agreement, since continuum damage would be minimized. The moment-curvature relationships for the unidirectional and fiber-dominated layups were linear, and the unloading portions of the curves retraced the loading portions. When this is the case and linear beam theory applies, it can be shown that J is equal to G_1 calculated using Eq. 3. This formulation is helpful when comparing energy release rate and J because G_1 is calculated for a particular point (as J is for the linear and nonlinear cases), avoiding the averaging of the area method. Figure 39 is the load-displacement record from a fiber-dominated specimen which displayed the development and breakdown of a tie zone, causing the delamination resistance to increase and then suddenly drop with crack growth. The corresponding G_1 and J are plotted in Fig. 40. Both initiation and arrest values are shown. The two methods are in reasonably close agreement, supporting the interpretation of the difference between energy release rate and J for the angle-ply layup as being caused by damage. Even when damage is not present, the simple expression in Eq. 3 does not always hold. When geometric nonlinearity is present due to large rotations of the legs, the energy release rate must be calculated using either the area method

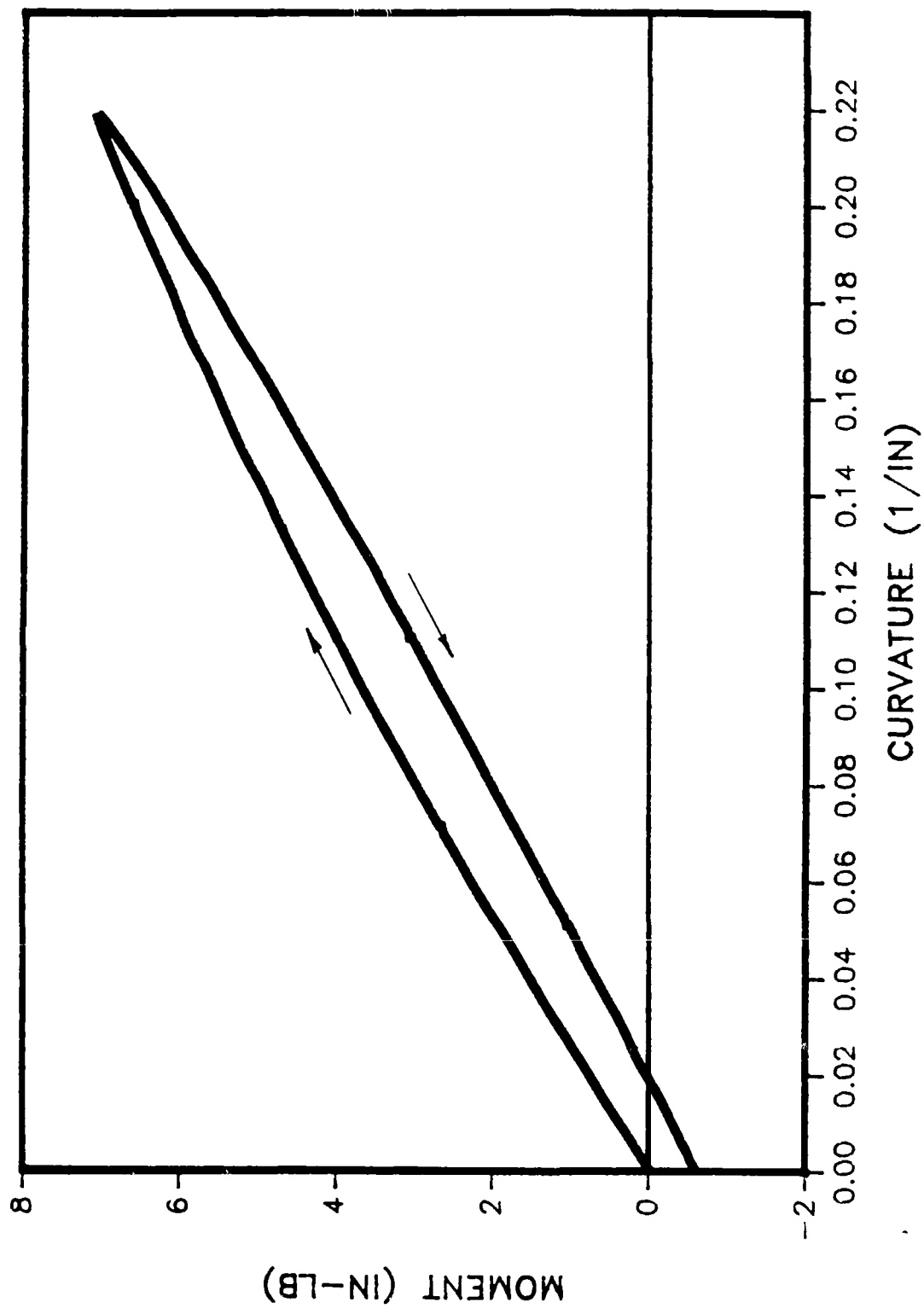


Figure 38. Moment vs. curvature diagram for an angle-ply layup

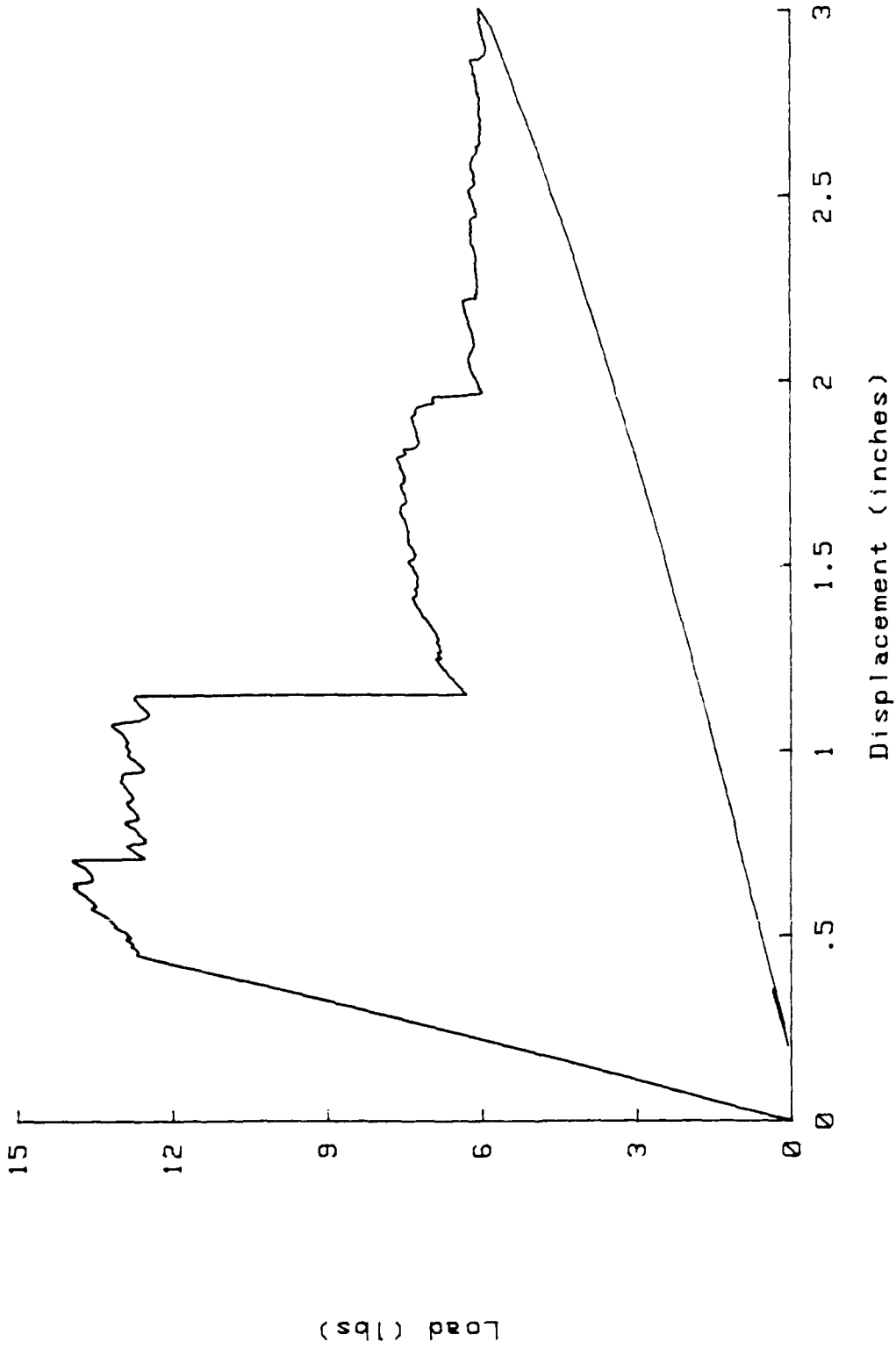


Figure 39 Load vs. displacement plot for a fiber-dominated DCB specimen
The layup is [+45/0_g/(-+45)₂/0_g/-+45].

AD-A192 821

FRACTURE PHYSICS OF DELAMINATION OF COMPOSITE MATERIALS

2/3

(U) INGLE, A AND M. UNIV. COLLEGE STATION MECHANICS AND
MATERIALS E. E. READING, PA. AL. OCT 87 HW-482, 84-12

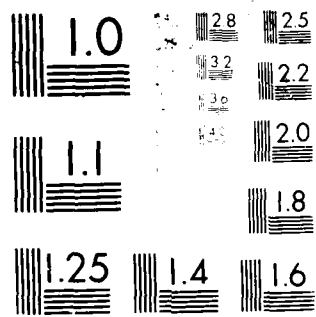
UNCLASSIFIED

AFOSR-7N-88-0020 AFOSR-84-0034

F/G 11/4

ML





(possibly losing information due to averaging) or using nonlinear beam theory¹⁷.

Geometry Dependence of J--The usefulness of J as a characterizing parameter depends on its independence of geometry, such as specimen width. To investigate the effect of specimen width, angle-ply specimens 1/2, 1, and 2 inches wide were tested. Representative results are given in Fig. 41. The high values for the 1 inch wide specimen for shorter crack lengths were found to be associated with the complex fracture morphology which developed near the starter crack. For more nearly self-similar crack advance, it appears that width does not have much effect on the fracture toughness measured over the range of widths and crack lengths studied. Recent work at Texas A&M²⁸ indicates that the state of stress in the legs of the DCB specimen is in the transition range between plane strain and plane stress over the practical range of crack length to width aspect ratios. However, the effects of the transition on J were not seen for the aspect ratios used in our tests. However, there is another aspect of specimen behavior which does show a marked width effect. Unlike unidirectional composites, multidirectional composites exhibit significantly curved crack fronts in DCB tests. The curvature depends on the width of the specimen. Figure 42 compares the normalized crack front profile for 1/2 inch, 1 inch, and 2 inch wide specimens for several crack lengths. Apparently the crack front curvature has two sources: the antielastic curvature of the DCB leg and free edge effects.

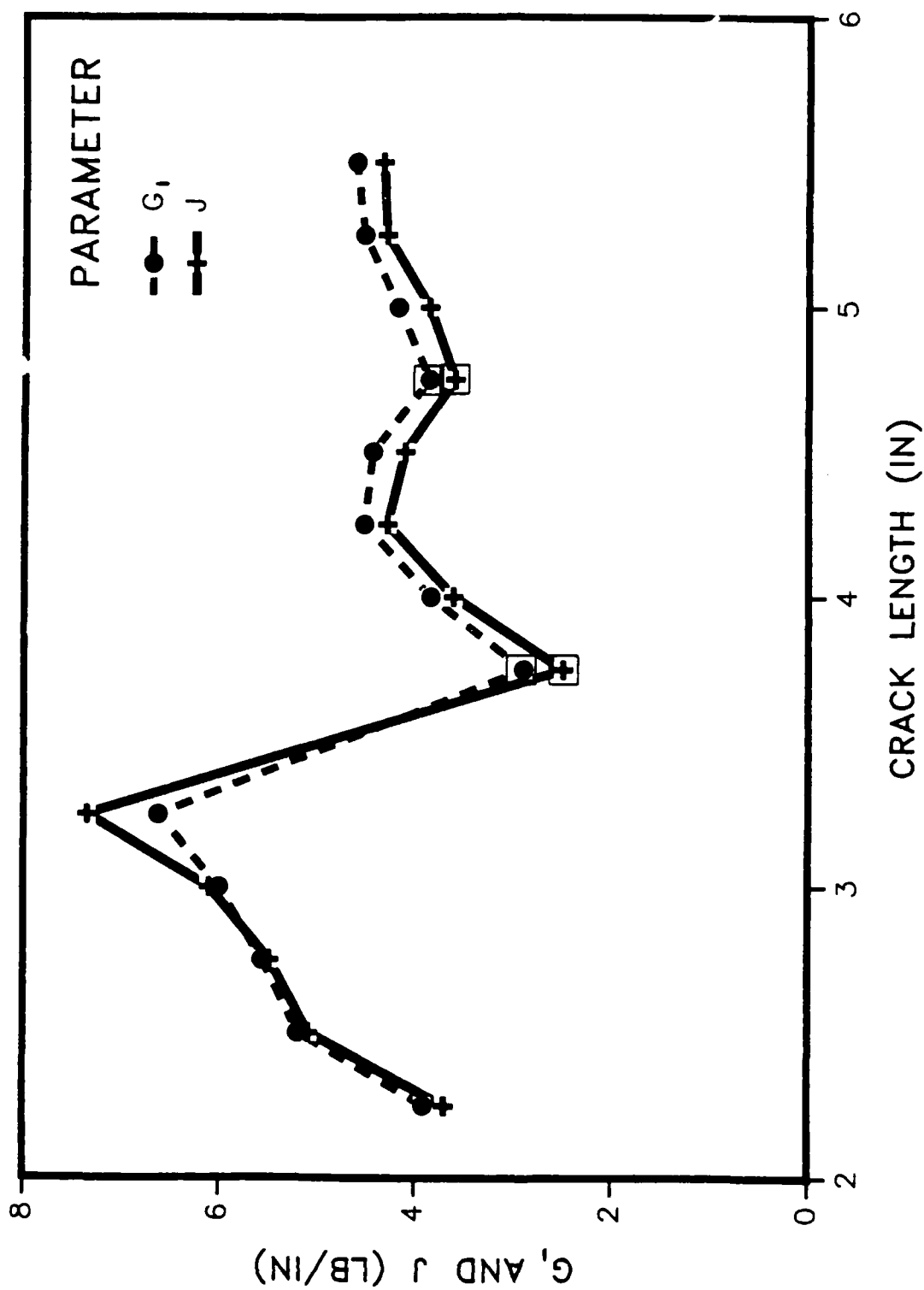


Figure 40. G_I and J vs. crack length for the fiber-dominated specimen of figure 4.4. Arrest values are marked by squares around data points. The layup is $[+45/0_8/(-45)_2/0_8/-45]$.

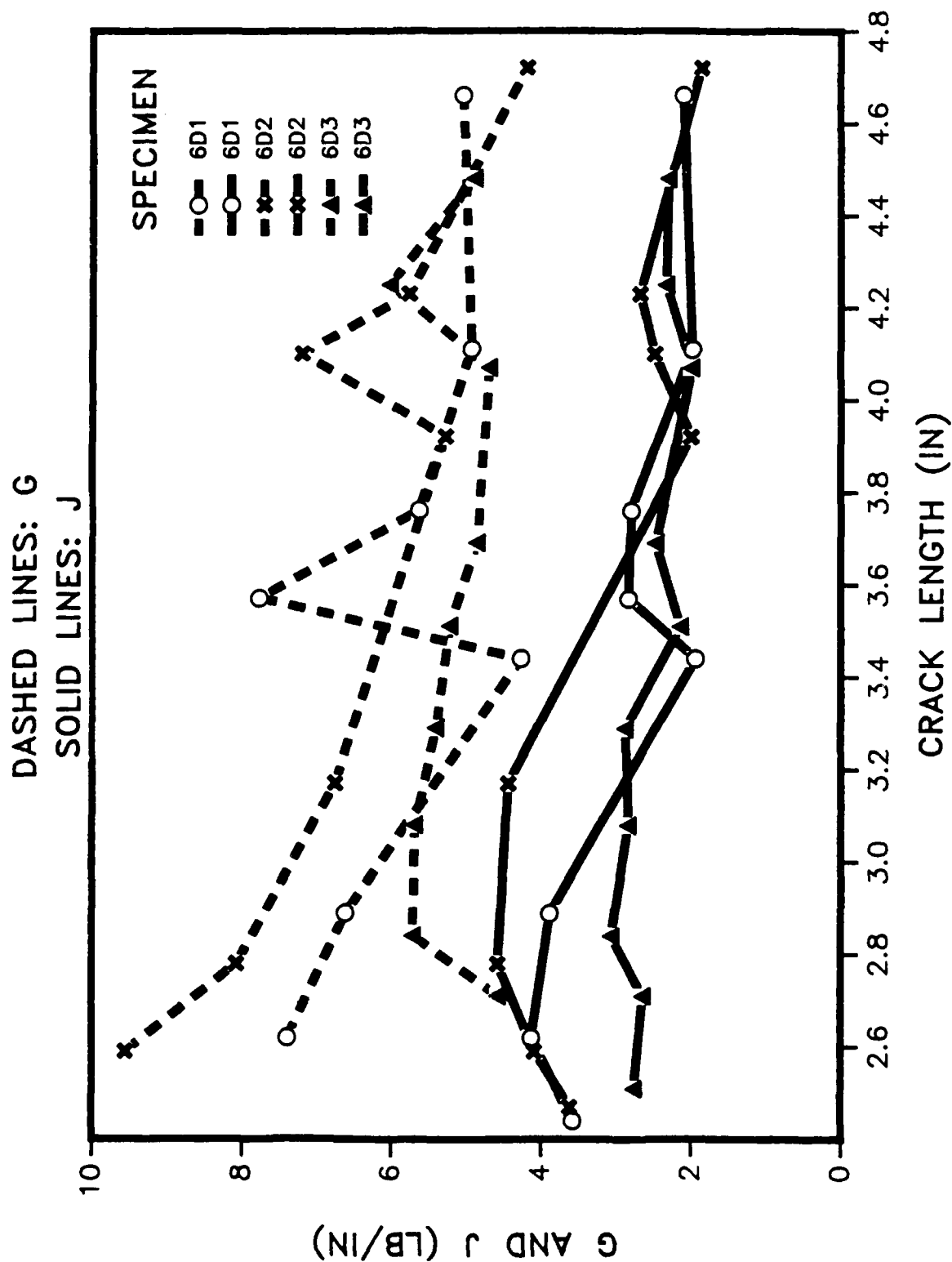


Figure 41. G and J vs. crack length for three angle-ply specimens

The general trend appears to be decreasing curvature with increasing crack length, but there is considerable scatter in the behavior. The differences between the shapes of the three plots are plain. The curvature associated with edge effects is dominant for the 1/2 inch specimen, but becomes less significant for increasing widths. These profiles were taken from fracture surfaces where the crack arrested after jumping forward, marking the surface.

Effect of Stacking Sequence on J--The effect of layup on J was studied. It was found that when complex mechanisms of fracture involving fiber breakage, ply jumping, extensive fiber bridging, etc., were absent, the results for various layups were often comparable. However, multidirectional layups often displayed such mechanisms. Other investigators^{21,22} have reported similar behavior. Figure 43 illustrates the variety of behaviors observed. The unidirectional specimen had a uniform toughness over a large range of crack lengths. The fiber-dominated layup led to large variations in J associated with tie zone development and breakdown. Typically the fiber-dominated layup produced data with the most scatter. Data interpretation was often difficult. Such large variations in toughness for similar layups have been reported elsewhere²¹. Practically, this is unfortunate, since one would like to use this layup to study the effect of various fiber angles at the delamination plane without resorting to making measurements of the moment-curvature relationship (since the relationship is

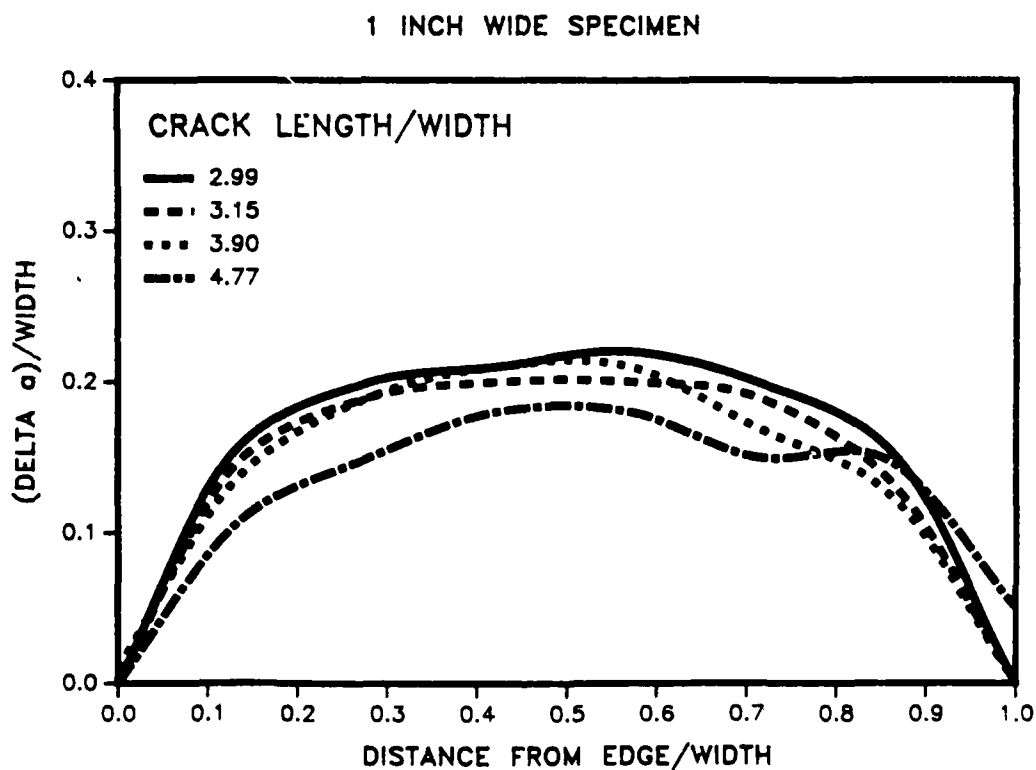
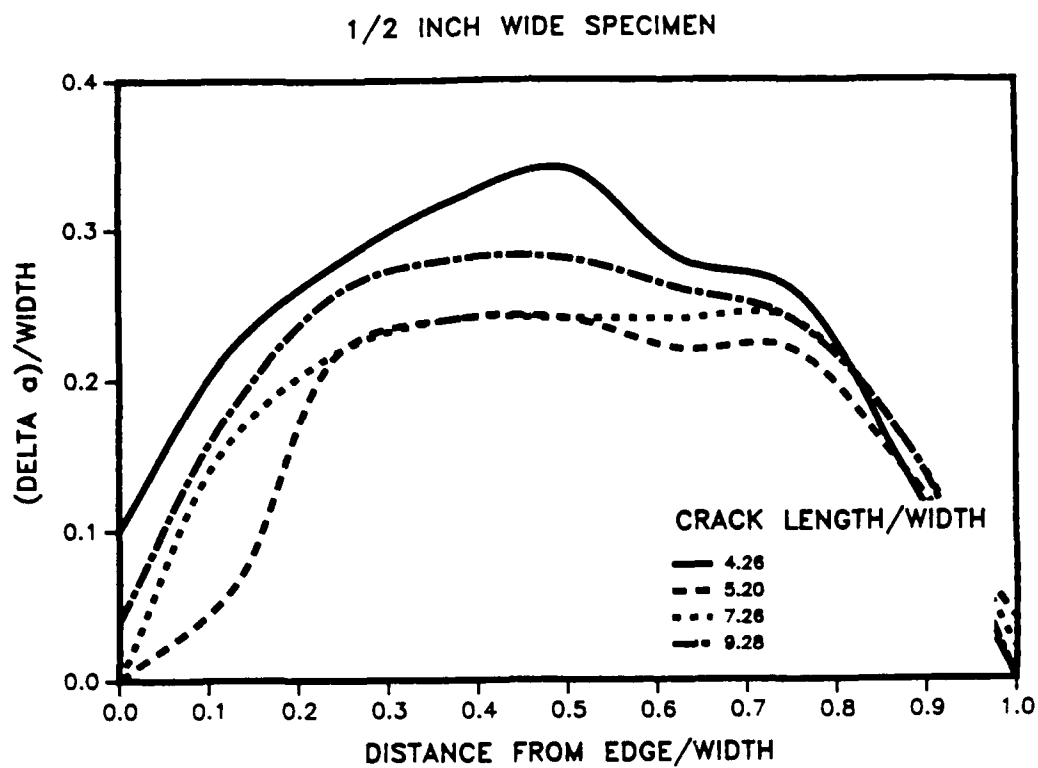


Figure 42. Normalized crack front profiles for three angle-ply DCB specimens of different widths. The profiles for various crack lengths have been superimposed.

2 INCH WIDE SPECIMEN

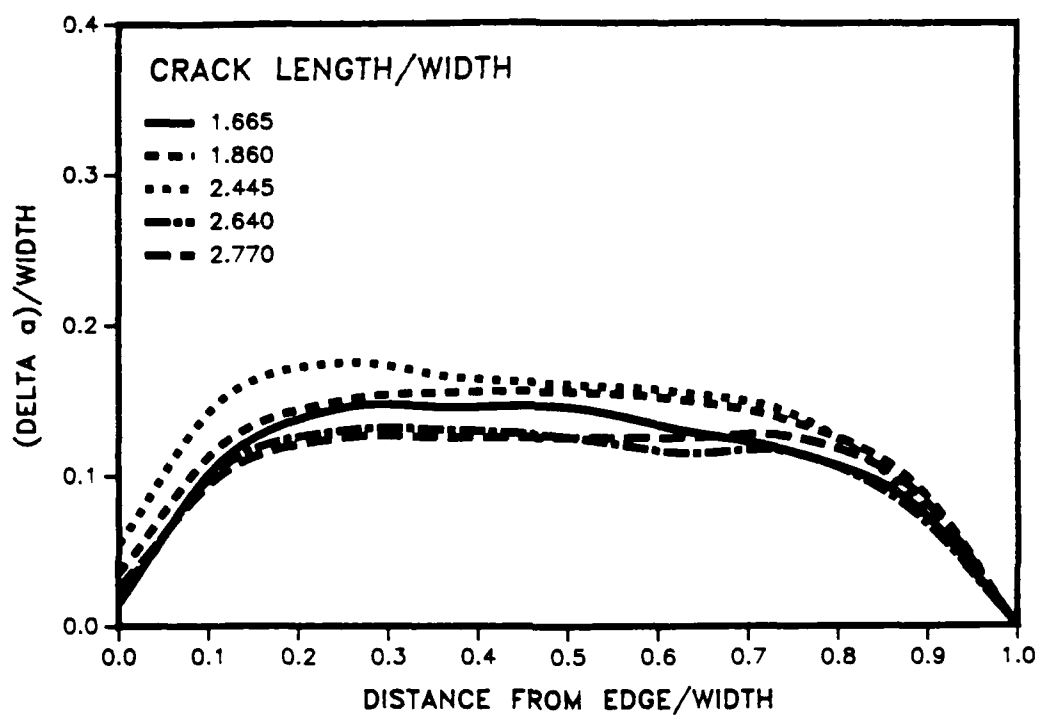


Figure 42. (continued)

linear so that Eq. 3 can be used). The angle-ply layup, being a "softer" layup, and with distributed (energy absorbing) damage, exhibited less crack jumping and scatter in the data. However, as shown in Fig. 43, complex fracture mechanisms were sometimes present early in the test before the delamination plane had been established.

The effect of fracture morphology is further illustrated in Fig. 44 where features on the fracture surfaces are related to the toughness measured. Note that once a more or less uniform fracture morphology was established, the toughness values settled into better agreement. The two angle-ply specimens shown were next to each other in the plate of material before cutting. Dark and light bands were formed when the crack tip jumped forward, then arrested. Dark regions were formed during rapid crack advance; light regions correspond to slow crack growth. These studies of the effect of layup illustrate a major difference between unidirectional and multidirectional laminate delamination behavior. The opportunity for more mechanisms of fracture leads to a greater complexity of behavior. It is therefore essential that attention be paid to the fracture surface morphology when interpreting the data.

Effect of Crack Speed on J--Tests were done to investigate the dependence of J on crack speed. The results for a unidirectional layup and a fiber-dominated layup are given in Fig. 45. In both cases there is a slight decreasing

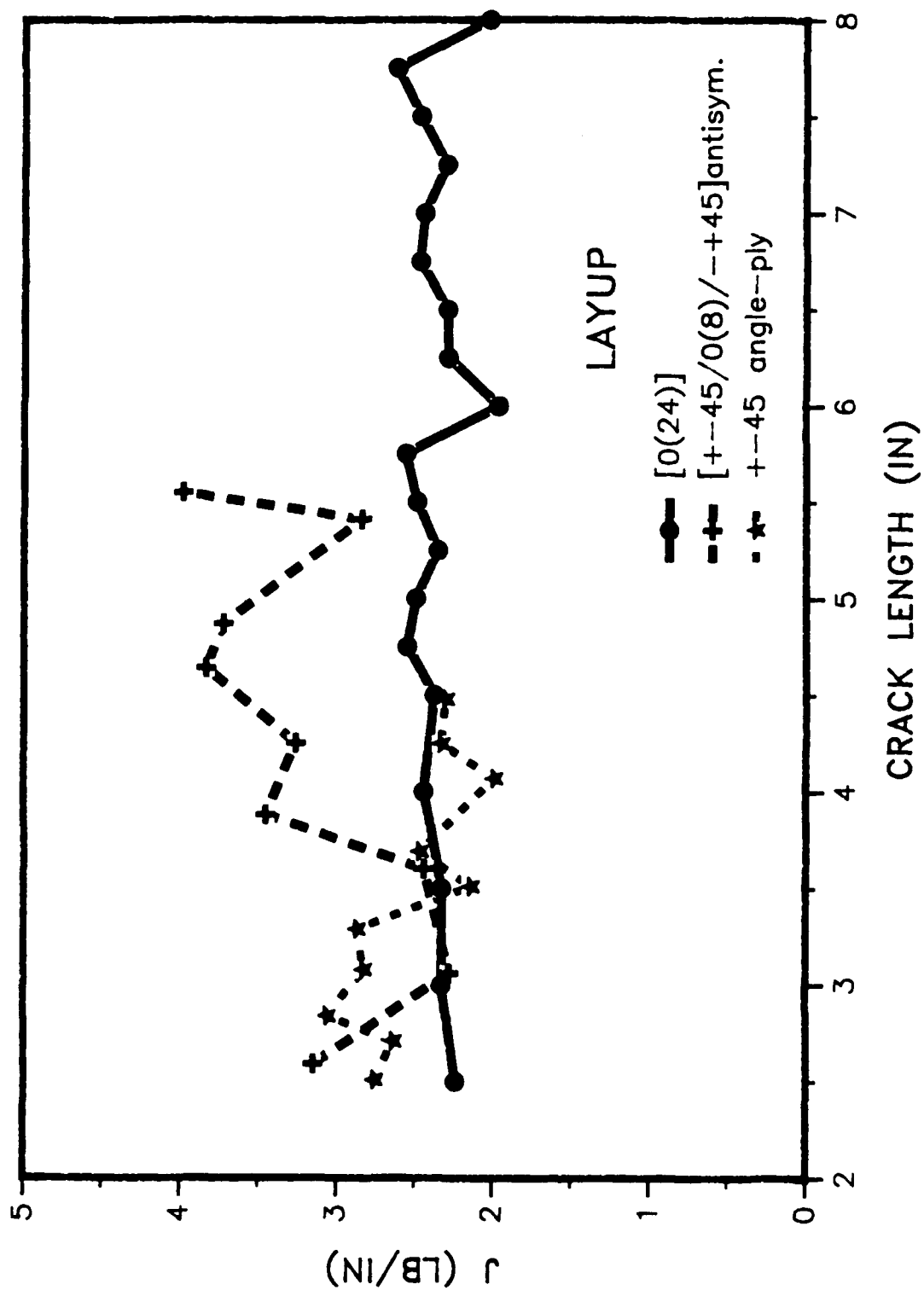


Figure 43. J vs. crack length for three different layups

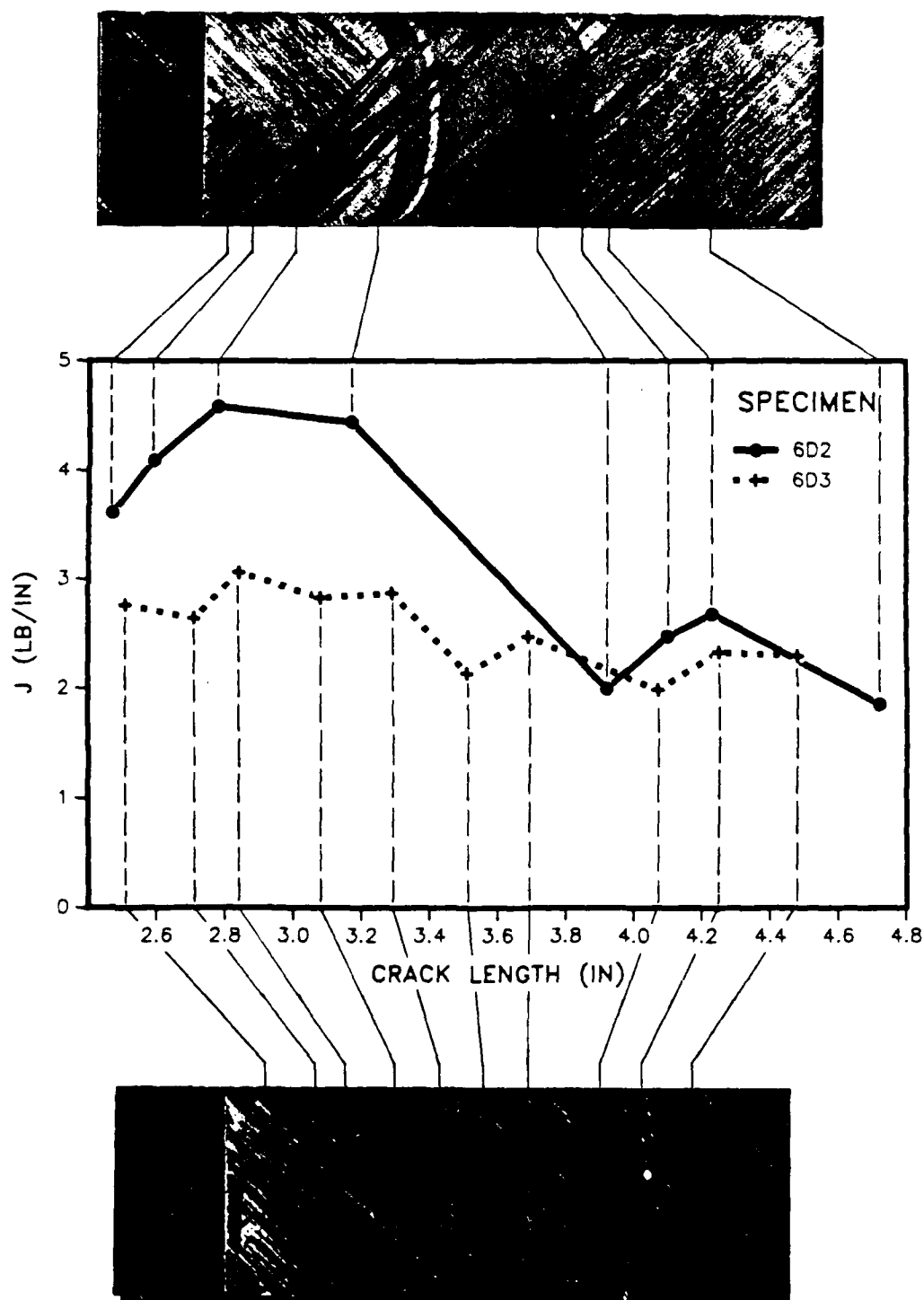


Figure 44. Correlation of fracture surface morphology with measured delamination fracture toughness for two angle-ply specimens

trend in J with increasing crack speed. This trend agrees with the observation that when sudden crack jumping occurred, a low value of toughness was usually measured. It is significant to note that no strong trend can be established for the range of crack speeds experienced by one specimen. Thus, rate effects are not important in interpreting data for individual specimens in this material tested at ambient temperature.

Fracture Surface Morphology and J--The importance of considering the fracture morphology when interpreting the delamination toughness data has already been mentioned. Macro- and microfractography were done to document the fracture mechanisms which were observed. Two items are of particular interest. First, when off-axis plies were present at the fracture plane, toughness values were sometimes elevated even in the absence of complex fracture mechanisms. Apparently this was due to increased surface roughness caused when bundles of fibers were pulled away from the fracture surface. This feature was only observed for layups with off-axis plies at the delamination plane. For a more brittle system the phenomenon was found to give differences of a factor of two in toughness between unidirectional and off-axis specimens²⁵. Figure 46 is a cross-section of a specimen (normal to the direction of crack propagation) at the fracture surface. A bundle of fibers is separated from the surface at this plane, but is attached to it at another point.

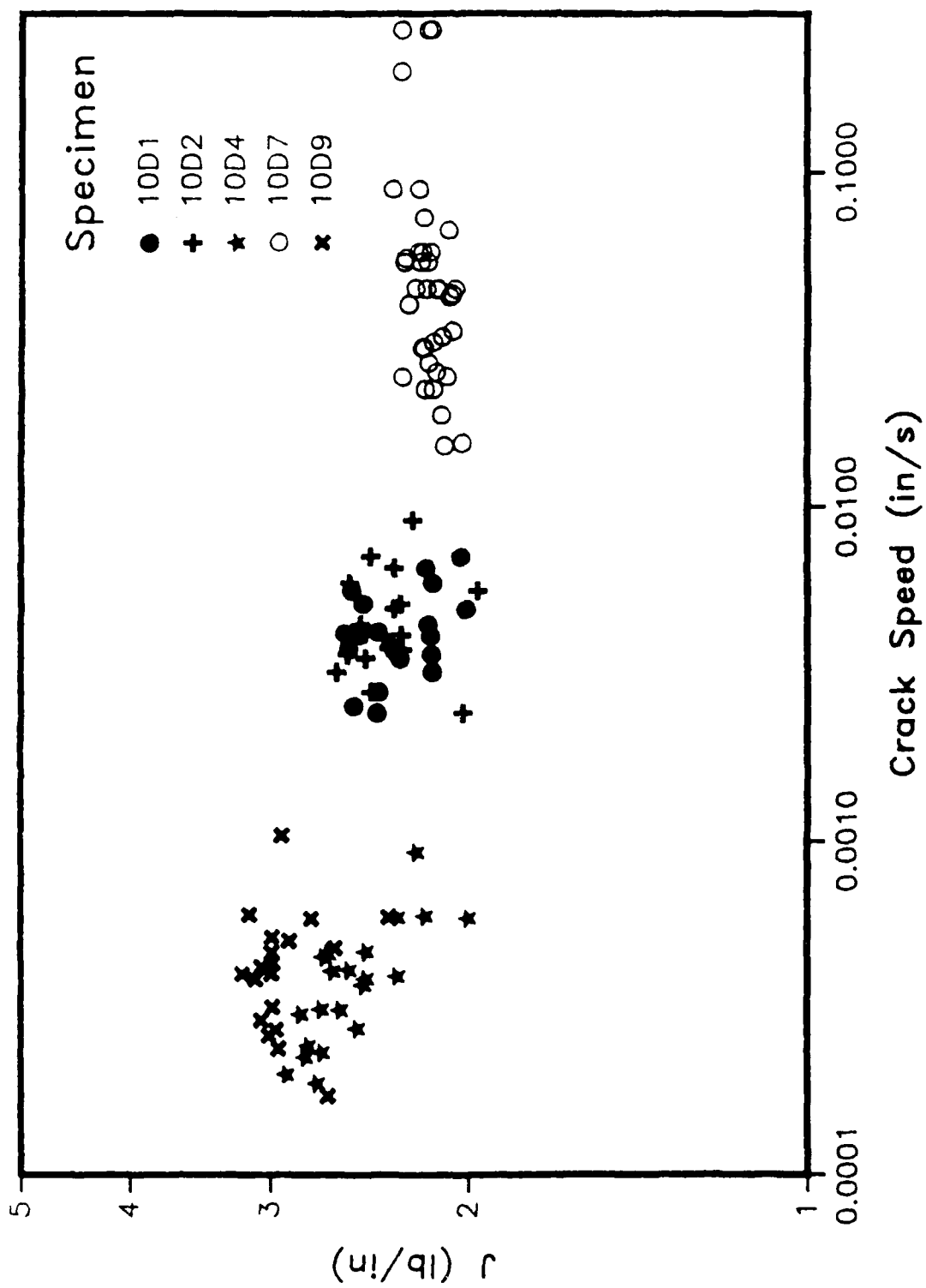


Figure 45. J vs. crack speed for unidirectional DCB specimens

A second phenomenon which is of significance is that in almost all specimens tested, delamination was found to occur within a ply rather than between two plies. Figure 47 shows a typical situation on a polished cross section at a fracture surface. Note that the fracture plane does not pass through the interply region, but stays a few fiber diameters away from it. Practically, the presence of resin-rich regions and ply interfaces has only an indirect impact on the mode I delamination toughness when such steady-state morphology is present.

Future work under the follow-on grant is expanding on these investigations of the effect of geometry, layup, rate effects and fracture surface morphology. Further experiments are being performed to explore the effect of specimen width, especially as it relates to crack front curvature. The effect of the number of plies and the bending stiffness of the legs of the DCB specimen is being addressed. Also, tests are being conducted with various fiber angles at the delamination plane. The dependence of delamination toughness on crack speed for matrix-dominated layups is also being investigated over a wider range of displacement rates. An attempt will be made to systematize the correlation between fracture surface morphology and delamination toughness. In addition to these continuing activities, new studies are beginning to improve our understanding of the effect of continuum damage on the apparent toughness. This will probably include delamination tests which simulate mechanical

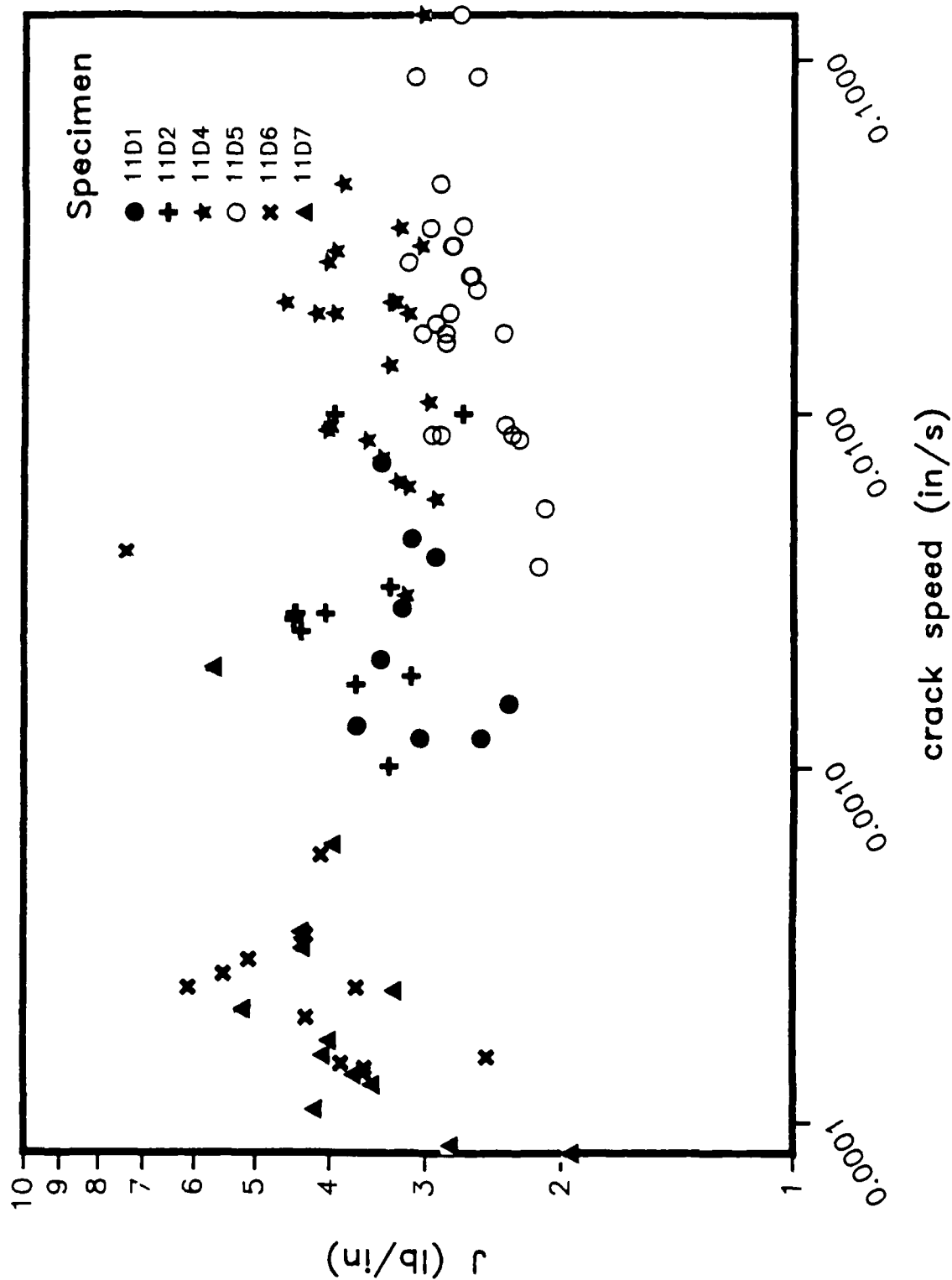


Figure 46. J vs. crack speed for fiber-dominated DCB specimens. The layup is $[\pm 45/0_g/(-+45)_2/0_g/-+45]$

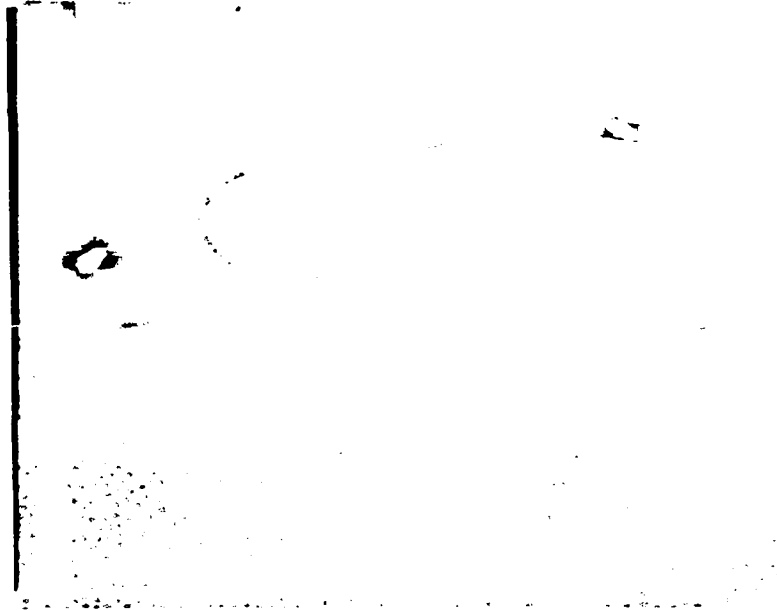


Figure 47a Micrograph of a polished section of a failed DCB specimen showing the fracture surface. A bundle of fibers has been pulled away from the surface. (150X)



Figure 47b. Micrograph of a polished section of a failed DCB specimen showing the fracture surface. The large circles at the top are the material used to mount the specimen for polishing. (100X)

states in real structures, such as tests using a modified DCB specimen with bending and stretching inputs.

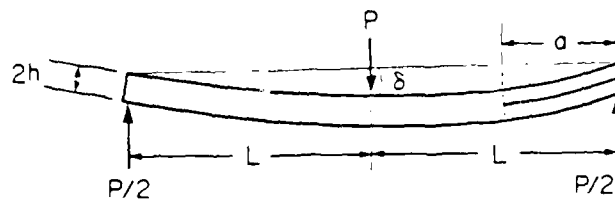
4.4.2 Mixed Mode and Mode II Delamination of Composite

Materials

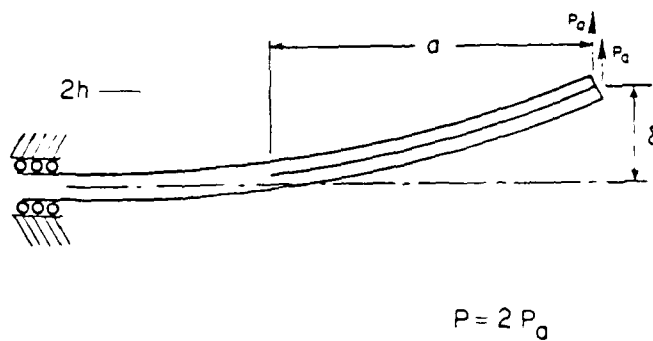
Our efforts in the characterization of mixed mode and mode II delamination of composite materials have fallen into three categories: (1) a comparison of the end notch flexure and the end loaded flexure tests to see if they give consistent values of G_{IIC} ; (2) development of a J-integral approach to evaluate mode II delamination fracture toughness for composites made of resins which have significant nonlinear behavior and/or split laminate specimens which give significant geometric nonlinearity during testing; and (3) determination of the G total as a function of the percentage of G_{II} as well as the state of stress ahead of the crack tip for mixed mode loading. The results of our efforts in these areas will be summarized in the three subsections that follow.

4.4.2.1 Comparison of the End Notch Flexure Test and the End-Loaded Split Laminate Test for Delamination of Composite Materials

Several test configurations have been proposed for measuring the resistance to delamination under mode II loading, including the end-notched flexure (ENF) test and the end-loaded split laminate (ELS) test. The end-notched



(a) ENF test configuration and associated parameters.



(b) ELS test configuration and associated parameters.

Figure 48. Mode II delamination tests.

flexure test configuration can be seen in Fig. 48a. This test consists of a laminate beam with a split on one end, loaded in three point bending. The end loaded split laminate test consists of a split laminate beam specimen which is loaded at the cracked end and fixed at the opposite end (see Fig. 48b). The experimental results from the ENF and ELS test methods may be evaluated to give G_{IIC} using equations derived using linear beam theory; i.e., assuming geometric linearity and linear elastic material behavior^{30,31}. A review of the current literature indicates that both test configurations are currently being used to measure G_{IIC} ³⁰⁻³².

During a recent finite element analysis³³, the ENF test was found to be a pure mode II fracture test within the constraints of small deflection theory. The study also revealed that the interlaminar normal stress is identically zero along the beam center line and the interlaminar shear stress exhibits the expected singularity. A similar analysis was performed for the ELS test configuration in this project using the code described in 4.3. The results which were presented in section 4.3.1.2 also indicate pure mode II stressing along the center line.

4.4.2.1.1 Analysis

End-Notched Flexure (ENF) Test--The ENF test consists of loading a split laminate beam specimen using a three point bend fixture. Figure 48a shows the ENF test configuration and associated test parameters. Calculation of the strain

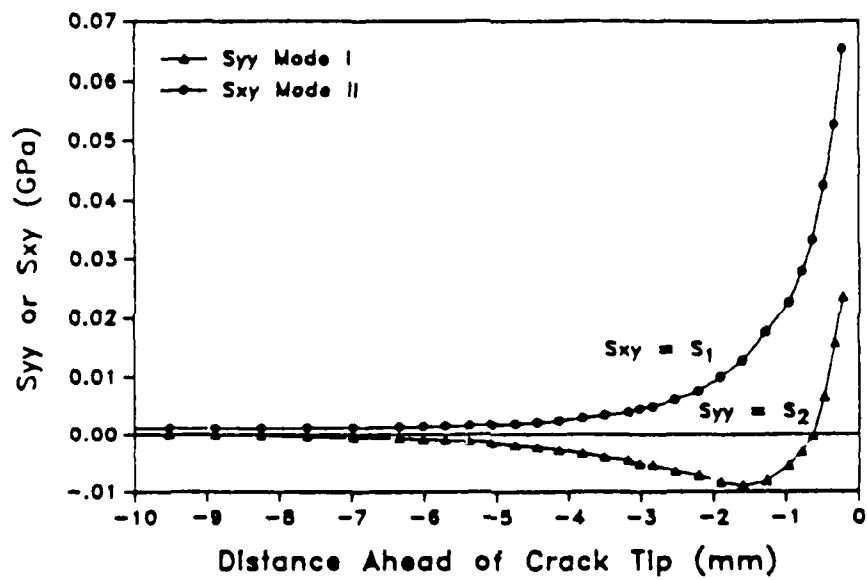


Figure 49. Stress distribution ahead of the crack tip for mode I and mode II loading.

energy release rate G_{II} assuming linear beam theory and linear elastic material behavior gives the following result³⁴,

$$G_{II} = \frac{9P^2 a^2 C}{2b (2L^3 + 3a^3)} \quad (4)$$

where a is the initial crack length, b is the width, C is the measured compliance, L is half-span length, and P is the applied load at the center pin. The strain energy release rate G_{II} can also be obtained by means of an experimental method for determining the relationship between compliance and crack length. In this case, G_{II} is given by³⁴

$$G_{II} = \frac{3P^2 m a^2 b_o}{2b^2} \quad (5)$$

where m is obtained from

$$C = m a^3 + \text{const.} \quad (6)$$

This equation is obtained by making a least squares fit of a straight line to experimental data from measured compliance against crack length cubed. This data is obtained from load-deflection curves at different crack lengths of one of the tested coupons of width b_o .

End-Loaded Split Laminate (ELS) Test--The energy release rate for pure mode II in this case is determined by asymmetrically loading a split-laminate beam specimen.

Figure 48b shows the ELS test configuration and associated test parameters. Linear beam theory and linear elastic material behavior are assumed by the analysis. A complete explanation of this analysis can be found in reference 31. From this analysis, G_{II} can be expressed by

$$G_{II} = \frac{9P^2 a^2}{4b^2 E_{II} h^3} \quad (7)$$

P is the load applied at the cracked end of the beam (see Fig. 48b). The modulus E_{II} measured in bending can be shown to be

$$E_{II} = \frac{P}{2b \delta h} (3a^3 + L^3) \quad (8)$$

where δ is the total beam tip deflection.

Area method--In all the methods of data reduction previously described, the critical energy release rate was calculated by knowledge of the critical load P_c at onset of crack growth, and the crack length 'a' prior to crack extension. Therefore, G_{IIc} is a measure of the energy required per unit area of crack growth to initiate crack propagation. However, as the crack propagates, G_{IIc} does not necessarily remain constant, in which case distinct propagation and arrest values of G_{IIc} can exist.

Where nonlinear load-displacement curves are observed in mode II testing, the above relationships based on linear

analysis are no longer accurate. An alternate approach for evaluating the fracture toughness for nonlinear behavior is the area method. In this case, G_{II} is still the energy required to create a new crack per unit area of crack surface created. G_{II} can then be given by

$$G_{II} = \frac{U}{b \Delta a} \quad (9)$$

U is the area between the load-deflection curve for loading and unloading for a very small change Δa of crack growth (see Fig. 50). An important advantage of this method is that only elastic material behavior is required to predict G_{II} . Therefore, for geometrically non-linear and/or non-linear elastic material responses, this method gives an average release rate for the observed crack extension. For unstable crack growth, it gives an average value for G_{IIC} which typically falls between the initiation and arrest values measured for linear behavior. The load-displacement record should return to the origin to guarantee that no significant far field damage is included in U in Eq. 9. The inclusion of energy dissipation in far field damage in the fracture energy term U in Eq. 9 would give an erroneously high estimate of G_{IIC} . For materials where G_{II} is independent of crack growth rate and crack growth increment (i.e., systems with minimal fiber bridging and/or plastic wake), the average and initiation G_{II} should be identical. Furthermore, where slow stable crack growth occurs, the average G_{IIC} calculated from

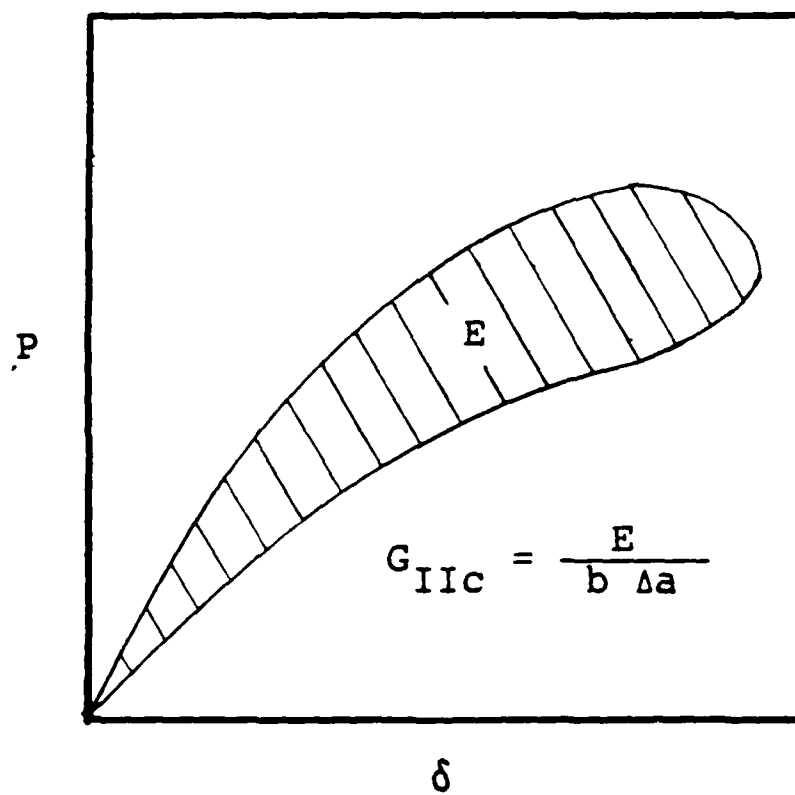


Figure 50. Alternate interpretation of G_{IIC} (area method)

the area method should equal the G_{IIC} for initiation calculated from linear beam theory. Another advantage of this method is that G_{II} is obtained without knowledge of the materials's elastic properties and it is always given by Eq. 9, regardless of the test configuration used.

4.4.2.1.2 Experimental Procedure

Split laminate beam specimens approximately 152.4 mm long, 25.4 mm wide, and 4.83 mm thick for the end-notched (ENF) test and 292.1 mm long, 25.4 mm wide, and 3.05 mm thick for the end-loaded split laminate (ELS) test were cut from 24 ply laminated panels of Hercules AS4/3502 and Hexcel T6C145/F185 graphite/epoxy composites. The starting crack was introduced in both panels by putting a teflon insert 0.127 mm thick at the midplane during layup. Loading tabs were bonded to the cracked end of the ELS test specimens with a two-part structural adhesive. A Tenslac UN-10A gray brittle coating was also applied to the edges of the specimen to facilitate measurement of crack length by making the location of the crack tip more evident.

End-Notched Flexure Testing--Five specimens for each graphite/epoxy system were tested using a three point bend fixture with outer loading points 101.6 mm apart attached to a closed loop servo-hydraulic test machine. Prior to testing, the specimens were precracked in order to provide a sharp crack tip from which to initiate the mode II fracture. Load point displacements were measured by the ram

displacement and loads were monitored by a 2225 N load cell. Real-time analog plots of the load-deflection curve were made on an x-y recorder. The tests were conducted by positioning the crack tip approximately midway between the center and one of the outer loadings pins. Under displacement control conditions and a ram rate of 2.54 mm/min, the specimens were loaded until delamination crack growth occurred. Then, the specimens were unloaded.

Since machine stroke displacement was used to measure specimen deflection, a machine compliance experiment was performed to make the necessary deflection corrections to the data obtained during the mode II delamination tests.

G_{IIC} calculations were made using Eq. 4 and measured compliances after appropriate machine compliance corrections had been made. It should be noted that corrections associated with shear compliance were not taken into consideration because no reliable values of the shear modulus G_{12} were available. However, these corrections are usually small and the omission was not thought to have a significant effect on the measured G_{IIC} values. The measured compliances were obtained by curve fitting the best straight line to the load-displacement data from the loading part of the test. Equations 5 and 6 were also used to calculate G_{IIC} . To use these two equations, a compliance calibration was performed with one of the tested specimens. Finally, G_{IIC} values calculated by the area method were determined by means of Eq. 9. The energy absorbed in the creation of a new cracked

surface was approximated numerically by integrating the area under the load/deflection curves obtained.

End-Loaded Split Laminate Testing--Two specimens for each graphite/epoxy system chosen for this study were tested in a closed loop servo-hydraulic machine. A mode I precrack was introduced to the specimens to sharpen the initial crack created by the teflon insert and to provide an initial crack length to beam length (a/L) ratio of approximately 0.55, where stable crack growth is expected³⁵.

Mode II delamination testing was done under displacement control at a rate of 10.16 mm/min and 6.35 mm/min. Loads were recorded with a 445 N load cell. Displacements were monitored using the ram displacement of the test machine. The tests were conducted by loading the specimens until the crack was allowed to grow approximately 10 mm to 38 mm. At that point the test was stopped and the new crack location marked and recorded. This procedure was repeated several times with the same specimen until the crack tip was approximately 12.7 to 25.4 mm from the uncracked end.

The critical energy release rate G_{IIC} was calculated by means of Eqs. 7 and 9. The modulus E_{11} was calculated from the load-deflection test data and Eq 3. The energy absorbed in the creation of a new cracked surface was approximated numerically by integrating the area under each loop in the load-deflection curves.

4.4.2.1.3 Results and Discussion

End Notched Flexure (ENF) Test Results--Table 2 shows the ENF test results for both graphite/epoxy systems investigated. Method I corresponds to G_{IIC} values obtained using beam theory equations (Eq. 4) and measured compliances. Method II results are based on the compliance calibration (Eqs. 5 and 6). Method III refers to data reduction based on the area method (Eq. 9) and the energy dissipated under the load-deflection curve. Delamination crack growth occurred at typical load values of 556 to 612.5 N for AS4/3502 graphite/epoxy and was unstable for this material. Figure 51 shows a typical load-deflection curve of AS4/3502 graphite epoxy showing the sudden drop of load as unstable delamination crack growth occurs. This indicates that the G_{IIC} values measured using the area method will be an average of the initiation value and the value for rapid, unstable crack growth. The very small nonlinearity just prior to crack extension is probably associated with the development of a crack tip damage zone.

The average critical energy release rate G_{IIC} for AS4/3502 using methods I, II, and III of data reduction were 560 J/m^2 , 648 J/m^2 , and 613 J/m^2 , respectively.

Figure 52 shows a typical load-deflection curve obtained for mode II delamination testing of T6C145/F185 graphite/epoxy. Crack growth was stable as seen in the upper part of the curve. However, the point at which crack growth occurred is not well defined. Therefore, the maximum load reached during each test was used to estimate the onset of

Table 2.- End-notched Flexure (ENF) Test Results.

Material	Specimen	G_{IIC} (J/m ²)		
		I	II	III
AS4/3502	1	525	648	613
	2	508	630	595
	3	560	682	613
	4	543	648	630
	Av.	543	648	613
<hr/>				
T6C145/F185	1	*	*	2240
	2	-	-	2695
	3	-	-	2485
	4	-	-	1995
	Av.	-	-	2398

* No calculation of G_{IIC} is possible due to significant nonlinearity in load/deflection curves. If one uses linear portion of curves to measure compliance and P_{max} for crack extension (ignoring nonlinear behavior near P_{max}), G_{IIC} lower bound values of 1225 may be calculated.

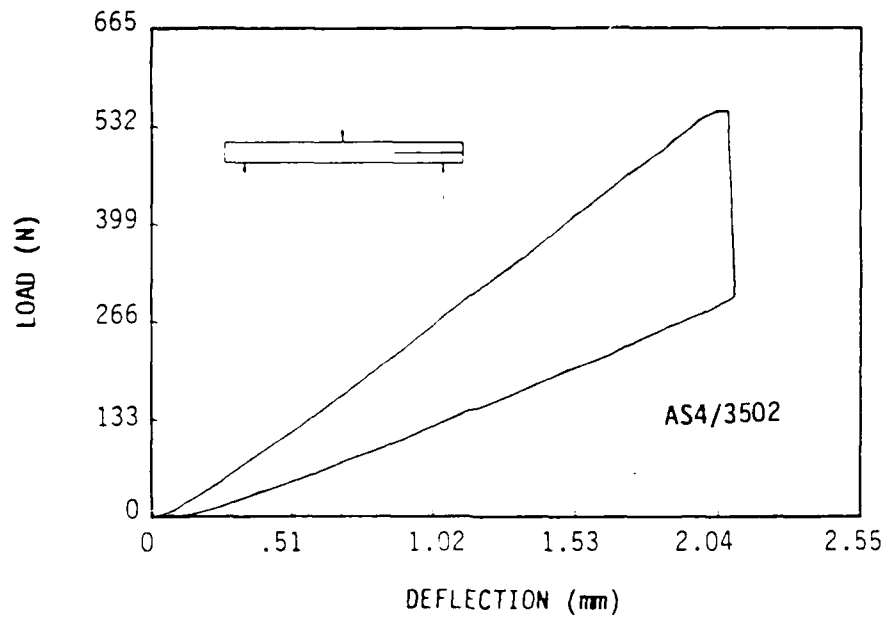


Figure 51. Typical mode II delamination load/deflection record of AS4/3502 using the end-notched flexure test.

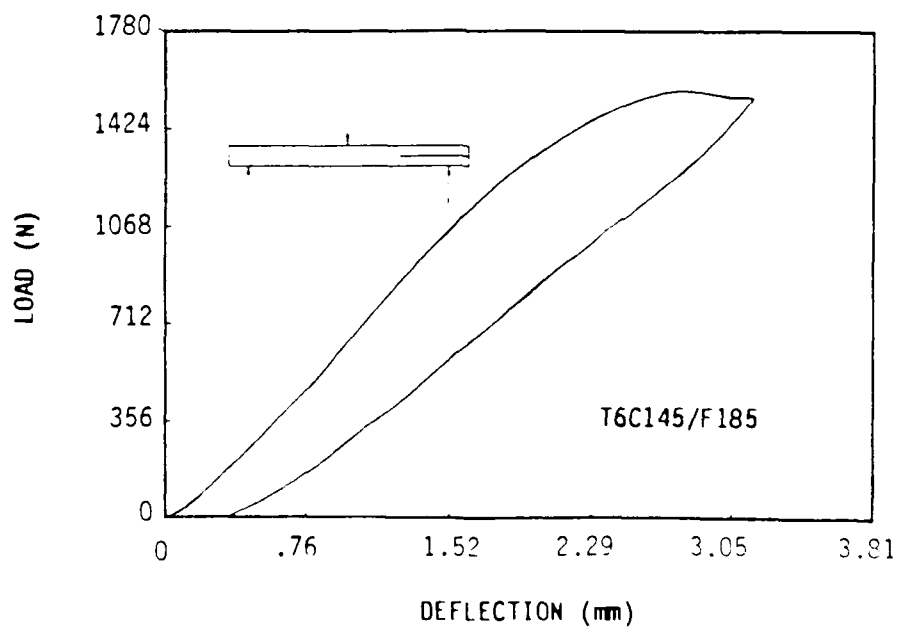


Figure 52. Typical mode II delamination load deflection record of T6C145/F185 using the end-notched flexure test.

crack growth. These values were between 1390 and 1632 N. The curve also indicates inelastic behavior of the material (i.e., the unload curve did not return to the origin). Therefore, the assumptions of the test have been violated. It should be noted that the load-deflection curves at different crack lengths used for the compliance calibration also showed non-linear behavior. However, the energy release rate obtained by the area method gives a better approximation of the critical energy release rate G_{IIC} because at least the geometrically non-linear behavior of the specimen is taken into consideration by this method. The calculated average G_{IIC} of 2400 J/m^2 should be considered an upper bound estimate of the mode II critical energy release rate of T6C145/F185 because the inelastic behavior is not accounted for in this analysis. A J-integral approach to be discussed in the next section has been developed to obtain a more meaningful measure of the mode II delamination fracture toughness of this system.

End-Loaded Split Laminate (ELS) Test Results--The ELS test results are seen in Table 3. Method I corresponds to G_{IIC} calculated using Eq. 7 and with E_{11} calculated from Eq. 8 and test data. Method II corresponds to the area method (Eq. 9). An average E_{11} of 125.5 GPa for AS4/3502 and 109.9 GPa for T6C145/F185 were calculated. Figure 53 shows a typical load-deflection curve obtained by testing one of the AS4/3502 specimens. As seen in this figure, unstable crack growth is observed for the first crack extension. This is

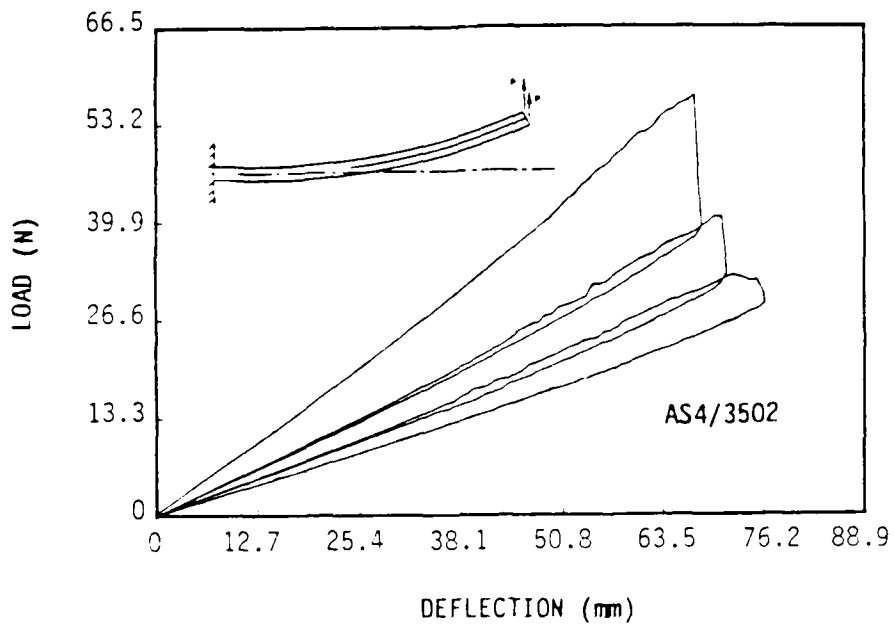


Figure 53. Typical mode II delamination load/deflection record of AS4/3502 using the end-loaded split laminate test.

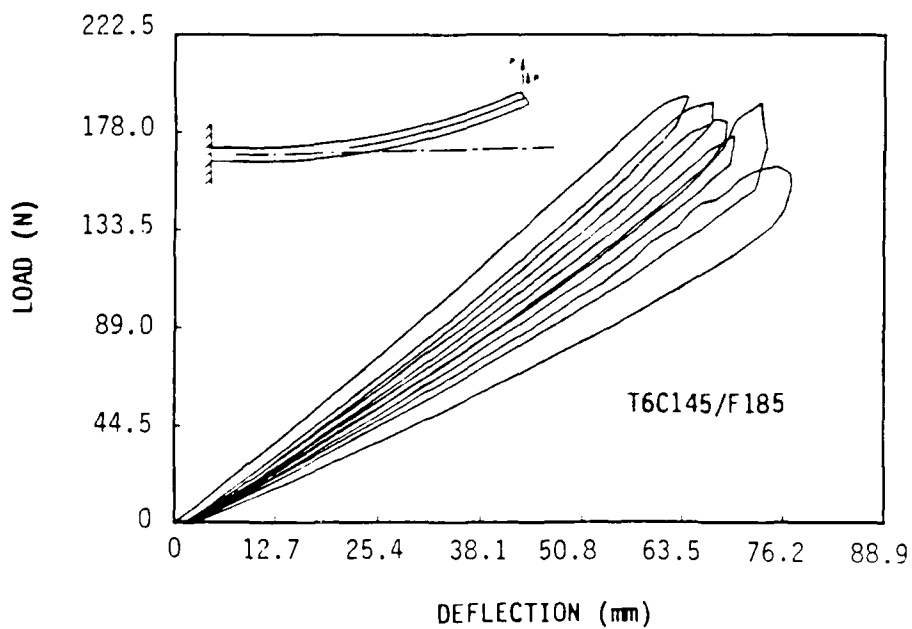


Figure 54. Typical mode II delamination load/deflection record of T6C145/F185 using the end-loaded split laminate test.

Table 3.- End-loaded Split Laminate (ELS) Results.

Material	Specimen	G_{IIc} (J/m ²)	
		I	II
AS4/3502	1	630	595
		613	560
		613	543
		648	543
	2	595	525
		595	525
		508	508
	Av.	595	545
T6C145/F185	1	*	
		1645	2153
		2030	2030
		2275	2415
		2275	2363
	2	2188	1873
		2275	2118
		1960	2643
		2223	2240
		2415	2083
		2590	2170
		2713	2765
		2800	2328
	Av.	2275	2260

* Nonlinearity is too great to satisfy linear beam theory assumptions implicit in the approach

surprising, since an a/L ratio of at least 0.55 was introduced to all ELS specimens during the mode I precracking done prior to mode II testing; according to stability analysis, crack growth should have been stable³⁶. This is probably the result of the additional energy storage in the fixtures. Also, the linear beam theory used in the stability analysis did not take into account the nonlinearity observed, especially at displacements greater than 50.8 mm. An average G_{IIC} of 595 J/m² (method I) and 543 J/m² (method II) were found for AS4/3502. These results are within 10 percent of each other. However, considerable scatter was observed in the G_{IIC} data from each specimen (Table 3). This scatter is believed to be the result of the significant amount of error involved in measuring crack locations which is done by monitoring the crack as it propagates. In contrast, this scatter was very small in the ENF results. A typical load-deflection curve for T6C145/F185 is seen in Fig. 54. Stable crack growth is observed for all load/unload loops. This is evidenced by the smooth decrease in loading rate followed by a gradual decrease in load. It should be noted that it is not known when crack growth started during this process, which was common to both types of mode II tests for this material. At least some of the observed nonlinear behavior is due to inelasticity since the curves fail to return to the origin as the specimen is unloaded. Nonlinear behavior due to large displacements and rotations is also observed for deflections greater than 50.8 mm.

The average mode II energy release rate values for T6C145/F185 were found to be 2275 J/m^2 (method I) and 2260 J/m^2 (method II). However, a systematic or monotonic increase in G_{IIc} for method I can be observed throughout the test. This is the result of the nonlinearity in the load/deflection curve seen in Fig. 54. Although this nonlinearity is less severe than the nonlinearity observed for this material tested using the ENF test, it is sufficient to invalidate the data analysis done using linear beam theory (method I). The scatter of the results for method II (area method) is more random and is associated with the experimental difficulty in obtaining a precise measure of the change in crack length. However, these values are an overestimation of G_{IIc} because the curves did not return to the origin as the specimens were unloaded. Thus, some far field energy dissipation is unavoidably included in G_{IIc} .

A comparison of the results predicted using both test configurations indicate that for AS4/3502 (a brittle composite) similar and valid results were obtained for the ENF and ELS tests. In contrast, for T6C145/F185 neither the ENF nor the ELS tests give valid results, since the assumptions associated with each test method were violated. Therefore, in order to properly characterize the fracture toughness of this material and tougher graphite/epoxy composites in general, an analysis which allows for material and geometric nonlinearity such as a J-integral analysis is needed. It is worth noting that similar results were

obtained for the ENF and ELS when data was analysed using the area method. However, both results should be considered upper bounds of the mode II critical energy release rate of the material. In the next subsection, an analysis for J_{IIC} will be presented.

4.4.2.2 J-Integral Approach for Mode II Delamination Fracture Toughness Evaluation

Most of the current analyses to measure delamination resistance in composites are elastic analyses based on linear fracture mechanics (i.e. energy release rate). However, these analyses may become inappropriate when the inelastic material behavior observed in the delamination process is sufficient to give nonlinear behavior in the measured load-displacement curves and/or permanent deformation on unloading. This inelastic behavior may be due to microcracking or extensive resin deformation. In fact, Corleto and Bradley have noted that under mode II loading, composite systems with tough matrices show considerable non-linear behavior due to extensive microcracking and yielding of the resin prior to macroscopic delamination crack extension³⁷.

Successful fracture characterization of metals with inelastic behavior (i.e. small scale yielding) has been done by means of Rice's path-independent J integral³⁸. The use of this parameter as a fracture criterion has been based on a consideration of the Hutchinson-Rice-Rosengren (HRR)³⁹⁻⁴⁰

crack tip model where the stress and strain fields ahead of a crack may be characterized in intensity by J . McClintock⁴¹ has further demonstrated that for deformation plasticity theory a singularity in r (the radial distance from the crack tip) exists which is strongly related to the J integral. However, the path independence of this integral may not hold true when variable damage develops as a result of unloading. Therefore, the J integral is limited to linear, nonlinear elastic, and elastic-plastic behavior under monotonic loading. Alternatively, the critical value of J may be thought of as giving the energy release rate required for crack growth for nonlinear elastic materials.

In the case of fiber reinforced composite materials, the use of the J integral as a failure criterion has been very limited and confined to experimental approaches (i.e., indirectly measuring J from load-displacement data via its energy interpretation⁴²⁻⁴⁵). However, Agarwal et.al⁴², have shown that for short fiber composites, the stress-strain behavior of the composite may be closely approximated by the Ramberg-Osgood relation (i.e., $\sigma_{ij} = \sigma_1(\epsilon_p)^n$), justifying the use of the J integral as a fracture criterion for short fiber reinforced composite materials. Furthermore, they argued that since the local unloading of the matrix resulting from microcracking and debonding at the interface does not necessarily also occur in the fibers, this observed crack tip damage does not lead to material unloading to the same extent as a crack extension does in metals. Therefore, although the

requirement of no unloading is not completely met, its influence will be quite small for some applications, and thus, may be ignored for some applications.

In a recent investigation, an additional approach for characterizing fracture of inelastic composite materials has been made by Schapery⁴⁶. He uses strain-energy like potentials to characterize material response (i.e., $\sigma_{ij} = \partial W / \partial \epsilon_{ij}$). Theoretical support for the existence of these potentials is given by the thermodynamics of reversible processes. The potentials are free energy and internal energy for isothermal and adiabatic processes, respectively. Schapery argues that if a potential of this nature exists, it is often possible to use Rice's J integral theory³⁸ to simplify fracture analysis.

In the present analysis, an approach similar to Schapery's is proposed to evaluate the mode II fracture toughness of composite laminates with inelastic behavior. J is defined for the end-loaded split laminate test (mode II) specimen and the implications of the analysis reviewed. Also, some limited assessment of the proposed method has been done. A more complete evaluation of the utility of J_{II} to evaluate mode II delamination fracture is being undertaken in the new contract.

4.4.2.2.1 Theoretical Model

Figure 5 shows the unsymmetric end-loaded split laminate test used to determine the critical energy release

rate G_{IIc} for the mode II delamination of fiber-reinforced composite materials. The test consists of loading an split laminate at the cracked end, with the opposite end fixed to achieve a mode II stress state at the crack tip. As has been previously noted, inelastic behavior has been observed for composite systems with tough matrices²⁹. Further, inelastic behavior is expected if a significant volume fraction of off angle fibers are present in the layup. This inelastic behavior then invalidates the standard elastic methods used to measure fracture toughness. In order to develop an analysis where inelastic behavior is accounted for, consider Rice's J integral, as extended to crack growth in inelastic media with large deformation by Schapery⁴⁷.

$$J = \int_{C_1} [w_0 dx_2 - T_i (\partial u_i / \partial x_1)] dL \quad (10)$$

where w_0 is the work potential density, T_i the tractions along C_1 , and u_i the displacements. A rigorous proof and support for the use of work potentials to characterize the behavior of materials and structures with damage is given elsewhere. Figure 56 shows the counterclockwise integration path C_1 . The contribution to J from this contour comes from the left and right vertical segments only, since for the outer horizontal segments, $dx_2 = T_1 = T_2 = 0$ which also holds true for the inner vertical segments (crack surfaces) if friction is assumed to be negligible between the crack surfaces. Further, assuming small strains and that the left vertical segment experiences small rotations and right

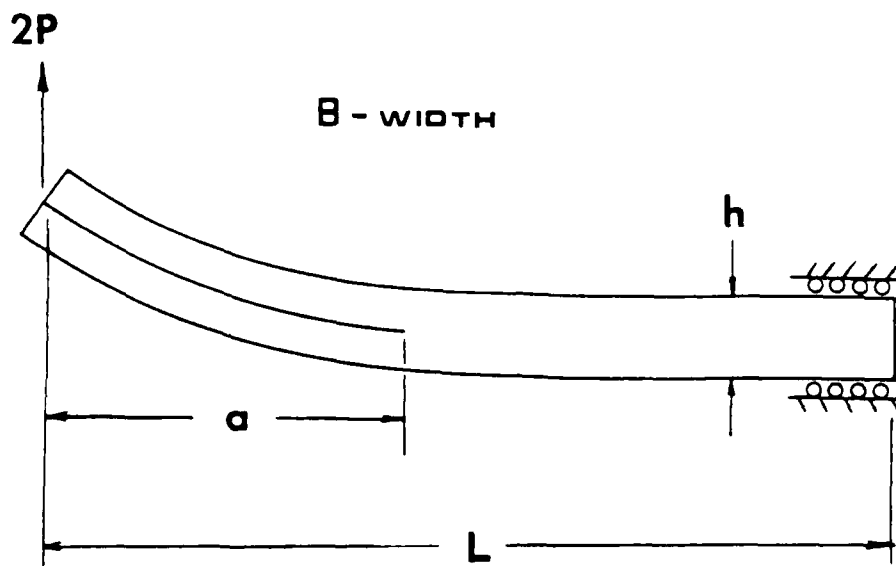


Figure 55. End-loaded split laminate test used for mode II delamination of composites.

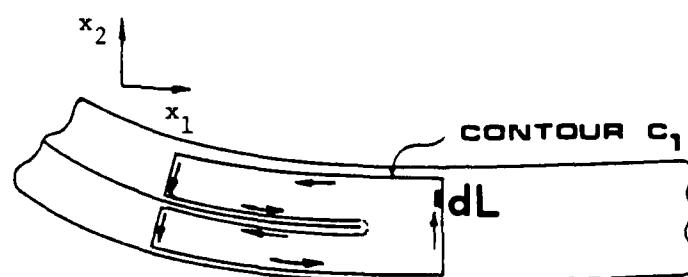


Figure 56. Contour used to evaluate J_{II} for the end-loaded split laminate test.

vertical segment is evaluated far enough away from the crack tip and fixed end as to avoid nonuniformity in the stress field, using small rotation theory

$$J_{II} = \frac{2}{B} \left[\int_0^M k \, dM - P \frac{du_2}{dx_1} \right]_L - \frac{1}{B} \left[\int_0^M k \, dM - 2P \frac{du_2}{dx_1} \right]_R \quad (11)$$

where M and du_2/dx_1 are the moment and slope, respectively. The subscript L and R indicate evaluation of the integrals corresponding to the left and right vertical segments, respectively. B is the width of the specimen. If $k = d^2u_2/dx_1^2$ is used to obtain the slope, Equation 11 reduces to

$$J_{II} = \frac{1}{B} \left[2 \int_0^{M_a} k \, dM \right]_L - \left[\int_0^{M_a} k \, dM \right]_R \quad (12)$$

where M_a corresponds to the moment at the crack tip. (See Appendix I for a detailed derivation of this equation). Equation 12 indicates that the result is independent of the location of the segments and both are equal to that evaluated at the crack tip. This path independence will be met as long as the crack propagates at a constant maximum moment M_a . For a long laminate that is initially homogenous in the x_1 direction, constant M_a indicates that the stress and strain state in the neighborhood of the crack tip is independent of crack length (self similar growth conditions). Under this condition, the energy release rate G_{II} can be shown to be equal to J_{II} calculated using Eq. 12. Further, since small

rotations are only required from the fixed end up to the neighborhood of the crack tip, Eq. 12 will also be valid for large rotations at the loaded end. See Ref. 46 for further explanation of the ability of this type of analysis to characterize fracture.

Equation 12 can be shown to reduce to G_{II} as given by linear beam theory by substituting $k=M/EI$, and noting that $M=M_a=Pa$ for the left segment, $M=M_a=2Pa$ for the right segment, and $I_L=I_R/8^{48}$. This gives,

$$J_{II} = \frac{6 P^2 a^2}{B E I_R} \quad (13)$$

where I_R is the moment of inertia of the uncracked segment of the beam.

4.4.2.2.2 Experimental Methods

Limited experimental verification of J_{II} as given by Eq. 12 has been done with a 1.0 x .121 in. x 8.0 in. and a 1.0 in. x .188 in. x 6.0 in. split laminate of unidirectional AS4/3502 and T6T145/F185 composites, respectively. The former one has a brittle matrix and the latter one a tough matrix. Typical mode II delamination tests have been performed on both composite systems, carefully recording the moment arm (distance from load line to crack tip) and load at onset of crack growth. Moment-curvature relationships (e.g., Fig. 57) for these composites have been obtained with beams having one-half (cracked portion) and full lay-up (uncracked

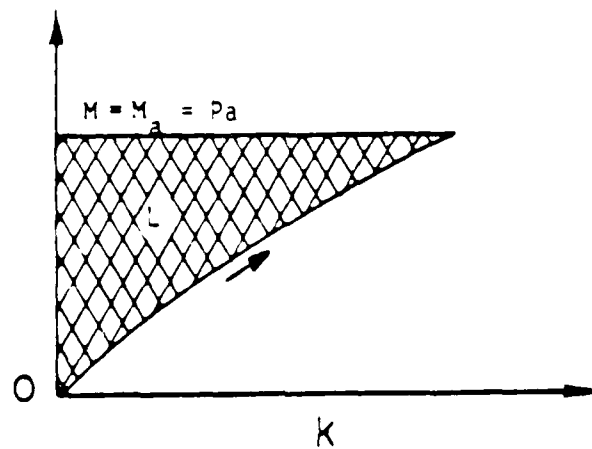
portion) of the split laminates tested in mode II delamination. Finally, J_{II} calculations were obtained with

$$J_{II} = \frac{I}{B} [2 (\text{shaded area L}) - (\text{shaded area R})] \quad (14)$$

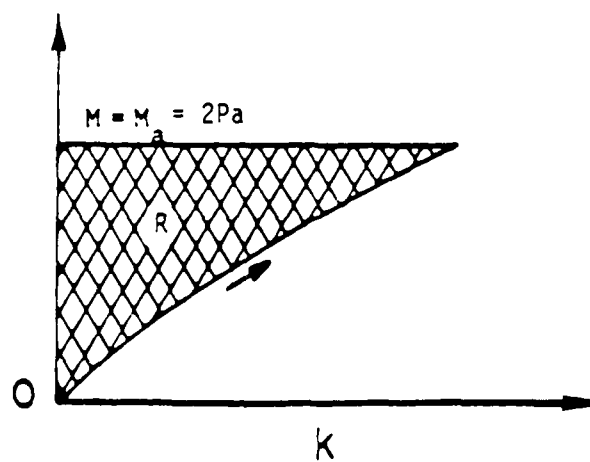
where shaded area L and shaded area R are shown in Fig. 57.

4.4.2.2.3 RESULTS AND DISCUSSION

Figure 58 shows the load/deflection curves obtained for the delamination tests. Stable as well as unstable crack growth occurred on both systems. Figures 59 and 60 correspond to the moment-curvature relationships. For both systems these relationships were linear. Figures 61 and 62 show the J_{IIc} and G_{IIc} values measured, plotted as a function of crack length for AS4/3502 and T6T145/F185, respectively. Also, Tables 4 and 5 show the overall results obtained during the tests. An average J_{IIc} of 2.5 lb/in and a G_{IIc} of 2.7 lb/in for AS4/3502 and J_{IIc} of 12.0 lb/in and G_{IIc} . In the case of AS4/3502 the difference between J and G amounts to no more than 10 percent. This small discrepancy can be explained by carefully observing the load/deflection record in Figure 58a. Notice how the curves consistently have a steeper slope as the load increases indicating a stiffening effect. Obviously, G_{II} which is based on linear beam theory will measure higher values of the energy release rate. This stiffening effect is not well understood yet but in this case, it seems that it is not due to large rotations and



(a) Moment-curvature for loading of left segment of split laminate beam (cracked)



(b) Moment-curvature for loading of right segment of split laminate beam (uncracked)

Figure 57. Moment-curvature test needed to experimentally evaluate J_{II} .

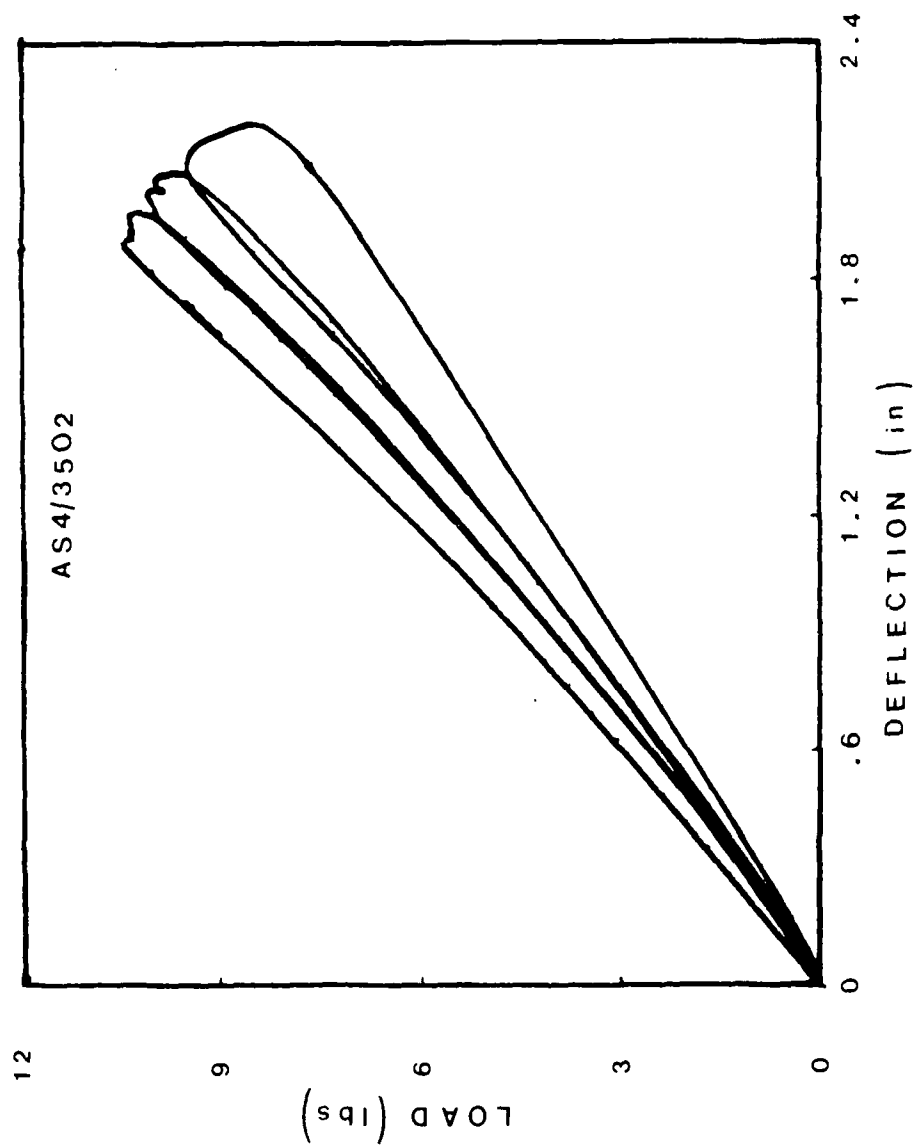


Figure 58. Typical mode II delamination load/deflection record of unidirectional AS4/3502 and T6T145/F185 composites.

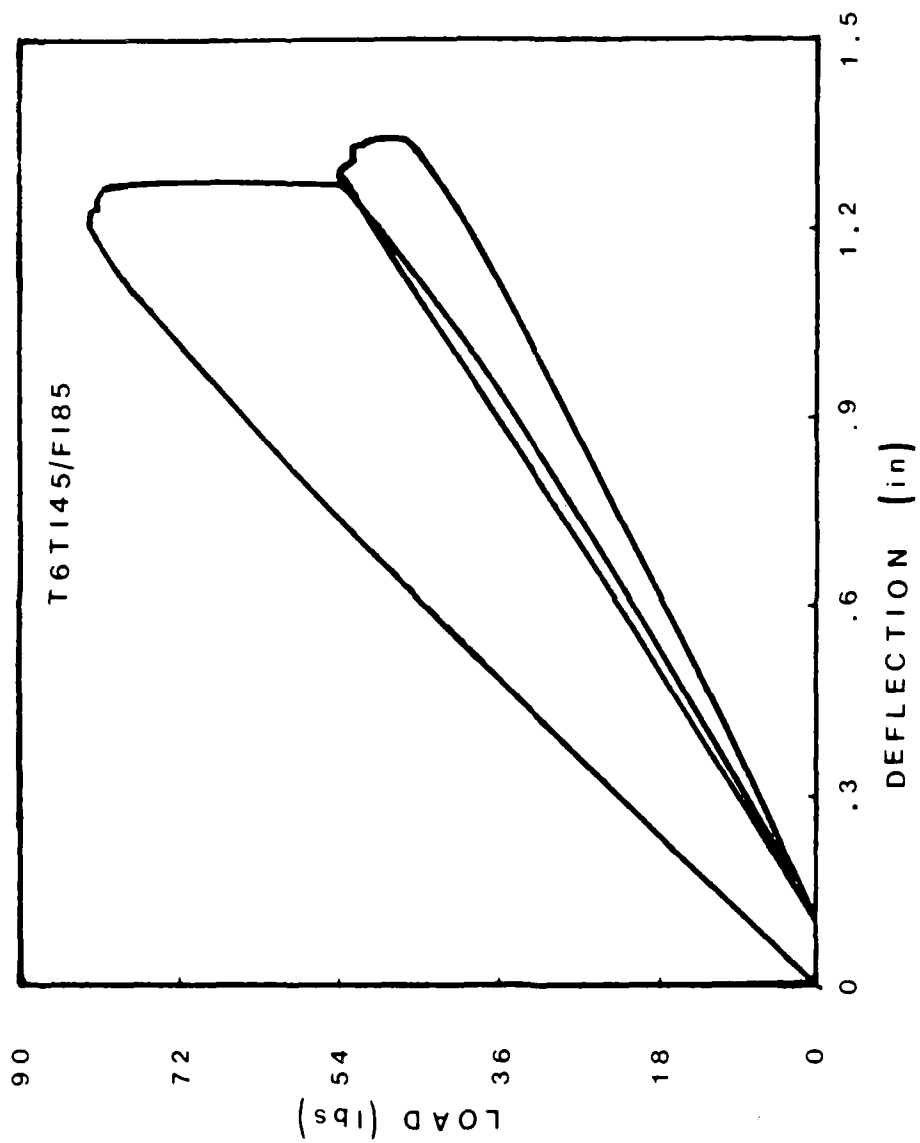


Figure 58. (Continued).

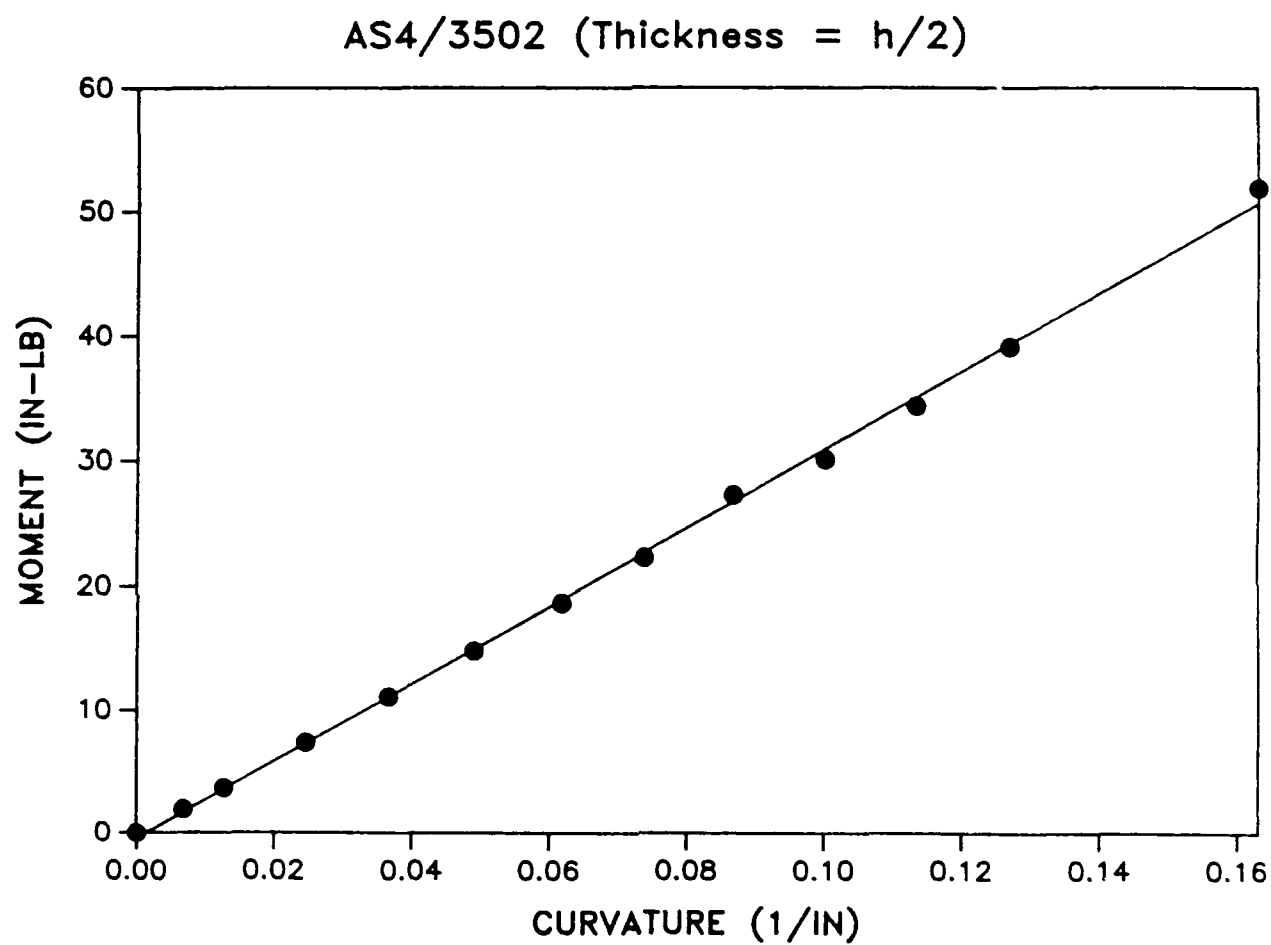


Figure 59a. Moment-curvature relationship corresponding to the cracked portion of unidirectional AS4/3502 composite.

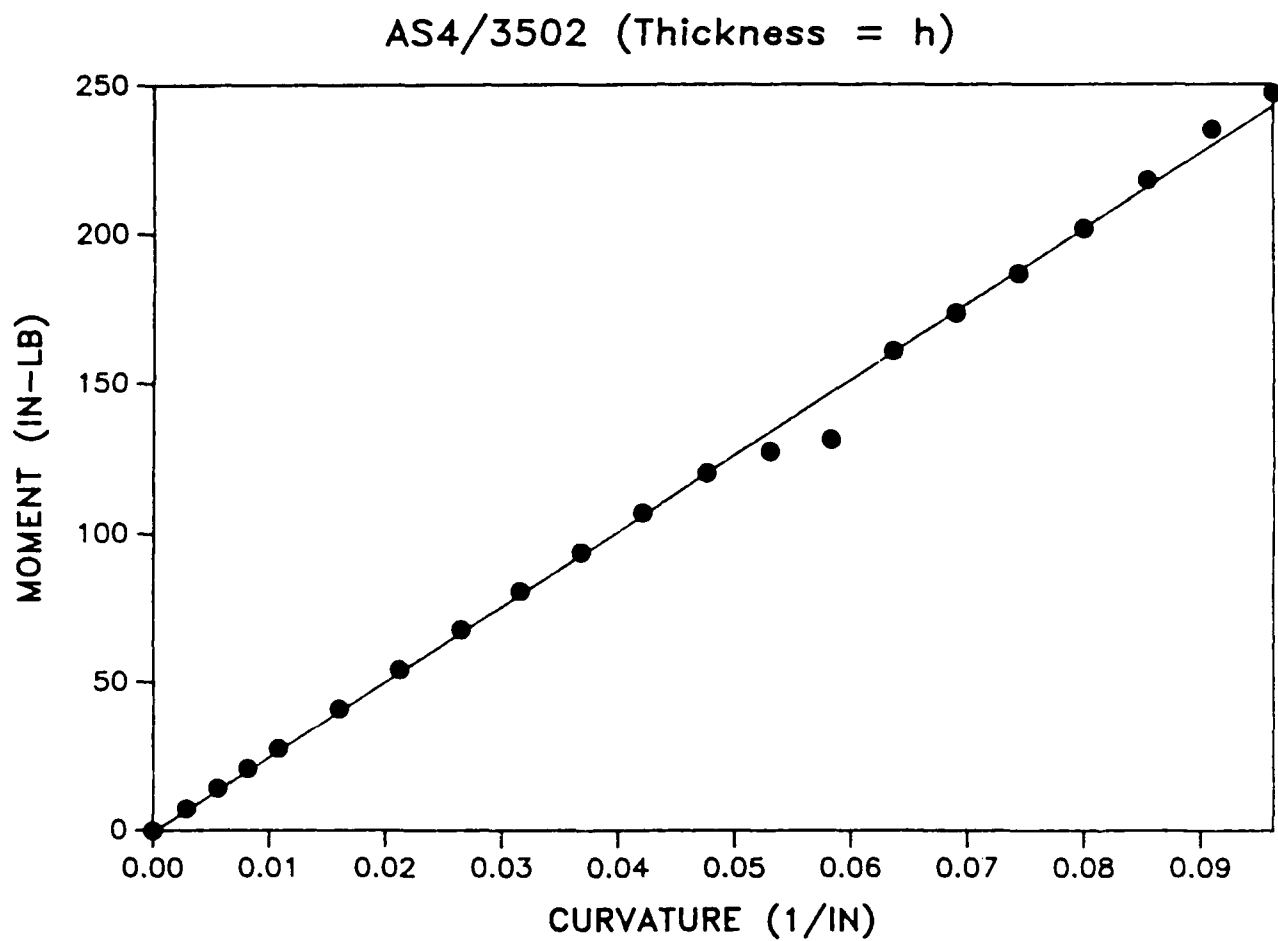


Figure 59b. Moment-curvature relationship corresponding to the uncracked portion of unidirectional AS4/3502 composite.

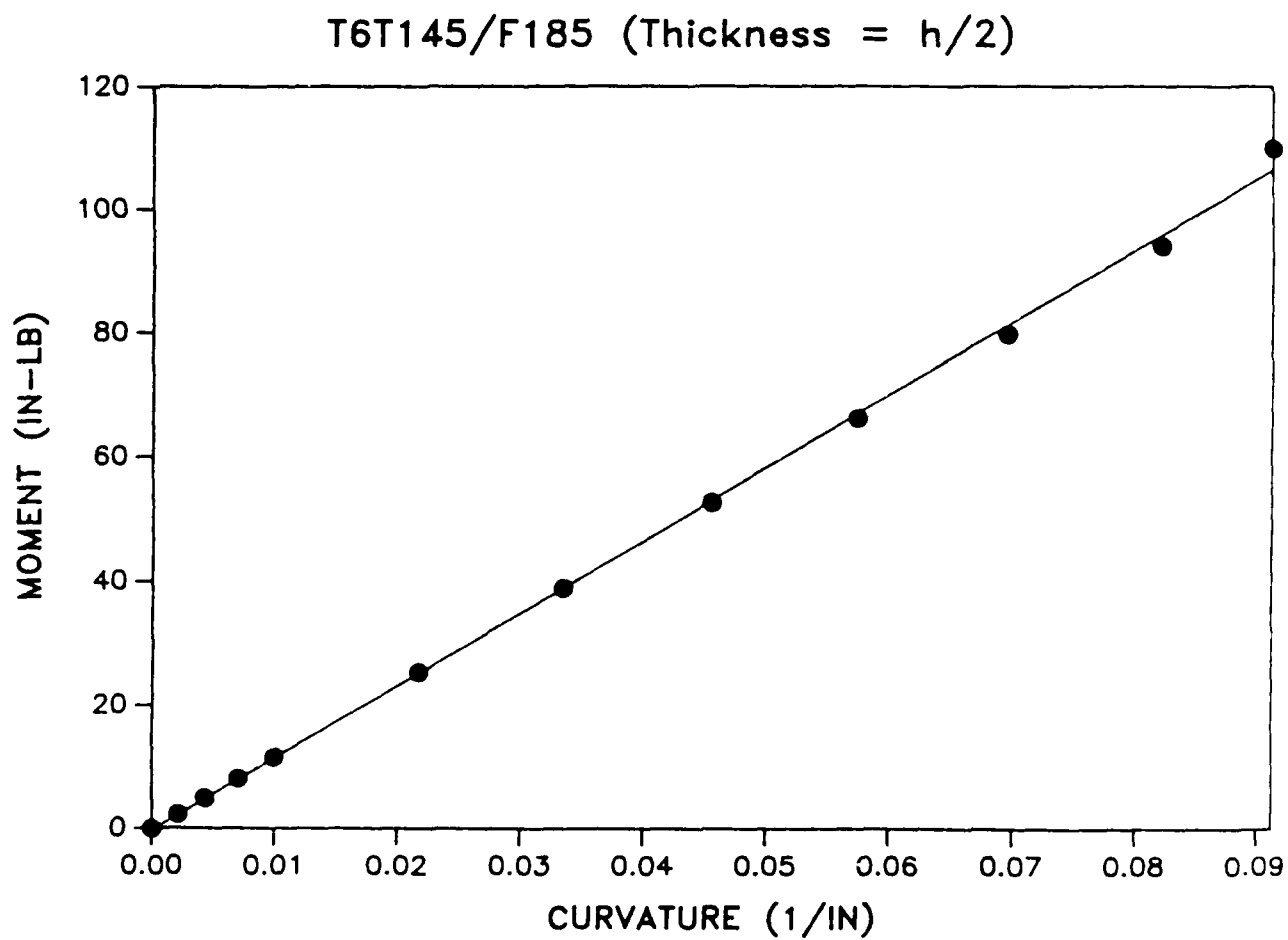


Figure 60a. Moment-curvature relationship corresponding to the cracked portion of unidirectional T6T145/F185 composite.

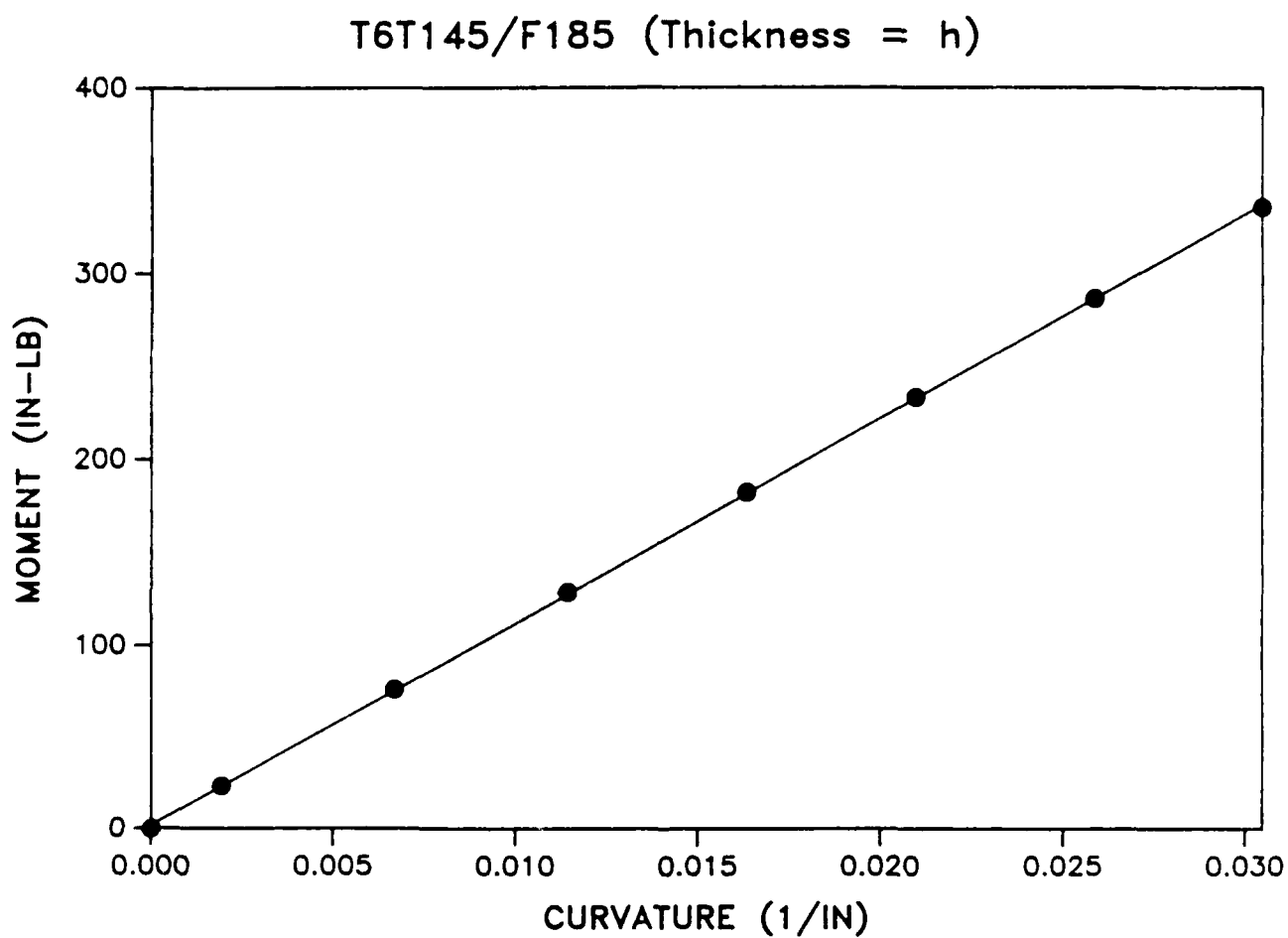


Figure 60b. Moment-curvature relationship corresponding to the uncracked portion of unidirectional T6T145/F185 composite.

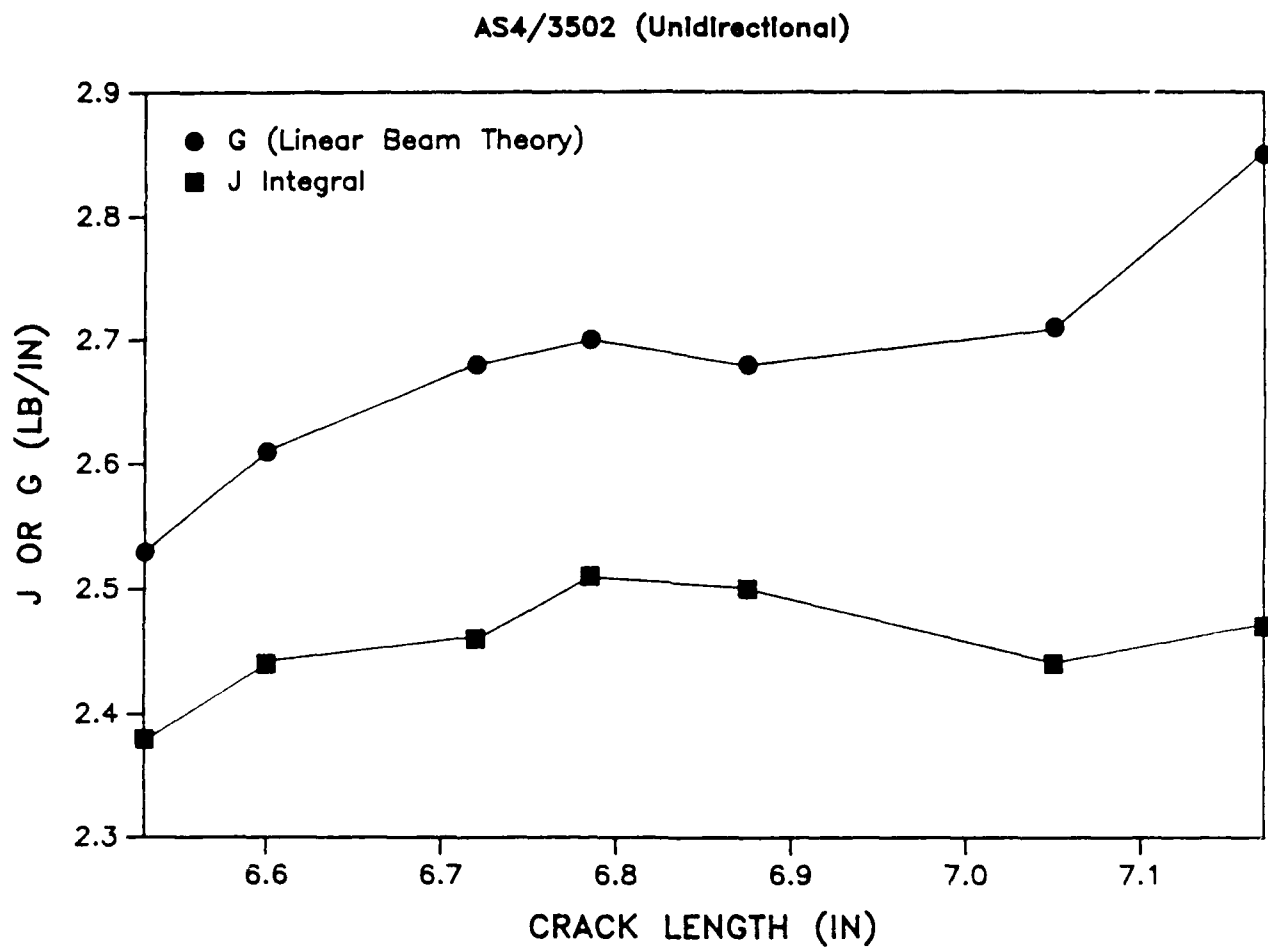


Figure 61. Mode II fracture toughness as a function of crack length of unidirectional AS4/3502 composite.

deflections since the a/L ratios for this test are within the linear regime. Instead, friction between the cracked surfaces can be a factor contributing to the problem, especially as the crack grows. If this is the case, the proposed J_{II} will not take into consideration these friction effects, and thus, will give an artificially high indication of the energy required per unit area of crack growth.

For T6T145/F185, G_{IIC} is at least 20 to 25% higher than J_{IIC} . Observing the load/deflection record (Fig. 58b) for this system during delamination, it can be seen that the curves failed to return to the origin upon unloading, indicating inelastic deformation during the test. It is very clear that G_{IIC} will yield a overestimate of the critical energy release rate because some energy was dissipated in the far field, but was included in the energy associated with creating an new surface. Corleto and Bradley have noted that the inelasticity for these composite systems with tough matrices is the result of considerable matrix deformation and yielding ahead of the crack tip (long damage process zone)³⁷. In contrast, J_{IIC} appears to successfully measure the fracture toughness of this material as evidenced by the lower J_{IIC} values measured. Further, the small scatter and consistency found in the measured J_{IIC} values indicate a constant crack tip moment when the crack was growing. Therefore, the path independence and self similar growth conditions assumed by the analysis were not violated.

Finally, even these this limited results are

Table 4. Mode II Fracture Toughness of Unidirectional AS4/3502 Composite.

Crack Length (in)	Moment Arm (in)	P_c	M_c (in-lb)	M_u (in-lb)	G_{IIc} (lb/in)	J_{IIc}
6.53	6.4	9.9	31.68	63.36	2.53	2.38
6.6	6.45	9.95	32.09	64.18	2.61	2.44
6.72	6.5	9.9	32.18	64.35	2.68	2.46
6.79	6.6	9.86	32.54	65.08	2.7	2.51
6.88	6.7	9.69	32.46	64.92	2.68	2.50
7.05	6.8	9.5	32.1	64.2	2.71	2.44
7.17	6.75	9.57	32.3	64.6	2.85	2.47
Avg.					2.68	2.46

P_c - Critical load.

M_u - Crack tip moment applied to uncracked portion of split laminate.

M_c - Crack tip moment applied to each of the cracked portions of split laminate

Table 5. Mode II Fracture Toughness of Unidirectional T6T145/F185 Composite.

Crack Length (in)	Moment Arm (in)	P_c (lb)	M_c (in-lb)	M_u (in-lb)	G_{IIc} (lb/in)	J_{IIc}
3.3	3.24	81.68	132.24	264.48	14.45	11.66
3.5	3.44	79.61	136.91	273.82	15.45	12.45
5.18	5.05	52.6	132.81	265.63	14.78	11.76
5.33	5.3	50.6	134.09	268.18	14.31	11.99
5.55	5.48	49.	134.26	268.52	14.35	12.02
Avg.					14.7	12.

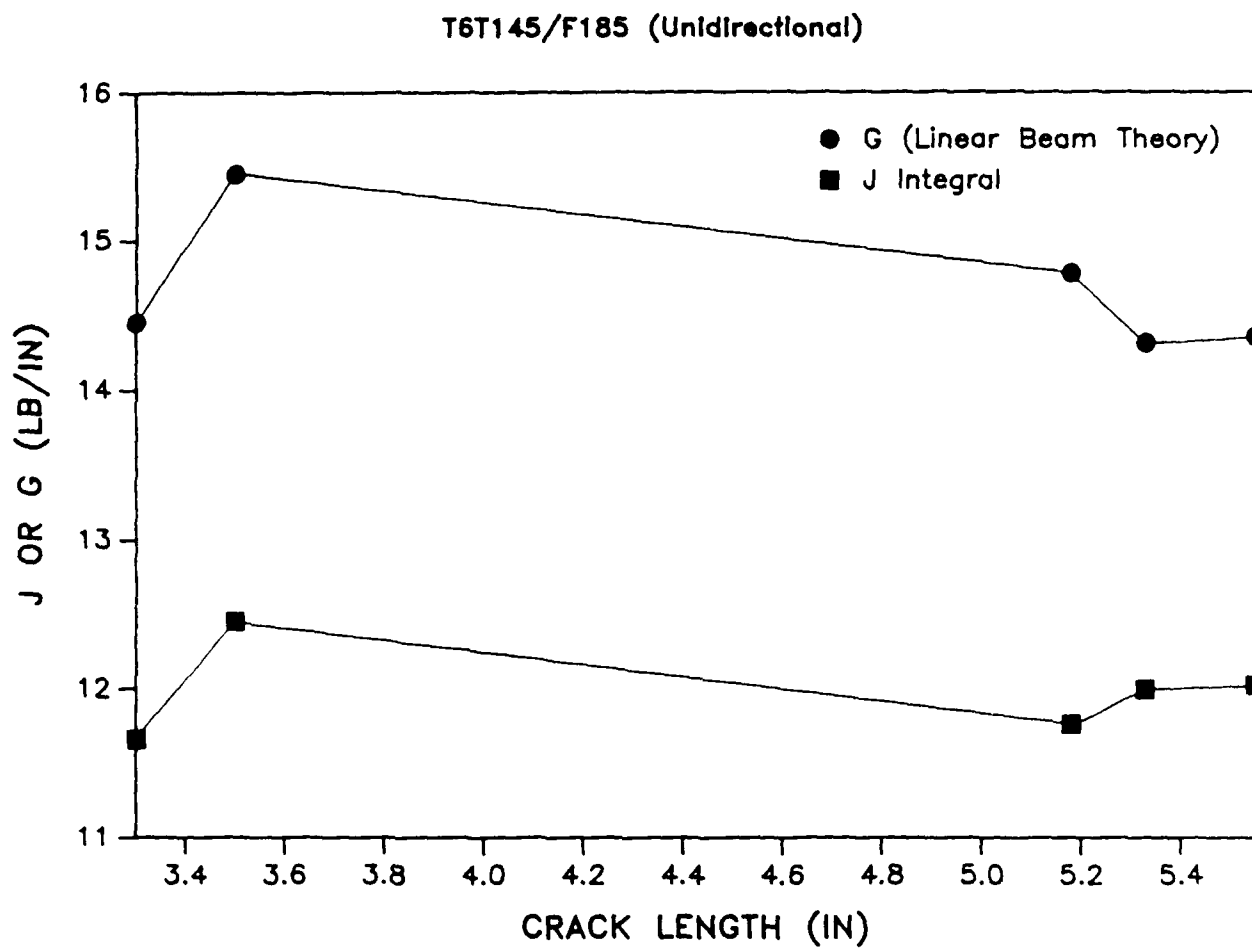


Figure 62. Mode II fracture toughness as a function of crack length of unidirectional T6T145/F185 composite.

encouraging, a complete assessment of this analysis will require testing composites with different extents of damage induced by layups dominated by off axis fiber orientations. Further, the effects of variable ply thickness and specimen widths on J should be assessed.

4.4.2.3 MIXED MODE DELAMINATION

Using a asymmetrically loaded split laminate (see Fig. 63), one can achieve a variety of combinations of mode I and mode II loading. The total energy release rate is given by the sum of the mode I and mode II values, $G_{IC} + G_{IIc}$, calculated using the relationships:

$$G_T = G_I + G_{II} = \frac{(P_S L_C)^2}{BEI} + \frac{3(P_A L_C)^2}{4BEI} \quad (15)$$

where I is the moment of inertia of one leg of the split portion of the laminate, $P_S = (P_U + P_L)/2$ and $P_A = (P_U - P_L)/2$. For composites made from brittle resins, the G_T is seen to increase with increasing percentage of mode II loading, especially above about 40% mode II. By contrast, the G_T for a composite made from a ductile resin system is found to have very little dependence on the % G_{II} used in achieving delamination. Typical results have previously been presented in Fig. 12 (section 4.1) with additional results provided in Table 4. The reason for this behavior has previously been explained in detail in section 4.1.

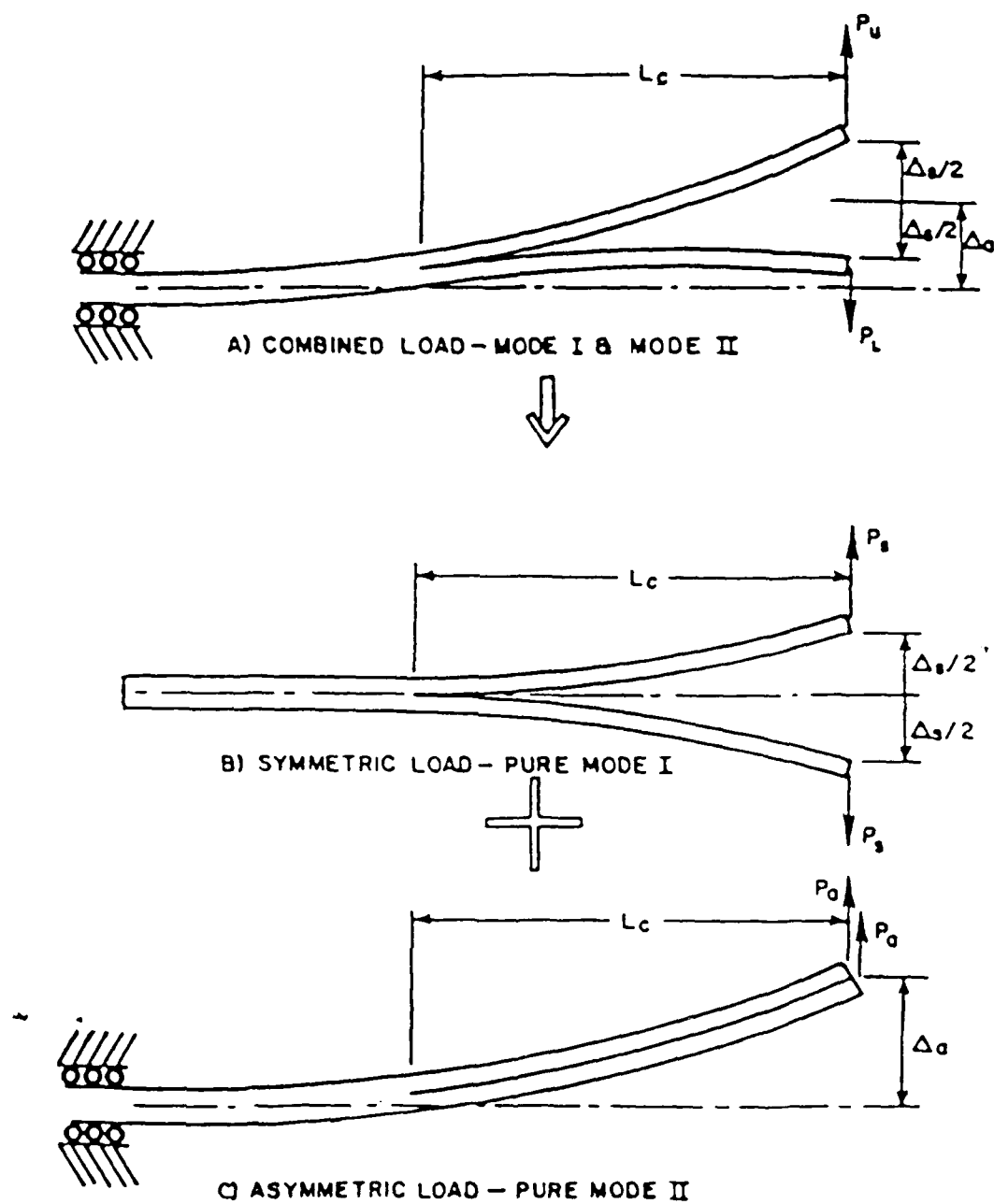


Figure 63

Schematic showing how asymmetric loading of split laminate can introduce a mixed mode I/mode II state of stress at the crack tip.

4.5 FRACTOGRAPHY AND FAILURE ANALYSIS

There has been considerable confusion over whether it is possible to determine crack growth direction in an unambiguous way from the direction the hackles point. The results of the in-situ observations in this study clearly indicate that hackles can point either in the direction of crack growth or opposite to the direction of crack growth, as previously seen in Fig. 9. Furthermore, the development of damage ahead of the crack tip gives some serious question about how reliable some of the surface features may be in determining crack growth direction. Unless all of the damage ahead of the crack tip develops in a very consistent way, using the artifacts that result from this damage can be misleading in fractographic interpretation. A great deal more work needs to be done to establish that such a regular pattern is present in the development of the damage zone that unambiguous information concerning the crack growth direction can be inferred from fracture surface details. More details in this regard are contained in papers 5.4 and 5.6 section 5.0 of this report.

REFERENCES

1. Standard Test Method for Plane-Strain Fracture Toughness of Metallic Materials, American Society for Testing and Materials Test E-399-81, Philadelphia, 1981.
2. Bradley, W.L. and Cohen, R.N., "Matrix Deformation and Fracture in Graphite Reinforced Epoxies", Delamination and Debonding of Materials ASTM STP 876, W.S. Johnson, Ed., American Society for Testing and Materials, Philadelphia, 1985, pp. 389-410.
3. Williams, D.R., Davidson, D.L., and Lankford, L., "Fatigue-crack-tip Plastic Strains by the Stereoimaging Technique", Experimental Mechanics, Vol. 20, No. 4, April 1980.
4. Davidson, D.L., Lankford, L., "Fatigue Crack Tip Strains in 7075 Aluminum Alloy by Stereoimaging and Their Use in Crack Growth Models", Special Technical Publication 811, ASTM, 1983.
5. Davidson, D.L., "The Observation and Measurement of Displacements and Strains by Stereoimaging", SEM 1979, 2, SEM, Inc., AMF, O'Hare, IL.
6. Avery, and Berlin, Interpretation of Aerial Photography, fourth addition, Burgess, 1985.
7. Barsoum, R.S., "On the Use of Isoparametric Finite Elements in Linear Fracture Mechanics", International Journal for Numerical Methods in Engineering, Vol. 10, pp. 25-27, 1976.

8. Henriksen, M. Engineering Department, Colorado School of Mines Golden, Colorado, 80301.
9. Hercules Manual of AS4/3502 Graphite/Epoxy, Hercules Corporation, Magma, Utah.
10. Vanderkley, P.S., "Mode I - Mode II Delamination Fracture Toughness of a Unidirectional Graphite/Epoxy Composite a M.S. Thesis, Texas A&M University, College Station, Texas, 1981.
11. Jordan, W.M., and Bradley, W.L., "Effect of Resin Content on the Delamination Fracture Behavior of Graphite Epoxy Laminates", presented at the 29th National SAMPE Symposium, April 3-5, 1984, and appearing in the proceedings entitled: Technology Vectors, pp. 1422-1437.
12. Hunston, D.L., "Composite Interlaminar Fracture: Effect of Matrix Fracture Energy", Composites Technology Review, vol. 6, 1984, pp. 176-180.
13. O'Brien, T.K., Johnston, N.J., Morris, D.H., and Simonds, R.A., "A Simple Test for the Interlaminar Fracture Toughness of Composites", SAMPE Journal, July/August 1982, pp. 8-15.
14. Wang, S.S., and Mandell, J.F., "Analysis of Delamination in Unidirectional and Crossplied Fiber Composites Containing Surface Cracks", NASA Technical Report NASA-CR-13524, May 1977.
15. Russell, A.J., and Street, K.N., "Moisture and Temperature Effects on the Mixed-Mode Delamination

- Fracture of Unidirectional Graphite/Epoxy", ASTM STP 876, 1985, pp. 349-370.
16. Whitney, J.M., Browning, C.E., and Hoogsteden, W., "A Double Cantilever Beam Test for Characterizing Mode I Delamination of Composite Materials", Journal of Reinforced Plastics and Composites, vol. 1, Oct. 1982, pp. 297-313.
 17. Devitt, D.F., Schapery, R.A., and Bradley, W.L., "A Method for Determining the Mode I Delamination Toughness of Elastic and Viscoelastic Composite Materials", Journal of Composite Materials, vol. 14, Oct., 1980, pp. 270-285.
 18. Weatherby, J.R., "Evaluation of Energy Release Rates in Unidirectional Double Cantilevered Beam Fracture Toughness Specimens", Mechanics and Materials Center Report MM 4665-82-9, Texas A&M University, December 1982.
 19. Wang, S.S., Suemasu, H., and Zahlan, N.M., "Interlaminar Fracture of Random Short-Fiber SMC Composite," Journal of Composite Materials, vol. 18, Novol. 1984, pp. 574-594.
 20. Keary, P.E., Ilcewicz, L.B., Shaar, C., and Trostle, J., "Mode I Interlaminar Fracture Toughness of Composites Using Slender Double Cantilever Beam Specimens", Journal of Composite Materials, vol. 19, March 1985, pp. 154-177.
 21. Nicholls, D.J., and Gallagher, J.P., "Determination of

- G_{IC} in Angle Ply Composites Using a Cantilever Beam Test Method", Journal of Reinforced Plastics and Composites, vol. 2, Jan. 1983, pp. 2-17.
22. Chai, H., "The Characterization of Mode I Delamination Failure in Nonwoven, Multidirectional Laminates", Composites, vol. 15, Oct. 1984, pp. 277-290.
23. Pipes, R.B., and Pagano, N.J., "Interlaminar Stresses in Composite Laminates Under Uniform Axial Extension", Journal of Composite Materials, vol. 4, No. 4, Oct. 1970, pp. 538-548.
24. Jordan, W.M., "The Effect of Resin Toughness on the Delamination Fracture Behavior of Graphite/Epoxy Composites", Ph.D. dissertation, Texas A&M University, Dec., 1985.
25. Schapery, R.A., Jordan, W.M., and Goetz, D.P., "Delamination Analysis of composites with Distributed Damage Using a J Integral", Proc. of the Int. Symp. on Composite Materials and Structures, Beijing, China, June 10-13, 1986.
26. Kuo, A.Y., and Wang, S.S., "A Dynamic Hybrid Finite Element Analysis of Delamination in Composites", T.&A.M. Report No. 466, University of Illinois, April, 1984.
27. Schapery, R.A., "Deformation and Fracture Characterization of Inelastic Composite Materials Using Potentials", Polymer Engineering and Science, vol. 27, 1987, pp. 63-76.

28. Davidson, B.D., and Schapery, R.A., "Effect of Finite Width and Crack Tip Constraint on Deflection and Energy Release Rate of a Double-Cantilever Specimen", to appear in Journal of Composite Materials.
29. Tse, M.K., Hibbs, M.F., and Bradley, W.L., "Delamination Fracture Studies of Some Toughened Graphite/Epoxy Composites, Including Real Time Fracture Observation in Scanning Electron Microscope". ASTM Symposium on Toughened Composites, Houston, Texas, March 13-15, 1985.
30. Murri, G.B., " G_{IIC} Measurement of Toughened Matrix Composites Using the End-Notched Flexure (ENF) Test". ASTM Committee D30.02 Task Group on Interlaminar Fracture Toughness, Dallas, Texas, 1984.
31. Vanderkley, P.S., "Mode I-Mode II Delamination Fracture Toughness of a Unidirectional Graphite/Epoxy Composite". Master of Science Thesis, Texas A&M University, Dec. 1981.
32. Russell, A.J. and Street, K.N., "The Effect of Matrix Toughness on Delamination: Static and Fatigue Under Mode II Shear Loading of Graphite Fiber Composites". Presented at the NASA/ASTM Symposium on Toughened Composites, Houston, Texas, March 13-15, 1985.
33. Gillespie, J.W., Carlsson, L.A., and Pipes, R.B. "Finite Element Analysis of the End-Notched Flexure Specimen for Measuring Mode II Fracture Toughness". Center for Composite Materials, University of

Delaware, Newark, Delaware. To be published in Composite Science and Technology.

34. Carlsson, L.A., Gillespie, J.W., and Pipes, R.B. "On the Analysis and Design of the End-Notched Flexure (ENF) Test Specimen for Mode II Testing". Center for Composite Materials, College of Engineering, University of Delaware Newark, Delaware. To be published in the Journal of Composite Materials.
35. Henriksen, M., Engineering Department, Colorado School of Mines, Golden, Colorado, 80301.
36. Schapery, R.A., Mechanics and Materials Center, Texas A&M University, College Station, Texas, 77843. (Private communication).
37. Corleto, C.R., and Bradley, W.L., "Mode II Delamination Fracture Toughness of Unidirectional Graphite/Epoxy Composites". Presented at the ASTM Second Symposium on Composite Materials: Fatigue and Fracture, Cincinnati, Ohio, April 1987.
38. Rice, J.R., "A Path Independent Integral and the Approximate Analysis of Strain Concentration by Notches and Cracks", J. Appl. Mech. vol. 35, pp. 379-387, 1986.
39. Rice, J.R., Rosengren, G.F., "Plane Strain Deformation Near a Crack Tip in a Power Law Hardening Material", J. Mech. Phys. Solids vol. 16, pp. 1-12, 1968.
40. Hutchinson, J.W., "Singular Behavior at the End of a Tensile Crack in a Hardening Material", J. Mech. Phys.

Solids vol.16, pp. 13-31, 1968.

41. McClintock, F., "Plasticity Aspects of Fracture".
Fracture, Chap. 2, Vol. III (Edited by Liebowitz).
Academic Press, New York, 1971.
42. Agarwal, B.D., Patro, B.S., Kumar, P., "J Integral as
Fracture Criterion for Short Fibre Composites: An
Experimental Approach", Engineering Fracture
Mechanics, vol. 19, No. 4, pp. 675-684, 1984.
43. Agarwal, B.D., Kumar, P., and Khanna, S.K.,
"Determination of the Fracture Toughness of Fabric
Reinforced Composites by the J Integral Approach.
Compos. Sci. Technol., vol. 25 No. 4, pp. 311-323,
1986.
44. Keary, P.E., Ilcewicz, L.B., Shaar, C. and Trostle,
J., "Mode I Interlaminar Fracture Toughness of
Composites Using Slender Double Cantilever Beam
Specimens", J. of Compos. Mater. vol. 19, pp. 154-177,
1985.
45. Ilcewicz, L.B., Keary, P.E., Trostle, J.,
"Interlaminar Fracture Toughness Testing of Composite
Mode I and Mode II DCB Specimens", Boeing Commercial
Airplane Company, Advanced Composites Development
Program, P.O. Box 3707, M/S 6C-11, Seattle,
Washington.
46. Schapery, R.A., "Deformation and Fracture
Characterization of Inelastic Composite Materials
Using Potentials", Polymer Engineering and Science,

vol. 27, No. 1, 1987.

- 47. Schapery, R.A., "Correspondence Principles and a Generalized J Integral for Large Deformation and Fracture Analysis of Viscoelastic Media", Inter. Jour Fracture vol. 25, pp. 195-223, 1984.
- 48. Vanderkley, P.S., "Mode I-Mode II Delamination Fracture Toughness of a Unidirectional Graphite/Epoxy Composite", Master of Science Thesis, Texas A&M University (1981).

5.0 PUBLICATION RESULTING IN WHOLE OR IN PART FROM WORK SUPPORTED BY AFOSR (Note all manuscripts not provided in annual reports previously are provided in Appendix II).

- 5.1 Jordan, W.M. and Bradley, W.L., "Effects of Resin Content on Delamination Fracture Behavior of Graphite/Epoxy Laminates", Technology Vectors, 1984, pp. 1422-1437. (1984-1985 annual)
- 5.2 Jordan, W.M. and Bradley, W.L., "Micromechanisms of Fracture in Toughened Graphite-Epoxy Laminates", Toughened Composites, ASTM STP 937, Norman J. Johnston, Ed., American Society for Testing and Materials, Philadelphia, 1987, pp. 95-114. (Appendix II)
- 5.3 Hibbs, M.F., Tse, M.K. and Bradley, W.L., "Interlaminar Fracture Toughness and Real-Time Fracture Mechanism of Some Toughened Graphite-Epoxy

- Composites", Toughened Composites, ASTM STP 937, Norman J. Johnston, Ed., American Society for Testing and Materials, 1987, pp. 115-130. (Appendix II)
- 5.4 "The Meaning and Significance of Hackles in Composite Materials Failure Analysis", Jordan, W.M., Hibbs, M. and Bradley, W.L., Proceedings of International Conference: Post Failure Analysis Techniques for Fiber Reinforced Composites, Dayton, Ohio, July, 1985. (1985-1986 annual)
- 5.5 Chakachery, E.A. and Bradley, W.L., "A Comparison of the Crack Tip Damage Zone for Fracture of Hexcel F185 Neat Resin and T6T145/F185 Composite", Polymer Engineering and Science, Vol. 27, pp. 33-40. (Appendix II)
- 5.6 Hibbs, M.F. and Bradley, W.L., "Correlations Between Micromechanical Failure Processes and the Delamination Fracture Toughness of Graphite-Epoxy Systems," Fractography of Engineering Materials, ASTM STP 948, J.E. Masters and J.J. An, Ed., American Society for Testing and Materials, Philadelphia, 1987, pp. . (Appendix II)
- 5.7 Bradley, W.L. and Jordan, W.M., "The Relationship Between Resin Ductility and Composite Delamination Fracture Toughness", Proceedings of International Symposium on Composite Materials and Structures, Beijing, T.T. Loo and C.T. Sun, Ed., Technomic Publishing Co., Inc., Lancaster, PA, 1986, pp.

445-451. (1985-1986 annual)

- 5.8 Schapery, R.A., Jordan, W.M. and Goetz, D.P., "Delamination Analysis of Composites with Distributed Damage Using a J-Integral," Proceedings of International Symposium on Composite Materials and Structures, Beijing, T.T. Loo and C.T. Sun, Ed., Technomic Publishing Co., Inc., Lancaster, PA, 1986, pp. 543-549. (1985-1986 annual)
- 5.9 Corleto, C., Bradley, W.L., and Henriksen, M., "Correspondence Between Stress Fields and Damage Zones Ahead of Crack Tip of Composites Under Mode I and Mode II Delamination," Sixth International Conference on Composite Materials: ICCM-ECCM, Eds. Matthews, Buskell, Hodgkinson, and Martin, London, Elsevier Applied Science Publishers Ltd., Essex, England, 1987, Vol. 3, pp. 3.378-3.387. (Appendix II)
- 5.10 Jones, Jr., R.E. and Bradley, W.L., "Fracture Toughness Testing of Ductile Polymer Resins Using a J-Integral Approach," Nonlinear Fracture Mechanics, ASTM STP , John Landes, Ed., American Society for Testing and Materials, Philadelphia, 1988, pp. . (Appendix II)
- 5.11 Corleto, C.R. and Bradley, W.L., "Mode II Delamination Fracture Toughness of Unidirectional Graphite-Epoxy Composites," Composite Materials: Fatigue and Fracture, ASTM STP , Paul Lagace, Ed., American Society for Testing and Materials, Philadelphia, PA,

1988, pp . (Appendix II)

- 5.12 Hibbs, M.F. and Bradley, W.L., "Crack Tip Strain Field Measurements Determined In-Situ in Scanning Electron Microscope for Mode I Crack Extension in a Polymeric Material," Proceedings of Society of Experimental Mechanics Fall Conference-1987 (also submitted to Journal of Experimental Mechanics). (Appendix II)

6.0 PRESENTATIONS MADE THAT WERE BASED ON WHOLE OR IN PART ON WORK PERFORMED UNDER SPONSORSHIP OF THIS AFOSR GRANT.

- 6.1 "Correspondence Between Stress Fields and Damage Zones Ahead of Crack Tip of Composites Under Mode I and Mode II Delamination", Sixth International Conference on Composite Materials, London, England, July 1987.
- 6.2 "Fracture Studies in Neat and Fiber Reinforced Thermoset Resins", invited presentation for Gordon Research Conference on Thermosetting Plastics, New London, New Hampshire, June, 1987.
- 6.3 "Micromechanics of Compressive Failures in Composite Laminates", with Gail Guynn, and Mode II Delamination Fracture Toughness of Unidirectional Graphite/Epoxy Composites", with Carlos Corleto, ASTM Symposium on Fatigue and Fracture in Composite Materials, Cincinnati, Ohio, April, 1987.
- 6.4 "The Effect of Fiber Volume Fraction, Interfacial

- Bonding and Fiber Alignment on the Compressive Strength of Thermoplastic Composite Materials", invited presentation to the Corporate Research and Development Center of Phillips Petroleum, Bartlesville, Oklahoma, March, 1987.
- 6.5 "The Application of Fracture Mechanics to Plastics" and "In-Situ Fracture Studies in the Scanning Electron Microscope of Delamination in Composite Materials", invited presentation to the Dow Chemical Corporate Research and Development Center, Midland, Michigan, January, 1987.
- 6.6 "Various Problems in Measuring the Fracture Toughness of Ductile Plastics Using J-Integral Approach", invited presentation, the ASTM subcommittee meeting to set up round robin on fracture toughness characterization of plastics, Phoenix, AZ, November, 1986.
- 6.7 "Relationship Between Neat Resin Fracture Toughness and Delamination Fracture Toughness of Composite Materials", invited presentation to Phillips Petroleum Corporate Research and Development, Bartlesville, Oklahoma, November, 1986.
- 6.8 "Fracture Toughness Testing of Polyethylene Using a J-Integral Approach", International Symposium on Nonlinear Fracture Mechanics, Nashville, TN, October, 1986.
- 6.9 "The Relationship Between Resin Ductility and

- Composite Delamination Fracture Toughness",
International Symposium on Composite Materials, and
Structures, Beijing, China, June, 1986, invited.
- 6.10 "On Mode II Delamination Fracture Toughness
Measurements in Composite Materials," ASTM Annual
Meeting, Charleston, S.C., March, 1986, invited.
- 6.11 "Direct Observation of Fracture in Composites,"
lecture for Gordon Research Conference on Composites,
Santa Barbara, CA, January 1986, invited.
- 6.12 "The Meaning and Significance of Hackles in Composite
Materials," International Conference: Post Failure
Analysis Technique for Fiber Reinforced Composites,
Dayton, Ohio, July, 1985 (sponsored by Wright
Patterson), invited.
- 6.13 "A Comparison of the Crack Tip Damage Zone for
Fracture of Hexcel F185 Neat Resin and T6T145/F185
Composite Material," International Symposium on
Nonlinear Deformation, Fracture and Fatigue of
Polymeric Materials, Chicago, September, 1985,
invited.
- 6.14 "Correlations Between Micromechanical Failure Processes
and Delamination Fracture Toughnesses of
Graphite/Epoxy Composites," ASTM Symposium on
Fractography of Modern Engineering Materials,
Nashville, November, 1985, invited.
- 6.15 "Micromechanisms of Fracture in Toughened
Graphite/Epoxy Laminates," ASTM Symposium on Toughened

Composites, Houston, TX, March, 1985.

- 6.16 "Delamination Fracture Studies of Some Toughened Graphite/Epoxy Composites, Including Real-Time Fracture Observations in Scanning Electron Microscope," ASTM Symposium on Toughened Composites, Houston, TX, March, 1985.
- 6.17 "Delamination Fracture Behavior of Graphite/Thermoplastic Composite Systems," invited, NASA Langley, Hampton, VA., February, 1985.
- 6.18 "Micromechanics Modelling of Delamination Fracture in Graphite/Epoxy Composites," Gordon Conference on Composite Materials, Santa Barbara, CA., Jan., 1985.
- 6.19 "In-Situ Studies in Delamination of Graphite/Epoxy: Recent Results", Air Force Composite Materials Review Dayton, Ohio, Oct., 1984, invited.
- 6.20 "In-Situ Studies of T6T145/F185 Composite Materials," presented at the 6th International Fracture Symposium, New Delhi, India, Dec., 1984.
- 6.21 "In-Situ SEM Studies of Fracture of Plastics and Fiber Reinforced Plastics". Dow Chemical, Research Center, Freeport, TX, July 1984, invited.

7.0 PROFESSIONAL PERSONNEL ASSOCIATED WITH RESEARCH EFFORT

- 7.1 William M. Jordan, Ph.D., awarded, December, 1985, dissertation title: "The Effects of Resin Toughness on the Delamination Fracture Behavior of Graphite/Epoxy Composite".

- 7.2 Carlos Corleto, M.S., awarded, June, 1986, thesis title: "Mode II Delamination Fracture Toughness of Unidirectional Graphite/Epoxy Composites". Currently working on Ph.D. in area of Mode II Delamination with expected graduation date of December, 1988.
- 7.3 Mike Hibbs, Ph.D. candidate with expected graduation date of Fall, 1987, working on strain field mapping around crack tip.
- 7.4 Douglas Goetz, Ph.D. candidate for May, 1988, is working on J-Integral approach for Mode I delamination of multiaxial layups (supported half by Bradley and half by Schapery).

APPENDIX I
Derivation of J for the end-loaded split laminate test

Assumptions:

- (1) material homogeneity with respect to x_1 axis.
- (2) small rotations from fixed end of beam to the neighborhood of the crack tip. Therefore, the following apply:

u_2 , vertical displacement of the center line of beam

$$u_1 = x_1 \frac{du_2}{dx_1} ; \quad \frac{\partial u_1}{\partial x_1} = x_2 \frac{d^2 u_2}{dx_1^2} = \epsilon_{11} ;$$

$$k = d^2 u_2 / dx_1^2, \text{ curvature ; } \quad \frac{\partial u_2}{\partial x_1} \quad \frac{du_2}{dx_1}, \text{ slope}$$

- (3) friction forces at crack interface are negligible (this is accomplished in the specimen by placing a teflon insert between the crack surfaces).

Analysis:

Using Rice's J integral as extended by Schapery⁴⁷,

$$J = \int_{C_1} [w_0 dx_2 - T_i (\partial u_i / \partial x_1)] dL \quad (A1)$$

J_{II} for the specimen configuration of Fig. I.1 will be given by

$$J_{II} = J_1 + J_2 + J_3 + J_4 + J_5 + J_6 + J_7 \quad (A2)$$

where J_i correspond to the contribution of J_{II} coming from the counterclockwise contour C_1 shown in Fig. I.2. $J_1 = J_3 = J_5$

= 0 since $dx_2 = T_i = 0$ for these cases (see Fig. I.2).

Therefore, the only contribution to J comes from J_2 , J_6 and J_4 . The two former ones are equal due to symmetry and will be evaluated close enough to the crack tip so that small rotation beam theory applies (assumption 2). J_4 will be

evaluated far enough from the crack tip and fixed end to avoid nonuniformities in the stress field. Let's consider J_4 first. Since $T_i = \sigma_{ij}n_j$ and noting that the limits of integration for path 4 are $-h/2$ and $h/2$ for the lower and upper limits, respectively,

$$J_4 = \int_{-h/2}^{h/2} w_0 dx_2 - \left[\int_{-h/2}^{h/2} \left(\sigma_{11} n_1 \frac{\partial u_1}{\partial x_1} + T_2 \frac{\partial u_2}{\partial x_1} \right) dL \right] \quad (A3)$$

Using the expressions stated in assumption 2, and further assuming that

$$w_0 = \int_0^{\epsilon_{11}} \sigma_{11} d\epsilon_{11} \quad (\text{neglecting shear})$$

and since $dL = dx_2$ and the unit outward normal $n_1 = 1$, Eq. A3 becomes

$$J_4 = \int_{-h/2}^{h/2} \left[\int_0^{\epsilon_{11}} \sigma_{11} d\epsilon_{11} \right] dx_2 - \int_{-h/2}^{h/2} \sigma_{11} \epsilon_{11} dx_2 - \frac{du_2}{dx_1} \int_{-h/2}^{h/2} T_2 dx_2 \quad (A3a)$$

Now by means of the following

$$\epsilon_{11} = -kx_2 ; d\epsilon_{11} = -x_2 dk ; \int_{-h/2}^{h/2} T_2 dx_2 = -\frac{2P}{B}$$

and performing a change of variables,

$$J_4 = \int_0^k \left(- \int_{-h/2}^{h/2} \sigma_{11} x_2 dx_2 \right) dk - k \int_{-h/2}^{h/2} (-\sigma_{11} x_2 dx_2) + \frac{2P}{B} \frac{du_2}{dx_1} \quad (A.3b)$$

Further,

$$\frac{M}{B} = \int_{-h/2}^{h/2} (-\sigma_{11} x_2 dx_2)$$

thus,

$$J_4 = \frac{1}{B} \int_0^k M dk - \frac{k}{B} M + \frac{2P}{B} \frac{du_2}{dx_1}$$

Integrating by parts ($u = M$ $du = dM$ $dv = dk$ $v = k$)

$$J_4 = \frac{1}{B} \left(M k - \int_0^M k dM \right) - \frac{M k}{B} + \frac{2P}{B} \frac{du_2}{dx_1}$$

$$J_4 = \frac{1}{B} \left(\frac{2Pdu_2}{dx_1} - \int_0^M k dM \right) \quad (A3c)$$

To evaluate J_6 or J_2 the same procedure as that followed for J_4 was performed. For these cases one must notice that $dL = -dx_2$ and $n_1 = -1$ and thus,

$$J_6 = \int_{h/2}^0 \int_0^{\epsilon_{11}} \sigma_{11} d\epsilon_{11} dx_2 + \int_{h/2}^0 \sigma_{11} \frac{\partial u_1}{\partial x_1} dx_2 - \frac{du_2}{dx_1} \frac{P}{B} \quad (A4)$$

which can be reduced to

$$J_2 = J_6 = \frac{1}{B} \int_0^M k dM - \frac{P}{B} \frac{du_2}{dx_1} \quad (A4a)$$

Adding J_2 , J_6 and J_4 ,

$$J_{II} = \frac{2}{B} \left[\int_0^M k dM - P \frac{du_2}{dx_1} \right]_L - \frac{1}{B} \left[\int_0^M k dM - 2P \frac{du_2}{dx_1} \right]_R \quad (A2a)$$

where the subscripts L and R indicate evaluation of the quantities inside the brackets corresponding to the left (paths 2 and 6) and right (path 4) vertical segments of the beam.

In order to establish the path independence of J_{II} , it will be evaluated at a distance x_1 from loaded end.

Left segment:

since $d^2u_2/dx_1^2 = k$, the slope of any segment in the cracked part of the beam at a distance x_1 from the loaded end is given by

$$\frac{du}{dx_1} = \frac{1}{2P} \left[\int_{2PL}^{2Pa} k dM \right]_R + \frac{1}{P} \left[\int_{Pa}^{Px} k dM \right]_L$$

Substituting this expression into Eq. A4a and evaluating the integral for x_1 ,

$$J_6 = \frac{1}{B} \left\{ \left[\int_0^{Pa} k dM \right]_L - \left[\int_0^{2Pa} k dM \right]_R \right\} \quad (A5)$$

where J_L refers to the contribution to J_{II} coming from the left segment of the beam (cracked part). As it can be seen, this expression is independent of path (i.e. independent of x_1).

Right segment:

The slope of any segment in the uncracked part of the beam at a distance x_1 from the loaded end is given by

$$\frac{du_2}{dx_1} = \left[\frac{1}{2P} \int_{2PL}^{2Px_1} k dM \right]_R$$

Substituting the above expression into J_4 and evaluating the integral for x_1 ,

$$J_4 = \frac{1}{B} \left\{ \left[\int_{2PL}^{2Px_1} k dM + \int_{2Px_1}^0 k dM \right]_R \right\} = J_R = - \frac{1}{B} \left[\int_0^{2PL} k dM \right]_R \quad (A.3d)$$

where J_R refers to contribution to J_{II} coming from right segment of beam.

Finally, by adding Eq2. A3d and A5, we obtain

$$J_{II} = \frac{1}{B} \left\{ 2 \left[\int_0^{Pa} k dM \right]_L - \left[\int_0^{2Pa} k dM \right]_R \right\} \quad (A6)$$

which is Equation 12 as shown in Theoretical Model section.

APPENDIX II

Papers published since 2nd annual report.

Mike F. Hibbs,¹ Ming Kwan Tse,² and Walter L. Bradley¹

Interlaminar Fracture Toughness and Real-Time Fracture Mechanism of Some Toughened Graphite/Epoxy Composites

Authorized Reprint from Special Technical Publication 937, 1987

Copyright American Society for Testing and Materials, 1916 Race Street, Philadelphia, PA 19103

REFERENCE: Hibbs, M. F., Tse, M. K., and Bradley, W. L., "Interlaminar Fracture Toughness and Real-Time Fracture Mechanism of Some Toughened Graphite/Epoxy Composites," *Toughened Composites, ASTM STP 937*, Norman J. Johnston, Ed., American Society for Testing and Materials, Philadelphia, 1987, pp. 115-130.

ABSTRACT: Five graphite/epoxy composites containing toughened epoxies prepared at Dow Chemical and AS-4 graphite fibers from Hercules have been studied in Mode I, mixed mode, and Mode II to determine their delamination fracture toughnesses G_c and the controlling micromechanism of fracture. The G_c values were determined using split laminate specimens. The delamination fracture process was observed in real time in the scanning electron microscope. To increase delamination fracture toughness, both an improved interface as well as higher resin toughness were found to be required. Increasing Mode II loading, particularly of the more brittle systems, gives a significantly greater resistance to crack propagation as measured by the total energy release rate required to propagate the crack.

KEY WORDS: composite material, delamination, mixed mode, Mode I, graphite/epoxy, toughened, in situ fracture

Nomenclature

- B Specimen thickness
- C Compliance of test coupon
- E Elastic modulus in the fiber direction
- G_I Energy release rate for Mode I loading (opening mode)
- G_{II} Energy release rate for Mode II loading (in plane shear)
- G_{Ic} Critical energy release rate for stable crack growth for Mode I loading
- G_{IIc} Critical energy release rate for stable crack growth for Mode II loading

¹Research assistant and professor, Mechanical Engineering Department, Texas A&M University, Engineering Research Center, College Station, TX 77843.

²Senior research engineer, The Dow Chemical Company, Resins Research, B-1215 Bldg., Freeport, TX 77541.

- G_{I+II} Total critical energy release rate for stable crack growth
 I Moment of inertia for cracked portion of split laminate
 L_c Crack length in split laminate
 P_s Symmetric load component ($P_u + P_L$)/2 (see Fig. 1)
 P_a Asymmetric load component ($P_u - P_L$)/2 (see Fig. 1)
 P_u Load applied to upper half of split laminate (see Fig. 1)
 P_L Load applied to lower half of split laminate (see Fig. 1)
 Δ Total opening displacement (see Fig. 1)

Introduction

Graphite/epoxy composite materials are beginning to be used in many new aerospace applications, as a result of their very high strength-to-weight and stiffness-to-weight ratios. However, design strains used in the aircraft industry are sometimes limited by concerns about delamination. The first generation resins developed for use in graphite/epoxy composite materials optimized stiffness and high glass transition temperature (T_g) by using a very high cross-link density. Unfortunately, such resins are quite brittle. Recent developments have centered on how to increase resin toughness with a minimum penalty in stiffness and T_g . As tougher resins systems are developed, however, a commensurate improvement in interfacial bonding will be required if the full benefit of the increased toughness is to be realized in practice.

The purpose of this study has been to evaluate the delamination toughness of five graphite/epoxy composite materials systems where the resin toughness and interfacial bonding strength have been systematically increased. The delamination fracture toughness for Mode I, Mode II, and mixed mode loading has been determined using split laminate specimens. The fracture process has been studied using real-time in situ fracture observations in a scanning electron microscope (SEM) with a specially designed stage which allows specimen fracture in the SEM. Postmortem fractography has been used to supplement the mechanistic portion of the study.

Experimental and Analytical Procedures

Sample Preparation

The five graphite/epoxy composites studied are toughened high temperature epoxies combined with AS-4 fibers from Hercules. Systems P4 and P5 are composites which consist of brittle resins and graphite fibers without the sizing which is often added to enhance interfacial bonding and protect the fibers during processing. Resin P4 is Dow Chemical XD7342 and P5 is Hercules 3501-6. Systems P6 and P7 are composed of the somewhat tougher Novalac epoxy, used with sized graphite fibers. The P7 system is a modified version of P6, altered to enhance both resin toughness and adhesion. A fifth system (Q6) is a much tougher cross-linkable thermoplastic epoxy (Dow XU71788) with sized fibers to enhance interfacial bonding.

Mechanical Testing

Delamination fracture toughness measurements for opening mode (G_{Ic}), shear mode (G_{IIc}), and mixed mode were made using split laminate specimens, sometimes called double cantilevered beam specimens (DCB), as shown in Fig. 1. These specimens were tested at room temperature (24°C) in stroke control at a rate of 0.0085 cm/s. A partial unload compliance measurement was made after each approximate 1 cm of crack growth. Stroke, displacement, and load were measured continuously as a function of time while crack length was measured discretely using visual measurements on the edge of the specimen. A check of the accuracy of the measurement of crack length by visual observation on the edge of the specimen was made by performing the final several centimetres of delamination at liquid nitrogen temperatures, which gives a distinctly different fracture surface appearance. This allowed the estimation of the degree of crack tunneling

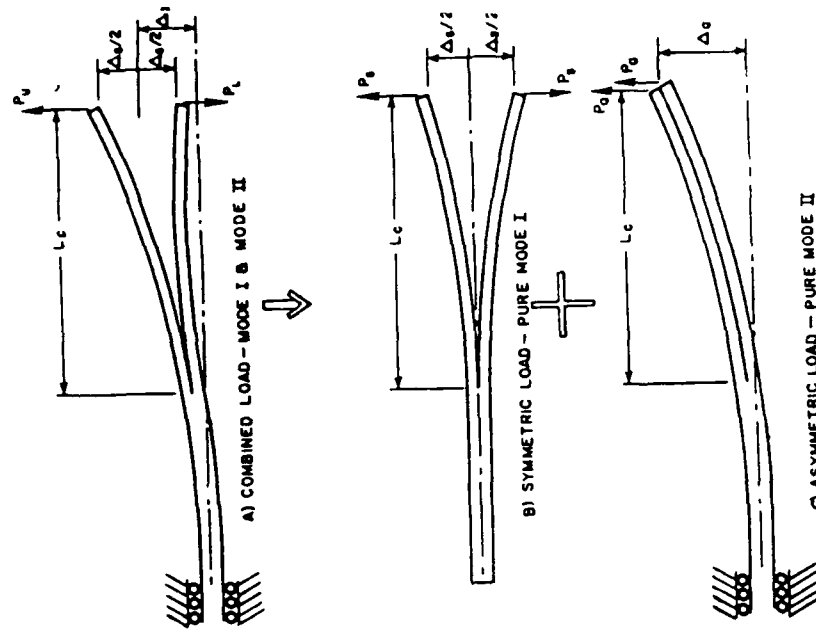


FIG. 1—Schematic showing how asymmetric loading of split laminate can introduce a mixed Mode I/Mode II state of stress at the crack tip

(or thumb nail formation) to determine whether surface measurements of crack length needed to be corrected. Typically, the correction to the crack measured on the edge of the specimen was +1.0 mm.

The mixed mode and Mode II tests were also performed using split laminate specimens. The uncracked end was supported against vertical displacements, but was free to move horizontally. The cracked end was then asymmetrically loaded, as shown in Fig. 1, and described more fully elsewhere by Vanderkley [1]. A 0.8-mm-thick Teflon® spacer was used between the ends of the cracked surfaces for the pure Mode II tests to avoid frictional loading between the two fractured surfaces. Confirmation that no significant frictional loading occurred was found in the fractographic examinations subsequent to mechanical testing. Using superposition, one can then analyze the Mode I and Mode II contributions to the total energy release rate using linear beam theory.

Analysis of Results

Mode I Analysis—The Mode I critical energy release rate for delamination G_{Ic} was calculated from the measured data in three ways. The linear beam theory was used in the first approach as described by Devitt et al. [2] where

$$G_{Ic} = P_1^2 L_c^3 / BEI \quad (1)$$

and

$$EI = 2P_1 L_c^3 / 3\Delta_1 \quad (2)$$

The area method was used in the second approach as suggested by Whitney [3] and can be shown to be identical to linear beam theory when all the unload compliances are linear and pass through the origin. For this approach, the following relationship is used for linear load displacement behavior:

$$G_{Ic} = (P_{s1}\Delta_{s2} - P_{s2}\Delta_{s1}) / 2B\Delta L_c \quad (3)$$

where P_{s1} and P_{s2} and Δ_{s1} and Δ_{s2} are consecutive loads and opening displacements for a crack extension ΔL_c . The area under the load-displacement record which represents the work required to grow the crack a finite distance is seen in Fig. 2.

The third approach used in this work was the compliance change method based on data analysis as suggested first by Wilkins [4]. In this approach

$$G_{Ic} = (nH^{1/n} / 2B) (P_1^{1+1/n} / \Delta_1^{1-1/n}) \quad (4)$$

where the constants n and H are determined from a least squares fit of $\log C = n \log L_c + \log H$, and C is measured at each unload. Using each of these approaches, it is possible to determine G_{Ic} at many points of crack growth along the specimen. Ideally, the calculated values of G_{Ic} will be relatively constant for various crack lengths during delamination. Some variation is occasionally observed during the early stages of crack growth. This variation may be associated with the development of a fiber bridging zone behind the crack tip, the

SAMPLE MH514C1 P5 SYSTEM

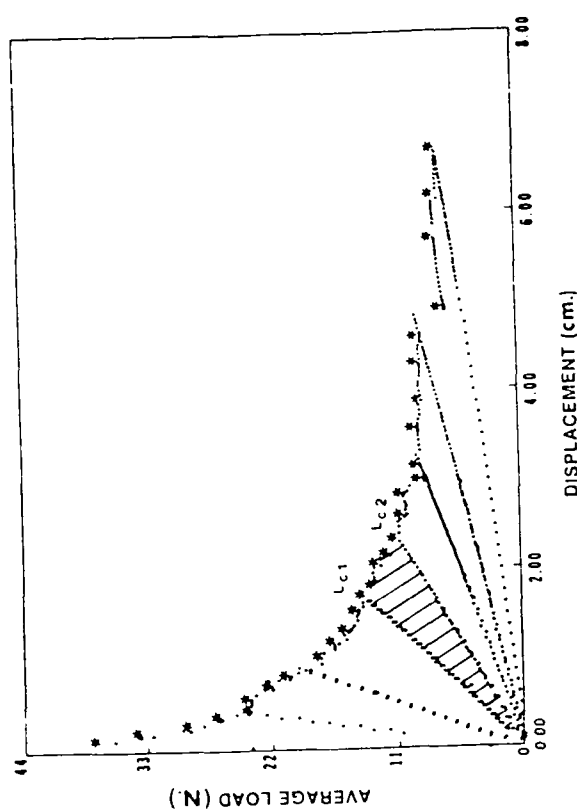


FIG. 2—Typical load/opening displacement curve for the P5 system. Cross-hatched area represents the energy expended for the crack extension. ($L_{c2} - L_{c1}$)

development of a steady-state damage zone ahead of the natural crack as it grows from the artificial crack produced by the Teflon, or a result of the fact that beam theory is strictly applicable only when the beam length (and crack length) is several times the beam width. The latter seemed to be the case in this study since no significant fiber bridging was noted and the calculated values of G_{Ic} actually decreased during the transient. Thus, only the "steady-state" values of G_{Ic} were considered when an average value of G_{Ic} was calculated. A typical load-displacement record is shown in Fig. 2 with the reduced results given in Table 1.

Mode II Analysis—The Mode II critical energy release rate for delamination fracture was initially calculated from measured quantities using a relationship based on linear beam theory, namely,

$$G_{IIc} = 3P_2^2 L_c^3 / 4BEI \quad (5)$$

However, it was noted that the load-displacement record for the Mode II tests were somewhat nonlinear and the calculated G_{IIc} values seemed artificially high. This suspicion was confirmed by comparison of our G_{IIc} values for System P5, obtained using Eq. 5 (based on linear beam theory), to results by Street and Russell [5] using an end notch flex test on a similar composite material. Reanalysis of the same measured load-displacement records for Mode II delami-

nation using the area method gave results for our P5 system that were similar to Street and Russell's results. The energy release rate was calculated as the area under the load-displacement record for a load-crack extension — unload divided by the increase in crack area $(L_{c2} - L_{c1}) \times B$ (see Fig. 2). It is worth noting that the area method implicitly implies that all energy dissipation occurs in the crack tip rather than in the far field. Because the nonlinear load-displacement records returned to the origin, this implied minimal energy dissipation outside the crack tip volume. In general, the reanalysis of the measured load-displacement records gave G_{IIc} values that were 60 to 70% lower than those calculated using linear beam theory. Thus, it was concluded that only the area method or a nonlinear beam analysis could be used to analyze the Mode II results. The area method was used for this work.

Relative good agreement between linear beam theory and the area method calculations of G_{IIc} were obtained, as seen in Table 1. However, Fig. 2 indicates that the load-displacement records for the Mode I tests were quite linear. Thus, good agreement would be expected. The higher G_{IIc} values necessitated much higher loads and deflections to give delamination for Mode II loading, and these higher loads gave the observed geometrically induced nonlinearity in the load-displacement behavior.

Mixed Mode Analysis — For the specimens loaded asymmetrically, as shown in Fig. 1, the total energy release rate was calculated by combining the Mode I and Mode II energy release rates calculated from linear beam theory (Eqs. 1 and 5) to give

$$G_{Tot,c} = G_{Ic} + G_{IIc} = (4P_f^2 + 3P_a^2)L_c^2/4BEI \quad (6)$$

The fraction of Mode II energy release rate was calculated by combining Eqs. 5 and 6 to give

$$G_{IIc}/G_{Tot,c} = \frac{3P_a^2}{4P_f^2 + 3P_a^2} \quad (7)$$

Finally, the fracture toughness of the neat material was determined using compact tension specimens tested according to ASTM Test for Plane-Strain Fracture Toughness of Metallic Materials (E 399). Because of the relative brittleness of the resins studied, it was not possible to precrack the specimens. Thus, a razor blade was used to pop in very sharp cracks.

Fractographic Examination

All fractured surfaces were subsequently examined in a JEOL-25 scanning electron microscope to determine the degree of resin fracture versus interfacial debonding. The nature of the resin fracture (brittle versus ductile) and the degree of microcracking which precedes fracture, as evidenced by scallops on the fracture surface, was also noted.

TABLE 1 — Sample calculation of composite mode I energy release rate (G_{Ic}) for a typical DCB specimen

Input Data				SYSTEM P5	
P_f , N	Δ , cm	L_c , cm	C, cm/N	Area Method G_{Ic} (A), J/m ²	Linear Beam Theory G_{Ic} (B), J/m ²
13.3	1.8	9.3	...	122	134
12.9	2.1	9.8	...	166	139
11.9	2.2	10.2	...	141	131
11.1	2.3	10.8	0.205	130	125
10.7	2.6	11.3	...	156	128
10.7	2.9	11.8	...	120	139
9.0	3.1	12.3	...	240	107
9.2	3.2	12.8	0.339	31	121
9.4	3.6	13.3	...	137	136
9.0	4.0	13.8	...	160	136
9.1	4.3	14.3	...	120	149
9.0	4.7	14.8	0.482	140	155
6.8	5.0	16.5	...	152	110
7.5	5.8	16.9	...	96	140
7.2	6.3	17.4	0.845	125	151
7.3	6.8	17.9	Ave. G_{Ic} : 0.845	139	134
			Standard Deviation:	43	12

Real-Time Observation of Delamination Fracture in SEM

The details of the delamination fracture process were determined using real-time observations of the fracture process in the scanning electron microscope, which displays the image on a cathodic ray tube (CRT). Delamination was achieved by pushing a wedge into the precracked portion of a small DCB-type specimen. The wedge tip was sufficiently blunt to ensure that the wedge remained well away from the crack tip, giving essentially pure Mode I loading. The crack propagation was then observed by viewing the edge of the specimen near the region of the crack tip. The experimental results were recorded on both video tape and on standard photographic film.

Experimental Results

Fracture Toughness Results

The Mode I (G_{Ic}), mixed mode ($G_{I/IIc}$), and Mode II (G_{IIc}) fracture toughness results are summarized in Table 2. As has been previously mentioned, the G_{Ic} values were calculated using three different approaches, but the results were generally quite similar, with the average values from each analysis method following within one standard deviation of each other (see Table 1). The average values of G_{Ic} obtained for each of the three analyses on each Mode I specimen were in turn averaged to obtain the values reported in Table 2. Mixed mode results analyzed using linear beam theory are also presented in Table 2 along with Mode II values analyzed using the area method. Fracture toughness values for the neat resin obtained from compact tension specimens are also included in Table 2. The delamination fracture toughness for Mode I loading was found to be greater than the neat resin toughness for the most brittle systems (P4 and P5) and similar to the neat resin toughness for the tougher systems (P6, P7, and Q6). Similar behavior has previously been reported by Bradley and Cohen [6].

Increasing the fraction of Mode II loading increases the total energy release rate for crack growth. Most of this increase was observed as the percentage of Mode II energy release rate increased from 40 to 100%.

Fractography

The fractured surfaces for specimens delaminated in Mode I loading are found in Fig. 3. As evident by the smooth, "clean" surfaces of the fibers, the fracture micromechanism in Systems P4, P5, and P6 is seen to be primarily interfacial debonding. Where a larger resin rich region is observed, a very brittle cleavage fracture is noted. Ductile resin failure is seen to be a fracture micromechanism completely coating the fibers indicating good interfacial adhesion. Resin is seen to be seen to have a combination of resin fracture and interfacial debonding. Fiber pullout is evident in both P4 and P5. The fracture surface in the systems with failure by interfacial debonding (P4, P5, and P6) has the appearance of a cor-

TABLE 2—Resin and composite energy release rates^a

Resin System	Resin G_{Ic} , kJ/m ²	Mode I, kJ/m ²	20% Shear, kJ/m ²	43% Shear, kJ/m ²	Mode II, kJ/m ²
P4	0.08	0.165 (45) ^b	0.373 (2)	0.532 (14)	0.769 (5)
P5	0.07	0.137 (64)	0.532 (1)	0.695 (14)	1.267 (4)
P6	0.14	0.165 (26)	...	0.334 (6)	1.532 (3)
P7	0.32	0.340 (29)	0.522 (1)	0.629 (9)	1.724 (2)
Q6	0.73	0.848 (21)	1.533 (1)	0.969 (10)	2.836 (1)

^a A summary of the energy release rates for the five resin systems. Mode I G_{Ic} was calculated by averaging the results from the area method, linear beam theory, and change in compliance analysis. The mixed modes, 20 and 43% shear energy release rates were calculated using linear beam theory. Mode II G_{IIc} was calculated using the area method.

^b () indicates the number of data points used to determine G_{Ic} .

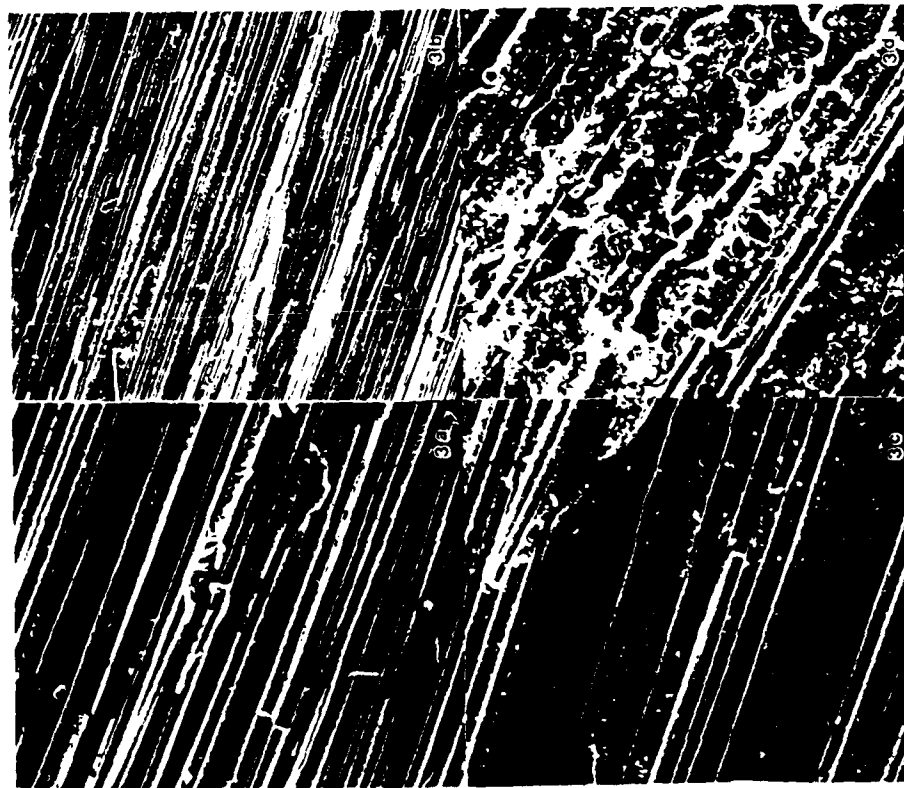


FIG 3—Postmortem fractography of Mode I delamination. (a) P4, $\times 450$; (b) P5, $\times 70$; (c) P6, $\times 450$; (d) P7, $\times 450$; and (e) Q6, $\times 1300$. P4, P5, and P6 are characterized by a smooth corrugated surface and fiber debonding. P7 displays some resin deformation with improved resin adhesion. Q6 shows extensive resin adhesion and at higher magnifications (f), failure can be clearly seen to be due to resin cracking and deformation.

rugated roof (or a plowed field), which has the effect of increasing the area of the fractured surface. This is typical of delamination fracture in composite systems with relative brittle resin.

The fractured surfaces for the various specimens with mixed mode loading up to 43% Mode II were essentially the same as for Mode I, except for a somewhat greater incidence of individual or multiple fiber pullout. A significantly different fracture surface for all of the systems fractured in Mode II was found, which correlates with the dramatic increase in total energy release rate (see Fig. 4). The

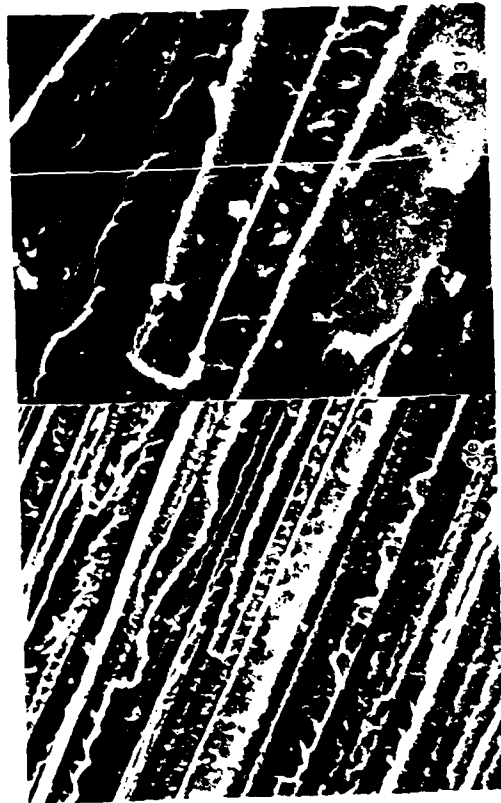


FIG 3—Continued

scalloped appearance of the fractured surfaces seen in Fig. 4 is typical of high Mode II delaminations of composite materials made from brittle resin systems and constitutes resin cracking.

Real-Time Observations of Delamination in SEM

In situ observations of fracture in the SEM of the P4 system are seen in Fig. 5. The primary crack is seen to proceed by interfacial debond. Some microcracking is seen to occur in the resin behind the primary crack tip and appears to occur concurrently with fiber bridging and eventual pullout.

Fracture of the Q6 system in the SEM is seen in Fig. 6. In contrast to P4, crack propagation occurs primarily by resin deformation and fracture, with only occasional interfacial debonding. Considerable resin deformation and microcracking is seen in regions outside the resin rich region between plies. This larger deformation and damage zone is undoubtedly the result of the better interfacial bonding which allows a greater stress buildup to occur in the crack tip region before crack advance occurs.

Discussion

Increasing the delamination toughness requires an increase in both the resin toughness and the interfacial bond strength. Otherwise, the resin toughness will not be extracted in delamination fracture as a result of "short circuiting" via fiber debonding. The two best composite systems were seen to be the ones with the best interfacial bonding (P7 and Q6) and with the greatest resin deformation before fracture. In this regard, Q6 was particularly good, showing fractographic evidence of considerable resin yielding and deformation.

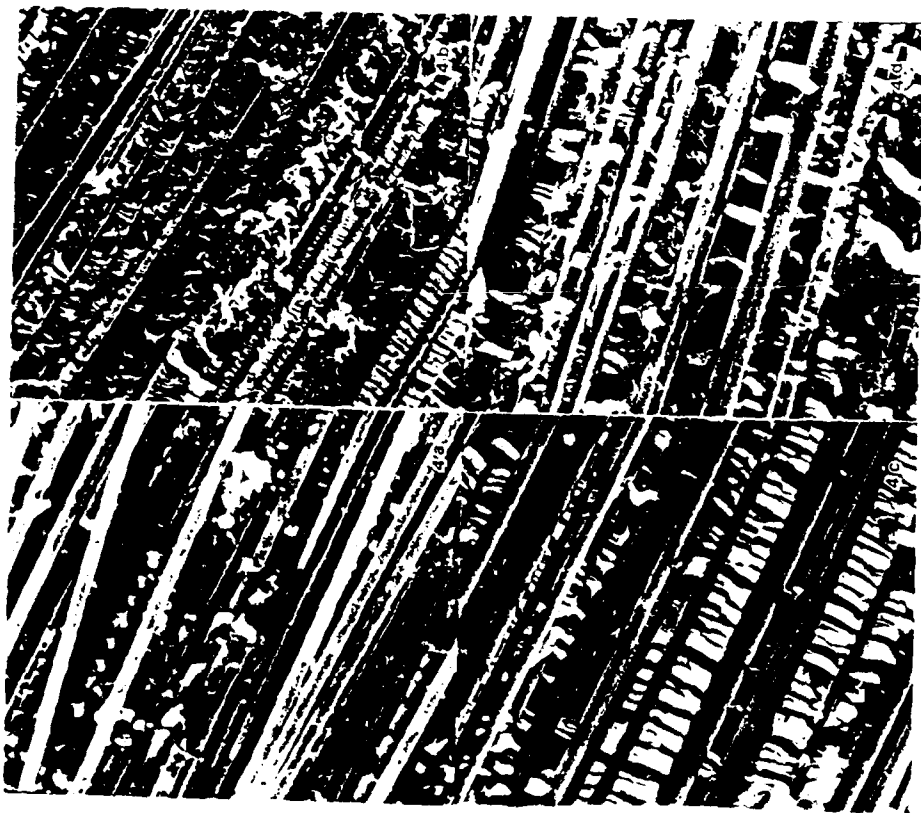


FIG. 4. Postmortem fractographs of Mode II delamination. All the systems tested exhibit a rougher or more scalloped fracture surface than seen in Mode I failure: (a) P4, (b) P7, (c) P5, and (d) P6. All at $\times 450$.

The delamination toughness for Mode I loading was found to be greater than the neat resin toughness for the most brittle systems, namely, P4 and P5. This type of behavior has previously been reported by Bradley and Cohen [6] and is explained in terms of a greater fracture area as a result of a "corrugated roof" fracture surface in the composite (see Fig. 3) as compared to a mirror smooth fracture surface in the neat resin. This greater fracture area along with fiber bridging and fiber breakage apparently compensates for the premature failure by fiber debonding before resin cracking, giving a net increase in toughness.

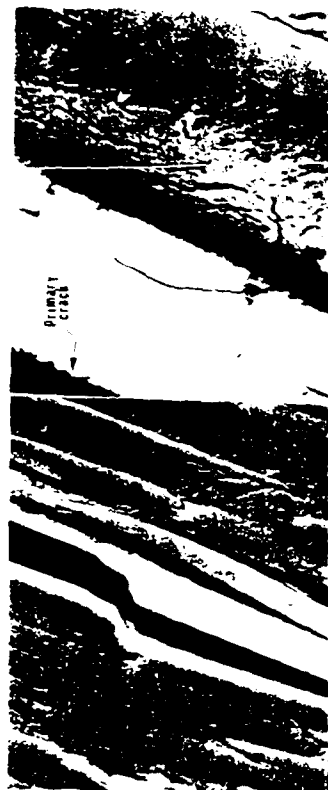


FIG. 5. In situ delamination fracture in P4. Primary cracking along an interlaminar boundary and fiber bridging. $\times 1000$ (left). Resin deformation and microcracking resulting from fiber bridging. Note the primary crack seen in the upper left corner. $\times 3000$ (right).

At higher resin toughness values, the Mode I delamination fracture toughness is seen to be similar to the neat resin toughness (see P6, P7, and Q6 in Table 2). This again agrees with earlier results by Bradley and Cohen [6] in which it was noted that the damage zone in the neat resin may be similar in height to the thickness of the resin rich region between plies, and thus, the fracture process will be similar in neat material and composite. This does appear to be the case for P7 and Q6. On the other hand, P6 seems to have failed primarily by fiber debonding.

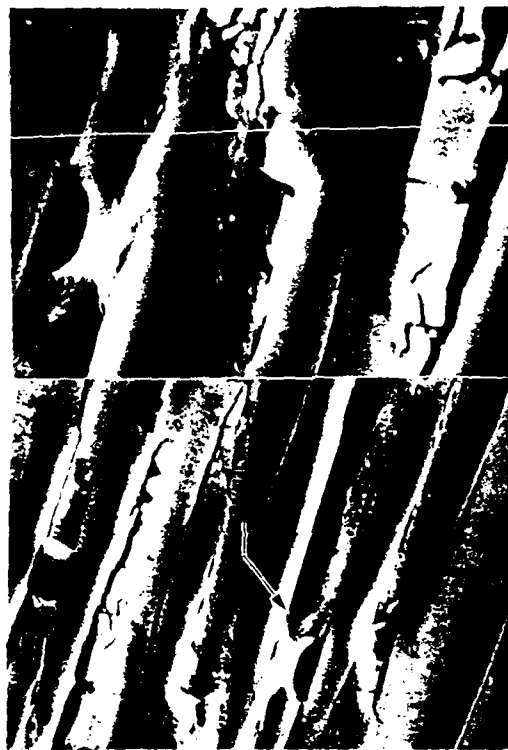


FIG. 6. In situ delamination fracture in Q6. Resin deformation and bridging near the primary crack tip. Numerous secondary cracks are seen adjacent to the primary crack. $\times 1100$ (left). Resin drawing and microcracking seen within the resin bridging. $\times 2000$ (right).

4. Apparently, the fiber bridging and breakage along with the corrugated roof of the surface which increases the fracture surface area help to compensate for the premature fracture at the fiber/matrix interface, allowing the delamination fracture toughness to be similar to the neat resin toughness, in spite of debonding. Further increases in toughness will not give commensurate increases in composite toughness [6, 7]. This is apparently due to the fact that as the damage zone where energy dissipation occurs becomes greater in size than the thickness in the resin rich region between plies can accommodate, the presence of the fibers in what would otherwise be damage zone prevents the same amount of energy dissipation as would occur in a neat, tough resin system.

The large increase in delamination fracture toughness with high Mode II contribution to the total energy release rate is accompanied by a large number of scallops appearing on the fractured surface in the systems studied. These scallops apparently result from the attempt of the primary crack to propagate in a brittle fashion on the principal normal stress plane, which for increasing Mode II is no longer parallel to the resin rich region between plies. As a result, a whole series of microcracks form and grow in the resin rich region between plies, terminating at the fibers which bound this region. The coalescence of these cracks constitutes the growth of the primary crack. This much more tortuous path for the crack is responsible for the increased resistance to crack growth evidenced in the increase in total energy release rate with increasing Mode II loading.

Delamination crack propagation in P4 as observed in the SEM occurs with growth along one interface with occasional jumps to an adjacent interface on the same fiber or an adjoining fiber. When this occurs, fiber bridging usually results with some microcracking as well. Because the crack propagation seeks out the weakest available interface along which to grow, propagation of the primary crack in P4 is always occurring at a sufficiently low stress so that microcracking of the matrix does not occur. Somewhat higher stresses may develop behind the primary crack as fiber bridging and pullout occur at somewhat more well bonded locations. It is under these circumstances that the matrix microcracking develops in such systems (see Fig. 5).

Summary

The results of this study indicate that the translation of resin toughness to Mode I delamination composite toughness is highly dependent on the adhesion of the resin to the fiber. In the brittle Systems P4 and P5, where the primary fracture mechanism was interfacial debonding, the composite Mode I energy release rate was about twice that for the neat resin. This increase was seen to be the result of the increased fracture surface area and occasional fiber bridging and pullout. Because of the interfacial debonding restricts the degree of resin participation in the fracture process, a twofold increase in resin toughness such as in the P6 system does not result in a twofold increase in composite toughness. Instead, the P6 resin system gave a delamination composite toughness similar to those of the brittle resin systems.

When the interfacial adhesion is enhanced, composite toughness can approach that of the neat resin toughness for moderately tough systems ($G_{Ic} \approx 600 \text{ J/m}^2$), since resin deformation and fracture is not preempted by interfacial failure. Alternatively, a combination of increased surface area or fiber bridging and breaking or both, and resin deformation can also give composite delamination toughness values which equal the neat resin toughness (for example, the P7 system).

In all of the graphite/epoxy systems of this study, the delamination toughness is seen to increase with higher percentages of Mode II shear loading. In the systems where Mode I delamination is dominated by interfacial debonding (P4, P5, and P6), this increased toughness in the mixed mode and Mode II loading conditions is the result of the microcracking in the resin rich region between plies on planes perpendicular to the principal normal stress plane. Such cracks can only grow a short distance before being obstructed by the fibers. Macrocrack advance requires the coalescence of these microcracks. This microcracking increases the fracture surface area and results in a more tortuous path for delamination crack growth. The increase from Mode I to Mode II delamination toughness was less dramatic in the P7 system where there was less interfacial debonding for Mode I fracture. This is expected since some of the resin toughness was already extracted in the Mode I delamination through resin deformation. In the Q6 system where resin adhesion was seen to be very good, the out of plane stress resulting from the shear loading was seen to increase only moderately the amount of resin deformation and resin cracking, resulting in only a threefold increase in delamination toughness as one changes from Mode I to Mode II loading. Finally, the more ductile resins do not tend to give brittle microcracking and scallops formation for Mode II loading. Thus, the fracture micromechanism is less effected by a change in loading mode.

Acknowledgments

This study was made possible by the material and financial support of the Dow Chemical Company.

References

- [1] Vanderkley, P. S., "Mode I-Mode II Delamination Fracture Toughness of a Unidirectional Graphite/Epoxy Composite," Master's thesis, Texas A&M University, College Station, TX, Dec. 1981.
- [2] Devitt, D. F., Schapery, R. A., and Bradley, W. L., "A Method for Determining the Mode I Delamination Fracture Toughness of Elastic and Viscoelastic Composite Materials," *Journal of Composite Materials*, Vol. 14, Oct. 1980.
- [3] Whitney, J. M., Browning, C. E., and Hoogsteeten, W., "A Double Cantilever Beam Test for Characterizing Mode I Delamination of Composite Materials," *Journal of Reinforced Plastics and Composites*, Vol. 1, Oct. 1982.
- [4] Wilkins, D. J., Eisenmann, J. R., Camin, R. A., Margolis, W. S., and Benson, R. A., "Characterizing Delamination Growth in Graphite-Epoxy," in *Damage in Composite Materials: Basic Mechanisms, Accumulation, Tolerance, and Characterization*, ASTM STP 775, K. L. Reifsnider, Ed., American Society for Testing and Materials, Philadelphia, 1982, pp. 168-183.

- [5] Russell, A. J. and Street, K. N., "Moisture and Temperature Effects on the Mixed-Mode, Delamination Fracture of Unidirectional Graphite/Epoxy," in *Delamination and Debonding of Materials*, ASTM STP 876, W. S. Johnson, Ed., American Society for Testing and Materials, Philadelphia, 1985, pp. 349-370.
- [6] Bradley, W. L. and Cohen, R. N., "Matrix Deformation and Fracture in Graphite-Reinforced Epoxies," in *Delamination and Debonding of Materials*, ASTM STP 876, W. S. Johnson, Ed., American Society for Testing and Materials, Philadelphia, 1985, pp. 389-410.
- [7] Hunston, D. L. and Bullman, G. W., "Characterization of Interlaminar Crack Growth in Composites: Double Cantilever Beam Studies," in *1985 Grant and Contract Review*, NASA Langley Research Center Materials Division, Fatigue and Fracture Branch, Vol. II, 13-14 Feb. 1985.

William M. Jordan¹ and Walter L. Bradley¹

Micromechanisms of Fracture in Toughened Graphite-Epoxy Laminates

Authorized Reprint from Special Technical Publication 937, 1987

Copyright American Society for Testing and Materials, 1916 Race Street, Philadelphia, PA 19103

REFERENCE: Jordan, W. M. and Bradley, W. L., "Micromechanisms of Fracture in Toughened Graphite-Epoxy Laminates," *Toughened Composites*, ASTM STP 937, Norman J. Johnston, Ed., American Society for Testing and Materials, Philadelphia, 1987, pp. 95-114.

ABSTRACT: The combination of low cross-link density and elastomer additions has been seen to give the most potent toughening for neat resins. A relatively small increment of the additional neat resin fracture toughening above 800 J/m² is actually reflected in the delamination fracture toughness of a composite. Mode II delamination toughness of brittle systems may be as much as three times the Mode I delamination fracture toughness, while a ductile system may have a Mode II delamination fracture toughness that is similar to the Mode I value. The energy absorbed per unit area of crack extension for delamination seems to be independent of ply orientation if proper accounting of the near and far field energy dissipation is made.

KEY WORDS: composite materials, delamination, Mode I, Mode II, mixed mode, toughened epoxy

Nomenclature

- B Specimen
- E Elastic modulus in the fiber direction
- G_{Ic} Critical energy release rate for stable crack growth for Mode I loading
- G_{IIc} Critical energy release rate for stable crack growth for Mode II loading
- $G_{Tot,c}$ Total critical energy release rate for mixed mode loading
- I Moment of inertia for cracked portion of split laminate
- L_c Crack length in split laminate
- P_s Asymmetric load component $(P_u + P_l)/2$ (see Fig. 1)
- P_a Symmetric load component $(P_u - P_l)/2$ (see Fig. 1)
- P_u Load applied to upper half of split laminate (see Fig. 1)

This work performed at Texas A&M University was supported by the Air Force Office of Scientific Research with Major David Glasgow as project monitor.

¹Research assistant and professor of mechanical engineering, Mechanical Engineering Department, Texas A&M University, College Station, TX 77843.

- P_L Load applied to lower half of split laminate (see Fig. 1)
 Δ , Total opening displacement (see Fig. 1)

Introduction

Graphite/epoxy composite materials are very attractive for a number of aerospace applications because of their high strength and stiffness to weight ratios. Furthermore, the ability to tailor the stiffness and thermal expansion coefficients of a laminate by using an appropriate layout for the composite laminate is a very attractive feature. The first generation of graphite/epoxy composites were developed to maximize stiffness and glass transition temperature T_g by utilizing a high cross-link density. However, these systems were found to delaminate rather easily when out-of-plane stresses were applied. Subsequently, attempts have been made to improve the composite toughness by improving the toughness of the resin systems. This has had somewhat disappointing results in that a large increase in resin toughness has not been found to give a proportionate increase in composite toughness. Scott and Phillips [1] found that a tenfold increase in resin toughness increased composite toughness by a factor of two. Similar results on different systems were found by Bascom et al. [2,3], Vanderkley [4], and Bradley and Cohen [5,6].

In this paper, we will consider the question of whether some types of resin toughening mechanisms are more effective than others in enhancing delamination toughness. In particular, toughening by reductions in cross-link density and elastomer additions will be considered. The efficacy of the toughening mechanisms for Mode I, Mode II, and mixed mode loading will be considered.

Experimental Procedures and Analysis

Materials

Four graphite epoxy composite systems have been studied in this research effort. Hercules AS4/3502 composite which utilizes a highly cross-linked, and therefore, relatively brittle, resin system was chosen to be compared with three tougher systems, namely, Hexcel T6T145/F155, T6T145/F185, and T6T145/HX205. The Hexcel F155 resin has a lower cross-link density (280 atomic mass units between cross-links²) than the Hercules 3502 resin (AMU between cross-links not available). The Hexcel F185 and HX205 resins have even lower cross-link densities (430 AMU between cross-links²). Thus, the three Hexcel resins differ from the Hercules 3502 resin in that they have lower cross-link densities with the associated lower T_g values and higher resin ductility.

A second difference between the Hexcel F155 and the Hexcel F185 resins and the Hercules 3502 resin is that the two Hexcel resins have elastomeric material added to enhance their respective toughnesses. Approximately 6% carboxy-

terminated butadiene acrylonitrile (CTBN) is included in the F155 resin. This CTBN rubber precipitates as a second phase with a diameter which varies from 0.1 to 1.0 μm [2,3]. The F185 resin includes both a 6% addition of the CTBN rubber which precipitates and approximately 8% of prereacted rubber which has been mechanically blended into the resin [2,3]. These prereacted rubber particles have a bimodal distribution of diameters with peaks at 2 and 8 μm . The Hexcel HX205 has had no elastomer additions. Whatever toughness it manifests is a result of its relatively low cross-link density, which is the same as the Hexcel F185 resin, as previously noted.

Unidirectional, 24-ply-thick panels of the AS4/3502 and the T6T145/F155 were laid up using prepreg from the respective manufacturers and then cured in an autoclave/press at Texas A&M University. Additional panels of T6T145/F185 containing some plus and minus 45° plies were prepared to study the effect of ply orientation across the delaminating plane on the delamination fracture toughness. Unidirectional, 24-ply-thick panels of T6T145/F185 and T6T145/HX205 were prepared at NASA Langley for this study.

All panels contained a 0.025-mm-thick strip of Teflon[®] laid to a depth of 3 cm from one edge of the panel between the center two plies to provide a crack starter. Since the Teflon strip introduces a relatively blunt notched "crack," a natural crack extension of at least 3 cm was made before the measurement of any critical energy release rates. Thus, the G_c values reported in this study are for crack growth rather than crack initiation.

Split laminate specimens 2.5 cm wide by 30 cm in length were cut from the composite panels (fibers running the length of the specimens for the unidirectional panels) for macroscopic testing, while much smaller specimens (3 cm long by 0.6 cm wide) were cut to be fractured in the scanning electron microscope.

Castings of neat resin were provided by Hexcel for the F155, F185, and HX205 systems. Rectangular specimens 1.27 cm wide by 0.318 cm thick by 3.56 cm long were machined from the neat resin castings to be tested on a dynamic mechanical spectrometer manufactured by Rheometrics, Inc. Standard tension specimens were also machined from the neat resin castings, as were compact tension specimens for fracture toughness testing. Standard compact tension specimens were prepared according to the ASTM Test for Plane-Strain Fracture Toughness of Metallic Materials (E 399) with $W = 5.08$ cm, but with a thickness of approximately 0.5 cm, which was the thickness of the castings.

Mechanical Properties Testing

Delamination Fracture Toughness Tests—Delamination fracture toughness tests were run at ambient temperature (24°C) in opening mode (Mode I), shear mode (Mode II), and mixed mode conditions on split laminate test specimens using an MTS materials testing system operated in stroke control at 0.0085 cm/s. Load and displacement were continuously measured, while the crack length was measured visually at the surface at discrete intervals (about once every 1 cm of

²R. Moulton, Hexcel Corporation, Dublin, CA, personal communication.

crack extension). Unload compliance measurements were made at intervals of about 2 to 3 cm.

Mixed mode and Mode II tests were also performed using split laminate specimens. This was accomplished by asymmetrically loading the cracked end of the split laminate while restricting vertical displacement of the uncracked end, which was still free to translate horizontally, as seen in Fig. 1. This procedure was first developed by Vanderkley [4] at Texas A&M University. The mixed mode loading can be analyzed by the superposition principle and noting that an asymmetrically loaded split laminate can be treated as the sum of pure bending and pure Mode I loading, with the pure bending giving essentially a pure Mode II state of stress (see Fig. 1). When the specimen is loaded as shown in Fig. 1 with the uncracked end and the upper arm of the split laminate held stationary and the lower arm of the split laminate displaced (through actuator displacement), the percentage of Mode II loading will vary continuously throughout the test from pure Mode I to a Mode II energy release rate that is approximately 40% of the total energy release rate.

Two special cases of the loading configuration seen in Fig. 1 may be noted. First, if the upper arm of the cracked end of the split laminate is unconstrained ($P_u = 0$), then the specimen will experience a constant fraction of Mode II

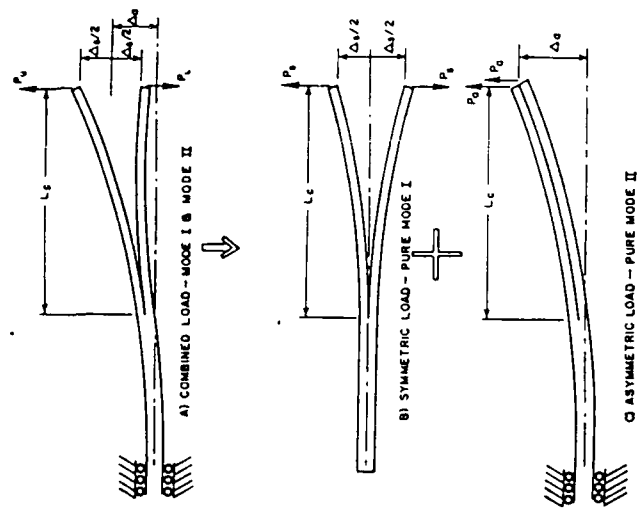


FIG. 1—Schematic showing how asymmetric loading of split laminate can introduce a mixed Mode I/Mode II state of stress at the crack tip.

loading throughout the test, which gives a Mode II energy release rate that is 43% of the total energy release rate. Second, if both upper and lower arms of the split laminate are pulled down with equal force using the actuator ($P_u = -P_d$), then a pure Mode II loading condition results. This loading arrangement is, in effect, one half of a three-point bend test, and thus, is very similar to the end notch flexural test developed by Russell and Street [7].

For the Mode II tests, a 0.79-mm Teflon spacer was placed between the crack faces of the split laminate specimen to minimize any frictional effects which might occur by the rubbing of the two surfaces together. This spacer would constitute a superimposed Mode I loading, but because the spacer was very thin, the Mode I energy release rate it produces is trivially small. A scanning electron microscopy (SEM) examination of the fractured surfaces after Mode II testing gave no indication of rubbing between the two fractured surfaces.

Neat Resin Fracture Toughness Tests—Fracture toughness tests were run on several of the neat resins where G_{Ic} values were either unavailable or were regarded with some suspicion (literature values on F185 were calculated assuming linear elastic fracture mechanics, which is questionable for such a ductile system). The procedures specified in either ASTM E 399 or ASTM Test for J_{Ic} , a Measure of Fracture Toughness (E 813) were followed, with a single-specimen, multiple compliance approach used for ASTM E 813 on the Hexcel F185 system. Fatigue precracking was used to introduce cracks in the compact tension specimens.

Rheometrics Tests—Rheometric tests were run on neat resin specimens. These specimens were subjected to dynamics torsional cycling over a wide range of temperatures which bracketed the glass transition temperature T_g . The loss and storage modulus were recorded as a function of temperature. The glass transition temperature was assumed to correspond to the temperature where the loss modulus value was a maximum.

Tension Tests—Tension tests were conducted on the neat resin systems according to ASTM Test for Tensile Properties of Plastics (D 638). Strain was measured using strain gages which were mounted on the front and back face of each specimen and were capable of measuring strain of up to 10%. Complete stress-strain behavior was determined for each specimen from which tensile strength, yield strength, and elongation were noted.

Analysis of Delamination Fracture Toughness Tests

Mode I Critical Energy Release Rate Analysis G_{Ic} For Delamination Fracture—Generally, the term critical energy release rate is used to refer to initial crack extension from some preexisting flaw or fatigue precrack. In this work it is used to refer to the work required per unit area of new crack surface created for stable crack propagation, rather than for initiation. The Mode I critical energy release rate was calculated using linear beam theory as described by Vanderkley [4] where

$$G_{IIc} = (P_u L_c)^2 / BEI \quad (1)$$

where P_u is the symmetric loading $(P_u + P_L)/2$, see Fig. 1), L_c is the crack length, B is the specimen width, and EI is the flexural stiffness of the arms of the cracked portion of the specimen.

The flexural stiffness was calculated from measured values of load P_u , displacement Δ_u , and crack length L_c using a relationship also derived from linear beam theory, namely,

$$EI = 2P_u L_c^3 / 3\Delta_u \quad (2)$$

A value for EI was calculated at each of the approximately twenty points per specimen where crack length was measured. An average value of EI for the specimen was then determined and used in Eq 1 to calculate G_{IIc} values, also at approximately twenty points for each specimen. Three split laminate specimens of each composite were tested in Mode I with the reported G_{IC} values being the average of approximately sixty calculated values.

The results from all Mode I tests were also analyzed using the unload compliance measurements analyzed using the method suggested by Wilkins et al. [8], with the calculated values of G_{IIc} typically falling within 3% of the values calculated using linear beam theory (that is, Eqs 1 and 2). The only Mode I tests for which it was not possible to use the linear beam theory analysis (or the Wilkins analysis) were the T6T45/F155 specimens containing all plus and minus 45° plies. Because of the lower compliance, a significant degree of geometric nonlinearity was noted in the load-displacement records for these specimens. Furthermore, some far field damage in the split laminate arms was evident in view of the fact that the load-displacement record did not return to the origin on unloading. As a result, the nonlinear beam theory analysis first developed by Devitt et al. [9] was used to analyze these results. However, this approach is only good for nonlinear elastic behavior. A J integral analysis is currently being developed to use in analyzing these results which include not only geometric nonlinearities but also nonlinear viscoelastic behavior of the resin.

Mixed Mode and Mode II Critical Energy Release Rate Analysis G_{IIc} For Delamination Fracture — For Mode II delamination fracture toughness analysis, the following relationship for Mode II critical energy release rate was derived by Vanderkley [4], again assuming linear beam theory (see Fig. 1):

$$G_{IIc} = 3(P_u L_c)^2 / 4BEI \quad (3)$$

where P_u is the asymmetric load $(P_u - P_L)/2$ and the other terms are as previously defined.

For all pure Mode II tests, the load-displacement records were found to be significantly nonlinear. Calculation of G_{IIc} values using Eq 3 based on linear beam theory gave artificially high values of G_{IIc} in comparison to the results of Russell and Street [7] on similar material. A critical energy release rate calculation for split laminate specimens based on nonlinear elastic beam theory has previously been published for Mode I loading [9], but not for Mode II loading.

Thus, we chose to use the area method approximation, whereby the area under a load-displacement record for loading, crack advance from L_1 to L_2 , and unloading is determined and assumed to be equal to the work required to increase the crack area by $B[L_2 - L_1]$, where B is the specimen width. This method assumes all of the work represented by the area bounded by the load, crack advance, unload-displacement curve goes into crack advance. Any far field energy dissipation would erroneously be lumped into the energy absorbed per unit area of crack extension relationship. Thus, the calculated values of G_{IIc} using this approach may be considered upper bound estimates. Nevertheless, our results for G_{IIc} using the area method were in reasonable agreement with Russell and Street's results [7] (which implies far field damage is minimal for the unidirectional, split laminate specimens studied in this work) and were much smaller than the values one would obtain by naively using linear beam theory on the obviously nonlinear load-displacement records obtained on the Mode II specimens.

Mixed Mode Critical Energy Release Rate Analysis G_{Tacc} For Delamination Fracture — Most of the load-displacement records for the mixed mode delamination tests were quite linear so that G_{IIc} and G_{IIc} could be calculated using Eqs 1 and 3 with G_{Tacc} calculated as the sum of G_{IIc} and G_{IIc} . Where this was not the case, no analysis was attempted since neither superposition nor linear beam theory would be appropriate.

Real-Time Observations of Delamination Fracture In Scanning Electron Microscope

Real-time observation of fracture in the scanning electron microscope (SEM) is a relatively new technology. Theocaris and Stassinakis, [10] have fractured composite specimens loaded in tension in the SEM while Beaumont [11] has fractured composite and polymeric systems using torsional loading in the SEM. In this study, small split laminate specimens were fractured in a JEOL 35 scanning electron microscope specially equipped with a loading stage. Delamination is obtained by pushing a delaminating specimen over a blunt stationary wedge. A blunt wedge was used so that crack growth would result from pushing apart the two crack surfaces in essentially Mode I loading, without any direct pressure applied at the crack tip by the wedge. The wedge tip remained well away from the crack tip so that Mode I conditions would dominate at the crack tip. The fracture process was recorded on video tape and standard sheet film. A post-mortem fractographic examination was made of the fractured macroscopic split laminate specimens and the miniature split laminate specimens fractured.

Experimental Results

Results from Mechanical Properties Tests

The results of the various mechanical properties tests are summarized in Tables 1 to 4. The glass transition temperature results are presented in Table 1,

TABLE 1—Glass transition temperature of resins

Resin System	Glass Transition Temperature, °C
3502	191*
F155	118
HX205	118
F185	109

* Obtained from literature from Hercules, Inc., Magna, UT 84044

TABLE 2—Resin tensile properties

Resin System	Yield Strength, MPA	Tensile Strength, MPA	Elongation, %
3502	58	69	3.10
F155	38	46	8.87
HX205	61	73	3.24

TABLE 3—Critical energy release rates G_c , J/m²

Material	AS4/3502	T6T145/F155	T6T145/HX205	T6T145/F185
Mode I (neat resin)	70 (13)	730 (14)	460	8100
Mode I (composite)	189	520	455	2205
20% Mode II	264	525	796	
43% Mode II		548	789	
Mode II	570	1270	1050	2440

TABLE 4—Effect of fiber orientation upon Mode I G_c

Material	Layup	G_c
F155	0(24)	520
F155	+45/-45/0(8)/-45/+45/ -45/+45/0(8)/+45/-45/ +45(2)/-45(4)/+45(2)/ -45(2)/+45(4)/-45(2)/	600
F155		1400*

* Note this is not a true G_c value because of inadvertent inclusion of far field damage, as explained in text

where the 3502 is seen to have the highest T_g , F185 has the lowest, and HX205 and F155 have an identical value of T_g . The three more ductile systems, HX205, F185, and F155, all have T_g values well below the relatively brittle 3502. The tension tests results are summarized in Table 2. No as-cast 3502 resin was obtained. Thus, a tension test was not run on this resin. The F155 and the HX205 have nearly identical tensile properties, which is not surprising since they have

the same T_g . The F185 resin is much more soft and ductile than the F155 or the HX205, as expected. Though tensile properties were not obtained for the 3502 resin, it would be expected to be somewhat stronger with a smaller elongation to failure than the other three resins.

The neat resin fracture toughness values G_{Ic} are summarized in Table 3 and correlate nicely with the T_g results and the tension test results presented in Tables 1 and 2. The ratio of composite delamination toughness G_{Ic} to neat resin fracture toughness G_{Ic} is seen to decrease as the resin toughness increases, as previously noted by Bradley and Cohen [6] and Hunston [12]. A second important trend to note from Table 3 is that the Mode II delamination toughness is always higher than the Mode I delamination toughness, with a ratio of Mode II delamination toughness to Mode I delamination toughness of approximately $\times 3$ for the brittle system decreasing to a value just barely larger than $\times 1.0$ for the most ductile system.

The effect of fiber orientation across the plane of delamination on delamination fracture toughness G_{Ic} is seen in Table 4. For a specimen with plus or minus 45° plies across the interface that is debonding, but with a stiffness similar to a unidirectional composite, the delamination critical energy release rate was found to be very similar to the results for unidirectional laminates (600 compared to 520 J/m²). Chai [13] has previously noted a similar result; namely, that ply orientation across the plane of delamination does not significantly affect the delamination fracture toughness for laminates with similar stiffness. The much larger value for G_{Ic} indicated for the second multiaxial layup is a result of far field damage as a result of nonlinear viscoelastic behavior by the resin. As will be seen presently, the resin carries a significant load in the axial direction for a composite laminate with all $\pm 45^\circ$ plies. This significant resin loading not only in the crack tip region but at other locations removed from the crack tip will cause the resin to undergo nonlinear viscoelastic deformation. This energy dissipation in the far field should not be counted in the crack tip energy dissipation per unit area of crack extension. However, our G_I calculation using the area method does not distinguish between crack tip and far field energy dissipation. Thus, the G_{Ic} value of 1400 J/m² indicated in Table 4 is not really a G_{Ic} , but includes G_{Ic} plus far field damage.

Results From Real-Time Observations of Delamination Fracture in Scanning Electron Microscope SEM

The observations of fracture in the SEM had as its purpose the determination of the details of the delamination fracture process for the various systems to gain a better understanding of how resin toughness can be translated into delamination fracture toughness. The damage zone size around the crack tip as well as the critical event (that is, resin fracture, interfacial debond, and so forth) can be determined from such observations.

In situ fractography for the four composite systems are shown in Figs. 2 through 5. The damage zone as evidenced by fine microcracking is seen to be

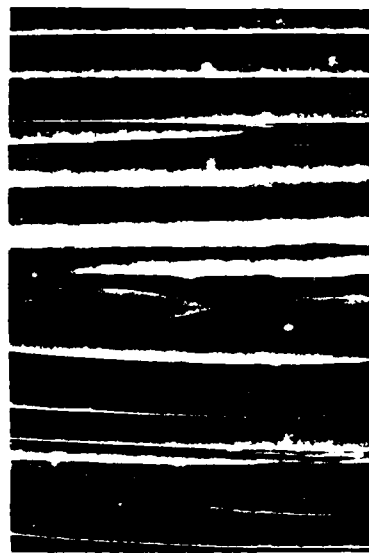


FIG. 2.—*In situ delamination of AS4/3502 showing debonding with very little resin damage (top, at $\times 1000$).*

very small for the AS4/3502 and the critical fracture event is usually interfacial debonding (see Fig. 2). In Fig. 2, the cracking appears to be through the resin, but is in fact along a fiber just beneath the surface, as indicated by the charging (light-colored region) adjacent to the fracture plane. Crack advance in the AS4/3502 was usually discontinuous. As the wedge was inserted further into the specimen, crack advance would not occur continuously but in a burst of interfacial debonding which resulted in significant crack advance. This unstable mode of crack growth suggests that the interfacial bonding in this system is quite heterogeneous. Crack arrest probably occurs at some locally better bonded region. The energy release rate must be increased to initiate crack growth. However, once the locally better interfacial bonding is overcome, crack advance occurs until the energy release rate decreases (which it does for crack extension under displacement controlled loading) to a value lower than the local resistance G_{ic} , which is probably at the next region of better interfacial bonding.

A much more extensive damage zone is seen around the crack tip for T6T145/F155 (see Fig. 3). The microcracked zone is much larger in extent than for the AS4/3502 and has a much greater density of microcracks. In spite of this fact, a significant amount of crack extension occurred by interfacial failure. It did not appear that the interfacial failure in the T6T145/F155 was always a result of debonding. Rather, it sometimes appeared that the microcrack density was greater adjacent to fibers, and therefore, made coalescence more likely in that region. Thus, it was rather an exception to see a bare fiber in the postmortem fractography of the T6T145/F155 while bare fibers were quite common in the AS4/3502.

The in situ fractography for the T6T145/HX205 is presented in Fig. 4 where the damage zone is again seen to be characterized by significant microcracking. The extent of the damage zone is somewhat greater than for the T6T145/F155, but the density of microcracking is much less. Failure seemed to proceed in the

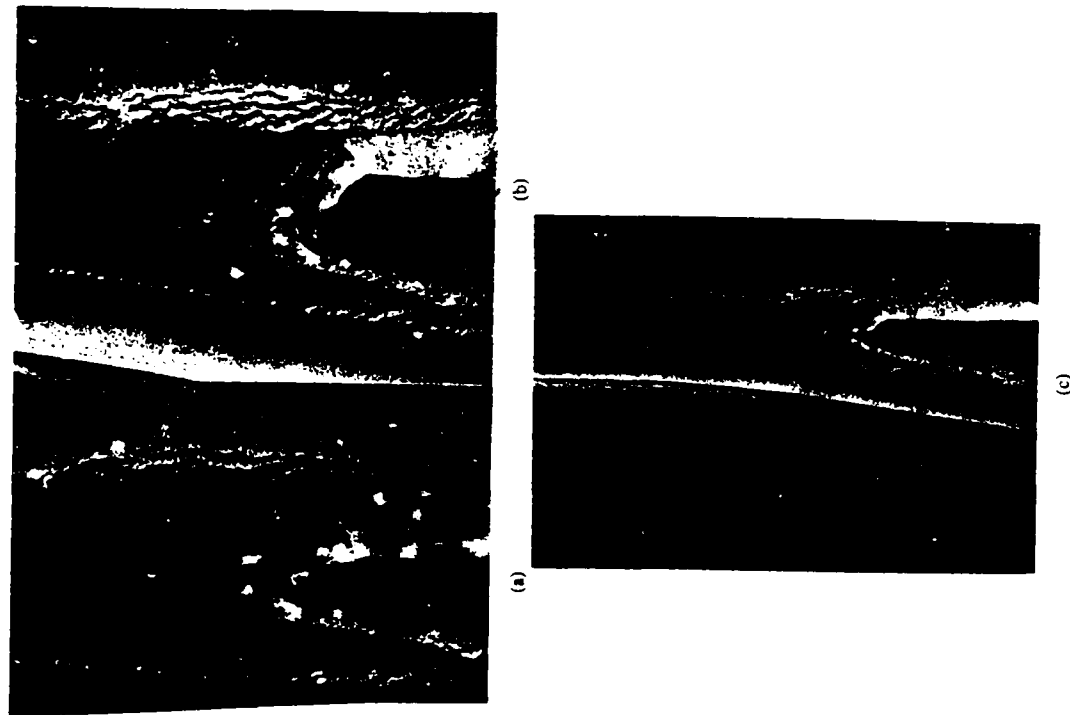


FIG. 3.—(a) *In situ delamination of T60045/F155 showing extensive microcracking around the crack tip (left, at $\times 3900$).* (b) *In situ delamination of T6T145/F155 showing coalescing of microcracks to form macroscopic crack growth (right, at $\times 3000$).* (c) *In situ delamination of T6T145/F155 system. Debonding as well as microcracking is visible ($\times 1000$).*

interfacial area between resin and fiber, not by debonding but by coalescence of microcracks which seemed to exist in greater number in the interfacial region in the T6T145/HX205.

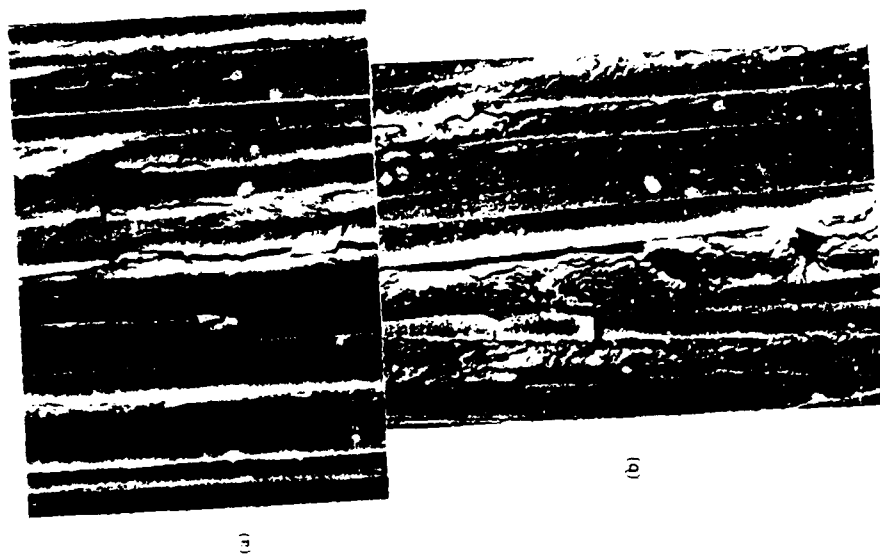


FIG. 4 — (a) In situ delamination of HX205 system. Main crack grows is preceded by developing of large microcrack zone ahead of the crack tip (top, at $\times 1000$). (b) In situ delamination of HX205 system. Extensive microcracking that coalesces into macroscopic crack growth (bottom, at $\times 1000$).

Finally, the damage zone around the crack tip in the T6T145/F185 is seen in Fig. 5 to be both large in extent and high in density of microcracks. Again, the failure is still frequently near the interface, but a result of a higher density of microcracks in this region rather than debonding. Very few regions of bare fiber are noted in the postmortem fractography.

The in situ fracture behavior of the T6T145/F155 composite with off-angle plies is seen in Fig. 6. Because the fibers are at an angle of 45° to the length of the specimen, Mode I loading of the split laminate gives significant loading of the resin along the length of the specimen as well as in the Mode I opening direction. Thus, while microcracking similar to that observed in the specimens made from



FIG. 5 — (a) In situ delamination of T6T145/F185 system. Large microcrack zone ahead of crack tip with a significant extent above and below plane of crack (left, at $\times 1000$). (b) In situ delamination of T6T145/F185 system. Resin tearing as well as microcracking is evident (right, at $\times 1000$).



FIG. 6 — (a) In situ delamination of T6T145/F155 system with fibers at 45° (left, at $\times 1000$). (b) In situ delamination of F155 system with fibers at 45° . Note microcracks that point back to microscopic crack tip (right, at $\times 1000$).

a unidirectional laminate is still evident, the orientation is different and voiding at the resin/fiber interface is noted. In fact, coalescence of these voids seems to play a significant role in the delamination fracture process in a split laminate with a large number of off-axis plies.

Typical damage zone sizes around the crack tip of the various composites tested have been quantified and are summarized in Table 5.

Results of Postmortem Fractographic Examination of Fractured Surface of Delaminated Specimens

The postmortem fractographic examination included specimens fractured for Mode I, Mode II, and mixed mode loading conditions. The results for the AS4/3502 consistently indicated bare fibers (except possible sizing) and interfacial debonding, whereas the three ductile systems gave only occasional indication of fiber debonding. Postmortem fractographic results for T6T145/F155 and T6T145/HX205 are seen in Figs. 7 and 8. The duplex appearance to the fracture surface in the T6T145/F155 appears to be the result of a variable thickness of the resin rich region between plies. Only a few bare fibers are noted.

Figures 9 through 11 present highlights of the results from the postmortem fractographic examination of the specimens fractured in Mode II and mixed mode. At the time this work was done, our stage was not yet adapted for Mode II testing in the SEM. Thus, the postmortem fractographic results on the Mode II and the mixed mode delamination fractures constitute all of the fractographic information obtained for these loading conditions. The distinctive features on the fractured surface of the three more ductile composite systems loaded with a significant percentage of Mode II loading are leaf-like artifacts whose orientation relative to the delamination plane increase monotonically with increasing percentage of Mode II loading. The more brittle AS4/3502 had a very regular array of what appear to be sigmoidal shaped microcracks which have coalesced to give macrocrack advance.

Discussion

The significant results to be discussed in this section are as follows:

- (1) the efficacy of rubber particle additions and lower cross-link density in enhancing neat resin fracture toughness;

TABLE 5—Damage zone size and corresponding delamination fracture toughness.

Material	Size of Damaged Zone, Mm			G_{Ic} , J/m ²
	Ahead of Crack Tip	Above or Below Delamination Plane		
AS4/3502	20	5		189
F155	20	10		520
F155 ± 45	50	10		...
HX205	75	35		455
F185	200	35		2205

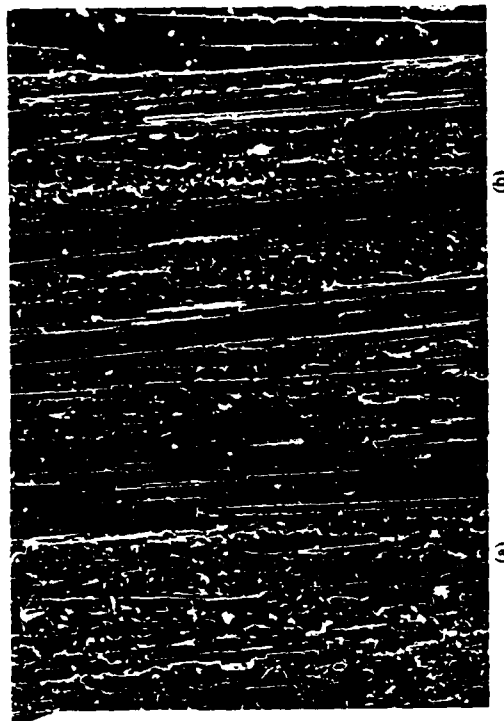


FIG. 7—(a) Postmortem fractography of F155 composite delaminated in Mode I conditions (near center of specimen) (upper left, at $\times 100$). (b) Postmortem fractography of F155 composite delaminated in Mode I conditions (near edge of sample) (upper right, at $\times 100$).

- (2) the efficacy of rubber particle additions and lower cross-link density in enhancing composite delamination fracture toughness;
- (3) the change in fracture toughness with increasing fraction of Mode II shear loading; and
- (4) the effect of ply orientation and laminate stiffness on delamination fracture toughness.

These macroscopic fracture toughness results will be discussed in light of the in situ and postmortem fractographic observations.

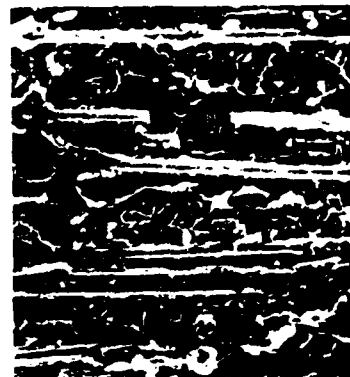


FIG. 8—Postmortem fractography of HX205 composite delaminated in Mode I conditions (lower center, at $\times 300$).

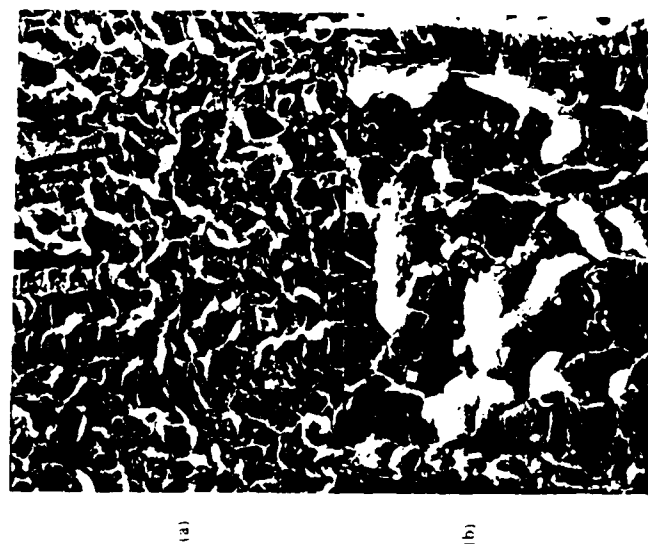


FIG. 9 — (a) Postmortem fractography of F155 composite delaminated in 43% Mode II conditions (top surface of fractured specimen) (top, at $\times 450$). (b) Postmortem fractography of F155 composite delaminated in 43% Mode II conditions (bottom surface of fractured specimen). Note leaf-like artifacts are oriented in opposite direction to those on the top surface (center, at $\times 1500$).



FIG. 10 — Postmortem fractography of HX205 composite delaminated in 43% Mode II conditions (bottom, $\times 300$).

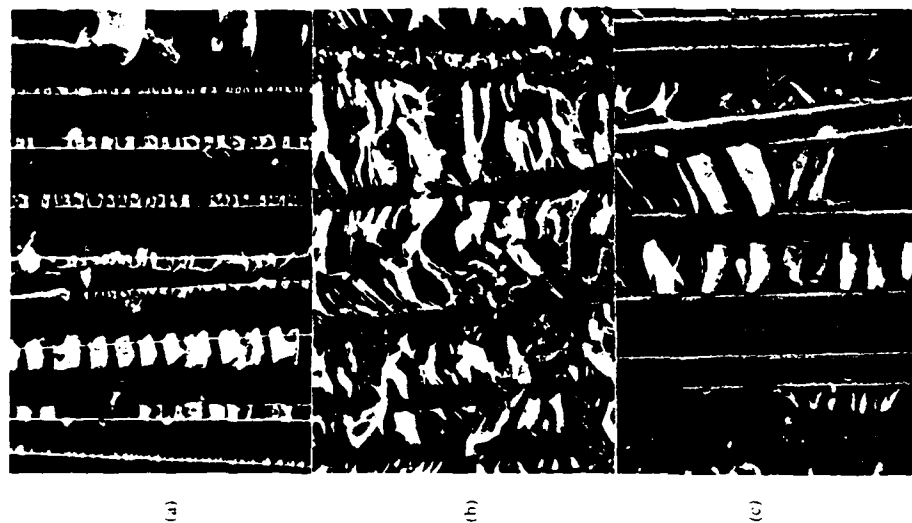


FIG. 11 — (a) Postmortem fractography of AS4/3502 composite delaminated in Mode II conditions. Zipper-like artifacts appear to be formed by coalescence of series of sigmoidal shaped microcracks (top, $\times 1500$). (b) Postmortem fractography of F155 composite delaminated in Mode II conditions. Note extensive resin deformation. (center, at $\times 1000$). (c) Postmortem fractography of HX205 composite delaminated in Mode II conditions. Note extensive resin deformation (bottom, at $\times 1000$).

Neat Resin Fracture Toughness

The neat resin toughness was found to correlate with T_g and with elongation in a tension test for the four systems studied. Note that the F155 and the HX205 had quite similar tensile properties and T_g , though they were toughened somewhat differently, that is, HX205 relied entirely on decreasing the cross-link density while the F155 used a combination of reduction in cross-link density (compared

to an epoxy like Hercules 3502) and rubber particle additions. The F155 had a better fracture toughness for both neat resin and composite delamination than did the HX205. Materials with similar tensile elongations may have significantly different fracture toughnesses since fracture toughness depends on the ductility under a triaxial rather than a uniaxial state of stress. Since rubber particle additions can relieve this triaxial state of tension by voiding, the same elongation in a tension test may correlate with a higher fracture toughness for rubber particle toughened resins.

The beneficial effect of rubber particle additions is particularly evident in the F185, whose neat resin toughness is $\times 18$ that of the HX205 even though their tensile ductilities differ by only a factor of $\times 3$. The elastomer additions while giving some enhancement to tensile elongation give a dramatic increase to the fracture toughness. Yee and Pearson [14] have noted that a resin needs to have some intrinsic capacity to deform in response to shear stress if it is to be benefited by rubber particle additions, which principally increase the shear stress in the crack tip region by relaxing constraint. Again, the very large fracture toughness of the F185 compared to the other systems suggests a strong synergistic effect between lowering the cross-link density, which increases the freedom to deform in response to shear stress and rubber particle additions, which allow larger shear stresses to be developed at the tip of a crack.

Translation of Neat Resin Toughness into Delamination Toughness

There appear to be at least two reasons why tougher resin systems give a much smaller fraction of their neat resin fracture toughness in delamination toughness. First, a tougher resin has a deformation zone that is much more extensive than the resin rich region between plies. In the composite, the fibers act like rigid filler in this deformation zone, which reduces the degree of load redistribution away from the crack tip, and thus allows the critical strain or critical stress condition for local failure at the crack tip to be achieved more easily. For resins where the deformation/damage zone ahead of the crack tip is on a scale of less than or equal to the height of the resin rich region between plies, one might expect the neat resin toughness and the delamination toughness to be similar if interfacial failures do not dominate the delamination fracture behavior. Only in the case of the F185 is there extensive damage outside of the resin rich region between plies, and only in this system is there a dramatic difference in the neat resin fracture toughness and the composite delamination fracture toughness.

A second way the fibers may prevent delamination fracture toughness from achieving neat resin fracture toughness is that they allow heterogeneous nucleation sites for fracture. For Mode I loading, all four of the composite systems studied had failure primarily in the interfacial region. Even where fiber bonding is good, the interfacial region seems to have a greater density of microcracks (or deformation), which leads to premature failure of the composite before extraction of the full toughness from the resin system.

Mode II Delamination Fracture Toughness

The more brittle the system, the greater is the ratio of G_{IIc} to G_{Ic} . This is the generalization from this work and other unpublished work at Texas A&M University. The increase in total energy release rate for increasing Mode II in brittle systems can be understood to be the result of a whole series of brittle sigmoidal shaped microcracks, impeded in their growth on their respective principle normal stress plane by the presence of the fibers. This both increases the area of fracture surface created and constitutes a more tortuous path for crack propagation, each of which would require greater energy dissipation per unit area of crack extension.

Where the fracture is more ductile, the energy dissipation does not seem to be such a sensitive function of the imposed state of stress. For example, the fracture mode and the appearance of the fracture surface were similar for pure Mode I and pure Mode II loading of T6T145/F185. For such systems, one would expect $G_{IIc} \approx G_{Ic}$, which was the case for T6T145/F185.

The Effect of Off-Angle Plies

The in situ fractography seen in Fig. 6 clearly indicates that significant resin deformation is occurring along the axis of the specimen. This specimen with all $\pm 45^\circ$ plies would certainly experience significant resin loading in the direction of the specimen axis as a result of bending stresses. While similar stresses would also be experienced by a unidirectional laminate specimen, the fibers would carry essentially all of the loading in the axial direction. It is this additional deformation, not only in the crack tip region, but presumably all along the specimen that is the far field damage previously mentioned as being responsible for giving an artificially high value for G_{Ic} of 1400 J/m². It is worth noting that the specimen with $\pm 45^\circ$ plies at the interface where delamination is occurring, but mainly unidirectional plies otherwise had a delamination fracture toughness similar to that for the unidirectional laminate. A J integral analysis being developed at Texas A&M University has given approximately 600 J/m² for G_{Ic} for the laminate with all $\pm 45^\circ$ plies. If this proves to be a reliable result, then it suggests that the delamination fracture toughness in composite materials may be a material property independent of stacking sequence if the near and far field damage are properly separated.

Summary

The combination of low cross-link density and elastomer additions has been seen to give the most potent toughening for neat resins. A relatively small increment of the additional neat resin fracture toughening above 800 J/m² is actually reflected in the delamination fracture toughness of a composite. Mode II delamination toughness of brittle systems may be as much as three times the Mode I delamination fracture toughness while a ductile system may have a

Mode II delamination fracture toughness that is similar to the Mode I value. The energy absorbed per unit area of crack extension for delamination seems to be independent of ply orientation if proper accounting of the near and far field energy dissipation is made.

Acknowledgment

The generous support of this work by the Air Force Office of Scientific Research (Major David Glasgow, project monitor) is acknowledged. Rich Moulton's (Hexcel Corporation) assistance in providing the materials studied is also recognized. The authors also acknowledge the technical support given by the Electron Microscopy Center of Texas A&M University.

References

- [1] Scott, J. M. and Phillips, D. C., "Carbon Fibre Composites with Rubber Toughened Matrices," *Journal of Materials Science*, Vol. 10, 1975, pp. 551-562.
- [2] Bascom, W. D., Bitner, J. L., Moulton, R. J., and Siebart, A. R., "The Interlaminar Fracture of Organic-Matrix, Woven Reinforcement Composites," *Composites*, Jan. 1980, pp. 9-18.
- [3] Bascom, W. D., Ting, R. Y., Moulton, R. J., Riew, C. K., and Siebert, A. R., "The Fracture of an Epoxy Polymer Containing Elastomeric Modifiers," *Journal of Materials Science*, Vol. 16, 1981, pp. 2657-2664.
- [4] Vanderkley, P. S., "Mode I-Mode II Delamination Fracture Toughness of a Unidirectional Graphite/Epoxy Composite," Master's thesis, Texas A&M University, College Station, TX, Dec. 1981.
- [5] Cohen, R. N., "Effect of Resin Toughness on Fracture Behavior of Graphite/Epoxy Composites," Master's thesis, Texas A&M University, College Station, TX, Dec. 1982.
- [6] Bradley, W. L. and Cohen R. N., "Matrix Deformation and Fracture in Graphite Reinforced Epoxies," presented at ASTM Symposium on Delamination and Debonding of Materials, Pittsburgh, PA, 8-10 Nov. 1983.
- [7] Russell, A. J. and Street, K. N., "Moisture and Temperature Effects on the Mixed-Mode Delamination Fracture of Unidirectional Graphite/Epoxy," *Delamination and Debonding of Materials*, ASTM STP 876, S. Johnson, Ed., American Society for Testing and Materials, Philadelphia, 1985.
- [8] Wilkins, D. J., Eisemann, J. R., Cumin, R. A., and Margolis, W. S., "Characterizing Delamination Growth in Graphite-Epoxy," in *Damage in Composite Materials: Basic Mechanisms, Accumulation, Tolerance and Characterization*, ASTM STP 775, American Society for Testing and Materials, Philadelphia, 1982.
- [9] Devitt, D. F., Schapery, R. A., and Bradley, W. L., "A Method for Determining the Mode I Delamination Fracture Toughness of Elastic and Biscoelastic Composite Materials," *Journal of Composite Materials*, Vol. 14, Oct. 1980.
- [10] Theocaris, P. S. and Stassinakis, C. A., "Crack Propagation in Fibrous Composite Materials Studied by SEM," *Journal of Composite Materials*, Vol. 15, March 1981, p. 133-141.
- [11] Mao, T. H., Beaumont, P. W. R., and Nixon, W. C., "Direct Observations of Crack Propagation in Brittle Materials," *Journal of Materials Science Letters*, Vol. 2, 1983.
- [12] Hunston, D. A., "Composite Interlaminar Fracture: Effect of Matrix Fracture Energy," presented at ASTM Symposium on Toughened Composites, Houston, TX, March 1985.
- [13] Chai, H., "The Characterization of Mode I Delamination Failure in Non-Woven, Multi-Directional Laminates," *Composites*, Vol. 15, No. 4, Oct. 1984, pp. 277-290.
- [14] Yee, A. F. and Pearson, R. A., "Toughening Mechanism in Elastomer-Modified Epoxy Resins — Part I," NASA Contractor Report 3719, 1983, experimental work completed.

A Comparison of the Crack Tip Damage Zone for Fracture of Hexcel F185 Neat Resin and T6T145/F185 Composite

E. A. CHAKACHERY and W. L. BRADLEY

Texas A&M University
College Station, Texas 77843

Hexcel F185 neat resin and T6T145/F185 graphite fiber-reinforced composite were subjected to Mode I loading in the compact tension (CT) geometry (fibers parallel to the crack) and the energy per unit area of crack extension, J_{Ic} , determined to be 8100 and 1600 J/m² respectively. *In-situ* fracture studies using scanning electron microscopy on a CT-type specimen of F185 showed extensive microcracking in a damage zone ahead of the crack tip, which was similar to the microcracking observed in the whitened area ahead of the crack tip in the macroscopic CT specimens. A simple calculation using a rule of mixtures approach suggests that the diminished size of the damage zone and the presence of rigid fibers in the damage zone in the composite are not a sufficient explanation for the significantly lower delamination toughness of the composite compared to the neat resin. From this it may be inferred that the strain to failure locally in the damage zone ahead of the crack in the composite may also be lower than that which can be tolerated in the neat resin. Evidence for this idea comes from the observation that microcrack coalescence seems to occur preferentially at the fiber/resin interface.

INTRODUCTION

Delamination in graphite fiber-reinforced resin composites is well known to limit the extensive use of these materials in some structural applications. Much effort has been directed in the past decade towards improving the delamination fracture toughness of graphite/epoxy composites (1 to 10). Since the delamination crack propagates through the interlaminar resin rich region, the emphasis has been on obtaining epoxy resins with improved fracture toughness. The addition of elastomeric modifiers was shown (1 to 6) to dramatically increase the fracture toughness, G_{Ic} , of the matrix resin, but resulted in a quite modest increase in the delamination fracture toughness of the composite (7, 8). This was shown (8 to 10) to be primarily due to the reduced volume of resin deformation in the damage zone ahead of the delamination crack tip since the fibers act as rigid fillers in the ductile matrix. Evidence in support of this conclusion was obtained (9, 10) from the observation that a decrease in the fiber volume fraction resulted in an increase in the delamination fracture tough-

ness. The current investigation was undertaken to attempt to correlate the delamination fracture toughness of the composite with the fracture toughness of the neat resin. The determination of the fracture processes occurring in the vicinity of the crack tip in both the composite and the neat resin was a necessary first step. If these events are nominally the same, then there may be a relationship between neat resin toughness and delamination toughness.

To study the relationship between neat resin fracture toughness and composite delamination fracture toughness, *in-situ* observations of each fracture process have been made in the scanning electron microscope (SEM). These observations have been correlated with macroscopic measurements of a composite made from this neat resin. A simple model has been proposed to relate the microscopic observations of the fracture processes to the observed macroscopic measurements of fracture toughness.

The resin system selected for this study was the F185 formulation commercially available from Hexcel Corp. It is a relatively tough resin (9 per cent elongation in a 25 mm specimen) with a reported fracture toughness of

AD-A192 021

FRACTURE PHYSICS OF DELAMINATION OF COMPOSITE MATERIALS

3/3

(U) TEXAS A AND M UNIV COLLEGE STATION MECHANICS AND
MATERIALS CE W L BRADLEY ET AL. OCT 87 NOL-8021-87-12
AFOSR-TN-88-0020 AFOSR-84-0064

UNCLASSIFIED

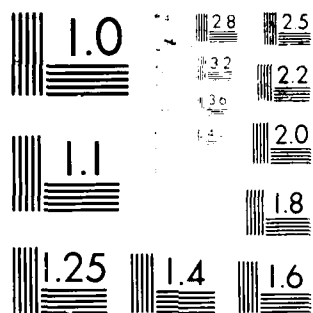
F/C 11/4

ML

END

DATE
FILMED
5 88

1511



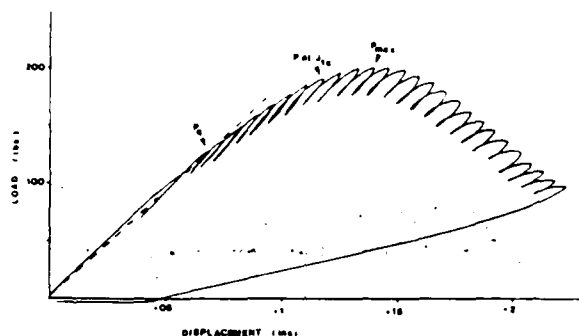


Fig. 1. Load-displacement record for 1T compact tension specimen of F185 resin showing considerable non-linearity.

gral analysis according to ASTM E813-81. A well defined J-R curve was obtained from which a J_{Ic} value of 8100 J/m² was determined. This is considerably higher than the value of 6000 J/m² reported by the manufacturer (11). This difference may be due to our use of fatigue precracking rather than razor notching or due to our use of a nonlinear rather than linear analysis. If we use the linear elastic analysis in ASTM E399-81, we obtain a K_Q value of 2700 J/m² from the 5 percent secant offset value of P_Q . However, P_{max} is much greater than 1.1 P_Q , and the specimen thickness is less than that required by ASTM-E399 for K_Q to be equal to K_{Ic} . Thus, the linear elastic analysis is invalid for our specimen size. If we use P_{max} and the actual crack length at P_{max} in a LEFM calculation, we obtain a " K_{Ic} " which has an equivalent G_{Ic} of 6300 J/m² which is similar to the 6000 J/m² obtained by Bascom and coworkers (2) using a similar approach. We believe that the value of 8100 J/m² obtained in this work using fatigue precracked specimens and a J-integral analysis is a more meaningful measure of the fracture toughness of the F185 resin.

A J-integral approach was also used to analyze the data obtained in the CT specimens of the composite. The J_{Ic} for transverse crack growth thus obtained was 1600 J/m² which compares very well with recent results by Bascom (13). The macroscopic test results may be summarized as follows: the neat resin fracture toughness was 8100 J/m², whereas the delamination and transverse cracking in the composite gave toughness values of 1900 J/m² and 1600 J/m² respectively. Thus, crack growth in the composite parallel to the fiber direction is much easier than crack growth in the neat resin.

In-Situ and Post Mortem Fracture Observations in SEM

Fracture studies conducted in the SEM on the F185 neat resin indicate that the zone ahead of the crack tip undergoes extensive microcracking (Fig. 2). There has been some recent controversy as to whether these are actually micro-

cracks in the resin or microcracks in the 150A thick gold-palladium coating applied to the specimens to minimize charging. To try to verify that these are actual microcracks in the material, we have recently polished two sides of an AS4/3501-6 graphite/epoxy composite, coated one side with a 150A thick layer of gold-palladium in the usual way, delaminated the specimen in the SEM, removed the specimen with the wedge intact to avoid viscoelastic recovery and closure of the microcracks, and then coated the other side with gold-palladium in the usual way, and then examined it in the SEM with the wedge still intact. The results of this exercise are presented in Figs. 3(a) and 3(b). The microcrack morphology on the side coated and then deformed is essentially indistinguishable from the microcrack morphology seen on the side deformed and then coated. Thus, we believe that the Au/Pd coating is not responsible for the microcracking seen on the surface of our composite specimens.

The microcracked region ahead of the crack tip of the F185 neat resin (Fig. 2) extends 60 to 70 μ m above and below the crack tip and is shaped somewhat like a kidney bean. Crack propagation under fixed grip conditions occurred in a discontinuous manner via a time-dependent coalescing of the microcracks ahead of a blunted crack tip. With each successive extension, crack advance of 120 to 150 μ m was observed, resulting in a very sharp crack tip with relatively few microcracks ahead of it. The applied crack opening displacement was then increased essentially instantaneously, and with this increase, the microcrack density ahead of the crack tip would gradually increase with time, accompanied by crack tip blunting at the formerly sharp crack tip. Again, a critical density of microcracks (or crack tip strain) is reached and crack extension occurs by microcrack coalescence as before. Evidence of this process is seen in the post-mortem fractographic examination as relatively flat regions of crack extension, separated by the small lips that probably arise from crack tip blunting, preceding the next crack extension (Fig. 4). This appearance is typical over the whole fracture surface, indicating that the phenomena observed at the surface is typical of the bulk fracture behavior.

If crack extension does indeed occur by microcrack coalescence, then the relatively flat regions between lips seen in Fig. 4(a) and (b) should be found on examination at higher magnification to be composed of many small facets with ledges between them. This is exactly what is observed at 10,000 \times magnification, as shown in Fig. 4(c). It is worth noting that even at this very high magnification, the individual facets do not seem to have fractured by a brittle cleavage. The surface is relatively textured, with cavitation presumably at the rubber particle additions, which suggests that the microcracking is



Fig. 4. Fracture surface of F185 resin. Crack growth is from left to right. (a) 330 \times . Away from the free surface. Arrows indicate a lip formed by crack tip blunting after a growth sequence. (b) 330 \times . Just adjacent to the free surface. (c) 10,000 \times . Detail of a relatively flat region in (a). Cavitation due to phase separated CTBN. Facets separated by ledges probably correspond to microcrack coalescence.

tip can be made equally well in either case. The possibility also exists that microshear bands formed perpendicular to the surface can give rise to sharp contours, which, when viewed on edge, appear as microcracks on the surface. It should also be noted that microcracking and

deformation have the same beneficial effect of redistributing the load away from the crack tip and lowering the local stresses at the crack tip. Thus, from a physical point of view, either process enhances toughness.

In-situ delamination studies on T6T145/F185 composite show that the resin microcracks quite extensively in the vicinity of the crack tip. The microcracking extends from the interlaminar region and into the ply about 50 μm above and below the crack (Fig. 5). Here, as in the resin, the crack propagates by microcrack coalescence and in the same discontinuous manner. At each stage, however, the crack tip blunting is apparently less than in the F185 resin and the discontinuous extension varies from 40 to 100 μm . The coalescence of microcracks occurs predominantly at the fiber resin interface. Thus it appears that the presence of the fibers prevents the development of the full resin toughness from being realized due to premature microcrack coalescence at the fiber resin interface.

The presence of the rigid fibers also restricts the height above and below the delamination plane over which deformation and microcracking occurs (100 μm in the composite, compared to 130 μm in the resin). However, the region of microcracking ahead of the crack tip is actually increased from 25 μm in the resin to about 50 μm in the composite.

The fracture surface of the delaminated specimens showed evidence of cavitation, voiding, and microcracking (Fig. 6). The resin region of the composite delamination fracture surface shows more coarse cavitation than in the neat F185 resin fracture surface, where voids were relatively fine and more homogeneously dispersed. Furthermore, the voids seem to be more dense in the resin adjacent to the fibers (Fig.

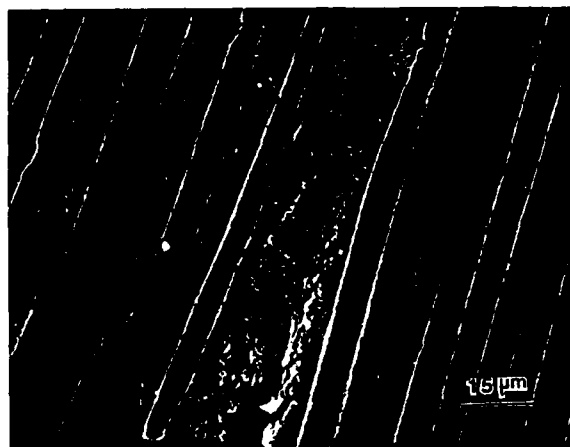


Fig. 5. 1000 \times . *In situ* delamination of T6T145/F185 composite showing microcracking in the damage zone ahead of the crack tip. Note microcracking is more dense adjacent to the fibers. Preferential microcrack coalescence near the resin fiber interface where the microcracks are inclined to the primary crack.

m² in the composite delamination fracture toughness. The first two of these three factors can be quantified based on actual observations. If one assumes that microcracking begins for strains above a threshold strain, then the extent of the microcracked zone can be used to quantify the magnitude of the h in Eq 2.

A cross-section of the composite prepared metallographically to reveal the microstructure (Fig. 8) may be used to determine the volume fraction of fibers in the hypothetical tensile specimen ahead of the crack tip. Since the volume fraction is quite nonuniform, the microstructure was divided into three regions: the resin rich region between plies with a fiber volume fraction of 19 percent; the ply region with a volume fraction of fibers of 76 percent and a transition zone with a volume fraction of approximately 33 percent. The relative heights of these three regions are shown in the schematic in Fig. 9, along with the height of the

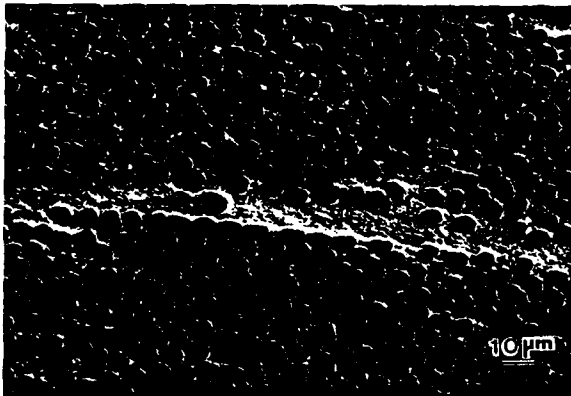


Fig. 8. 600x. Cross section of T6T145/F185 showing interlaminar resin rich region.

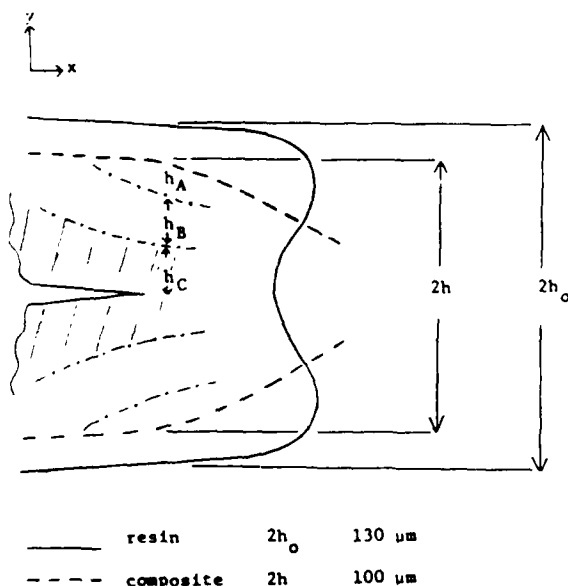


Fig. 9. Schematic showing relative height of damage zone in F185 resin and T6T145/F185 composite.

microcracked zone in the F185 resin. Using a simple rule of mixtures approach, and taking account of the smaller microcracked (and deformed) zone, one may estimate the delamination fracture toughness to be 4000 J/m² as shown below:

$$G_{lc} = \frac{J_{lc}}{h_0} [h_A(1 - V_f^A) + h_B(1 - V_f^B) + h_C(1 - V_f^C)]$$

This calculation implicitly assumes that the local strain to fracture in the F185 resin and the composite are the same, and that the stress distribution is also similar, at least on average.

Since the measured value of delamination fracture toughness in this system is 1900 J/m², the estimated value of 4000 J/m² is seen to be quite excessive. It also strongly suggests what the *in-situ* fractography has already indicated: namely, that preferential microcrack nucleation at the fiber/resin interface leads to premature failure, preventing the realization of 4000 J/m² that might otherwise be possible. This suggests that more attention to the interphase region is required if a greater fraction of the intrinsic toughness of the neat resin is to be manifested in delamination fracture toughness of the fiber-reinforced composite material.

SUMMARY

1. The delamination fracture toughness of the T6T145/F185 composite is 1900 J/m², whereas the fracture toughness of the neat F185 resin is 8100 J/m².

2. Microcracking in the resin appears to be a significant deformation mode for load redistribution at the crack tip.

3. Crack propagation occurs in a discontinuous manner through microcrack coalescence ahead of the crack tip.

4. In the composite, the microcracking is coarser and coalescence seems to occur preferentially at the resin-fiber interface.

5. The height of the deformation zone, above and below the plane of crack propagation, is greater in the resin than in the composite.

6. Comparison of the relative heights of the damage zone yielded 4000 J/m² as a calculated delamination G_{lc} for the composite, which is an over-estimation by a factor of two.

7. It may be inferred that the strain to failure in the composite is lowered, probably due to premature microcrack coalescence at the resin fiber interface.

ACKNOWLEDGMENTS

The authors wish to acknowledge the generous financial support of both the National Aeronautics and Space Administration, Langley Research Center, (Dr. John Crews, Project Monitor) and the Air Force Office of Scientific Research (Major David Glasgow, Project Monitor). Special thanks are due Laurie Veeder for her careful macroscopic testing.

Crack Tip Strain Field Measurements Determined
In-Situ in Scanning Electron Microscope of Mode I Crack
Extension in Polymeric Material

by
M. Hibbs and W.L. Bradley
Mechanical Engineering
Texas A&M University
College Station, TX 77843

published in
Proceedings of Society of Experimental Mechanics
Fall Conference - 1987
Savannah, Georgia

**Crack Tip Strain Field Measurements Determined In-Situ in Scanning
Electron Microscope for Mode I Crack Extension in a Polymeric Material**

by

M. Hibbs and W.L. Bradley
Mechanical Engineering
Texas A&M University
College Station, Texas 77843

INTRODUCTION

It has been recognized for some time that increasing the resin toughness in composite materials does not give a proportionate increase in the delamination fracture toughness of these materials.^{1,2} It has been suggested that the reason for this smaller increment of increase in delamination toughness compared to the increment of increase in toughness in the neat resin is due to reduction in crack tip strain possible in the composite due to interference of the fibers.

The addition of fibers to a ductile resin system could potentially reduce the crack tip strain for at least three reasons.³⁻⁵ First, failure in the composite might occur at the fiber/matrix interface prior to the extraction of the full potential ductility out of the resin. Second, the presence of fibers could give local constraint in the vicinity of the crack tip, lowering the total strain to failure observed. Third, the fibers can act as rigid filler, which could reduce the plastic zone size in resins which have a neat resin plastic zone size which is greater than the size of the resin rich region between plies in the composite.

Chakachery and Bradley⁵ and Jordan and Bradley⁶ have observed qualitatively the above mentioned reduction in plastic zone size, comparing crack growth in a ductile resin to delamination in a graphite/epoxy composite made from the same resin. Chakachery and Bradley⁵ attempted to quantify with a simple phenomenological model the reduction in fracture toughness in going from a tough resin to delamination in a composite made from this resin. They were unsuccessfully in fully accounting for the observed reduction in fracture toughness, most likely because their model implicitly assumed that the local strain field in each case was similar, with the difference in toughness resulting primarily from the presence of rigid filler; namely, carbon fibers. Obviously, a more realistic model would need to take into account the difference in the strain field around

the crack tip for neat resin compared to delamination of a composite made of this resin.

The purpose of this study has been to develop a technique which would permit the direct measurement of the strain field around a crack tip with sufficient resolution to see how distinctive the fields are for cracks in neat resin versus delamination cracks in composites made from the same resin. The approach used has been to burn a very fine dot map onto the polished surface (perpendicular to the plane of the crack) of a specimen using the electron beam in a scanning electron microscope. The exact coordinates for each of these points are determined before and after loading the specimen, allowing the determination of the displacement of each point. This displacement field may then be differentiated to give the strain field around the crack tip.

EXPERIMENTAL PROCEDURE

With considerable trial and error, a technique has been developed to burn a very systematic dot pattern onto the polished surface of the specimens. The beam of the electron microscope had to be adjusted to give dots that were sufficiently large to remain easily recognizable after considerable deformation but small enough to give adequate resolution. The very regular dot pattern seen in Fig. 1A was burned onto the surface using a JEOL-35 scanning electron microscope with the assistance of an image processing system manufactured by Kontron. The spacing seen in Figure 1A is approximately 10 microns. A finer dot spacing is possible, but not very useful unless the size of the dots can also be reduced, while retaining their visibility after large deformation.

The resin system selected for use in this study was Hexcel F185. This resin was selected because it is known to be relatively ductile (10% elongation in a tensile test), and therefore would be expected to give significant strain in the vicinity of the crack tip prior to failure. Furthermore, this system has a large reduction in toughness in going from the neat resin to delamination of the composite (8000J/m^2 to 2000J/m^2)⁵. Thus, it was considered ideal for this study.

Hexcel F185 resin was cast into rectangular plates. It was then machined into compact tension specimens which were subsequently fatigue precracked. Then the specimens were polished on a microprocessor to a 0.03 micron finish. Finally, the dot map was burned on the surface using the electron beam in the SEM, as shown in Figure 1A. The crack tip is seen at the bottom of Figure 1A,

just below the dot map. After loading which resulted in a small amount of crack growth which moved the crack tip just into the dot map, the deformation field is clearly seen through the distortion of the dot map (see Figure 1B). The displacement field and the associated strain field were determined using the image processing system in conjunction with a computer program written to numerically differentiate the displacement field data.

RESULTS AND DISCUSSION

The reduced results are presented in Figures 2-4. The normal strains as well as the principal shear strain are seen as a function of their respective x-y coordinate locations around the crack tip, which has a coordinate of $x=59.14$, $y=57.48$. The compact tension specimen was loaded in the x-direction with crack growth in the y-direction.

It should be emphasized that the three dimensional plotting routine used to present the results graphically does local smoothing prior to plotting. The polynomial curve fit for the smoothing operation interpolates as well, giving a much finer grid in the graphical results than was actually utilized (contrast actual grid size, Figure 1A, to grid size seen in the three dimensional plotting (Figures 2-4).

The elastic strain at yielding in F185 as measured in a tensile test is about 1.2%. Thus, the region of nonlinear deformation around the crack tip is seen to be quite extensive. If it is remembered that carbon fibers typical have diameters of about 7 microns, then the nonlinear deformation zone would extend to at least five fiber diameters above and below the plane of delamination if the composite has a similar strain field around the tip of a growing delamination crack to that observed in Figs. 2-4 for the F185 neat resin. Qualitative indications of a deformation zone of this size in a delaminating T6T145/F185 composite, but without direct measurement of the strain field, have been noted by Bradley and Cohen⁷.

A second important observation is the magnitude of the local strain at the crack tip. The elongation measured in a tensile test is 10%, with no apparent necking. Thus, one might have assumed for micromechanics modelling that the local strain to failure would be 10%, or possibly less due to the effects of constraint. However, it is clear that the tensile elongation greatly underestimates the true local strain to failure at the tip of a growing crack in F185. The measured value of 48% should be considered a lower bound since it is

measured over a 10 micron gage at the crack tip in a very steep strain gradient and would increase to an even higher value as crack advance gave ductile fracture to this material. The critical value for local strain to failure for delamination crack growth is probably somewhat lower than the value for crack growth in the neat resin for reasons previously discussed.

One concern that should be mentioned is the question of whether the surface strain measurements are in any way representative of the bulk strain distribution. In materials where cavitation or microcracking does not occur, one would expect a significant difference between the strain distribution for the plane-stress state of stress that exists at the surface and the strain distribution that would exist for the plane-strain state of stress in the bulk. However, F185 with rubber particle toughening does cavitate, relaxing the through thickness stress. Thus, for this system we believe the surface strain distribution is representative of the bulk strain distribution.

Comparable results for crack growth in a delaminating composite were not available at the time of the preparation of this manuscript but should be available for the presentation at the meeting.

SUMMARY

A technique for the direct measurement of the strain field around a growing crack has been developed. Results on F185 resin indicate a large non-linear deformation zone around the crack tip and a surprisingly large local, crack tip strain to failure.

REFERENCES

1. Bascom, W.D., Bitner, J.L., Moulton, R.J., and A.R. Siebert, "The Interlaminar Fracture of Organic-Matrix, Woven Reinforcement Composites", Composites, Vol. 11, 1980, pp9-18.
2. Hunston, D.L., "Composite Interlaminar Fracture Effects of Matrix Fracture Energy, Comp. Tech. Review, Vol. 6, 1984, pp.176-181.
3. Hunston, D.L., Moulton, R.J., Johnston, N.J., and Bascom, W.D., "Matrix Resin Effects in Composite Delamination: Mode I Fracture Aspects," ASTM STP 937, Johnston, N., Ed., American Society for Testing and Materials, Philadelphia, in press.
4. Tse, M.K., Hibbs M.F. and Bradley, W.L., "Delamination Fracture Studies of Some Toughened Graphite/Epoxy Composites, Including Real-Time Fracture Observations in Scanning Electron Microscope, ASTM STP 937, Johnston, N., Ed., American Society for Testing and Materials, Philadelphia, in press.
5. Chakachery, E. and Bradley, W.L., "A Fracture of Hexcel F-185 Neat Resin and T6Ti45/F185 Composite," Polym. Sci. and Eng., in press.
6. Jordan, W.M. and Bradley, W.L., "Micromechanics of Fracture in Toughened Graphite/Epoxy Laminates," ASTM STP 937, Johnston, N., Ed., American Society for Testing and Materials, Philadelphia, in press.

7. Bradley, W.L. and Cohen, R.N., "Matrix Deformation and Fracture in Graphite Reinforced Epoxy," ASTM STP 876, Johnson, S., Ed., American Society for Testing and Materials, Philadelphia, 1985.



Figure 1A (left) and 1B (right) showing the dot map on the surface of a compact tension specimen prior to loading (left) and after loading to give crack extension (right). Original magnification - 100X; 10 micron marker indicated on photographs.

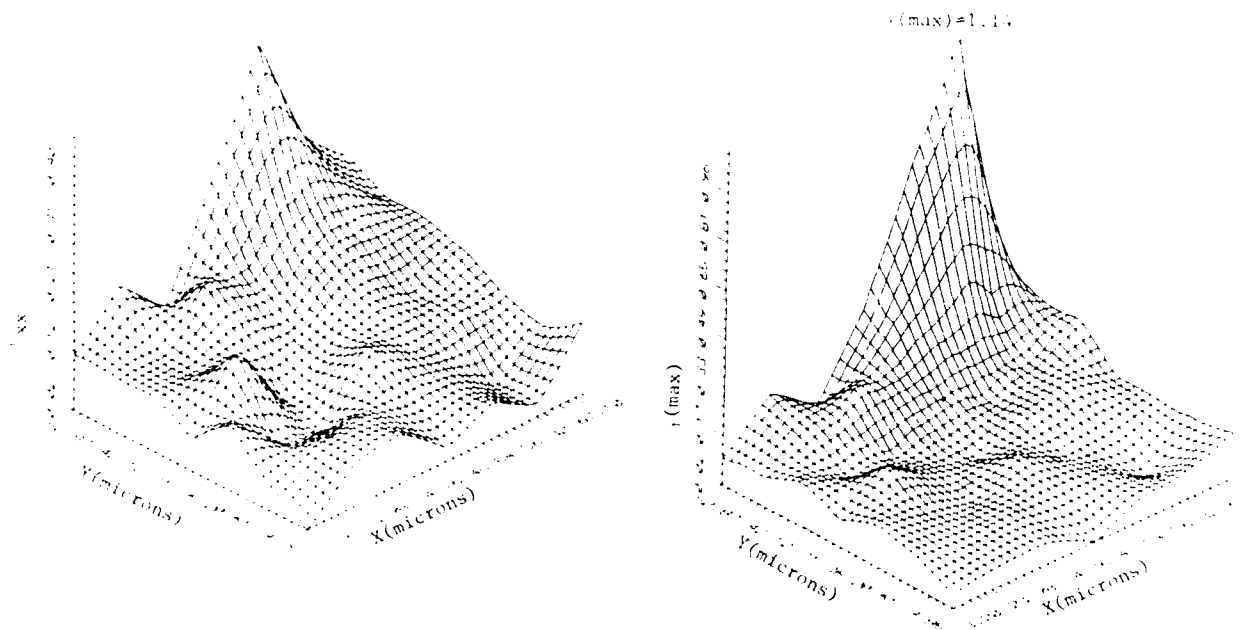
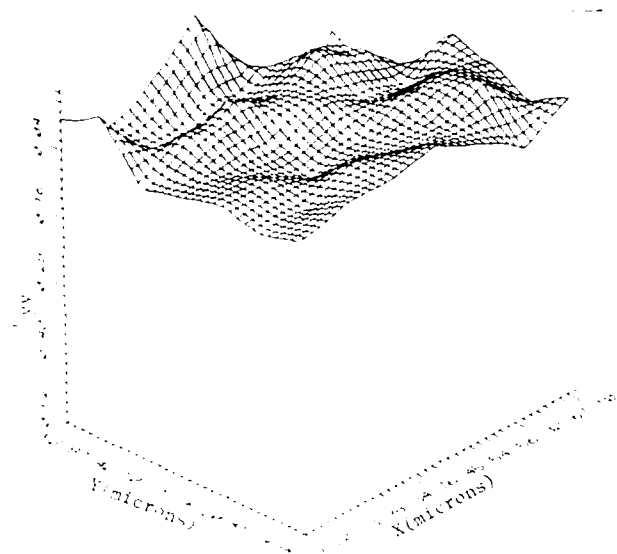


Figure 2-4 which give the strain fields for ϵ_{xx} , ϵ_{yy} and ϵ_{max} . Note the crack tip coordinate is $X = 59.14$, $Y = 57.48$.



Correspondence Between Stress Field and Damage
Zones Ahead of Crack Tip of Composites Under Mode I
and Mode II Delamination

Carlos Corleto, Walter Bradley, and
Mogens Henriksen

Proceedings of Sixth International Conference on Composite
Materials: ICCM-ECCM, Eds. Mathews, Buskell, Hodgkinson, and
Martin, London, Elsevier Applied Sciences Publisher Ltd.,
Vol. 3, pp. 3.378-3.387 (1987).

CORRESPONDENCE BETWEEN STRESS FIELDS AND DAMAGE ZONES AHEAD OF
CRACK TIP OF COMPOSITES UNDER MODE I AND MODE II DELAMINATION

Carlos Corleto, Walter Bradley
Department of Mechanical Engineering,
Texas A&M University,
College Station, Tx 77843,
USA

and

Mogens Henniksen
Engineering Department,
Colorado School of Mines,
Golden, Co 80301
USA

ABSTRACT

The Stress field ahead of the crack tip of a split laminate specimen loaded under mode I and Mode II delamination has been determined by means of a finite element analysis. The results have then been compared to the observed damage zone developed ahead of the crack tip for the same loading conditions. A direct correspondence has been found between the stress fields, damage zones observed, and resistance to delamination of composites for this modes of delamination fracture.

INTRODUCTION

Fiber-reinforced composite materials usually offer poor resistance to delamination. As a result, a complete understanding of the delamination process is needed to properly design composite structures and develop materials with improved fracture toughness characteristics. An important area of investigation is the determination of the stress field ahead of the crack tip for the various modes of delamination fracture (i.e. mode I, mode II, and mode III), by means of finite element analyses. Furthermore, these stress fields can be related to the corresponding observed damage zones that develop ahead of the growing crack as determined from in-situ observations in the scanning electron microscope. This combination of analyses with direct observation of delamination has been very useful in

developing an overall understanding of the relationship between macroscopic resistance to crack propagation and modes of delamination fracture.

In this investigation, the stress field ahead of the crack tip of a split laminate specimen loaded under mode I and mode II delamination conditions has been determined by means of a finite element analysis. The results were then compared to the observed damage zone developed ahead of the crack tip for the same loading conditions.

MATERIALS AND METHODS

The determination of the stress field ahead of the crack tip of the split laminate specimen loaded under mode I and mode II was accomplished by first generating a two dimensional mesh 52.4 mm long and 2.54 mm thick consisting of 79 nodes and 294 elements as shown in Figure 1a. Triangular six-noded elements were used around the crack tip with mid-side nodes displaced to the quarter point [1], and a substantial refinement of the mesh around the crack tip was made to overcome the difficulty imposed by the stress singularity present at the crack tip. This has been a linear analysis made with a finite element algorithm developed by Henriksen [2]. The algorithm is based on a nonlinear code updated with Lagrangian formulation using six and/or eight noded isoparametric elements with two degrees of freedom per node. Elastic constants for a unidirectional laminate of AS4/3502 graphite/epoxy composite to be used in the analysis were obtained from Hercules [3].

Mode I loading was simulated by applying a symmetric load at the cracked end of the mesh as shown in Figure 1b. Mode II loading was introduced by asymmetrically loading the cracked end (see Figure 1c). The load level applied corresponds to approximately the load at onset of crack growth for these two modes of failure, as determined from experimental measurements in combination with beam linear beam theory [4]. Stress contour plots were obtained from the output data and the stress distribution was plotted as a function of distance ahead of the crack tip.

Two sizes of split laminate specimens were used for direct observation of delamination in the scanning electron microscope, one 38.1 mm long, 5.08 mm wide and 1.14 mm thick, and the other 30.48 mm long, 5.08 mm wide, and 1.14 mm thick. Hercules unidirectional AS4/3501-6 graphite/epoxy composite material was used for mode I and mode II observations of the damage zones, respectively. The real time observations

of delamination were made in a JEOL-35 scanning electron microscope. Mode I delamination was achieved by pushing a wedge into the precracked portion of the longer split laminate specimens, using the tensile stage of the scanning electron microscope. The wedge was sufficiently blunt to ensure that it remained well away from the crack tip, giving essentially pure mode I loading. Mode II delamination was achieved by means of a specially designed three point bend fixture installed to the tensile stage of the scanning electron microscope. All surfaces observed were coated with a 150 Å thick gold/palladium film to minimize charging effects associated with the nonconductive nature of the epoxy matrix of the composite. The experimental results were recorded on standard tri-x film.

RESULTS AND DISCUSSION

Figures 2 and 3 show the finite element results for both mode I and mode II loading. Figure 2a is a S_{yy} (normal) stress contour plot from the vicinity of the crack tip for mode I loading. The normal stress S_{yy} which for this loading and geometry is the principal normal stress S_2 , rapidly decreases ahead of the crack tip. Figure 2b corresponds to the S_{xy} (shear) stress contour plot for a mode II condition. Note how the shear stress drops off much more slowly with distance ahead of the crack tip than does the normal stress for mode I loading (Figure 2a). Furthermore, the shape of the stress field is more narrow and elongated. For this loading condition, S_{xy} = maximum shear stress = S_1 . Figure 3 shows the stress distribution as a function of distance ahead of the crack tip for mode I and mode II. In the case of the normal stress for mode I, the stress drops off rapidly until it is compressive at a distance of 0.76 mm ahead of the crack tip. Finally, it gradually approaches a zero stress level at approximately 8 mm from the crack tip which is maintained all the way to the end of the beam. It should be noted that the compressive stresses observed are not expected to significantly influence the fracture mode at the crack tip because it develops far enough away from the crack tip. In the case of the shear stress distribution ahead of the crack tip for mode II, it monotonically decreases to a constant value. As it can be seen, the shear stress ahead of the crack tip for mode II loading decays much slower than the normal stress for mode I loading. These results indicate that the stress concentration at the crack tip is distributed over a larger distance for mode II loading than for mode I loading. For mode II, the extent

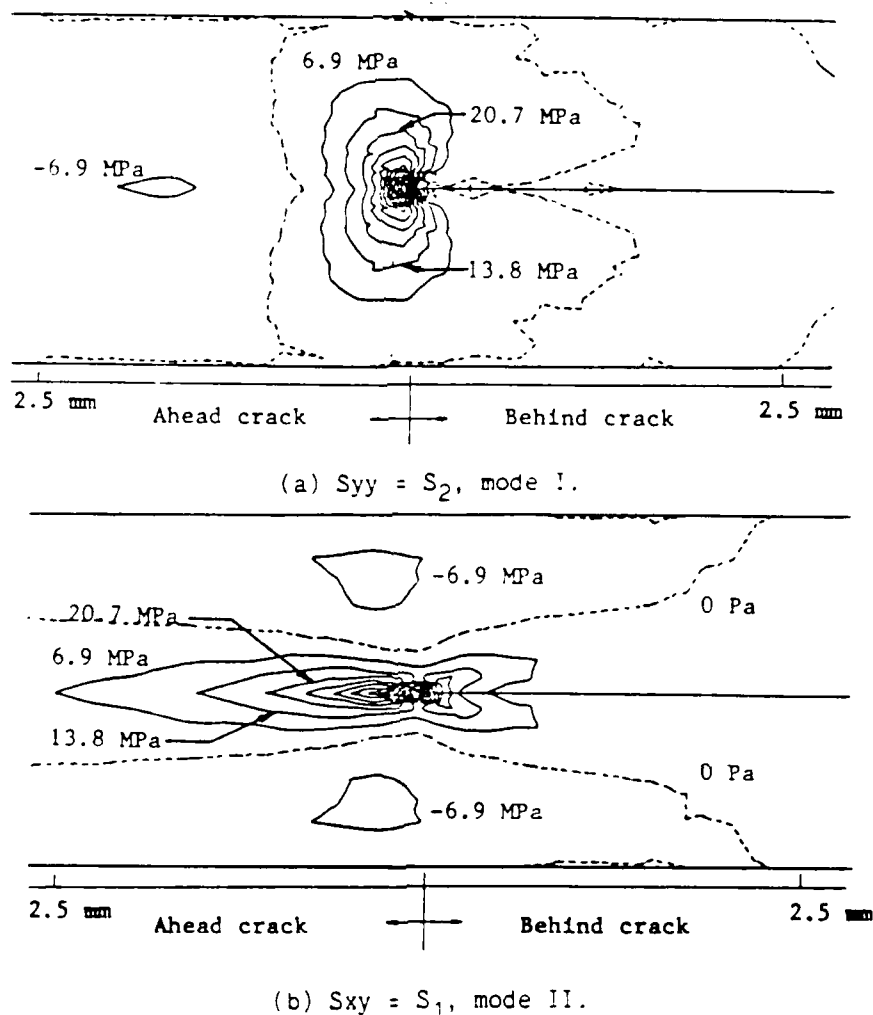


Figure 2. Stress contour plots.

of the stressed material above and below the center plane being much smaller than for mode I, as seen in the stress contour plots in Figure 2.

Figure 4 corresponds to the observed damage zones developed ahead of the crack tip for both mode I and mode II delamination of AS4/3501-6. The mode I damage zone is characterized by extensive microcracking of the resin extending at least 90 microns ahead of the macroscopic crack tip and approximately 7.5 microns above and below the primary plane of crack advance. In the case of mode II, the damage zone extends much further ahead of the crack tip (at least 180 microns) than the mode I damage zone, and is approximately 5 microns in extent above and below the primary crack plane.

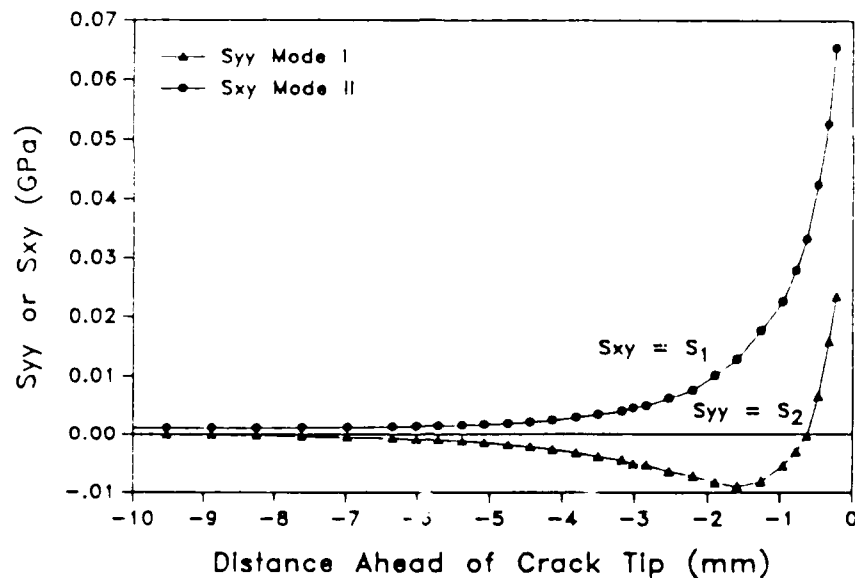
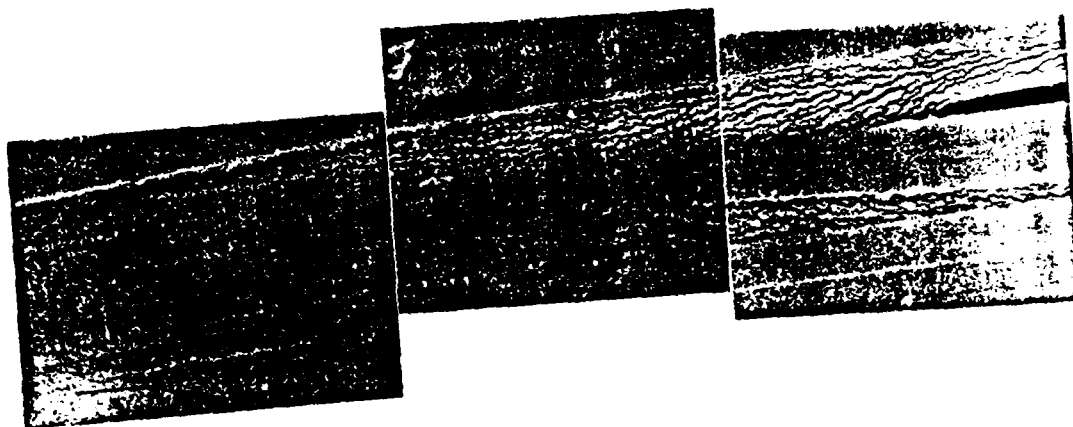
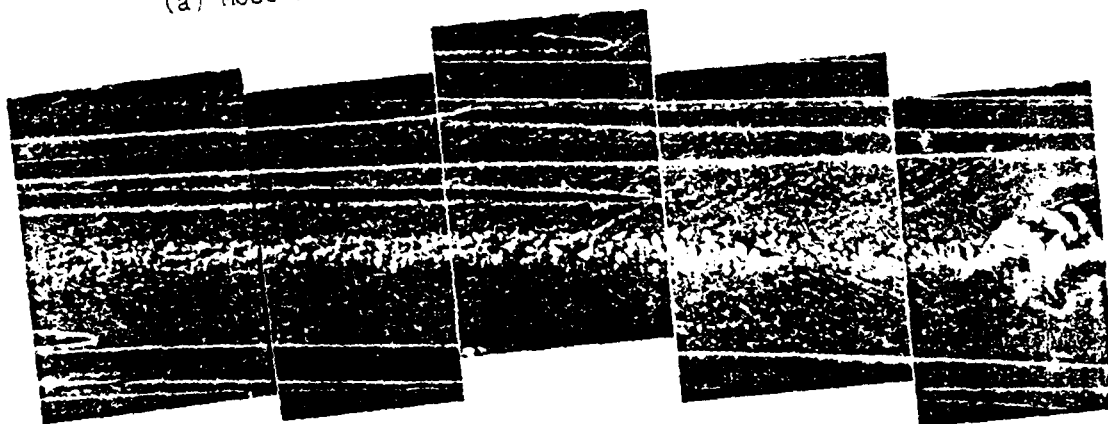


Figure 3. Stress distribution ahead of crack tip for mode I and mode II.

A careful comparison of the stress fields of Figures 2,3 and the damage zones shown in Figures 4 for mode I and mode II delamination, reveals a direct correspondence between them. The more gradual decrease in the magnitude of the shear stress with distance from the crack tip for mode II (Figure 3), along with the elongated shape of the shear stress contour plot seen in Figure 2b indicates that the stress concentration at the crack tip is distributed over a larger range, causing the size of the damage zone ahead of the crack tip to be elongated (Figure 4b). In contrast, the rapid decay of the magnitude of the normal stress for mode I with distance from the crack tip (Figure 3) and the more circular shape of the normal stress contour plot of Figure 2a indicate that the stress concentration at the crack tip is much more localized, causing the extent of the damage zone ahead of the crack tip to be smaller than for mode II delamination. Furthermore, the extent of the stressed material above and below the plane of delamination is seen in the stress contour plots to be much smaller for mode II than for mode I. Thus, the damage zone (Figure 4) changes from wide to narrow as one goes from mode I to mode II. These findings indicate that the greater resistance to delamination for mode II loading ($G_{IIC} = 570 \text{ J/m}^2$) than for mode I loading ($G_{IC} = 190 \text{ J/m}^2$) in AS4/3502, a similar material as AS4/3501-6, may be explained in part as resulting from the different decay rate of the stress field and the



(a) Mode I damage zone developed ahead of crack tip.



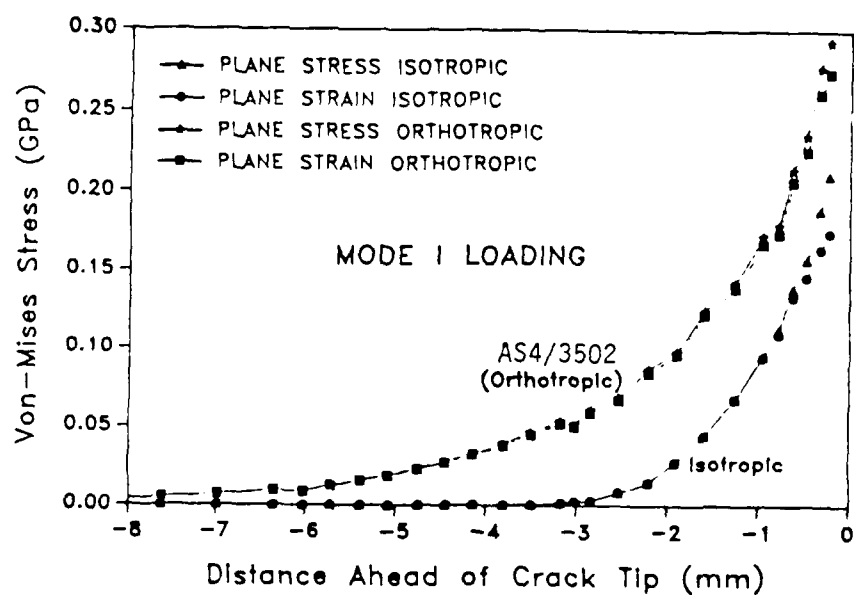
(b) Mode II damage zone developed ahead of crack tip.

Figure 4. Damage zones ahead of crack tip.

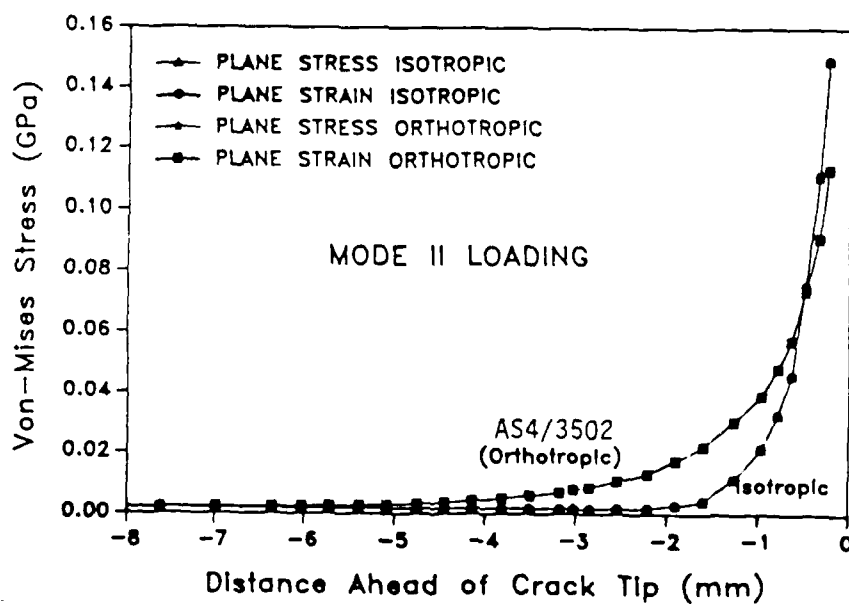
resulting difference in damage zone size and shape ahead of the crack tip for the two loading conditions.

It should be noted that even though the finite element analysis assumed global linear elastic orthotropic material behavior, it still predicted the overall trend in damage zone size and shape, despite the actual nonlinear behavior of composites in the crack tip region.

When dealing with damage zones development, the effect of the state of stress, namely plane stress versus plane strain, may be important. This is particularly true where the principle shear stress plays a role in the deformation or fracture process. The damage zones shown in Figure 4 are



(a)



(b)

Figure 5. Von-Mises stress for mode I and mode II loading.

obviously from the edge of the specimen where a plane stress condition occurs. Therefore, in order to have a first order approximation as to the effect the difference in the state of stress at the surface of the

specimen where our direct observations are made, and at the center where plane strain conditions prevail, the Von-Mises stress for mode I and mode II was plotted as function of distance ahead of the crack tip. The results in Figure 4a indicate that for mode I, the difference in the Von-mises stress (or root mean square shear stress) in plane stress versus plane strain is approximately 10% . In the case of mode II, the difference is negligible as evidenced in Figure 4b. Therefore, it appears that for these orthotropic materials, the difference between plane stress and plane strain is not too significant and our surface observations of damage zone size and detail should not be very different than subsurface behavior. Previous studies in which the post mortem appearance of the fracture surface near a free edge to that at the center of a specimen are consistent with this interpretation [6]. A final observation from Figure 4 is that the stress field ahead of a crack tip decays much more slowly for an orthotropic material with the crack parallel to the fibers than for an isotropic material.

CONCLUSION

In summary, it has been found that the different size and shape of the damage zone observed when comparing mode I to mode II delamination is consistent with the difference in the size and shape of the stress field predicted by the finite element analysis. Furthermore, these differences are also consistent with the difference in resistance to delamination of brittle graphite/epoxy composites for the two types of delamination studied. Also, there appears to be a very small difference between plane stress and plane strain states of stress for orthotropic materials. Therefore, the damage zones observed during in-situ delamination in the scanning electron microscope should not vary significantly from the actual damage zone that develops at the center of the specimens (plane strain damage zone).

REFERENCES

- 1.- Barsoum, R.S. On the Use of Isoparametric Finite Elements in Linear Fracture Mechanics. International Journal for Numerical Methods in Engineering, Vol., 10 pp. 25-27, 1976.
- 2.- Henriksen, M. Engineering Department, Colorado School of Mines Golden, Colorado, 80301.
- 3.- Hercules Manual of AS4/3502 Graphite/Epoxy. Hercules Corporation

Magma, Utah.

- 4.- Vanderkley, P.S., Mode I - Mode II Delamination Fracture Toughness of a Unidirectional Graphite/Epoxy Composite, a Thesis, Texas A&M University, College Station, Texas, 1981
- 5.- Jordan, W. M. The Effect of Resin Toughness on Fracture Behavior of Graphite/Epoxy Composites, PhD Dissertation, Texas A&M University College Station, Texas, 1985.
- 6.- Jordan, W.M., and Bradley, W.L., Effect of Resin Content on the Delamination Fracture Behavior of Graphite Epoxy Laminates, presented at the 29th National SAMPE Symposium, April 3-5, 1984, and appearing in the proceedings entitled: Technology Vectors, pp. 1422-1437.

Fracture Toughness Testing of Polyethylene Pipe Materials

Robert E. Jones, Jr. and Walter L. Bradley

Department of Mechanical Engineering

Texas A&M University
College Station, TX 77843

Revised 6/1/87

Accepted, 7/1/87 for publication in ASTM
Special Technical Publication

entitled

Nonlinear Fracture Mechanics

ABSTRACT: Multi-specimen J integral tests which are defined in the Standard Test for J_{1C} , A Measure of Fracture Toughness (ASTM E 813-81) have been conducted on side-grooved compact tension specimens of medium and high density polyethylene. Specimens were precracked with a razor blade, as has been common practice to date, or were fatigue pre-cracked. Tests were performed over a 50X range of crosshead rates in the quasi-static regime. Results indicated that the razor notching gives a J-R curve which is significantly higher than that obtained using fatigue precracked specimens. A significant variation in the J-R curve was noted for changes in the displacement rate due to the viscoelastic character of the polyethylene. The orientation of the specimens, which were cut from actual pipe, was found to have a significant effect on the fracture toughness. The fracture toughness results were correlated with fractographic results and the behavior of side-grooved vs. non-side-grooved specimens was compared.

KEY WORDS: Polyethylene, Fracture (materials), Compact Tension Test, Fatigue (materials)

INTRODUCTION

Thermoplastics are seeing increased use as structural materials. With this increased structural use a need has arisen for a method of determining useful fracture mechanics parameters for failure prediction. Thermoplastics such as polyethylene (PE) which have a high degree of ductility and exhibit strong viscoelastic behavior present a problem for linear elastic fracture mechanics (LEFM) testing procedures. Previous investigators [1,2] have used the concepts of LEFM with tough PE in an effort to determine a valid plane strain fracture toughness (K_{Ic}). They encountered difficulty in doing so at temperatures near normal operating conditions for PE piping. However, it has been shown [3] that an elastic-plastic J integral approach as defined in the Standard Test for J_{Ic} , A Measure of Fracture Toughness (ASTM E 813-81) will yield plane strain toughness values for tough PE which meet the requirements of the standard for valid J values when tested in the normal operating temperature regime.

The question then arises as to the validity of a non linear elastic analysis such as the J integral when applied to a viscoelastic material. There is no currently approved standard for determining the fracture toughness of viscoelastic materials. However, R.A. Schapery [4] has shown that the J integral may be applied to fracture in viscoelastic media. Schapery assumes in his analysis that the work of fracture in the process zone is independent of the crack growth rate and that the significant viscoelastic effect (rate dependence) is through the time

dependent behavior in the stress field which surrounds the process zone.

A number of questions remain unresolved in the application of fracture mechanics testing of tough thermoplastics such as PE. This study examined the effects of several experimental parameters on the apparent J_{IC} toughness of PE tested at room temperature. Test rate, precrack acuity, and specimen thickness were examined. Previous investigators [1-3] have employed primarily a three point bend configuration in their tests. In this study a compact tension (CT) configuration as defined in ASTM E 813-81 was used for all tests. Due to the highly drawn nature of pipe materials, a directional dependence in toughness of actual pipe material was suspected. Experiments were performed to confirm this. In addition to alignment of molecules, extrusion of pipe usually introduces residual stresses which may influence the effective toughness of pipe in service. Previous investigators have worked primarily from sheet stock or flattened, annealed pipe in preparing specimens. Since actual field performance is of interest with pipe materials, both annealed and unannealed specimens were tested in this study.

PROCEDURE

Equipment-Fracture testing was performed on a servo-hydraulic closed loop test stand with load-line displacement measured by a linearly varying differential transformer mounted on the specimen holding pins. Data acquisition and reduction were accomplished with a micro-computer connected to an analog to

digital signal processor. Specimens were observed during testing through an optical stereo microscope and post mortem fractography was performed in a scanning electron microscope (SEM).

Specimen Preparation-2.54 cm CT specimens with uncracked ligament lengths, b , of 1.5 cm were prepared from a high density pipe grade polyethylene PE 3306 described in the Standard Specification for Thermoplastic Gas Pressure Pipe, Tubing, and Fittings (ASTM E 2513-75b). Non-annealed specimens were produced in two thicknesses, 0.635 cm and 0.556 cm, which were reduced 20 percent by side-grooving to 0.508 cm and 0.445 cm respectively. Annealed specimens were cut from stock which had been heated to 130 °C, flattened, and then annealed for two hours at that temperature. Specimens cut from this stock were 0.572 cm thick after being reduced 20 percent by side-grooving. Two additional specimens were cut to a thickness of 0.508 cm. One was reduced in thickness 20 percent with sidegrooves. With the exception of one set, specimens were cut with the starting notch in the longitudinal pipe direction; thus, they are termed transverse specimens in the standard ASTM nomenclature. The remaining set of specimens was cut to test transverse pipe properties and are termed longitudinal specimens in the ASTM nomenclature. The angle of the sidegrooves was 45 degrees and where fatigue precracking was used specimens were precracked before side grooves were machined. Razor notched specimens were side grooved before notching.

Fatigue-Specimens were fatigue precracked in accordance with the procedure outlined in ASTM E 813-81 with the exceptions noted below. It was found that fatigue at 40 percent of the limit load specified by the standard produced no noticeable sharpening of the crack tip and no crack advance. Therefore the requirement that the final stage of crack growth be at this level was ignored. Specimens were fatigued at a rate of ten Hz and a load of 70 percent of P_L for 30 000 cycles to produce the precrack. Sidegrooves were cut after precracking because it was found that the fatigue crack front tended to run ahead at the surface of the specimen when they were machined prior to fatiguing.

Razor Notching-Razor notches were made using the test stand and specially designed fixtures. A new razor blade was used for each specimen to obtain the sharpest possible crack tip.

Tests-Tests were run at an ambient laboratory temperature of 21 °C. The standard crosshead rate for tests was 0.0254 cm/min. One set of tests was run at 0.00254 and another at 0.127 cm/min to examine rate effects. Immediately after loading, specimens were immersed in liquid nitrogen and then broken in the test stand. The liquid nitrogen fracture produced clear boundaries between the actual crack growth, the Dugdale type process zone, and the undamaged material. Approximate measurements of the crack advance were made during the tests using an optical microscope to permit a good distribution of crack lengths which would result in a more reliable J-R curve. Final crack length measurements were made from micrographs taken in the SEM. To permit viewing in the SEM, one half of each specimen was sputter coated with 150A of a

gold-palladium alloy. The crack advance visible on the resulting micrographs was measured at eleven points evenly spaced across the specimen width. The mean of the nine inner points and the average advance at the two surfaces was taken as the crack advance. The micro-computer used to record load displacement data was also used to calculate the areas under the load displacement curves. J_{1C} was found from the resistance curve plotted according to the procedure in ASTM E 813-81.

RESULTS

J Integral Testing-Resistance curves like the one shown in Figure 1 were generated for each test. The results are summarized in Table 1. The non-sidegrooved thin specimen (0.508 cm) showed a high degree of crack tip tunneling which made it unusable in the J determination. However, the identical specimen sidegrooved 20 percent to a thickness of 0.4064 cm yielded a straight crack front. The sidegrooved thin specimen yielded a J value that fell just below the J-R curve for the thicker specimens used in the remainder of the tests.

ASTM E813-81 establishes minimum dimensions for specimens which are necessary in testing of metals, for the J analysis to be valid. The requirements are:

- a. $b, B \geq 25 J_{1C}/S_y$
- b. $\frac{dJ}{da} < S_y$

These have been calculated for each of the tests and are listed in Table 1. Though the yield strength of PE can vary greatly with strain rate, all tests easily satisfied the second requirement.

6

However, according to the standard, the unannealed razor notched CT specimens were slightly smaller than the specified minimum. This was also the case in the high crosshead rate test using annealed material. These values are reported for comparison since the standard does not strictly apply to this material. Tests satisfying these requirements were not possible since thicker stock was not available.

Fatigue precracking resulted in a drop in J_{1C} of 33 percent when compared to razor notched specimens in both annealed and unannealed samples. Annealing decreased the measured J_{1C} by 47 percent in both fatigue precracked and razor notched tests. The longitudinal specimens yielded a J_{1C} which was 11 percent greater than that determined for the transverse specimen tests.

Blunting Line-In several of the multi-specimen tests, one test was terminated before the onset of crack advance across the entire crack front. The resulting points should have fallen on the blunting line. As can be seen in Figure 2, the high rate test required a steeper blunting line. When a yield stress measured at a strain rate which corresponded to the rate of the fracture test was used, the appropriate blunting line resulted.

Fractography-Comparison of the surfaces of the low rate and medium rate fracture tests shows a marked similarity in morphology but a significant difference in the scale of features. (Figures 3 and 4). The difference in size of fibrils and voids corresponds to the trend identified by Chan and Williams [5] and Lee and Epstein [6]. The lower rate has smaller voids and shorter fibrils. The average diameters of the voids were measured from

SEM micrographs by Lowry [7] and are listed in Table 2.

Of special interest was the observation that the Dugdale type process zone varied in length with test rate. The average lengths of process zones in three annealed razor notched specimen tests are listed in Table 2. This variation was not what one would expect if the yield stress rate sensitivity was primarily responsible for increases in toughness while the work done in the process zone remained constant with changing rate. In fact, since the yield strength increases with strain rate, the process zone should have gotten smaller as strain rate increased. This would have been due to the increased constraint induced by the higher yield strength of the surrounding material. This is clearly illustrated by the Dugdale equation

$$r/a = \sec(\pi\sigma/2S_y) - 1$$

Since S_y is increasing in the surrounding material with the increasing rate, r should be decreasing. Post mortem examination indicated that this is not the case in this material.

DISCUSSION

Crack advance was observed to follow the process described by S.K. Bhattacharya [8]. A Dugdale type region formed ahead of the crack tip. Within this process zone voiding begins. These voids grow and coalesce creating a fibrillated structure. Further crack tip opening causes fibril failure and the crack advances.

Annealing-The 47 percent drop in J_{1C} which occurred with annealing is extremely significant. This may be due to an accelerated physical aging caused by the annealing process. It is also possible that annealing relieved residual stresses which

inhibit crack advance in the unannealed material. J.G. Williams [9] has measured significant residual stresses in extruded pipe. In fact, the annealed specimens yielded a symmetric crack front while unannealed material exhibited uneven crack advance suggestive of the presence of residual stresses. These residual stresses could have been responsible for the higher resistance to crack growth in the original pipe material. It is also possible that annealing modified the crystalline structure of the material. Density measurements indicated a change in crystallinity of less than one percent. However, spherulite size may have been changed by the heat treatment, thus altering the toughness. The annealing technique is commonly used when working with pipe material but these results indicate that material so treated may not reflect true pipe behavior.

Rate-The effect of rate on the magnitude of J_{1C} was much greater than expected. The 300 percent increase in magnitude of J_{1C} observed with the increase in test rate from the intermediate rate to the high rate was surprising. From linear viscoelasticity it can be shown that crack growth rate is related to stress intensity by:

$$\dot{a} = K^2(1+1/n)$$

if fracture energy is not a function of rate. For PE n can be taken to be approximately 0.2 and the equation becomes:

$$K_{1C} = \dot{a}^{1/12}$$

By using the relationship between K and J for linear elastic materials we can say that some equivalent " J_{1C} " is thus proportional to $\dot{a}^{1/6}$. Thus a fifty fold increase in test rate

1

(crack growth rate) will yield a 90 percent increase in J_{1C} . Clearly this is not adequate to account for the increase in measured J with the increasing test rate. Thus Schapery's [4] assumption that the fracture energy is independent of crack growth rate does not hold in this system. Stated another way, the far field viscoelastic effects are not sufficient to account for the 300 percent increase in measured J_{1C} . Some two thirds of the increase remain unaccounted for.

The changes in measured J_{1C} which correspond to changes in the length and surface morphology of the process zone suggest that the fracture process, and therefore the energy dissipated in the process zone, is, in fact, rate dependent. The J integral can be related to other material and fracture parameters. If we take the standard relationship between J and CTOD:

$$J = m \cdot S_y \cdot d_{CTOD}$$

and assume that m is rate independent then J can be increased by increasing the yield stress, S_y , or the CTOD.

As has already been stated, yield stress increases with increasing strain rate. The strain rate dependence of the stress-strain behavior of PE is demonstrated in Figure 5. The increase in yield strength and rate of strain hardening as the strain rate is increased are clearly apparent. However the increase in yield stress over the range of strain rates used in these tests is less than 25 percent. This is not nearly enough to account for the 200 percent increase in J which remains after far field viscoelasticity is taken into account.

From the above equation it is clear that an increase in CTOD

can account for the increase in J. The voids in the process zone are ellipsoids, elongated in the direction of the load applied to the specimen. However, if it is conservatively assumed that the voids in the process zone are spherical, then the diameter of the voids on the fracture surface can be used as a lower bound for the CTOD. Comparison of the average diameters of the voids produced by the various test rates indicates a 900 percent increase in void size over the range of rates tested. This is much more than necessary to explain the increase in J but is evidence that the majority of the increase in the measured J with increasing strain rate comes from an increasing CTOD.

The increase in CTOD has two possible complementary explanations. The first arises from the thermally activated nature of the fracture process. A high rate of crack growth necessitates the breaking of more bonds and void formation from fewer sites than a lower rate which allows time for thermally activated disentanglement of polymer chains. Thus high rates produce larger and fewer voids and fibrils with a correspondingly larger CTOD which results when the larger masses of material are drawn to failure. The second possible explanation for the increase in CTOD is the possibility that any decrease in final elongation of the fibrils due to the higher rate may be overwhelmed by an increase in the amount of material drawn into the process zone. The higher yield strength of the process zone material under faster load rates could cause additional low strength material to be drawn in from the surrounding region. This process is illustrated in Figure 6. Material in the fibrils

has been highly elongated and its strength would correspond to point B in Figure 5. The material on the edge of the process zone is less severely deformed and would perhaps correspond to the material condition at A in Figure 5. At the higher strain rates the difference in strengths is much more pronounced, as can be seen in Figure 5, so more material will be drawn into the fibril.

Precracking-The 33 percent drop in toughness between razor notched and fatigue precracked specimens can probably be explained in terms of the process zone. Fatigue precracking introduces a process zone ahead of the actual crack tip. Razor notching does not do so and thus razor notched specimens require additional work input to cause voiding and fibrillation prior to crack advance.

The suitability of razor notching vs. fatigue precracking for these materials can be determined only on the basis of the actual nature of expected service damage. The observed decrease in process zone length with decreasing rate would suggest that in the case of long term static field failures a small process zone is to be expected. Thus razor notching which produces virtually no Dugdale type zone would be most appropriate. However, if the service load will be in fatigue or a mixture of fatigue and static loading, then fatigue precracking is appropriate.

Thickness- The results of the thickness comparisons would seem to indicate that very thin specimens can still yield valid J's if they are sidegrooved. The amount of tunneling observed on non-sidegrooved CT specimens indicates that sidegrooving is essential for J integral testing of PE when

specimen thickness is approximately 0.5 cm.

Orientation-The 20 percent increase in J_{1C} which was observed when specimen orientation was changed from the longitudinal to the transverse pipe direction clearly demonstrated the existence of residual alignment effects. Since extrusion will tend to align polymer chains parallel to the axis of the pipe, crack growth perpendicular to this axis should encounter greater resistance. This was the case.

Blunting Line-The pre-initiation blunting point measured for the high rate test clearly indicates that some account must be taken of the strain rate dependence of the yield stress of the material when the blunting line is calculated. If the appropriate yield stress is used the blunting line will more accurately reflect the actual behavior of the specimen.

Conclusions

Annealing of pipe materials prior to testing caused a 47 percent decrease in the measured fracture toughness.

Fatigue precracking yields a lower J_{1C} toughness than does razor notching. This drop is probably due to the presence of a preformed process zone in the fatigued specimen.

Specimen orientation in unannealed material influences the measured J_{1C} . Longitudinal specimens yield a higher apparent toughness than do transverse specimens.

Fractography indicates that CTOD increases with increasing rate. This increase is reflected in an increase in the measured J_{1C} .

Acknowledgements

The authors wish to thank Dow Chemical Co. for funds which made this work possible. Thanks are also due Lone Star Gas Co. for providing the pipe material for testing.

TABLE I
SUMMARY OF J_{1c} TEST RESULTS

	J _{1c} kN/m	dJ/da kN/m ²	25(J _{1c})/S _y cm
Fatigue Precrack			
unannealed	3.08	74	0.41
annealed	1.65	35	0.216
Razor Notched			
unannealed	4.67	44	0.61
annealed	2.43	35	0.33
annealed high rate	6.35	43	0.84
annealed low rate	1.94	12	0.25
longitudinal	5.25		0.69

TABLE II
PROCESS ZONE LENGTHS

RATE	PROCESS ZONE LENGTH	VOID DIAMETER
low (0.00254 cm/min)	0.266 mm	13 μm
medium (0.0254)	0.54 mm	19 μm
high (0.127)	1.23 mm	131 μm

References

- [1] Mandell, J.F., Roberts, D.R., McGarry, F.J.,
Polymer Engineering and Science, Vol 23, No.7,
May 1983, pp. 404-411
- [2] Chan, M.K.V., Williams, J.G., Polymer Engineering and
Science, Vol. 21, No. 15, Oct. 1981, pp. 1019-1026
- [3] Chan, M.K.V., Williams, J.G., International Journal
of Fracture, 1983, p. 145
- [4] Schapery, R.A., International Journal of Fracture,
Vol. 11 (1975) p. 369
- [5] Chan, M.K.V., Williams, J.G., Polymer, Vol. 24, No. 2,
Feb. 1983, pp. 234-244
- [6] Lee, C.S., Epstein, M.M., Polymer Engineering and
Science, Vol. 22 (1982) p. 549
- [7] Lowry, D., Texas A&M University, Personal Communication
- [8] Bhattacharya, S.K., Brown, N., Journal of Material
Science, Vol. 19, 1984, p.2519
- [9] Williams, J.G., Hodgkinson, J.M., Gray, A., Polymer
Engineering and Science, Vol. 21, No. 13, Sept. 1981,
pp. 822-828

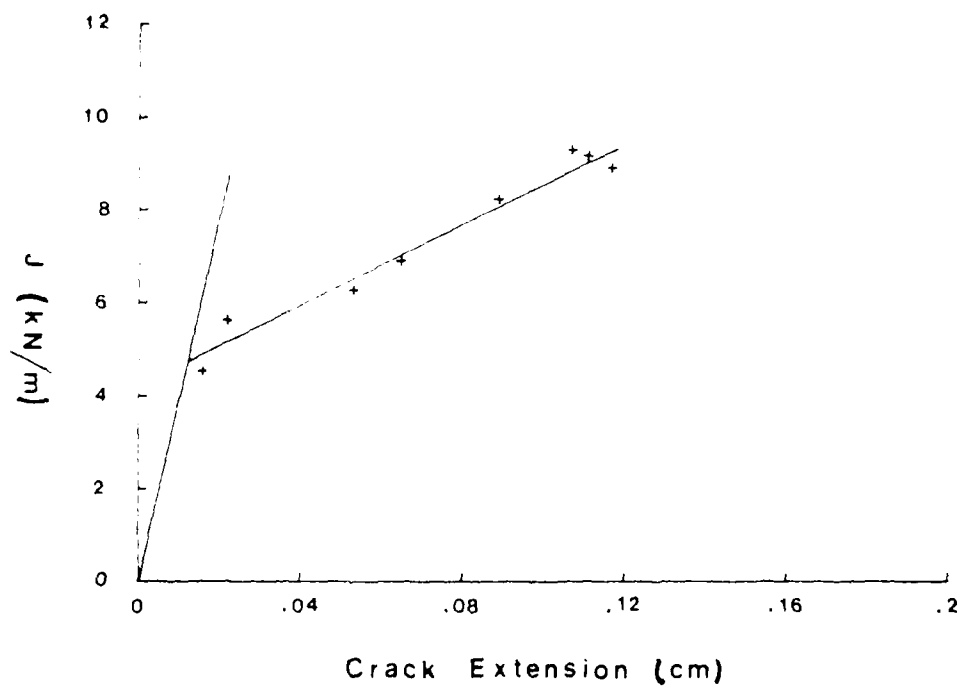
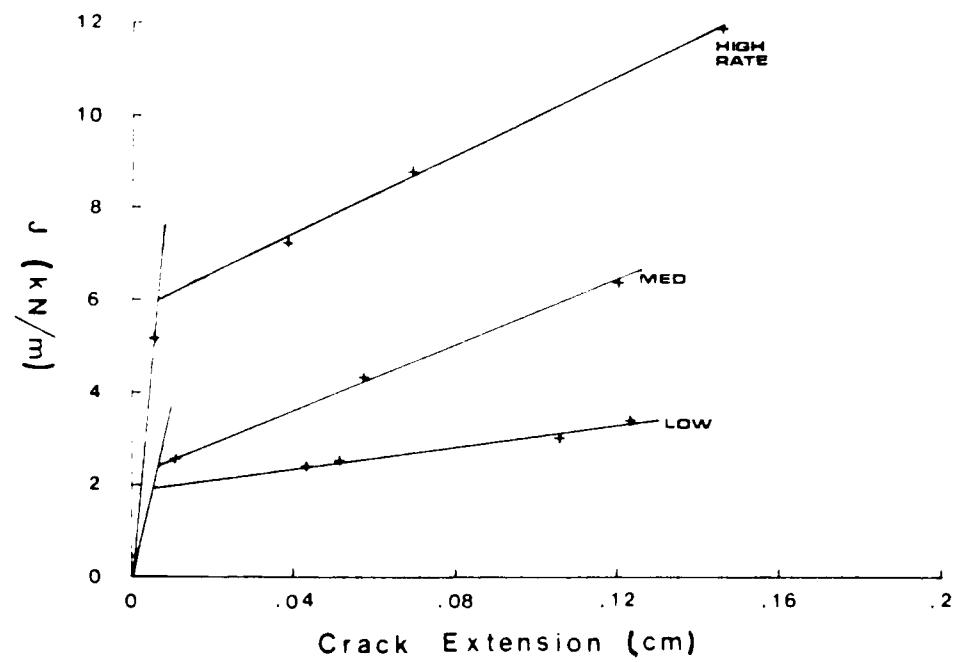
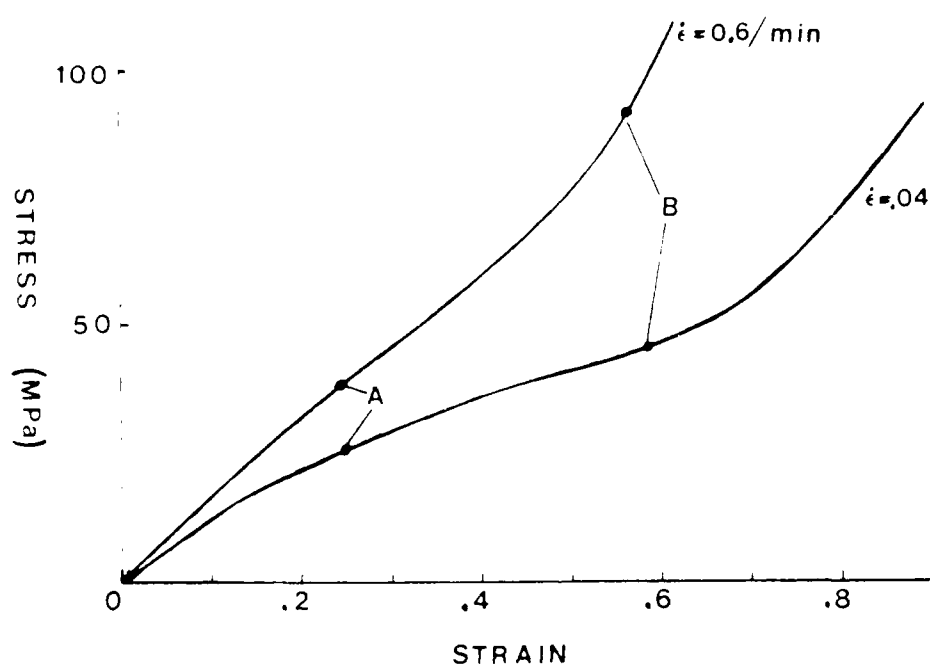


Fig. 1



F - 2



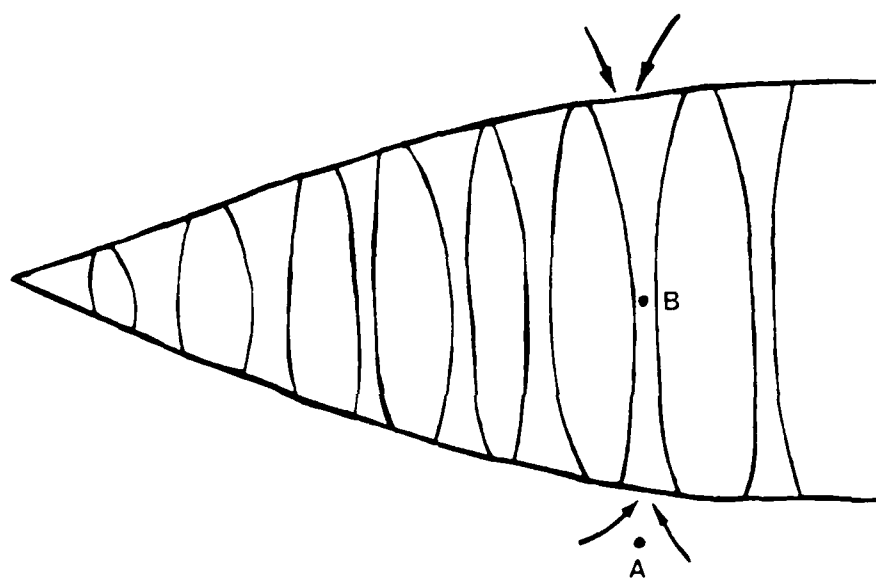


Fig 6

Mode II Delamination Fracture Toughness of
Unidirectional Graphite/Epoxy Composites

Carlos R. Corleto and Walter L. Bradley
Mechanical Engineering
Texas A&M University
College Station, TX 77843

Accepted for publication in
ASTM STP entitled
Composite Materials: Fatigue and Fracture

TITLE OF PAPER: Mode II Delamination Fracture Toughness of Unidirectional Graphite/Epoxy Composites.

AUTHORS: Carlos R. Corleto and Walter L. Bradley, Mechanical Engineering Department, Texas A&M University, College Station, Texas, 77843

KEY WORDS: Graphite/Epoxy, Delamination, Fracture Toughness, Failure Analysis, Mode II, Finite Element Analysis.

ABSTRACT:

The mode II delamination fracture toughness of a ductile and a brittle unidirectional graphite/epoxy composite has been studied using the end-notched flexure (ENF) test and the end-loaded split laminate (ELS) test. The stress field in the vicinity of the crack tip of a split laminate beam under mode II (ELS test) and mode I conditions has been determined by means of a finite element analysis. Also, the micromechanics of mode II fracture have been studied during in-situ and post-mortem observations of the fracture process. Both the ENF and ELS test give similar values for G_{IIC} . However, since elastic material behavior is assumed in the analysis, the G_{IIC} results for a ductile composite are somewhat uncertain because a small permanent deformation was observed. The ELS test has been found to provide a pure shear stress state in the vicinity of the crack tip. The formation of hackles provides a more tortuous path for the crack leading to an increased resistance to delamination under mode II conditions compared to mode I for brittle composites. However, extensive resin deformation and yielding play a more significant role in the fracture resistance of tough epoxy composites for mode II loading.

INTRODUCTION

One of the most important factors hindering the use of fiber reinforced composite materials in structural applications is their inherently poor damage tolerance for delamination. The resistance of composites to delamination can be well characterized by the delamination fracture toughness, measured as energy dissipated per unit area of crack growth. Where behavior is essentially linearly elastic, the fracture toughness can be measured as an energy release rate, G , of the material. Delamination in composites can occur due to tensile stresses (mode I), in-plane shear stresses (mode II), and tearing stresses (mode III). As a result, a complete understanding of these delamination processes is needed to properly design composite structures and develop materials with improved fracture toughness characteristics. Several areas must then be addressed in order to thoroughly understand delamination. First, a critical assessment of current methods used to measure resistance to delamination of composites is needed to verify the validity of the analysis for the various test configurations. Furthermore, the geometry independence of the measured energy release rates must be established by comparing measured values for different test geometries. Finite element analyses may be used to determine the state of stress at the crack tip where beam theory does not give details about the stress field. Second, a study of the physical mechanisms involved during the fracture process must be undertaken by means of in-situ and post-mortem fracture observations. Investigations of this nature should help in the understanding of the relationship between the macroscopic resistance to crack propagation and the micromechanics of fracture.

Recent investigations indicate that increasing mode II loading, particularly for brittle systems, results in a significantly greater resistance to crack propagation as measured by the total energy release rate required to propagate the crack [1]. This indicates the need to thoroughly understand mode II delamination in order to properly characterize this mode of

failure.

Several test configurations have been proposed for measuring the resistance to delamination under mode II loading including the end-notched flexure (ENF) test and the end-loaded split laminate (ELS) test. The end-notched flexure test configuration can be seen in Figure 1a. This test consists of a three point bend loading configuration by which a split laminate beam specimen is delaminated. The (ELS) test configuration shown in Figure 1b also uses a split laminate beam specimen loaded at the cracked end and fixed at the opposite end. Both the ENF and ELS test methods evaluate G_{IIC} from equations derived using linear beam theory and assume linear elastic material behavior [2,3]. A current review of the literature indicates that both test configurations are currently being used to measure G_{IIC} [2,3,4].

During a recent finite element analysis [5], the ENF test was found to be a pure mode II fracture test within the constraints of small deflection theory. The study also revealed that the interlaminar normal stress is identically zero along the beam center line and the interlaminar shear stress exhibits the expected singularity. No analysis of this nature has yet been done on the ELS test configuration.

As pointed out earlier, under increasing mode II loading, particularly for more brittle systems, a significantly greater resistance to crack propagation has been observed. Post-mortem observation studies in the scanning electron microscopy indicate that this increase in fracture toughness is the result of the development of hackles in the fractured surfaces [1]. Therefore, the hackle formation process as well as damage zone processes ahead of the crack tip need further study by means of additional in-situ and post-mortem delamination observations.

The objectives of this investigation have been (1) to measure the mode II delamination fracture toughness of a ductile and a brittle graphite/epoxy composite using the (ENF) test and the (ELS) test and compare the results, (2)

to determine the stress field in the vicinity of the crack tip of the (ELS) specimen under mode II and mode I loading conditions by means of a finite element analysis, and (3) to study the micromechanics of fracture using real-time and post-mortem observations of the fracture process and correlate them to the macroscopically obtained energy release rates for a brittle and ductile composite.

ANALYSIS

End-Notched Flexure (ENF) Test

The ENF test consists of loading a split laminate beam specimen using a three point bend fixture. Figure 1a shows the ENF test configuration and associated test parameters. Calculation of the strain energy release rate G_{II} assuming linear beam theory and linear elastic material behavior gives the following result [6],

$$G_{II} = \frac{9 P^2 a^2 C}{2 b (2L^3 + 3a^3)} \quad (1)$$

where a is the initial crack length, b is the width, C is the measured compliance, L is half-span length, and P is the applied load at the center pin. The strain energy release G_{II} can also be obtained by means of an experimental method for determining the relationship between compliance and crack length. In this case, G_{II} is given by [6]

$$G_{II} = \frac{3 P^2 m a^2 b_0}{2 b^2} \quad (2)$$

where m is obtained from

$$C = m a^3 + \text{const.} \quad (3)$$

This expression is the result of a least squares fit of experimental data from

measured compliances against their corresponding crack lengths cubed. This data is obtained from load-deflection curves at different crack lengths of one of the tested coupons of width b_0 .

End-Loaded Split Laminate (ELS) Test

The energy release rate for pure mode II in this case is determined by asymmetrically loading a split-laminate beam specimen. Figure 1b shows the ELS test configuration and associated test parameters. Linear beam theory and linear elastic material behavior are assumed by the analysis. A complete explanation of this analysis can be found in reference [3]. From this analysis, G_{II} can be expressed by

$$G_{II} = \frac{9 P^2 a^2}{4 b^2 E_{II} h^3} \quad (4)$$

P is the load applied at the cracked end of the beam (see Figure 4). The axial modulus E_{II} can also be shown to be

$$E_{II} = \frac{P}{2 b \delta h^3} (3a^3 + L^3) \quad (5)$$

where δ is the total beam tip deflection.

Area Method

In all the methods of data reduction previously described, the critical energy release rate was calculated by knowledge of the critical load P_c at onset of crack growth, and the crack length 'a' prior to crack extension. Therefore, G_{IIc} is a measure of the energy required to initiate crack propagation. However, as the crack propagates, G_{IIc} does not necessarily remain constant, in which case a propagation and arrest value of G_{IIc} can arise. An alternate approach for evaluating the fracture toughness is the area method. In this case, G_{II} is interpreted as the energy required to create a new cracked surface area. G_{II} can then be given by

$$G_{II} = \frac{U}{b \Delta a} \quad (6)$$

U is the area between the load-deflection curve for loading and unloading for a very small change Δa of crack growth (see Figure 2). An important advantage of this method is that only elastic material behavior is required to predict G_{II} . Therefore, for geometrically non-linear and/or non-linear elastic material responses, this method gives an average energy release rate for the observed crack extension. For unstable crack growth, it gives an average value for G_{IIC} which typically falls between the initiation and arrest values measured for linear behavior. The load-displacement record should return to the origin to guarantee that no significant far field damage is included in U in Equation (6). The inclusion of energy dissipation in far field damage in the fracture energy term U in Eq. 6 would give an erroneously high estimate of G_{IIC} . For materials where G_{II} is independent of crack growth rate, and crack growth distance (i.e., systems with minimal fiber bridging and/or plastic wake), the average and initiation G_{II} should be identical. Furthermore, where slow stable crack growth occurs, the average G_{IIC} calculated from the area method should equal the G_{IIC} for initiation calculated from linear beam theory. Another advantage of this method is that G_{II} is obtained without knowledge of the material's elastic properties and it is always given by Equation (6), regardless of the test configuration used.

EXPERIMENTAL PROCEDURE

Split laminate beam specimens approximately 152.4 mm. long, 25.4 mm. wide, and 4.83 mm. thick for the end-notched (ENF) test and 292.1 mm. long, 25.4 mm. wide, and 3.05 mm. thick for the end-loaded split laminate (ELS) test were cut from 24 ply precracked laminated panels of Hercules AS4/3502 and Hexcel T6C145/F185 graphite/epoxy composites. The starting crack was introduced on both panels by means of a teflon insert 0.127 mm. thick.

Aluminum and brass tabs were bonded to the cracked end of the ELS test specimens with a mixture of EA901 structural adhesive and B1 curing agent. An UN-10-A gray brittle coating was also applied to the lateral sides of the specimen to facilitate monitoring crack locations.

End-Notched Flexure Testing

Five specimens for each graphite/epoxy system were tested using a three point bend fixture with a total length of 101.6 mm, attached to a closed loop servo-hydraulic test machine. Prior to testing, the specimens were pre-cracked in order to provide a sharp crack tip from which to initiate the mode II fracture. Load point displacements were measured by the ram displacement and loads were monitored by a 2225 W. load cell. Real time analog plots of the load-deflection curve were made on an x-y recorder. The tests were conducted by positioning the specimens in the three-point bend fixture such that the location of the crack tip is approximately midway between the center and one of the outer loadings pins. Under displacement control conditions and a ram rate of 2.54 mm/min, the specimens were loaded until delamination crack growth occurred. Then, the specimens were unloaded.

Since machine stroke displacement was used to measure specimen deflection, a machine compliance experiment was performed to make the necessary deflection corrections to the data obtained during the mode II delamination tests.

G_{IIc} calculations were made using Equation (1) and measured compliances after appropriate machine compliance corrections had been made. It should be noted that corrections associated with shear compliance were not taken into consideration because no reliable values of the shear modulus G_{12} were available. However, these are usually small and this omission was not thought to have a significant effect on the measured G_{IIc} values. The measured compliances were obtained by curve fitting the best straight line to the data during the loading part of the test. Equations (2) and (3) were also

used to calculate G_{IIC} . To use these two equations, a compliance calibration was performed with one of the tested specimens. Finally, G_{IIC} values calculated by the area method were determined by means of Equation (6). The energy absorbed in the creation of a new cracked surface was approximated numerically by integrating the area under the load/deflection curves obtained.

End-Loaded Split Laminate Testing

Two specimens for each graphite/epoxy system chosen for this study were tested in a mode I/mode II fixture attached to a closed loop servo-hydraulic machine. A mode I precrack was introduced to the specimens to sharpen the initial crack created by the teflon insert and to provide an initial crack length to beam length (a/L) ratio of approximately 0.55, where stable crack growth is expected [7].

Mode II delamination testing was done under displacement control conditions at a rate of 10.16 mm/min and 6.35 mm/min. Loads were recorded with a 445 N load cell. Displacements were monitored using the ram displacement of the test machine. The tests were conducted by loading the specimens until the crack was allowed to grow approximately 10.16 mm to 38.1 mm. At that point the test was stopped and the new crack location marked and recorded. This procedure was repeated several times with the same specimen until the crack tip was approximately 12.7 to 25.4 mm from the uncracked end.

The critical energy release rate G_{IIC} was calculated by means of Equations (4) and (6). The axial modulus E_{11} was calculated from the load-deflection test data and Equation (5). The energy absorbed in the creation of a new cracked surface was approximated numerically, by integrating the area under each loop in the load-deflection curves.

Finite Element Analysis

The stress field in the vicinity of the crack tip of a split laminate beam specimen under mode II and mode I was determined using a finite element analysis. This was a linear analysis made with a finite element algorithm

developed by Henriksen [8]. The algorithm is based on a nonlinear code updated with Lagrangian formulation using six and/or eight noded isoparametric elements with two degrees of freedom per node.

To overcome the difficulty imposed by the singularity at the crack tip, a substantial refinement of the mesh in the vicinity of the crack tip, and the use of triangular six noded elements around the crack tip with mid-side nodes displaced to the quarter point has been done. These crack tip elements contain a singularity of the form $1/\sqrt{r}$, providing a stress field which agrees with the theoretical stress singularity of linear fracture mechanics. These 'special' nodes also contain rigid body motion and constant strain modes, thus satisfying all the necessary conditions for monotonic convergence [9].

The generated mesh consists of 791 nodes and 294 elements and can be seen in Figure 3. Mode I loading was simulated by applying a symmetric load at the cracked end of the mesh. Mode II loading was introduced by asymmetrically loading the cracked end (EIS test).

The material properties used in this finite element analysis were from typical properties of unidirectional AS4/3502 graphite/epoxy composite. Linear beam theory as well as linear elastic material behavior were assumed in the analysis. Stress contour plots were obtained from the output data and the stress distribution was plotted as a function of distance ahead of the crack tip.

Scanning Electron Microscopy

Split laminate specimens approximately 30.5 mm. long, 5.1 mm. wide, and 1.02 mm. thick of Hercules AS4/3502, and 30.5 mm. long, 5.1 mm. wide and 1.27 mm. thick of Hexcel T6C145/F185 graphite/epoxy composites were cut from 8 ply and 6 ply laminated panels of these two materials. Specimen dimensions were determined by the space allowed by the tensile stage of the scanning electron microscope, and stable crack growth criteria [6]. All specimens were polished with 0.3 alumina powder and cleaned ultrasonically in a scanning electron

microscope Freon 113 solution harmless to the resin.

Mode II observations of the delamination fracture process were determined using real-time observations in the scanning electron microscope. Mode II delamination was achieved by means of a especially designed three point bend fixture installed to the tensile stage of the scanning electron microscope. To confirm that these real-time observations were representative of the bulk delamination behavior post-mortem studies were performed.

All surfaces were coated with a 150 angstroms thick gold/palladium film to minimize charging effects associated with the nonconductive nature of the epoxy resins of the composites. The experimental results were recorded on both video tape and on standard tri-x film.

RESULTS AND DISCUSSION

End Notched Flexure (ENF) Test Results

Table 1 shows the ENF test results for both graphite/epoxy systems investigated. Method I corresponds to G_{IIC} values obtained using beam theory equations (Equation (1)) and measured compliances. Method II results are based on the compliance calibration (Equations (2) and (3)). Method 3 refers to data reduction based on the area method (Equation (6)) and the energy dissipated under the load-deflection curve. Delamination crack growth occurred at typical load values of 556 to 612.5 N for AS4/3502 graphite/epoxy and was unstable for this material. Figure 4 shows a typical load-deflection curve of AS4/3502 graphite epoxy showing the sudden drop of load as unstable delamination occurred. This indicates that the G_{IIC} values measured using the area method will not only include the energy required to create a crack surface but will also include energy dissipated in dynamic crack growth processes. The very small nonlinearity just prior to crack extension is probably associated with the development of a crack tip damage zone.

The average critical energy release rate G_{IIC} for AS4/3502 using methods I, II, and III of data reduction were 560 J/m², 648 J/m², and 613 J/m²,

respectively. These values are all within 15 percent difference of each other, which can be considered within the experimental error associated with the different methods of data reduction. In fact, Murri and O'Brien have indicated that G_{IIC} measurements may vary with method of data reduction up to 9% with no consistent pattern in the variation [10].

Figure 5 shows a typical load-deflection curve obtained for mode II delamination testing of T60145/F185 graphite/epoxy. Crack growth was stable as seen in the upper part of the curve. However, the point at which crack growth occurred is not well defined. Therefore, the maximum load reached during each test was used to estimate the onset of crack growth. These values were between 1390 and 1630 N. The curve also indicates an inelastic behavior of the material (i.e., the unload curve did not return to the origin). Therefore, all the assumptions of the test have been violated. It should be noted that the load-deflection curves at different crack lengths used for the compliance calibration also showed non-linear behavior. The G_{IIC} values predicted by methods I, II, and III are all ambiguous. However, the energy release rate obtained by the area method gives a better approximation of the critical energy release rate G_{IIC} because at least the geometrically non-linear behavior of the specimen is taken into consideration by this method. The calculated average G_{IIC} of 2400 J/m^2 should be considered an upper bound estimate of the mode II critical energy release rate of T60145/F185 because the inelastic behavior is not accounted for in this analysis. A J-integral approach needs to be developed to obtain a more meaningful measure of the mode II delamination fracture toughness of this system.

End-Loaded Split Laminate (ELS) Test Results

The ELS test results are seen in Table 2. Method 1 corresponds to G_{IIC} calculated using Equation (4) and with E_{11} calculated from Equation (5) and test data. Method 2 corresponds to the area method (Equation (6)). An average E_{11} of 125.5 GPa for AS4/3502 and 109.9 GPa for T60145/F185 were calculated.

Figure 6 shows a typical load-deflection curve obtained after testing one of the AS4/3502 specimens. As seen in this figure, unstable crack growth is observed for the first crack extension despite the (a/L) ratio of at least 0.55 introduced to all EIS specimens during the mode I precrack done prior to mode II testing, which according to the stability considerations of this loading and geometry should have been stable [8]. This is probably the result of the additional energy storage in the fixtures. Nonlinearity, especially at displacements greater than 50.8 mm, may also be associated with the limitations of linear beam theory used in the stability analysis. An average G_{IIC} of 595 J/m² (method 1) and 543 J/m² (method II) were found for AS4/3502. These results are within 10 percent difference of each other. However, considerable scatter was observed in the G_{IIC} data from each specimen (Table 2). This scatter is believed to be the result of the high degree of error involved in measuring crack locations which is done by monitoring the crack as it propagates. In contrast, this scatter was very small in the ENF results. A typical load-deflection curve for T60145/F185 is seen in Figure 7. Stable crack growth is observed for all load/unload loops. This is evidenced by the smooth decrease in loading rate followed by a decrease in load until the crack was arrested. It should be noted that it is not known when crack growth started during this process, which was a common uncertainty for this material for both types of mode II tests. At least some of the observed nonlinear behavior is due to inelastic behavior since the curves fail to return to the origin as the specimen is unloaded. Nonlinear behavior associated with the limitations of linear beam theory are also observed for deflections greater than 50.8 mm.

The average mode II energy release rate values for T60145/F185 were found to be 2275 J/m² (method 1) and 2260 J/m² (method 2). However, a systematic or monotonic increase in G_{IIC} for method I can be observed throughout the test. This is the result of the nonlinearity in the load/deflection curve seen in

Figure 7. Although this nonlinearity is less severe than the nonlinearity observed for this material tested using the ENF test, it is sufficient to invalidate the data analysis done using linear beam theory (method I). The scatter of the results for method II (area method) is more random and is associated with the experimental difficulty in obtaining a precise measure of the change in crack length. However, these values are an overestimation of G_{IIC} because the curves did not return to the origin as the specimens were unloaded.

A comparison of the results predicted using both test configurations indicate that for AS4/3502 (a brittle composite) similar results were obtained for the ENF and ELS tests. In contrast, for T60145/F185 both the ENF and ELS test do not give valid results since the assumptions associated with each test method were violated. Therefore, in order to properly characterize the fracture toughness of this material and tougher graphite/epoxy composites in general, an analysis which allows for material and geometric nonlinearity such as a J-integral is needed. It is worth noting that similar results were obtained for the ENF and ELS when data was analysed using the area method. However, both results should be considered upper bounds of the mode II critical energy release rate of the material.

Finite Element Analysis

Figure 8 shows the finite element results of a split laminate beam specimen tested under pure mode I conditions (double cantilever beam test). Figure 8a is a stress contour of the normal (S_{yy}) stress. A perfectly symmetric stress condition is shown through the beam thickness indicating the expected mode I loading. The stress is seen to rapidly increase as the crack tip is approached. Figure 8b shows the S_{yy} stress distribution ahead of the crack tip at the midplane of the specimen. The S_{yy} stress is a principal normal stress along this plane and it rapidly drops off with distance from the crack tip until it is compressive at a distance of 0.76 mm ahead of the crack

tip. Finally, it gradually approaches a zero stress level at approximately 8 mm from the crack tip, which is maintained all the way to the end of the beam. Similar behavior was observed when the stress field ahead of the crack tip was calculated by means of a high order plate theory [11]. An identical loading case but assuming isotropic material behavior, also indicated that compressive stresses developed in the specimen ahead of the crack tip. This suggests that these compressive stresses are due to geometry and loading rather than material anisotropy. However, this compressive stress state is not expected to significantly effect delamination because it develops far enough away from the crack tip. The dashed line also seen in Figure 8b indicates the magnitude of the shear stress S_{xy} , which is seen to be zero everywhere along the delamination plane for the mode I loading. Therefore, this confirms that a pure mode I loading macroscopically does indeed give a pure mode I delamination stress microscopically around the crack tip.

Figure 9 shows the results of a split laminate beam specimen subjected to an asymmetric loading case of pure mode II condition. Similar to the normal stress under mode I conditions, the shear stress is perfectly symmetric across the beam thickness suggesting a pure mode II loading condition on the specimen, as seen in Figure 9a. However, the shape of the stress field appears more narrower and elongated than for mode I loading. Figure 9b shows the stress field as a function of distance ahead of the crack tip. In this case, the shear stress can be seen to monotonically decrease to a constant value which extends all the way to the end of the beam. The dashed line indicates the normal stress distribution along the delamination plane to be zero; i.e., macroscopic mode II loading does indeed appear to give a microscopic mode II stress along the delamination plane. As can be seen, the shear stress ahead of the crack tip for mode II loading decays much more slower than the normal stress for mode I loading. Furthermore, for mode II loading the extent of the stress field above and below the delamination plane is much smaller for mode

II than for mode I, as seen in the stress contours plots. This results are consistent with the SEM observations of damage zone size and shape to be reported in the next section.

Scanning Electron Microscopy Observations of Mode II delamination

Figure 10 corresponds to real time observations under mode II delamination of AS4/3502 graphite/epoxy. Figure 10a shows part from the damage zone ahead of the crack tip which developed as the specimen was being loaded (left side of micrograph). This damage zone is characterized by extensive microcracking and it was found to be at least 180 μm long and extending about 5 μm above and 5 μm below the plane of delamination, and resembling the shape of a Dugdale type damage zone, long and narrow. This elongated damage zone is at least twice as long as the damage zone reported ahead of the crack tip for mode I delamination of the similar material AS4/3501-6 [12]. This is probably because for mode II, the resin rich region between plies behaves like a soft material between rigid plattens with all the strain being localized in this region, and also because of the slower rate of decay of the stress field under mode II compared to mode I revealed by the finite element analysis. The hackle formation process often associated with mode II delamination of composites made with relatively brittle resins can also be seen in Figure 10. First, microcracks start to form at approximately 45 deg. to the plane of the plies (Figure 10a), perpendicular to the principal normal stress direction. Then, macroscopic crack extension occurs as the sigmoidal shaped microcracks begin to coalesce, forming the hackles (Figures 10a and 10b). During this process, some resin deformation must have accompanied the coalescence of microcracks into hackles as the gap between adjacent hackles results from rotation at the base when microcrack coalescence takes place. Note how the final hackle orientation is steeper than the 45 deg. angle of orientation of the initial microcracks from which the hackles form. No clear indication of crack growth direction is given by the hackle orientation on the fractured

surfaces. Arrows at the upper left hand corner of all micrographs indicate crack growth direction. Figure 11 further illustrates the difficulty in trying to infer crack growth direction from hackle direction alone [13].

In-situ delamination observations of T6C145/F185 graphite/epoxy are shown in Figure 12, where the damage zone developed ahead of the crack tip as the material was being loaded is seen. This damage zone was approximately 1000 μm long and extended at least 25 μm above and 25 μm below the plane of delamination near the macroscopic crack tip, progressively decreasing to about 5 μm at the end of the damage zone. The damage zone is characterized by extensive microcracking. It is also approximately 15x larger by area than the damage zone for AS4/3502, indicating that much more energy is dissipated in the delamination process for this tougher material (T6C145/F185). Note also that the microcracks do not coalesce to form hackles as the macroscopic crack is created. Instead, the resin extensively deforms as the localized strain increases until a complete separation of the surfaces occurs due to local yielding (Figure 12b). Note the large strain undergone by the resin in areas well above and below the resin rich area where the crack formed. The extensive resin deformation and large damage zone observed explains the non-linear behavior observed in the load-deflection curves for this material (Figures 5a and 7). Furthermore, the much greater resistance to delamination of T6C145/F185 compared to AS4/3502 measured for mode II loading (2260 J/m^2 vs. 540 J/m^2) is consistent with these observations. The long narrow shape of the damage zone for both systems is consistent with what one would expect based on the finite element analysis.

Post-mortem fractography of the fractured surface under mode II delamination of AS4/3502 can be seen in Figure 13. The most significant artifact observed in these micrographs are the hackles formed on the fractured surface. Note the feather like appearance of the hackles which have developed at a very steep angle (larger than the 45 deg. angle at which the

microcracks were observed to develop during the in-situ observations). See Figure 13a. Therefore, the hackles undergo some rotation before full separation of the fractured surfaces occurs. This is in good agreement with the final hackle angle orientation from the in-situ observations (Figure 10). Figures 13b and 13c show the detailed river pattern markings that develop on the surface. No clear indication of crack growth direction is seen from the river pattern markings on the hackles or the direction in which the hackles point (Figure 10a). In fact, the direction the hackles and the river pattern markings point will be determined by whether microcrack coalescence occurs on the upper or lower boundary of the resin rich region between plies, and this is a random process.

Post-mortem observations of the fractured surface under mode II delamination of T6C145/F185 composite can be seen in Figure 14. Note the extensive random deformation undergone by the resin indicating that the resin failed due to yielding instead of the brittle type failure leading to hackle formation of the more brittle graphite/epoxy systems such as AS4/3502. Correlating these figures with Figure 10 from the in-situ observations of this material, it can be verified that the microcracks formed (in-situ) do not generally coalesce to form hackles. Rather, a much more ductile final fracture is noted.

As it has been shown already, the critical energy release rate for T6C145/F185 is approximately five times larger than for AS4/3502. Therefore, it can be inferred that although the formation of hackles provides a more tortuous path for the crack leading to an increase in fractured toughness in brittle composites, extensive resin deformation and yielding play a more significant role in the fractured toughness resistance of tougher graphite/epoxy systems. In fact, the reported fracture toughness of T6C145/F185 under mode I conditions where little to no hackle formation is observed is similar to the fracture toughness of the material under mode II

conditions [14].

CONCLUSIONS

- (1) Both the ENF and ELS test give similar values for the critical mode II energy release rate G_{IIC} . However, since elastic material behavior is assumed in the analysis, the G_{IIC} results for the ductile composite are somewhat uncertain because a small permanent deformation was observed.
- (2) Different size and shape of damage zone observed when comparing mode I to mode II is consistent with the difference in the size and shape of the stress field predicted by finite element analysis.
- (3) The damage zone developed ahead of the crack tip at the onset of crack growth under mode II delamination conditions is much larger by area for the composite made using a more ductile epoxy (E185) than for the composite made with a brittle epoxy (3502).
- (4) The formation of hackles provides a more tortuous path for the crack leading to an increased resistance to delamination under mode II conditions compared to mode I for brittle composites. However, the extensive resin deformation and yielding plays a more significant role in the fracture toughness resistance of tougher composites giving essentially similar fracture toughness values under mode I and mode II conditions.

REFERENCES

1. Tse, M. K., Hibbs, M. F., and Bradley, W. L. "Delamination Fracture Studies of Some Toughened Graphite/Epoxy Composites, Including Real Time Fracture Observation in Scanning Electron Microscope". ASTM Symposium on Toughened Composites, Houston, Texas, March 13-15, 1985.
2. Murri, G. B. "G_{IIc} Measurement of Toughened Matrix Composites Using the End-Notched Flexure (ENF) Test". ASTM Committee D30.02 Task Group on Interlaminar Fracture Toughness, Dallas, Texas, 1984.
3. Vanderkley, P. S. "Mode I-Mode II Delamination Fracture Toughness of a Unidirectional Graphite/Epoxy Composite". Master of Science thesis, Texas A&M University, Dec. 1981.
4. Russell, A. J. and Street, K. N. "The effect of Matrix Toughness on Delamination : Static and Fatigue Fracture under Mode II Shear Loading of Graphite Fiber Composites". Presented at the NASA/ASTM Symposium on Toughened Composites, Houston, Texas, March 13-15, 1985.
5. Gillespie, J. W., Carlsson, L.A. and Pipes, R. B. "Finite Element Analysis of the End-Notched Flexure Specimen for Measuring Mode II Fracture Toughness". Center for Composite Materials, University of Delaware, Newark Delaware. To be published in Composite Science and Technology.
6. Carlsson, L. A., Gillespie, J. W., and Pipes, R. B. " On the Analysis and Design of the End-Notched Flexure (ENF) Test Specimen for Mode II Testing. Center for Composite Materials, College of Engineering, University of Delaware Newark, Delaware. To be published in the Journal of Composite Materials.
7. Henriksen, M., Engineering Department, Colorado School of Mines, Golden Colorado, 80301.
8. Schapery, R. A., Mechanics and Materials Center, Texas A&M University, College Station, Texas, 77843. (Private communication).
9. Barsoum, R. S., International Journal for Numerical Methods in Engineering, Vol. 10, 1976, pp.25-37.
10. Murri, G. B., and O'Brien, T. K. "Interlaminar G_{IIc} Evaluation of Toughened-Resin Matrix Composites Using the End-Notched Flexure Test". NASA Langley Research Center Hampton, Virginia, 1985.
11. Whitney, J. M. Composites Science and Technology, Vol. 23, 1985 pp. 201-219.
12. Bradley, W. L., and Corleto, C. R. " The Significance of Hackles in the Failure Analysis of Graphite/Epoxy Composite Materials". Mechanical Engineering Division of the Texas Engineering Experiment Station, Texas A&M University, College Station, Texas, 1986.
13. Hibbs, M. F., and Bradley, W. L., "Correlations Between Micromechanical Failure Processes and the Delamination Fracture Toughness of Graphite/Epoxy Systems". ASTM STP 948 (to be published).
14. Jordan, W. M. "The Effect of Resin Toughness on Fracture Behavior of Graphite/Epoxy Composites", PhD Dissertation Texas A&M University, College

Station, Texas, 1985.

Table 1.- End-notched Flexure (ENF) Test Results.

Material	Specimen	G_{IIC} (J/m ²)		
		I	II	III
AS4/3502	1	525	648	613
	2	508	630	595
	3	560	682	613
	4	543	648	630
	Av.	543	648	613
<hr style="border-top: 1px dashed black;"/>				
T6C145/F135	1	*	*	
	2	-	-	2240
	3	-	-	2695
	4	-	-	2485
		-	-	1995
	Av.	-	-	2398

* No calculation of G_{IIC} is possible due to significant nonlinearity in load/deflection curves. If one uses linear portion of curves to measure compliance and P_{max} for crack extension (ignoring nonlinear behavior near P_{max}), G_{IIC} lower bound values of 1225 may be calculated.

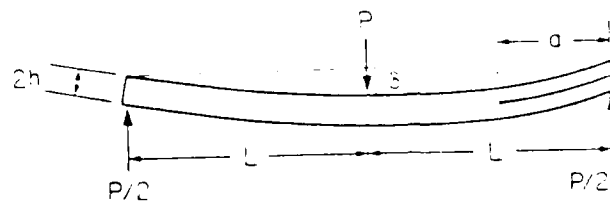
Table 2.- End-loaded Split Laminate (ELS) Results.

Material	Specimen	G_{IIC} (J/m ²)	
		I	II
AS4/3502	1	600	595
		613	560
		613	543
		648	543
	2	595	525
		595	525
		595	525
		508	508
	Av.		595 545
T60145/F135	1	★	
		1645	2153
		2030	2030
		2275	2415
		2275	2363
		2183	1873
		2275	2118
		1960	2643
	2	2223	2240
		2415	2083
		2590	2170
		2713	2765
		2800	2328
	Av.		2275 2260

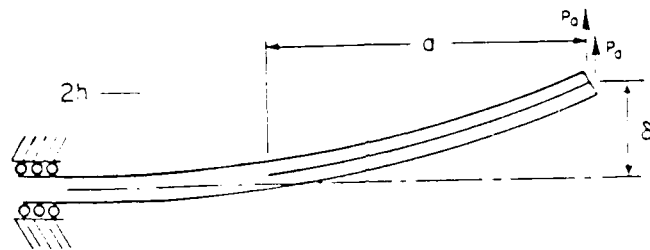
★ Nonlinearity is too great to satisfy linear beam theory assumptions implicit in the approach

FIGURE CAPTIONS

- Figure 1.- Mode II test configurations.
- Figure 2.- Alternate Interpretation of G.
- Figure 3.- Finite Element Mesh.
- Figure 4.- Typical load-deflection curve of AS4/3502 tested using the ENF test.
- Figure 5.- Typical load-deflection curve of T60145/F185 tested using the ENF test configuration.
- Figure 6.- Typical load-deflection curve of AS4/3502 tested using the ELS test configuration.
- Figure 7.- Typical load-deflection curve of T60145/F185 tested using the ELS test configuration.
- Figure 8.- Finite element mode I results.
- Figure 9.- Finite element mode II results.
- Figure 10.- Mode II in-situ delamination of AS4/3502.
- Figure 11.- Mode II in-situ delamination of AS4/3501-6 [13].
- Figure 12.- Mode II in-situ delamination of T60145/F185.
- Figure 13.- Mode II post-mortem fractography of AS4/3502.
- Figure 14.- Mode II post-mortem fractography of T60145/F185.



(a) ENF test configuration and associated parameters.



$$P = 2 P_d$$

(b) ELS test configuration and associated parameters.

Figure 1.

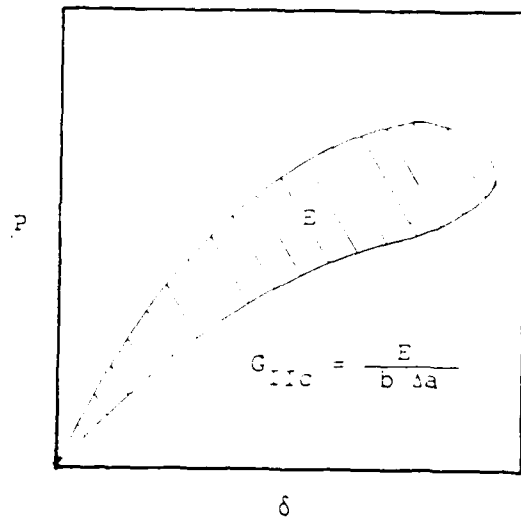


Figure 2.

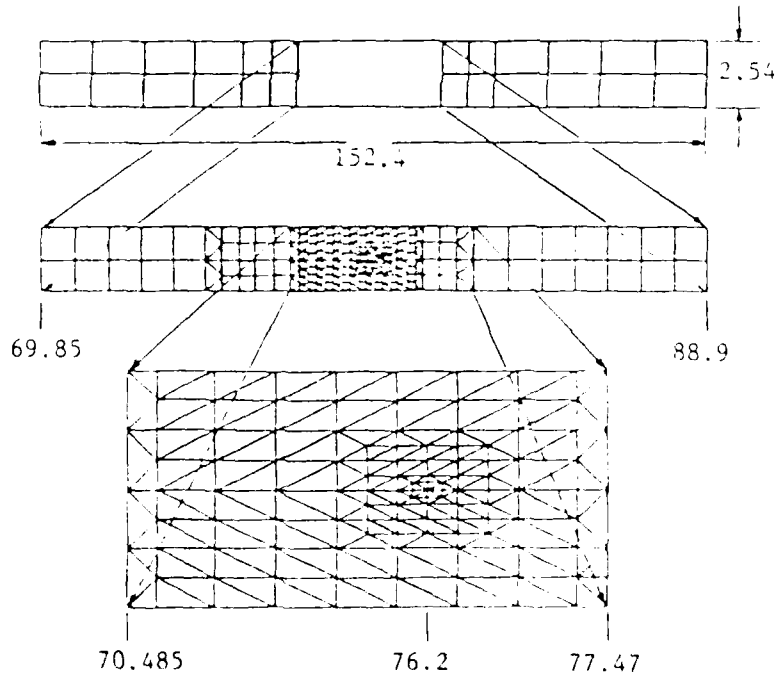


Figure 3.

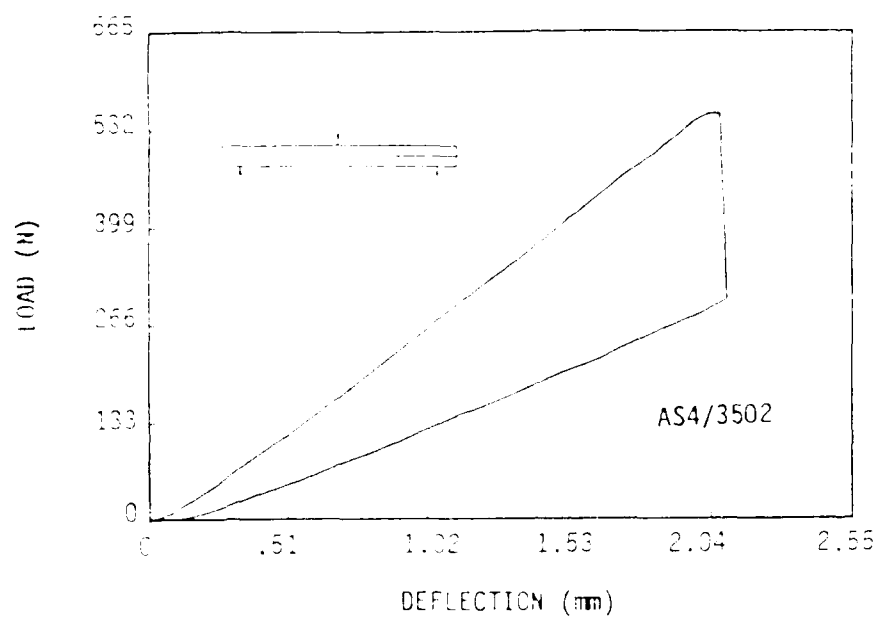


Figure 4.

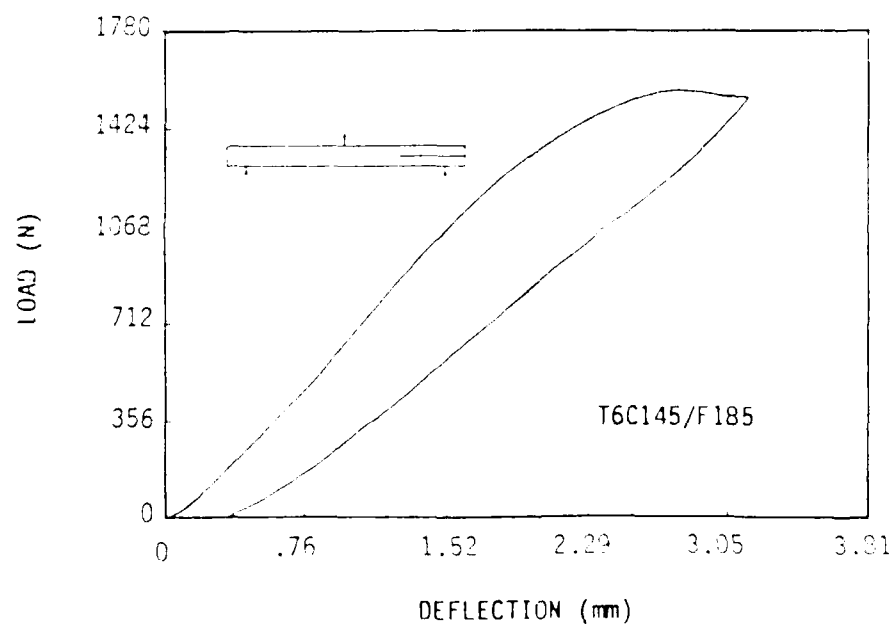


Figure 5.

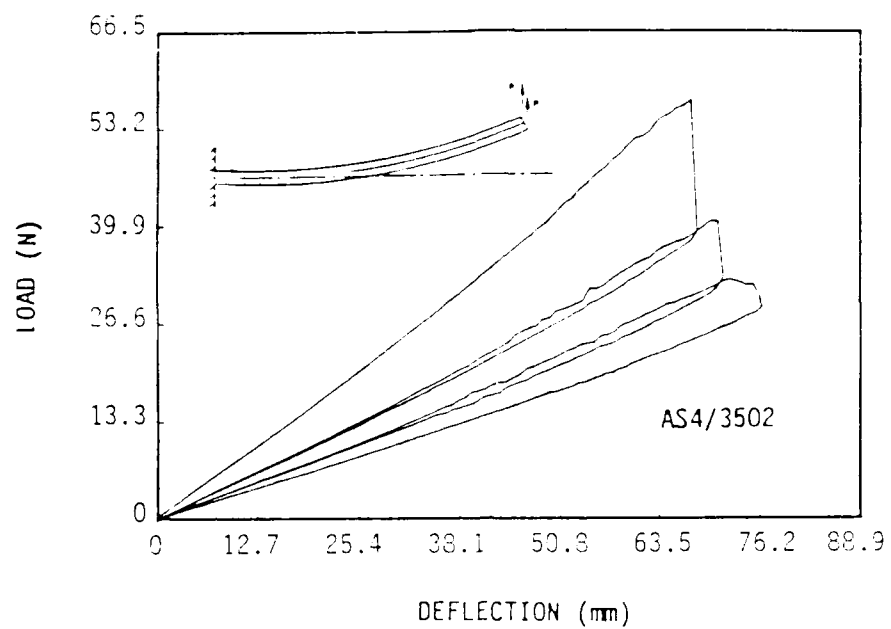


Figure 6.

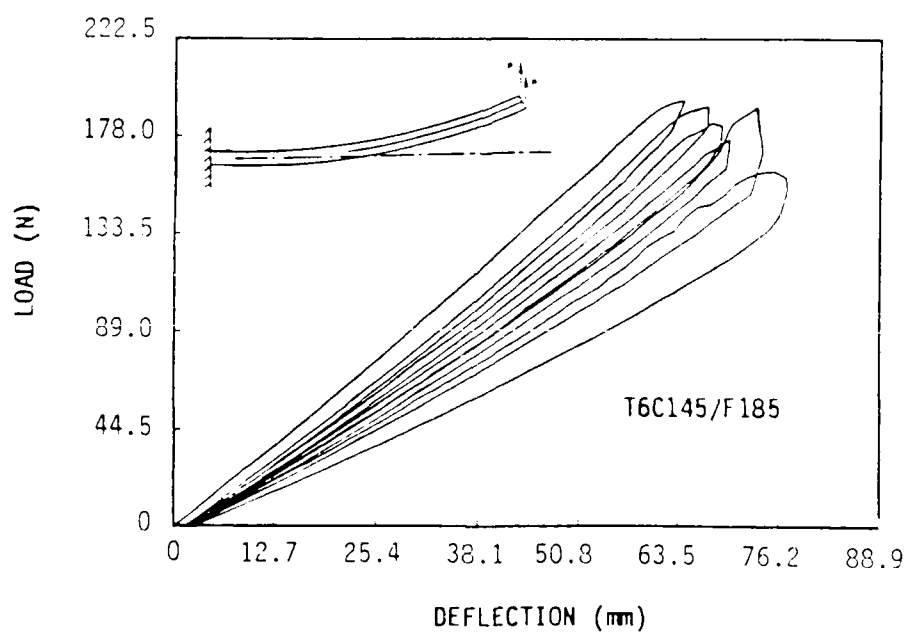
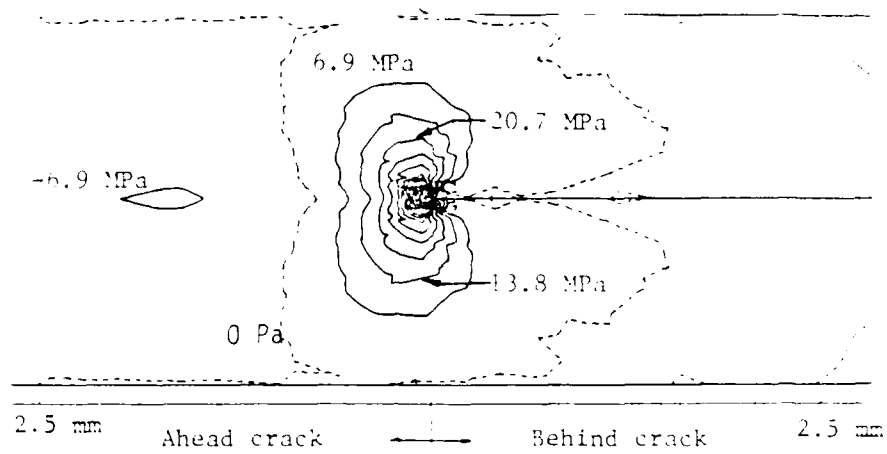
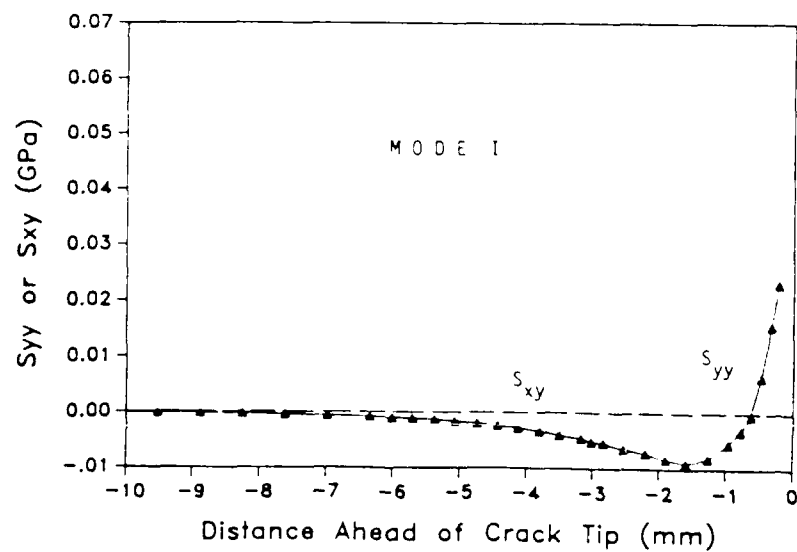


Figure 7.

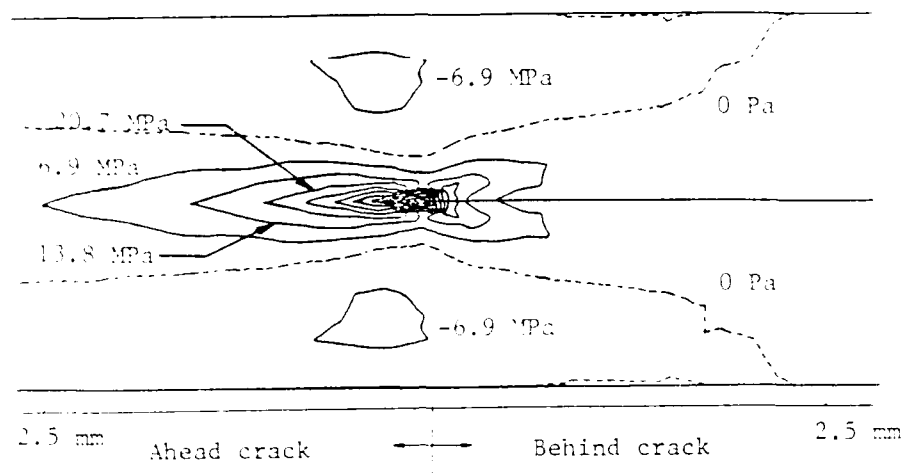


(a) S_{yy} (shear) stress contour plot.

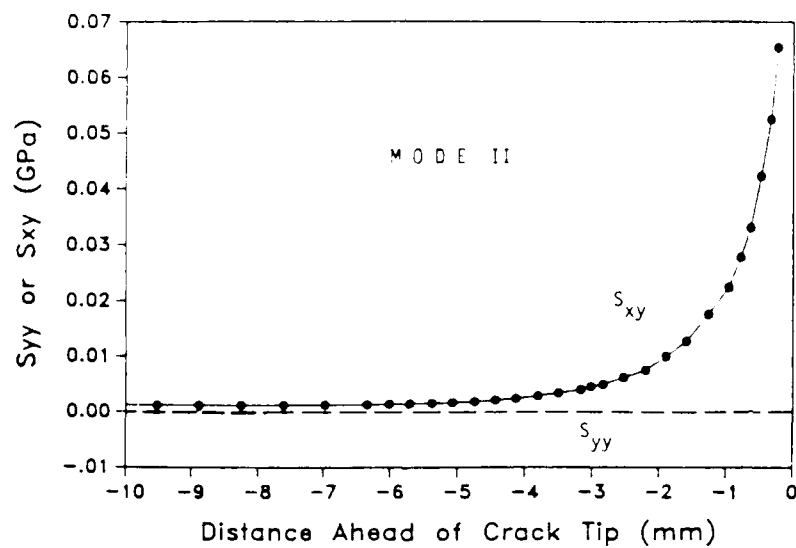


(b) Mode I stress field ahead of crack tip in the plane of delamination.

Figure 8.



(a) S_{xy} (normal) stress contour plot.



Mode II stress field ahead of crack tip in the plane of delamination.

Figure 9.

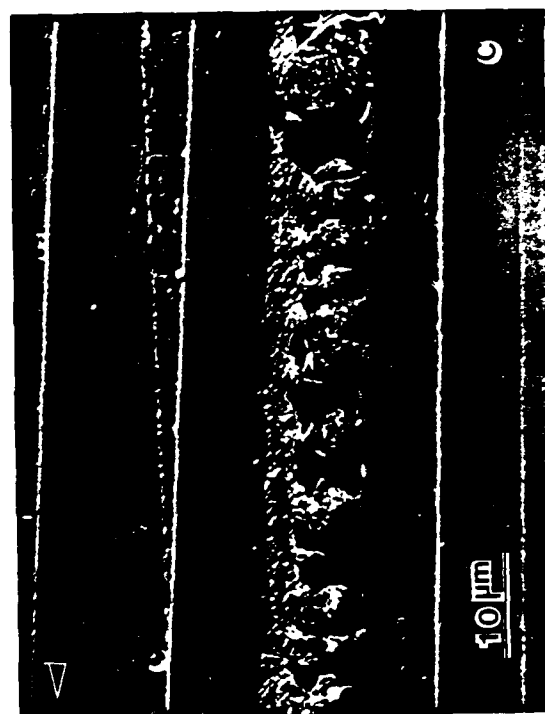
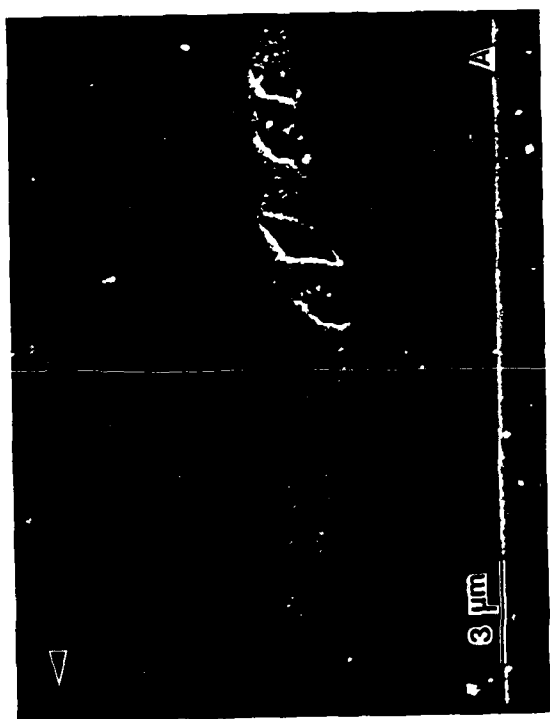
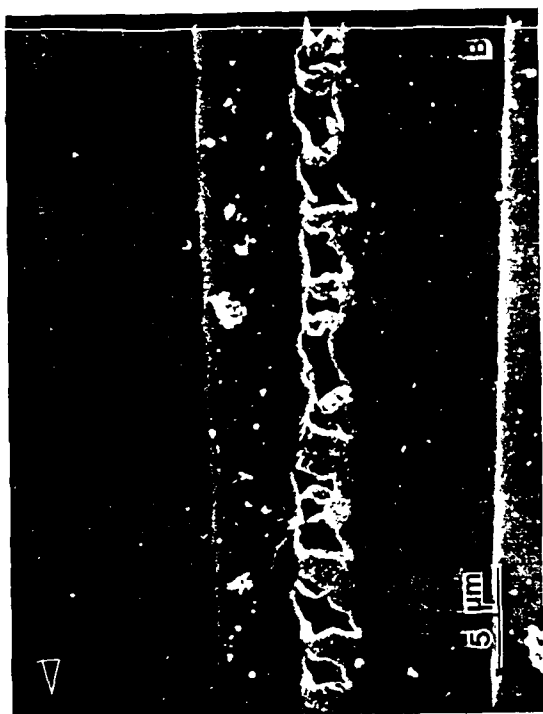


Figure 10

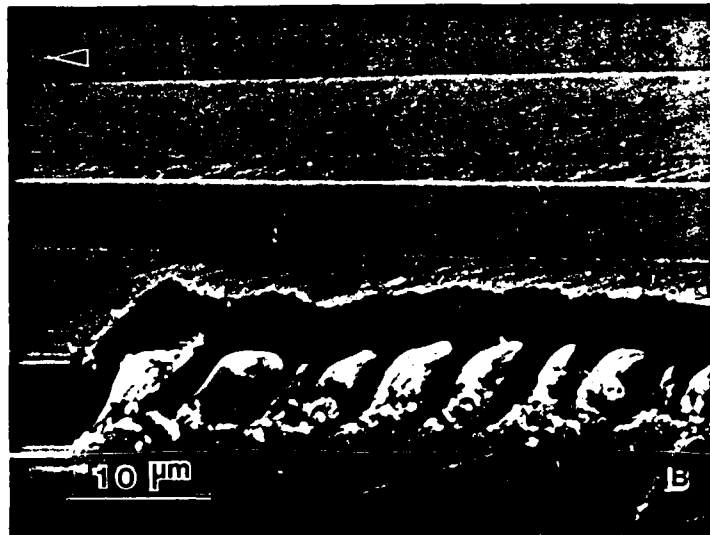
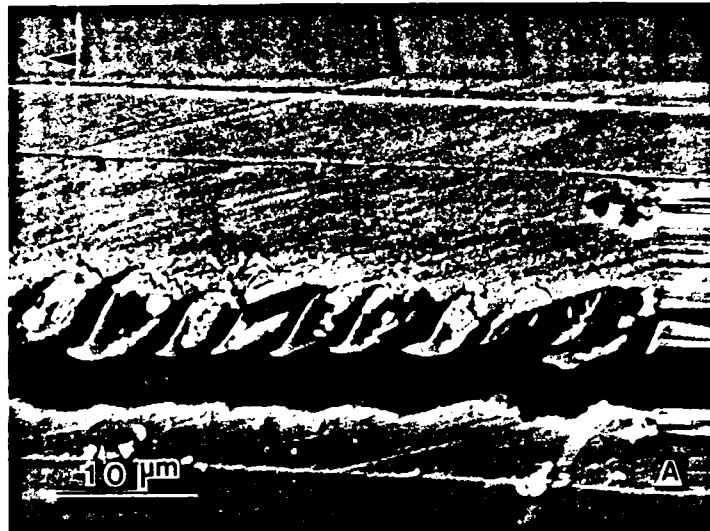


Figure 11

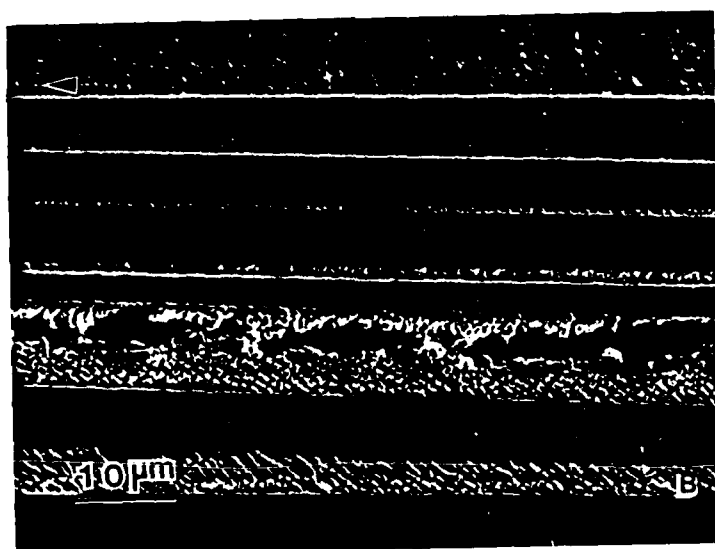
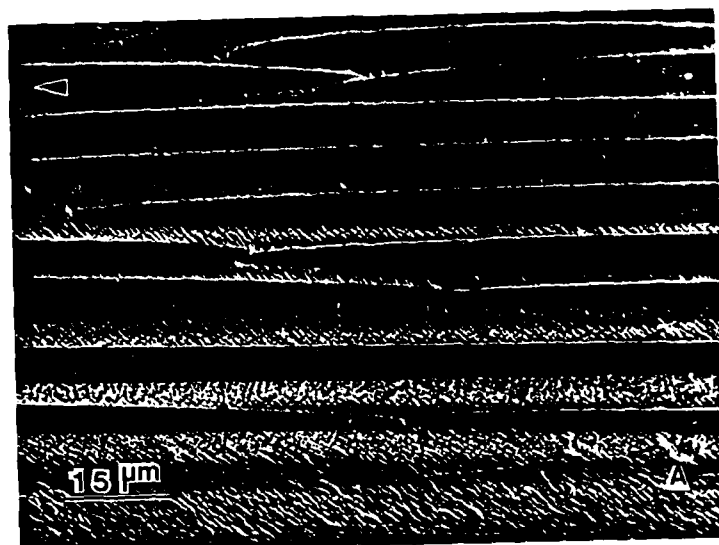


Figure 12



Figure 13

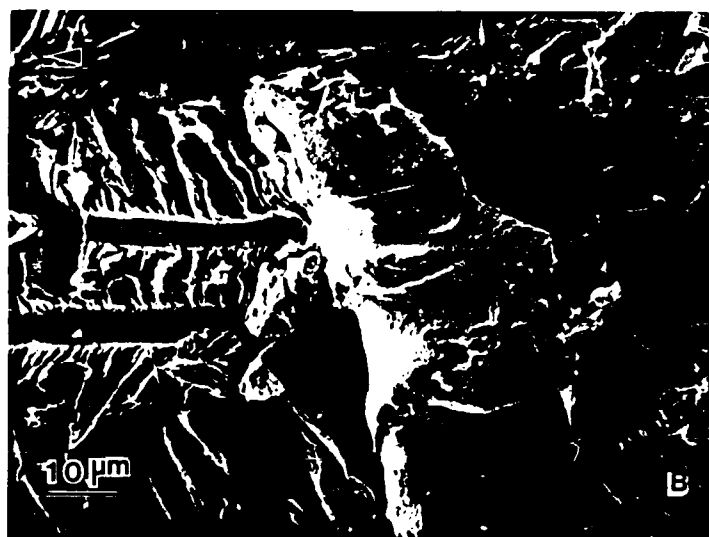


Figure 14

DATE
FILMED
68